STUDIES OF LOW-MASS INTERACTING BINARY STARS

Paul P. Rainger

A Thesis Submitted for the Degree of PhD
at the
University of St Andrews

1990

THE UNIVERSITY OF ST. ANDREWS

Studies of low-mass interacting Binary Stars.

Paul P. Rainger.

Submitted for the degree of Ph.D.

April 1990.

I, Paul Rainger, hereby certify that this thesis has been composed by myself, that it is a record of my own work and that it has not been accepted in partial or complete fulfilment of any other degree or professional qualification.

P. P. Rainger.

I was admitted to the Faculty of Science of the University of St. Andrews under Ordinance General No. 12 on 1st October 1986, and as a candidate for the degree of Ph.D. on 1st October 1987.

P. P. Rainger.

I hereby certify that the candidate has fulfilled the conditions of the Resolution and Regulations appropriate to the Degree of Ph.D.

R. W. Hilditch.

Acknowledgments

A work of this magnitude naturally involves a large degree of collaboration and it is a pleasure to acknowledge all those who contributed, in one way or another, to the successful completion of this project.

I must thank the numerous undergraduates, fellow research students, members of staff, and North East "Fifers" (past and present) who made my time at St Andrews so enjoyable, and whose encouragement and support (usually liquid) was invaluable. On a sadder note, this is probably the last Astronomy PhD Thesis to be produced wholly at the University Observatory.

I thank also the staff of the Observatorio del Roque de los Muchachos for their assistance during my observing sessions, and colleagues at St Andrews who helped with other observations presented in this work. Most of the telescope time was generously allocated by the PATT, with other observations made using the facilities of St Andrews University Observatory, the data being reduced using the computing facilities of St Andrews University and STARLINK. A big thank you goes to Louise Aikman, who kindly typed thousands of previously published photoelectric data points into the computer, and didn't complain once.

I am grateful to the staff of the Libraries both at St Andrews and the Royal Observatory Edinburgh, and the Centre de Donnees Astronomique de Strasbourg for their SIMBAD data base, all of whom helped in the considerable task of carrying out literature searches on the observed objects.

This work was financially supported mostly by the Science and Engineering Research Council in the form of a postgraduate studentship award, with important contributions in the "fourth" year from Menzies Campbell MP and my mother, who has encouraged and supported me throughout my University studies.

Finally, I am particularly indebted to my supervisor Dr. R.W. Hilditch, Dr. S.A. Bell and Dr. G. Hill for their collaboration on this project. The reduction and analysis programs of Steve Bell and Graham Hill provide the key to unlocking the secrets of a binary system, and Steve could always be relied on to know why the computer wasn't working. My supervisor, Ron Hilditch, showed a helpful interest throughout the work, and patiently guided me to what, at times, must have seemed an extremely distant finishing line.

And those whose heads are searching
in the clouds, to make discoveries,

maybe fail to see, what's on the ground

beneath their feet, not hard to find.

This book was presented to the Library
of St Andrews University by the author.

Abstract

Spectroscopic and photometric observations of eight contact/near-contact binaries are presented and analysed. Spectroscopic observations were obtained at 4200 Å (radial velocity spectra) and 6563 Å (hydrogen-alpha line profiles). New photometric observations were obtained at visual and infrared wavelengths, and other previously published light curves are also re-analysed. Absolute dimensions have been obtained for five systems ; TY Boo, VW Boo, BX And, SS Ari and AG Vir, and their evolutionary positions discussed. Four of the systems are found to be in marginal but poor thermal contact, exhibiting regions of apparent "excess luminosity" in their light curves. A qualitative analysis of these "hot spot" regions has been attempted for the first time using spot models now incorporated into a light curve synthesis programme.

Substantial time for this project was awarded on telescopes funded by the United Kingdom Science and Engineering Research Council (SERC), comprising 14 nights at the Issac Newton Telescope (INT) on La Palma, and 4 nights at the United Kingdom Infrared Telescope (UKIRT) on Mauna Kea. Additional observations were made during an 8 night commissioning run on the Jacobus Kapteyn Telescope (JKT) on La Palma, and extensive observations were made with the Twin Photometric Telescope (TPT) at St Andrews University Observatory between 1985 and 1989. These resulted in over 100 spectra at 4200 Å and over 50 spectra at 6563 Å (INT and JKT observations), over 300 infrared photometric observations (UKIRT), and over 3500 visual photometric observations (TPT).

Of the five systems analysed in detail in this work, TY Boo appears to be a normal shallow-contact W-type system.

Both VW Boo and BX And exhibit regions of "excess luminosity" around the ingress and egress of secondary minimum which are well modelled by a warm spot on the cooler component sitting symmetrically around the neck joining the pair. Such a phenomenon may be expected to arise naturally in systems which have come into contact but are not yet/currently in thermal contact, exhibiting a temperature difference between the components. BX And like other B-type systems seems to be reaching this

contact state for the first time, but the position of VW Boo is uncertain, and whilst evidence that it could be in the "broken contact" state predicted by the TRO Theory is far from conclusive, its lower orbital angular momentum clearly marks the system as worthy of further study.

SS Ari and AG Vir exhibit light curves with unequal quadrature heights. Attempts to treat the higher quadrature as a region of "excess luminosity" due to an energy transfer "warm spot" does not however provide a good model of this phenomenon. Since invoking a dark starspot model also does not provide a good explanation for such systems, it may be that this form of light curve distortion is due to an entirely different form of distorting surface phenomenon. Like BX And, AG Vir appears to be just reaching contact for the first time, but like VW Boo, the slightly lower angular momentum of SS Ari warrants further study.

Contents

List of Tables

List of Figures

Chapter 1

Introduction

1.1 Introduction

In recent years there has been much debate concerning both the evolution, and structural form, of close/contact binary star systems. Observational studies have investigated possible anomalous surface luminosity distributions, in the form of dark starspots, on both binary systems and single rotating stars. Surveys of binary parameters have looked for evidence of systems in the different evolutionary states predicted by theory.

The close, but detached, RS Canum Venaticorum (RS CVn) binaries exhibit erratic light curves which are almost certainly due to the presence of large-scale dark spots. The observational and theoretical evidence now seems overwhelming that stellar spots are a direct consequence of deep convection zones and rapid angular velocity (eg. Hall 1976, Mullan 1976a, 1976b, Gershberg 1978, Rodono 1980, 1981, Vogt 1983).

Work on starspots has to date however been primarily centered on the single, spotted, BY Dra stars, with the development of an analytical technique known as "Doppler Imaging" (Vogt & Penrod 1983a) which allows starspot features to be (at least partially) spatially resolved (see section 1.5.3.2).

The contact, W UMa binaries can be split into two sub-categories (Binnendijk 1965, 1970). The "A-type" systems have the more massive component covered during primary eclipse, and are found to be generally well over-contact. The "W-type" systems have the less massive component covered during primary eclipse, and are found to be in thin or marginal contact (eg. Lucy 1973).

The A-type systems are believed to be evolved, and essentially in equilibrium, exhibiting stable light curves. The W-type systems are believed to be unevolved, and show several signs of not being in equilibrium, exhibiting erratic light curve changes. The presence of large-scale dark starspots on the primary component has become the generally accepted explanation of W-type phenomenon (winning by default).

Surveys carried out at St. Andrews University Observatory of both early spectral type contact binaries (Bell 1987), and late spectral type contact binaries (McFarlane 1986), have provided evidence for two evolutionary paths for the formation of contact binaries (Hilditch 1989).

Recently interest has focused on a possible third grouping of W UMa binaries, the so called "B-type". Despite appearing to be well in contact, these systems exhibit a large temperature difference between components. Such systems are of great interest, since they may represent the evolutionary state of "broken contact" predicted by the TRO theory for the structure of contact binaries (see section 1.4.3). Also, rather than invoking dark starspots to model these systems, it has been proposed that an excess luminosity is required, indicative of the presence of a "hot spot", possibly due to mass transfer between the components (eg. Kaluzny 1986c, McFarlane 1986).

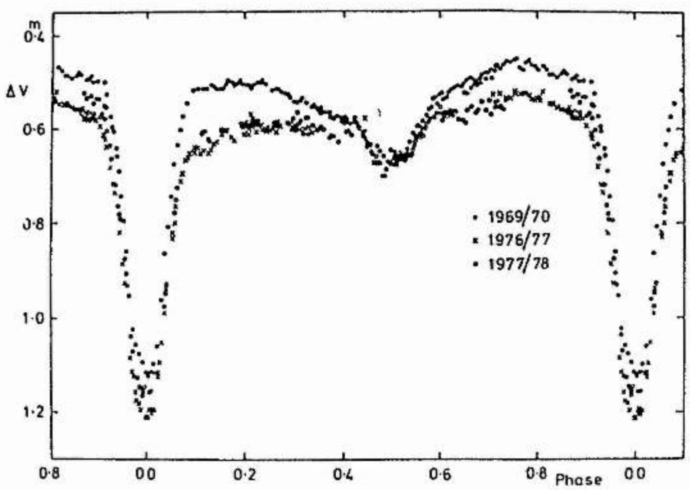

Figure 1.1: The light curve of SV Cam at different epochs. (Hilditch *et al.* 1979).

1.2 The RS Canum Venaticorum Systems

These close but detached binaries consist typically of a G/K subgiant, and a hotter F/G main-sequence companion. They display a variety of photometric and spectroscopic peculiarities which cannot be explained in terms of simple eclipse geometry, but which are almost certainly due to the presence of large-scale dark spots on the cool component, whose uneven distribution distorts the light-curve. (Figure 1.1).

Such spots have been modelled using a simplified kinematic dynamo (Shore & Hall 1980), and are formed by the eruption of enhanced toroidal fields. Shore & Hall also showed that such phenomenon would be related to both the evolutionary status, and the orbital parameters of the binary system. Although for a long time the evidence for spots was largely indirect, Ramsey & Nations (1980) claimed to provide direct evidence through a spectroscopic investigation of the *TiO*-band.

It is worth noting that starspot work on BY Dra stars has shown that although there is an analogy between starspots and Sunspots, there is some evidence (Vogt 1983)

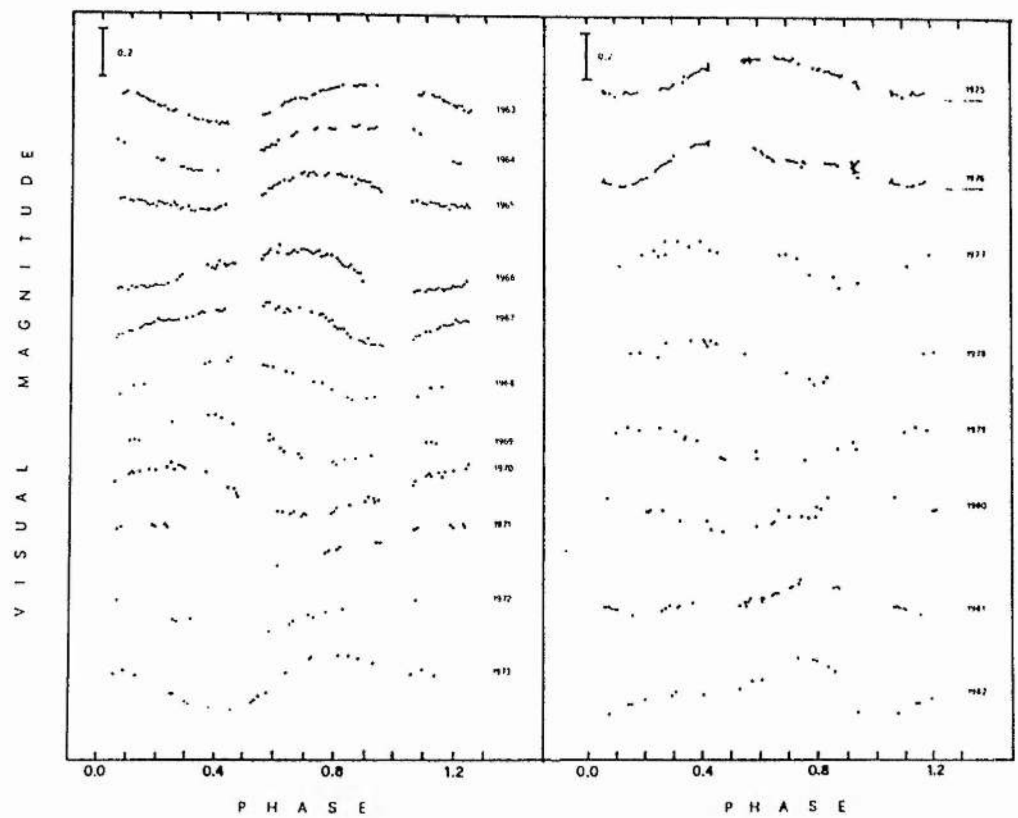

Figure 1.2: The outside-of-eclipse V light curve of RS CVn from 1962 to 1982, showing the migration of a "Photometric Wave". (Blanco *et al.* 1983).

that starspots are actually more analogous to Solar Coronal Holes and Complexes than to Sunspots, as regards to size, shapes, lifetimes, and migratory motions. If true, then starspots are probably more a manifestation of global-scale processes occurring deep within the star than are spots on the Sun. Furthermore, some published spot temperatures for BY Dra stars (Vogt 1981b, Oskanyan *et al.* 1977) have shown decreasing temperatures which become negative (ie. a hot spot) as the cool spot disappears.

One of the outstanding features of many RS CVn-type binaries is the changing shape of the "wave-like distortion" which is superimposed on the eclipsing light-curve, and demonstrates retrograde phase migration. (Blanco *et al.* 1983). (Figure 1.2).

If overall rotation is assumed to be synchronous, then this migration wave phenomenon can be interpreted as demonstrating that the spots must predominate in a surface zone that is rotating faster than the average, ie. the equatorial region. However such a conclusion, that certain zones on the star are subject to spots for years or decades, whilst the other hemisphere is essentially free of them, clearly needs explaining. (Rodono 1981, Rossiger 1982).

The RS CVn systems also display other unusual chromospheric and coronal activity, whose links with sunspot activity in the Sun has long been known. These include flare activity, strong *CaII* emission lines, high *UV*-excess, non-thermal radio frequency outbursts, and variable *X*-ray emission.

Although such systems are not yet actually in the process of tidal mass-transfer, the great majority of them clearly lie near the first phase of mass-transfer.

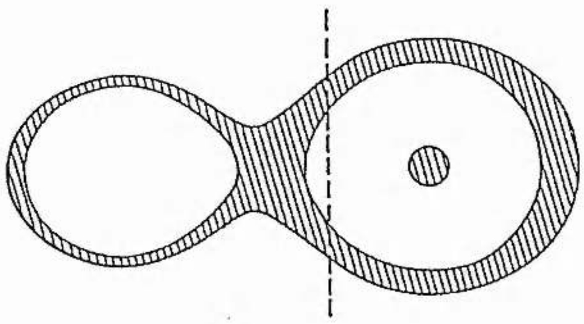

Figure 1.3: The Common Convective Envelope model for W UMa Binaries. Hatched areas donate convection zones. The vertical dashed line is the axis of rotation. (Lucy 1968b).

1.3 The W UMa Contact Binaries

These contact binaries traditionally have sinusoidal type light-curves, usually with roughly equal depth minima, periods less than a day, and dwarf spectra A to K. (A less distinct population of OBA, hot contact systems also exists). They have mass ratios not equal to unity, and components with similar effective temperatures, ie. over-luminous secondaries. Lucy (1968a,b) first suggested the Common Convective Envelope (CCE) model for these contact systems. (Figure 1.3).

In this model both components are surrounded by a CCE, leading to energy transfer from the more to less massive component to equalize the common surface brightness. The nature of this energy transfer is not understood (Robertson 1980), but almost certainly cannot exist in a state of equilibrium (Lucy 1976, Flannery 1976).

An alternative to this model is to argue that the binary components are simply evolved to some extent. This will almost certainly be the case for some systems, but various studies suggest that these cases are a minority of all systems. (Kaluzny 1985).

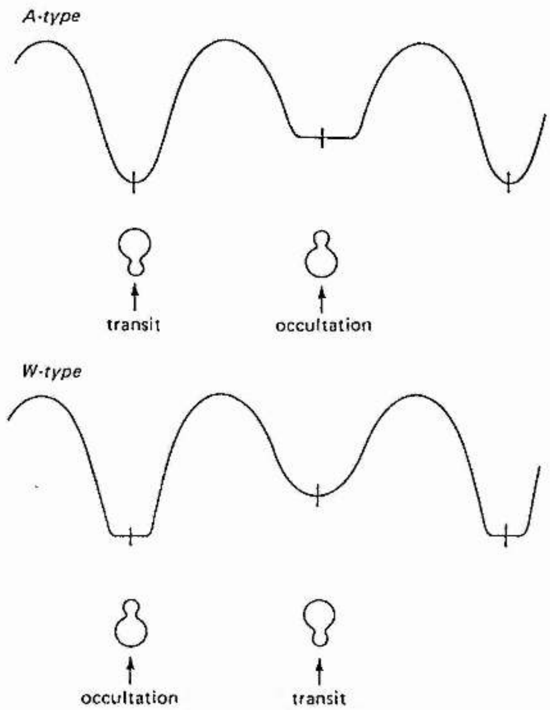

Figure 1.4: The W UMa Binaries are divided into A and W-types, dependent upon which component is eclipsed during primary or secondary minimum. (Rucinski 1985).

1.3.1 The A/W sub-division

It was noticed rather early that contact systems could be divided into two groups (called A and W-types by Binnedijk (1965, 1970)), depending upon which component is eclipsed during primary or secondary minimum. (Figure 1.4).

The origin, and reality, of this division is uncertain, but generally the late G-K spectral types are W systems, whilst A-F types form the A systems. Also, the A-types tend to have smaller mass-ratios, and are generally hotter and more massive. Studies show that the A-type systems are well over contact, with their surfaces substantially exceeding their Roche "inner contact surfaces". These systems are believed to be evolved, and essentially in equilibrium, exhibiting stable light curves. The W-type systems on the other hand are found to be in marginal/thin contact (Lucy 1973), and are believed to be unevolved. They show several signs of not being in equilibrium, with erratic period and light curve changes. Studies by Rucinski (1973, 1974), suggest that A-type systems have only shallow CCE's (but with a greater degree of contact), whilst W-types have deeper CCE's (with a lesser degree of contact). Table 1.1 compares and contrasts the two groups.

Mochnacki (1981) argued that the W-type systems were those containing unevolved components. In this case, the deeper CCE's in the W-types cause the secondaries to exhibite a larger surface brightness than expected, and the primaries a lower surface brightness. Hilditch *et al.* (1988) demonstrated empirically that this was indeed the case. Additionally the presence of dark starspots on the primary components, (Mullan 1975, Eaton *et al.* 1980) has been invoked to help explain the erratic light curve changes seen in these objects.

However, some observations of W-type systems (Kaluzny 1983), seem to be explained more adequately by the hypothesis of a temperature excess on the less massive component. Kaluzny also pointed out that for systems with large mass ratios, the assumption that spots are present only on the larger component is rather artificial. If the mass ratio is close to unity, the convective zones of both components would be of similar depth, so that spots, if they exist at all, should be created on both components.

It should also be noted that a few systems actually change their type. The classic example is TZ Boo, which has been observed to alternate between A-type and W-type several times during recent years (Rucinski 1985). This behaviour has again been explained in terms of a non-uniform surface brightness distribution over the common envelope, caused by the presence of dark starspots.

1.3.2 The "B-Type", Poor Thermal Contact, W UMa Binaries

Recently, a group of near/marginal contact binaries has received much attention. These are the so called "B-type"systems (Lucy & Wilson 1979), which seem to be in poor thermal contact, and often display asymmetric light curves, and unequal depth minima. (Figure 1.5).

Property	A	W	Remarks
1. Spectral type	earlier	later	differences slightly marked
2. Luminosity	higher	lower	differences slightly marked
3. Mass	larger	smaller	differences slightly marked
4. Activity (changes of light curves, asymmetries of maxima)	moderate or absent	strong or very strong (almost every system)	
5. Period	either changing or constant	always changing	Kelvin – Helmholtz time-scale or slightly slower
6. Mass-ratio	small $0.08 - 0.54$	larger $0.33 - 0.88$	upper limit more certain
7. Degree of contact	envelopes slightly thicker than in W-type	shallow envelopes	
8. Photometric conformity to the contact model	good	poor (less massive comp. hotter)	
9. Energy exchange takes place in	adiabatic parts of the conv. envelope	superadiabatic parts of the conv. envelope	
10. Peculiar systems	not too many: systems of very small q, early-type contact systems	many: SW Lac, $q = 0.88$; AB And and ER Ori, deviation from the mass-luminosity relation; many other with changing light curves	

Table 1.1: Comparison of A and W-type W UMa Binaries. (Rucinski 1973).

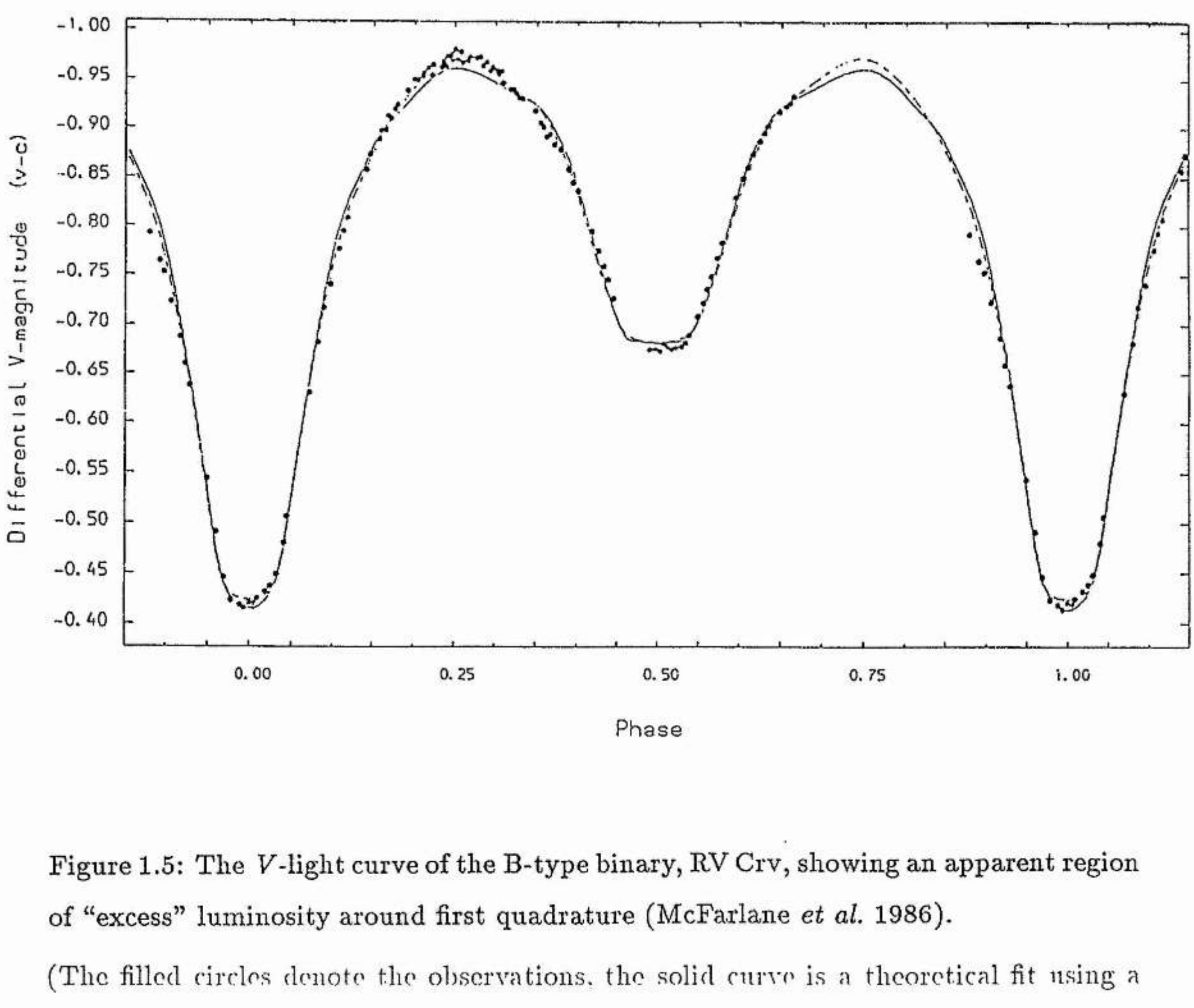

Figure 1.5: The V-light curve of the B-type binary, RV Crv, showing an apparent region of "excess" luminosity around first quadrature (McFarlane *et al.* 1986).

(The filled circles denote the observations, the solid curve is a theoretical fit using a convective atmosphere, and the dashed curve a radiative fit).

These systems are found to be in a state of marginal, but poor thermal contact (the differences in the depth of minima indicative of a large temperature difference between components). They are interesting in view of the predictions of the "Thermal Relaxation Oscillation (TRO) Theory" (Section 1.4.3). According to this theory, the unevolved W UMa systems undergo oscillations about a state of marginal contact. Thus, such systems should spend some time interval in a semi-detached/broken configuration, with the more massive component filling its Roche lobe. In this phase when thermal contact between components is weak, or does not exist, such systems would be expected to exhibit EB-type light curves. Hence, such objects are good candidates for W UMa systems in this broken contact phase.

Unlike the RS CVn and W-type W UMa systems, there is less evidence on these objects of the erratic light curve changes attributed to dark spot activity. However, it has been found, when modelling these asymmetric light curves, that good fits cannot be obtained, due to an apparent region of "excess" luminosity.

Naqvi & Gronbech (1976) first proposed the hot spot hypothesis to explain these asymmetries, and recently analysis of such systems (eg. Hilditch *et al.* 1984, Hilditch & King 1986, 1988, Kaluzny 1983, 1986a,b,c & McFarlane *et al.* 1986) have made similar conclusions. These found that the light curves could only be fitted when the albedo of the secondary component was treated as a free parameter. The solutions gave an albedo greater than unity, which was interpreted as an abnormally hot region on the neck of the secondary, presumably due to mass transfer. (Figure 1.6).

McFarlane *et al.* (1986) pointed out however that an abnormally cool region on the averted hemisphere would have the same effect as a hot region on the facing side. But in the analysis of the binary system RV Crv, McFarlane *et al.* (1986) did find possible evidence for a hot spot in spectroscopic data, where observations around $0^{\mathrm{P}}.25$ showed no indication of an additional peak in the cross-correlation function, due to the secondary, whilst data around $0^{\mathrm{P}}.75$ showed this expected peak, suggesting that light from a hot spot in view at $0^{\mathrm{P}}.25$ could be shrouding the contribution from the secondary.

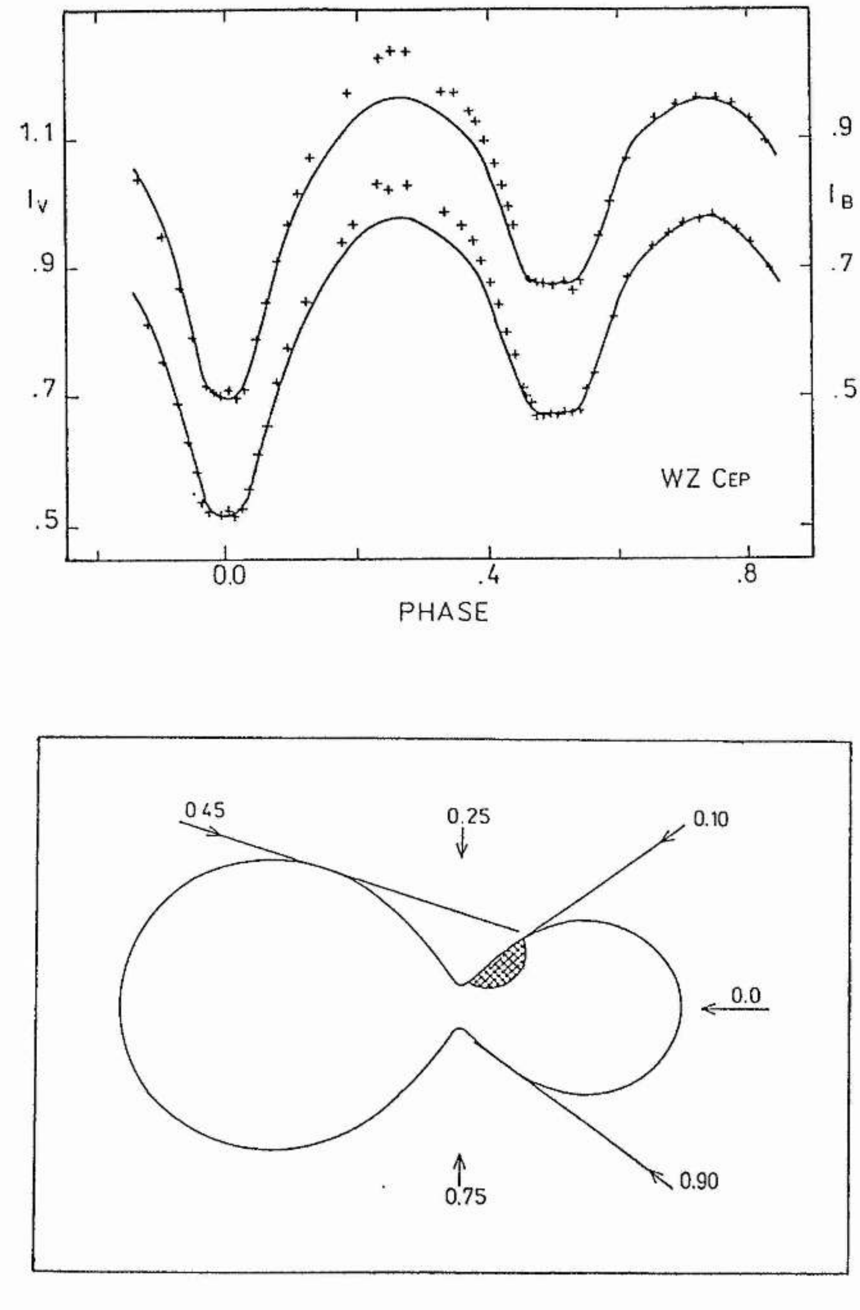

Figure 1.6: V and B light curves of WZ Cep (top). Crosses denote observations, the solid curves are theoretical fits. The phase region of observed excess luminosity suggests the location of a Hot Spot on the component configuration (bottom). (Kaluzny 1986a).

1.4 The Structure of Contact Binaries

1.4.1 Introduction

Although the internal structure of contact binaries has been the subject of intense debate over the last 20 years, no satisfactory theoretical model has yet to emerge which explains all the observed properties of the W UMa binaries.

There have been many reviews of the observational and theoretical work in the subject, those recently by Shu (1980), Smith (1984), Rucinski (1986), and Hilditch, King & McFarlane (1988) providing comprehensive coverage across the field.

It is clear that some contact systems (predominantly the A-types) are evolved, and it is possible to obtain stable contact binaries using models with differently evolved cores.

But some systems (predominantly the W-types) clearly contain unevolved main sequence components. Two different approaches have been taken to model such systems. The Contact Discontinuity (DSC) Theory sought to build an equilibrium model using zero-age main sequence stars of unequal entropy. The Thermal Relaxation Oscillation (TRO) Theory took the approach that the systems were not in equilibrium, but evolving on a thermal time-scale. There is both observational and theoretical evidence that zero-age contact systems could be essentially an evolving, time-dependent phenomenon. However, both theories assume the conservation of angular momentum.

It now seems certain that angular momentum loss (through magnetic braking) plays a crucial role in binary systems, not just in modifying the structural models, but in the entire evolutionary scenario.

Observations have suggested that two paths for evolution into contact are possible, via mass-reversal evolution, or via angular momentum loss. Angular momentum loss may also finally merge contact systems into single, rapidly-rotating stars (possibly FK Comae stars).

1.4.2 Observations

Observations of W Uma systems have provided useful constraints and tests for the theoretical models of contact binaries.

Contact systems seem to prefer small mass-ratios, avoiding q=1, thus at least for the unevolved systems, leading to the inevitable conclusion that there must be energy transport between components through the optically thick "neck". The energy transport mechanism is still largely unsolved, but is undoubtably very complex. Some simplified models have been constructed (eg. Hazlehurst & Myer-Hofmeister 1973), but the full hydrodynamical problem involves sonic flow in a complicated geometry, with coriolis forces, convection, turbulence and shocks.

Hilditch *et al.* (1988) compiled the masses, radii and luminosities for 31 well studied F-K contact, or near-contact binaries (ie. ones with spectroscopic mass ratios), and made several important conclusions.

As had been previously suspected, the primary components of the W-type systems were found to be generally unevolved main sequence stars, whilst the primary components of the A-type systems were generally near to the terminal-age main sequence. The secondary components of the A-type systems were also generally more over-sized than their W-type counterparts, indicative of the deeper-contact of the A-type systems. The magnitude of the luminosity transfer between components of the W-types systems was found to be in good agreement with that predicted by theory.

Two paths for evolution into contact were suggested ; (a) due to angular momentum loss from detached systems, via marginal-contact systems to the shallow-contact W-type systems, and (b) due to stellar evolution from detached systems, via case-A mass transfer to semi-detached systems and then marginal-contact systems, to the deeper-contact A-type systems.

The lack of observed B-type systems indicative of the broken-contact phase of the TRO theory has also been a problem. They only seem to appear at periods greater than about 0.4 day, and although some are certainly in genuine contact, they seem to exhibit strange surface-brightness distributions indicating the presence of bright spots in the neck area connecting the two components. It is interesting to note that a similar bright spot has been observed on the early-type binary system SV Cen (Drechsel *et al.* 1982). However, the three well-studied B-systems in the compilation of Hilditch *et al.* (1988) showed values of angular momentum and other properties which indicated that these systems could only be reaching contact for the first time, rather than being in a later cyclic phase.

1.4.3 The Contact Discontinuity Theory

The Contact Discontinuity (DSC) Model was proposed by Shu, Lubow, & Anderson (1976) who put an equal entropy common envelope on top of the unequal entropy, zero-age binary models of Bierman & Thomas (1972, 1973). This model satisfied observed light curve constraints, but required the maintenance of a temperature discontinuity between the common envelope and the secondary component.

Shu *et al.* (1980) argued that a temperature inversion layer could be maintained by dynamical energy transfer for both possible contact cases (Figure 1.7). However, Smith, Robertson & Smith (1980) showed that the DSC theory contained several serious and fatal inconsistencies, and there is general sceptism about whether a true equilibrium can be maintained in this way.

However, the DSC models may correctly describe contact binaries at particular stages of their thermal evolution, such as immediately after establishing contact in the TRO models.

1.4.4 The Thermal Relaxation Oscillation Theory

Rucinski (1973) proposed that observed instabilities in W-type light curves implied that these systems were not in thermal equilibrium. On this basis, the Thermal Relaxation Oscillation (TRO) Model was proposed by Lucy (1976) and Flannery (1976). This extended the original models of Lucy (1968a,b), allowing matter as well as energy to be exchanged between components. When the total mass and angular momentum are preserved, these models are found to undergo relaxation-type oscillations with alternate long-lasting contact phases and relatively short semi-detached phases (Figure 1.8).

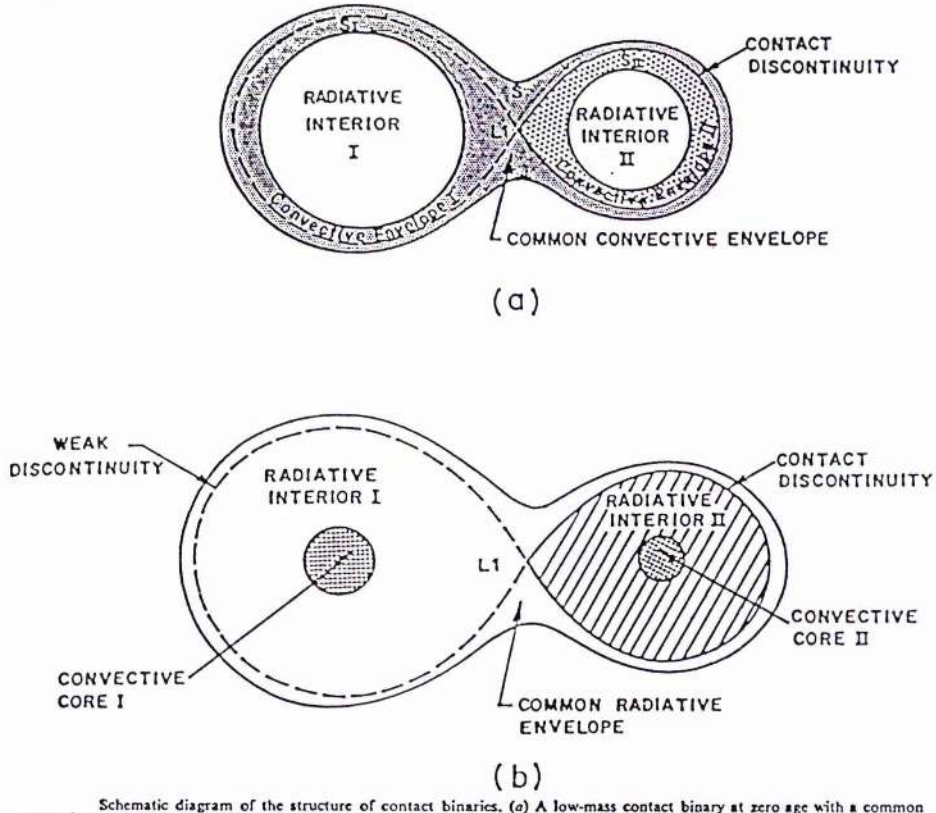

Schematic diagram of the structure of contact binaries. (*a*) A low-mass contact binary at zero age with a common convective envelope. The specific entropy s_{II} beneath the Roche lobe of star II is less than the specific entropy s_I beneath the Roche lobe of star I. For dynamical stability, the specific entropy s in the common envelope equals s_I. (*b*) A high-mass contact binary at zero age with a common radiative envelope. The temperature T_{II} immediately beneath the Roche lobe of star II is less than the temperature T_I immediately beneath the Roche lobe of star I. For dynamical stability, the temperature immediately above the inner critical surface equals T_I.

Figure 1.7: The Contact Discontinuity Model for the two possible cases : (a) Common Convective Envelope, and (b) Common Radiative Envelope. (Shu *et al.* 1976).

When the total mass and angular momentum are conserved, the system must undergo cycles around the state of marginal contact which is never reached. The mass transfer in the contact phase drives the system to larger separations and smaller mass-ratios until the contact is broken. The reversal branch corresponds to phases when the primary, swollen by the additional luminosity ΔL, sheds mass onto the secondary component, which is now devoid of the additional energy.

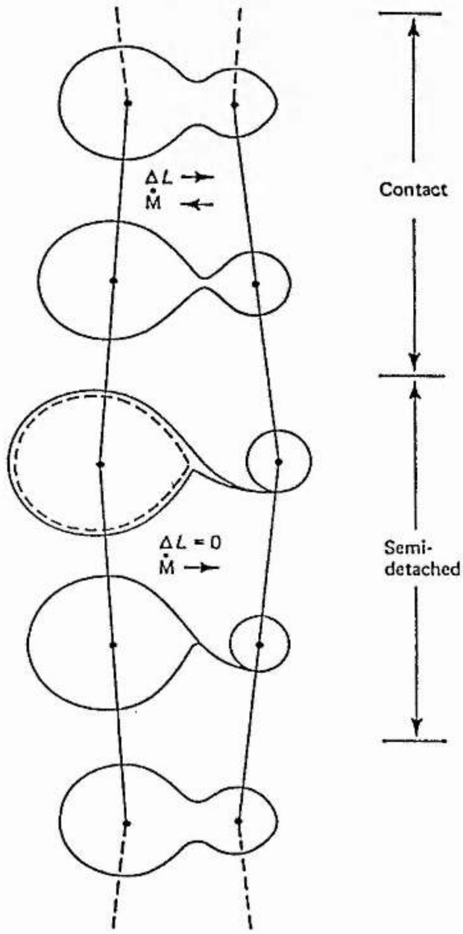

Figure 1.8: Lucy's Thermal Relaxation Oscillation model for a low-mass Contact Binaries. (Rucinski 1985).

The main problem with the TRO model has been the lack of observed systems in the semi-detached phase, ie. with B-type light curves, and periods less than 0.4 days. Although some candidates have been discovered, it is doubtful if they are really broken-contact examples of the TRO model, being equally well explained as either peculiar, evolved systems, not in broken-contact (Mochnacki 1981), or systems which are just evolving into a contact state for the first time (Hilditch *et al.* 1988).

1.4.5 Angular Momentum Loss

The Angular Momentum Loss (AML) Model (Mochnacki 1981 and Rahunen & Vilhu 1982) was proposed as a mechanism for keeping binary components in permanent contact, thus explaining the non-existence of semi-detached states predicted by the TRO theory. Angular momentum loss is used to hold the system in the contact phase of the TRO model, so that the semi-detached phase never (or very rarely) appears. Hence the system moves to smaller and smaller mass-ratios along contact branches of the TRO cycles.

The TRO and AML models have explained many observed features ; the preference for marginal contact, evolution towards smaller mass ratios, and the shape of the period-colour diagram. Rahunen (1981) followed the evolution of a binary system, artificially setting the AML rate to exactly the value needed to maintain marginal contact, and found a good fit with observation.

The main question mark over AML is the need for a self-regulating mechanism to ensure the loss rate is just sufficient to keep the system in contact. Too little and the system undergoes TRO-like oscillations. Too much and the components rapidly coalesce. Vilhu (1981) speculated that increasing contact would result in increased mixing in the common envelope, burying the surface magnetic field and decreasing the loss rate, thus providing the self-regulating mechanism. Rucinski (1986) also suggested that the amount of breaking in W UMa systems may be lower than that for similar non-contact stars, since the stellar cores under the CCE may be up to half a sub-type earlier than suggested by the envelope, thus having weeker deeply-rooted magnetic structures than might otherwise be expected.

1.5 Project Outline

1.5.1 Introduction

The development of theoretical models describing the evolution and structure of W UMa Binary systems has been impeded by a shortage of detailed information relating to short-period binaries.

The TRO theory in particular, has suffered from an apparent lack of observed systems whose components are either in a state of broken contact, or are in marginal contact, but possess widely differing temperatures.

Explanations of light-curve features in terms of anomalous surface luminosity distributions present a far from coherent picture of all the observed phenomena.

Crucially, the analysis of "spot" activity from light curve distortions is usually hampered by two problems :-

(a) In modelling spot activity to observed light curves, the lack of unique solutions is a severe problem, there being a fundamental relation between spot size and temperature.

(b) Interpretations of light curves are often made from theoretical fits where the mass ratio is treated as a free parameter. Yet it is well known that solution surface space exhibits a very shallow minimum with respect to the mass ratio parameter for systems exhibiting partial eclipses. Thus, model light curve fits cannot usually be certain without a spectroscopically defined mass ratio.

Furthermore, is it observationally possible to distinguish between an abnormally cool region on one hemisphere, as opposed to an abnormally hot region on the other hemisphere ?

1.5.2 Project Objectives

Recent work at St. Andrews University Observatory surveyed a sample of early and late-type contact binaries, obtaining detailed photometric and spectroscopic information, in order to determine accurately the physical parameters for a representative sample of systems across the contact binary field.

Given the problems outlined in Section 1.5.1, and the emergence of B-type systems (which may be in the crucial state of "broken contact" predicted by the TRO theory, as well as possibly exhibiting anomalous surface luminosity distributions), it was decided to move forward from the survey data to look more closely at the nature of the possible spot activity, particularly on B-type systems (given their possible evolutionary significance).

Initially, eight systems were selected for study, representing the range of typically observed phenomena.

SV Cam and XY UMa are short period RS CVn-type semi-detached systems whose light curves display the typical erratic variations attributed to dark spot activity.

BX And, SS Ari and AG Vir all exhibit B-type light curves, with unequal depths of minima. AG Vir had previously been studied by Kaluzny (1986c), who modelled the presence of a hot spot from light curve analysis.

TY Boo and VW Boo both exhibit light curves much more typical of the W UMa binaries, and neither system had previously been studied in great detail.

Finally the unusual system TZ Boo was also included, since it had been observed actually to change its type in recent years (Section 1.3.1).

All of these systems had had at least one photoelectric light curve published previously, but with the exception of TZ Boo, no spectroscopic mass ratios were available. Thus observations were planned to obtain spectroscopy, and where possible new photometry, in order to determine the physical parameters of each system; and then use this information to analyse H-α line profiles, and long wavelength-based colour observations (verses orbital phase) in an attempt to reveal the true nature of the surface luminosity distribution. (Section 1.5.3).

As the project evolved, the focus shifted away from a representative sample survey, and more towards the B-type systems, their structure and modelling of possible spot activity.

One reason for this shift was that the spectra obtained for the two RS CVn systems, SV Cam and XY UMa, revealed only the primary component. This lack of spectroscopic mass ratios, and other problems with "spot" related observations (outlined below), curtailed any useful analysis of these systems, and so the spectra obtained for these two systems are only briefly noted in Chapter 8.

Also the two observational techniques used to study the nature of any spot activity both suffered from problems. The *H-α* observations did not achieve a dispersion or signal to noise ratio great enough to enable the spot analysis hoped for, and so these observations are also only reported briefly in Chapter 8. Simultaneous visual and infrared photometric observations made to produce long wavelength based colours could not be reduced, due to an instrument malfunction (Section 2.3.2), but it was possible to produce infra-red light curves from the data, which may show extra evidence for the nature of spot activity.

Thus presented as the main part of this study, are the detailed analyses of five contact systems (BX And, SS Ari, AG Vir, TY Boo, and VW Boo). All appear to be in marginal contact. Four of the systems show signs of not being in equilibrium, and the nature of possible spot activity is considered.

A detailed analysis of TZ Boo was not possible due to distortions in the cross-correlation functions which are also noted in Chapter 8.

1.5.3 The Observational Programme

1.5.3.1 Spectroscopy and Photometry

Spectroscopic mass ratios were obtained for the five main systems presented here, and new optical photometry was obtained for two of these systems. The spectroscopic mass ratios allowed detailed analysis of light curves, to determine accurate physical parameters for each of the systems.

1.5.3.2 Doppler Imaging

The H-α line profile was monitored with orbital phase for seven of the target systems, to search for line profile changes due to localised chromospheric emission associated with spot activity.

It was hoped to extend the work done on dark spots on BY Dra stars and some RS CVn systems to the contact binaries. For example, Figure 1.9 shows the correlation between the H-α emission and starspot visibility observed for the single, rotating star II Peg.

Also, Vogt and Penrod (1983a,b) exploited these line profile changes, in a technique known as Doppler Imaging, to "map" spot activity. They showed how a dark spot would produce an emission bump in the absorption lines of a rotating star (Figure 1.10), and that for stars of intermediate inclinations, some two dimensional information could be derived. They applied the technique to the RS CVn binary, V711 Tau, to map spot positions on the primary component (Figure 1.11).

The observations made for this study are presented in Chapter 8, but the magitude of the proposed spot features, with the resolution and signal to noise obtained, proved insufficient to reveal any "emission bump" features. The work by Vogt on brighter BY Dra and RS CVn objects achieved noise to signal of less than 1%, whereas the noise to signal for the observations of these contact systems was typically 4-5%.

1.5.3.3 Long Wavelength based Colours

Observations over a wide wavelength base are required to help determine the nature of any anomalous surface luminosity distributions on marginal contact binaries. Observations of colours with orbital phase at both the visual (V-B) and the infra-red (J-K) alone have shown no significant variations, but calculations for colours over a large wavelength base (V-K) have suggested that any contribution due to spots would become noticeable.

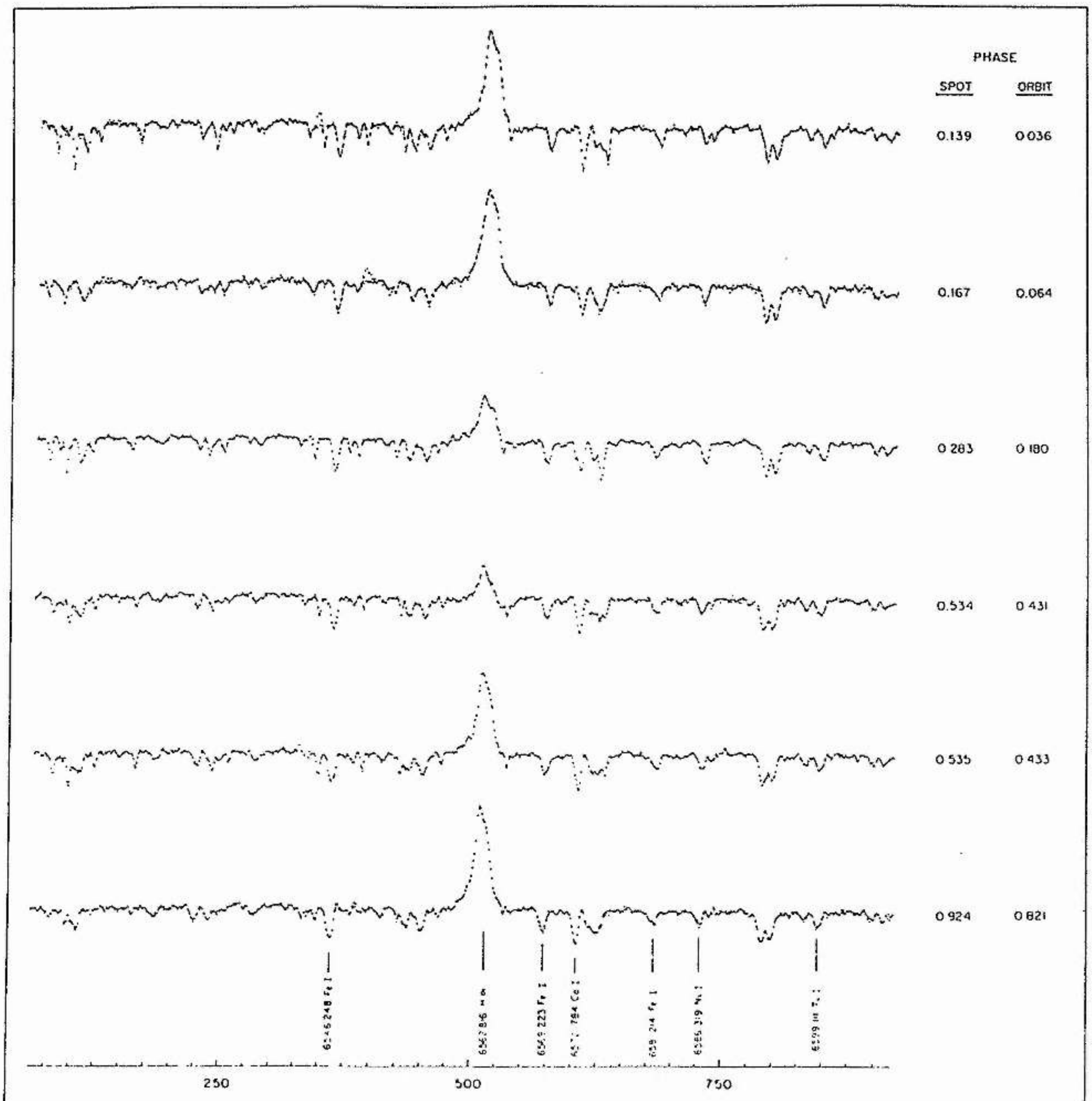

Figure 1.9: The changing H-α emission line profile of II Peg, as a "spot" region comes into and out of view. (Vogt 1981a).

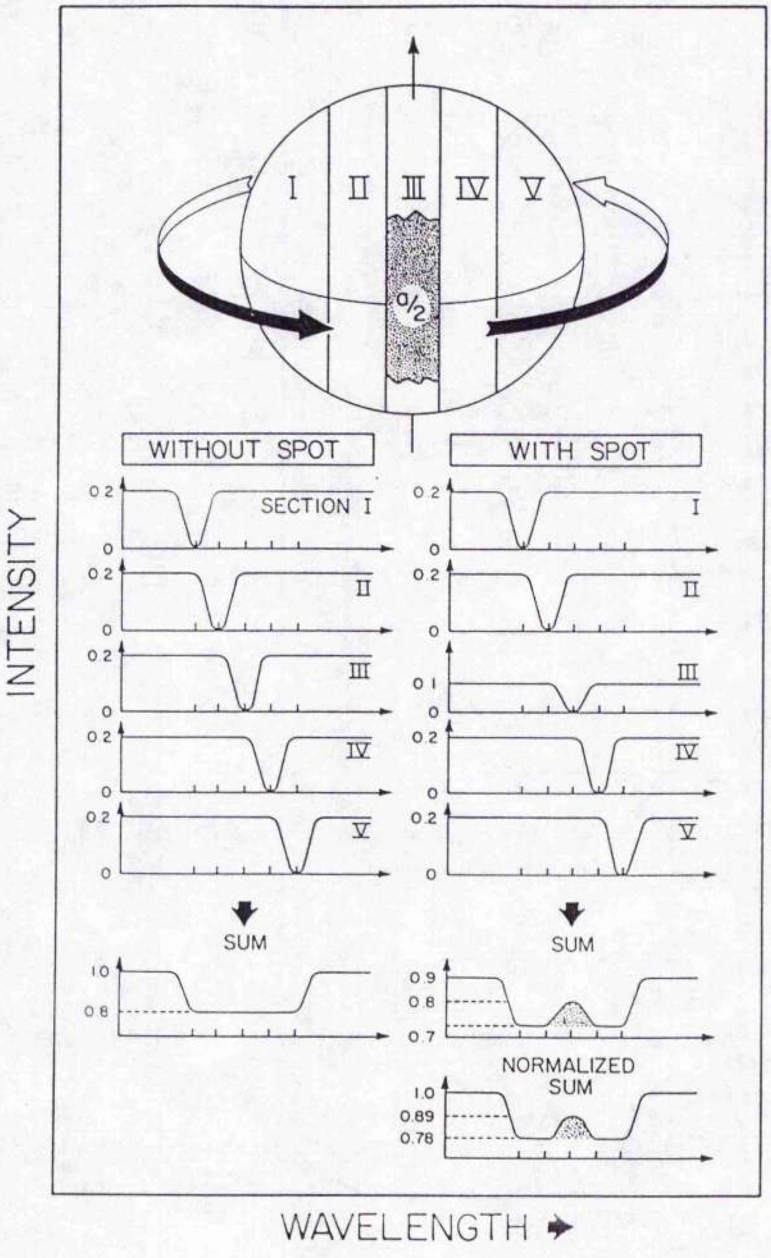

Figure 1.10: How a darkspot on a rotating star will produce an emission bump in the absorption line profiles as it moves through the line of sight. (Vogt & Penrod 1983b).

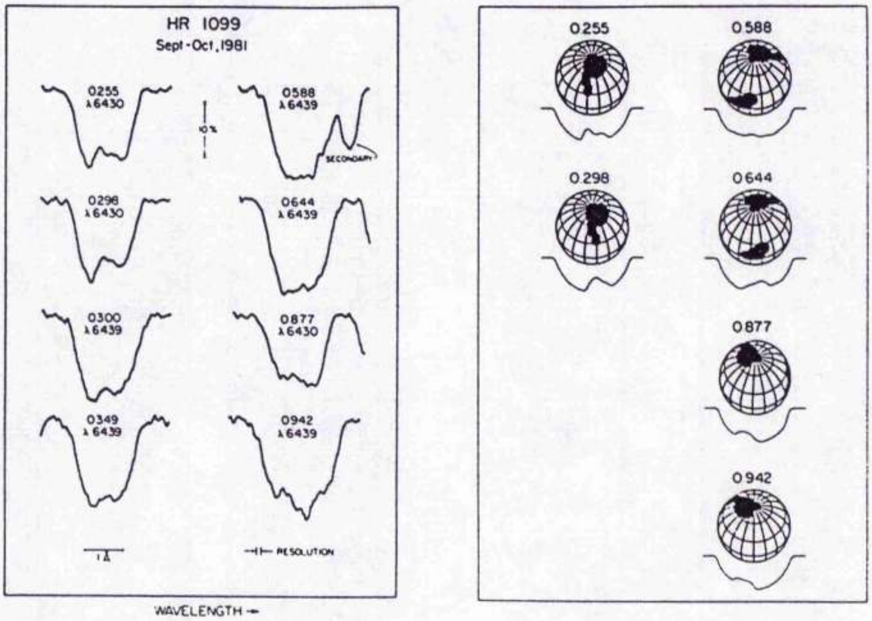

Figure 1.11: Doppler Imaging used to map spots on the primary component of the RS CVn Binary, V711 Tau. (Vogt & Penrod 1983b).

An ideal opportunity to obtain simultaneous visual and infra-red photometry arose during this study with the commissioning of a simultaneous visual photometer on the United Kingdom Infrared Telescope.

Unfortunately, an initial fault with this new visual photometer rendered the visual part of our data unuseable (Section 2.3.1), and although our observations made during the commissioning run helped to correct the instrumental fault, the long wavelength based colours hoped for could not be produced.

However, infra-red photometry was obtained for two of the systems presented here, providing valuable long wavelength light curves against which to test the system and spot parameters suggested from the analysis of other visual data.

1.6 References

Bell, S.A., 1987. *PhD thesis*, University of St. Andrews.

Biermann, P., & Thomas, H.C., 1972. *Astr. Astrophys.*, **16**, 60.

Biermann, P., & Thomas, H.C., 1973. *Astr. Astrophys.*, **23**, 55.

Binnendijk, L., 1965. *Kleini Ver. Bam. 4*, **40**, 36.

Binnendijk, L., 1970. *Vistas Astr.*, **12**, 217.

Blanco, C., Bodo, G., Catalano, S., Cellino, A., Marilli, E., Pazzani, V., Rodono, M., & Sacttriti, F., 1983. *IAU Colloquium 71*, 387.

Drechsel, H., Rahe, J., Wargau. W., & Wolf. B., 1982. *Astr. Astrophys.*, **110**, 246.

Eaton, J.A., Wu, C., & Rucinski, S.M., 1980. *Astrophys. J.*, **239**, 919.

Flannery, B.P., 1976 *Astrophys. J.*, **205**, 217.

Gershberg, R.E., 1978 *Mem. Soc. Astron. Italiana*, **49**, 781.

Hall, D.S., 1976. *IAU Colloquium 29*, 287.

Hazlehurst, J., & Myer-Hofmeister, E., 1973. *Astr. Astrophys.*, **24**, 379.

Hilditch, R.W., Harland, D.M., & McLean, B.J., 1979. *Mon. Not. R. astr. Soc.*, **187**, 797.

Hilditch, R.W., King, D.J., Hill, G., & Poeckert, R., 1984. *Mon. Not. R. astr. Soc.*, **208**, 135.

Hilditch, R.W., & King, D.J., 1986. *Mon. Not. R. astr. Soc.*, **223**, 581.

Hilditch, R.W., & King, D.J., 1988. *Mon. Not. R. astr. Soc.*, **231**, 397.

Hilditch, R.W., King, D.J., & McFarlane, T.M., 1988. *Mon. Not. R. astr. Soc.*, **231**, 341.

Hilditch, R.W., 1989. *IAU Colloquium 107*, 289.

Kaluzny, J., 1983. *Acta Astr.*, **33**, 345.

Kaluzny, J., 1985. *Acta Astr.*, **35**, 313.

Kaluzny, J., 1986a. *Acta Astr.*, **36**, 105.

Kaluzny, J., 1986b, *Acta Astr.*, **36**, 113.

Kaluzny, J., 1986c, *Acta Astr.*, **36**, 121.

Lucy, L.B., 1968a. *Astrophys. J.*, **151**, 1123.

Lucy, L.B., 1968b. *Astrophys. J.*, **153**, 877.

Lucy, L.B., 1973. *Astrophys. Space Sci.*, **22**, 381.

Lucy, L.B., 1976. *Astrophys. J.*, **205**, 208.

Lucy, L.B., & Wilson, R.E., 1979. *Astrophys. J.*, **231**, 502.

McFarlane, T.M., 1986. *PhD thesis*, University of St. Andrews.

McFarlane, T.M., Hilditch, R.W., & King, D.J., 1986. *Mon. Not. R. astr. Soc.*, **223**, 595.

Mochnacki, S.W., 1981. *Astrophys. J.*, **245**, 650.

Mullan, D.J., 1975. *Astrophys. J.*, **198**, 563.

Mullan, D.J. 1976a. *Irish Astronomical Journal*, **12**, 161.

Mullan, D.J., 1976b. *Irish Astronomical Journal*, **12**, 277.

Naqvi, S.I.H., & Gronbech, B., 1976. *Astr. Astrophys.*, **47**, 315.

Oskanyan, V.S., Evans, D.G., Lacy, C., & McMillan, R.S., 1977. *Astrophys. J.*, **214**, 430.

Rahunen, T., 1981. *Astr. Astrophys.*, **102**, 81.

Rahunen, T., & Vilhu, O., 1982. *IAU Colloquium 69*, 289.

Ramsey, L.W., & Nations, H.L., 1980. *Astrophys. J.*, **239**, L121.

Robertson, J.A., 1980. *Mon. Not. R. astr. Soc.*, **192**, 263.

Rodono, M., 1980. *Mem. Soc. Astron. Italiana*, **51**, 623.

Rodono, M., 1981. *Photometric and Spectroscopic Binary Systems*, editors Carling & Kopal, 285.

Rossiger, M., 1982 *Sterne*, **58**, 147.

Rucinski, S.M., 1973. *Acta Astr.*, **23**, 79.

Rucinski, S.M., 1974. *Acta Astr.*, **24**, 119.

Rucinski, S.M., 1985. *Interacting Binary Stars*, editors Pringle & Wade, 85.

Rucinski, S.M., 1986. *IAU Symposium 118*, 159.

Shore, S.N., & Hall, D.S., 1980. *IAU Symposium 88*, 389.

Shu, F.H., 1980. *IAU Symposium 88*, 477.

Shu, F.H., Lubow, L.H., & Anderson, L., 1976. *Astrophys. J.*, **209**, 536.

Shu, F.H., Lubow, L.H., & Anderson, L., 1980 *Astrophys. J.*, **239**, 937.

Smith, D.H., Robertson, J.A., & Smith, R.C., 1980, *Mon. Not. R. astr. Soc.*, **190**, 177.

Smith, R.C., 1984. *Quarterly Journal of the Royal Astronomical Society*, **25**, 405.

Vilhu, O., 1981. *Astrophys. Space Sci.*, **78**, 401.

Vogt, S.S., 1981a. *Astrophys. J.* **247**, 975.

Vogt, S.S., 1981b. *Astrophys. J.*, **250**, 327.

Vogt, S.S., 1983. *IAU Colloquium 71*, 137.

Vogt, S.S. & Penrod, G.D., 1983a. *IAU Colloquium 71*, 379.

Vogt, S.S., & Penrod, G.D., 1983b. *Publs astr. Soc. Pacif.*, **95**, 565.

Chapter 2

Observations, Reduction and Analysis

2.1 Spectroscopy

2.1.1 Introduction

The spectroscopic observations presented here were made by the author using the 2.5-m Isaac Newton Telescope (INT) at the Observatorio del Roque de los Muchachos, La Palma, and by Dr.R.P.Edwin using the 1.0-m Jacobus Kapteyn Telescope (JKT) also at the La Palma observatory. The observations were made during four observing periods at La Palma, as indicated in Table 2.1.

The objectives of the spectroscopic observations were two-fold :-

(i) To provide high-dispersion spectra throughout the orbital periods, centred on the rich field of photospheric iron-lines at 4200 Å in order to obtain well defined radial velocity measurements.

(ii) To monitor the Hydrogen-α line profile at 6563 Å against orbital phase to search for line profile changes due to localised chromospheric emission, from starspots, or from energy transfer between the components.

Object	Peroid of Observation
TZ Boo	1987 April 8 - 9
BX And	1987 November 7 - 9
SS Ari	1987 November 8 - 11
SV Cam	1987 November 7 - 11
	1988 February 4 - 11 †
XY UMa	1988 February 5 - 11 †
AG Vir	1988 April 28 - May 2
VW Boo	1988 April 28 - 30
TY Boo	1988 April 29 - May 2

Table 2.1: Dates of Spectroscopic Observations

† — observations made with the JKT.

An observing plan for each observing period at the telescope was prepared using the computer program PREDICT (Bell 1987) in order to maximise light curve coverage, and ensure increased radial velocity observations near quadratures, where there is the best chance of acquiring velocity measurements for both components of a binary.

PREDICT uses the position of the Observatory and object being observed, coupled with the best ephemeris available, to provide information on the position and orbital phase of the binary against time, for each night of observation selected.

2.1.2 Observations

Spectroscopic observations on the INT were made using the Intermediate Dispersion Spectrograph (IDS) with a coated GEC Charged Couple Device (CCD) detector. This spectrograph is situated at the $f/15$ Cassegrain focus of the INT, and can be used with two folded, short Schmidt design cameras of focal lengths 235-mm (Camera 1), or 500-mm (Camera 2).

The 500-mm camera was used throughout, with the Jobin-Yvon 1200 grating, to produce high dispersion spectra at 16.7 Å mm^{-1}. This provided a useful range of approximately 200 Å across each spectrum.

Observations were controlled using the INT software environment ADAM (Astronomical Data Acquisition Monitor). The grating's position angle was switched between radial velocity and H-α spectra, to centre each spectrum on 4200 Å and 6563 Å respectively. For H-α observations, red flat-fields, and red comparison lamp and standard star observations, a GG495 filter was used to prevent contamination.

Before each observing run, the spectrograph was focused and adjusted for tilt and rotation using ADAM routines. The focus was also checked at the start of each night. (Jorden & Lupton 1984).

Bias frames and flat-field integrations at both wavelengths were recorded at the beginning and end of each night. For the flat-fields, a Tungsten lamp source was used, with a slit width of 250 μm and 140 μm, and integration times of 200 s and 2 s, for the 4200 Å and 6563 Å flat-fields respectively.

All stellar integrations were alternated with comparison-source exposures at the corresponding wavelength, using a Cu-Ar lamp for wavelength calibration purposes, and to monitor any flexure in the instrument. Calibration integrations were 100 s with a slit width of 200 μm.

Stellar integrations were typically 1000 s at both wavelengths, this representing only a small fraction of the orbital phase of the target objects, as indicated in Table 2.2. The slit width was 200 μm, corresponding to $\approx 1''$ on the sky.

Object	Typical Integration/s	$\approx$ % of Orbital Period
TZ Boo	1000	3.9
BX And	1000	1.9
SS Ari	1000	2.9
SV Cam	1000	2.0
XY Uma	1000	2.4
AG Vir	800	1.4
VW Boo	1000	3.4
TY Boo	1000	3.6

Table 2.2: Typical Integration Times for Spectroscopic Observations

At regular intervals during each night of observation, radial velocity standard stars were also observed at both wavelengths to ensure that there were no systematic departures from the standard system, and to provide comparison spectra for cross-correlation of the radial velocity data. Standard stars were chosen to match the spectral types of the binary systems observed. The standard stars observed with each target binary system are listed in Table 2.3. The slit width for standard star observations was also 200 μm ($\approx 1''$ on the sky), and exposure times ranged from 600 s to 10 s, dependent on the brightness of each standard.

Also at regular intervals during each night, the CCD data frames collected were transferred on to magnetic tape in the FITS (Flexible Image Transport System) file format (Wells, Greisen & Harten 1981).

Standard Star	Spectral Type	Radial Velocity / $\mathrm{km\,s^{-1}}$	Target binaries observed between standard observations
HD75935	G8 V	-18.9 $\pm$ 0.3	TZ Boo
HD140913	G0 V	-20.8 $\pm$ 0.4	TZ Boo
HD693	F6 V	+14.7 $\pm$ 0.2	SS Ari & BX And
HD32963	G2 V	-63.1 $\pm$ 0.4	SS Ari & SV Cam
HD36673	F0 Ib	+24.7 $\pm$ 0.2	BX And
HD84441	G1 IIab	+4.8 $\pm$ 0.1	SV Cam & XY UMa
HD12929	K2 IIIab	-14.3 $\pm$ 0.2	SV Cam & XY UMa
HD122693	F8 V	-6.3 $\pm$ 0.2	TZ Boo, VW Boo, TY Boo, & AG Vir
HD145001	G8 III	-9.5 $\pm$ 0.2	VW Boo & TY Boo
HD103095	G8 Vp	-99.1 $\pm$ 0.3	VW Boo & TY Boo
HD89449	F6 IV	+6.5 $\pm$ 0.5	AG Vir

Table 2.3: Radial Velocity Standard Stars Observed

The same observing routine was followed for the spectroscopic observations made using the JKT. These observations were taken during a commissioning run at the telescope to fit a CCD detector (pixel size 22 μm), similar to the INT detector, onto the telescope's Richardson & Brealey design spectrograph which had been built at St Andrews. The twin of this spectrograph is in use at St Andrews University Observatory, and the design has been described in detail elsewhere (Edwin 1989). The dispersion of the JKT spectra was marginally higher at 20.0 Å $\mathrm{mm^{-1}}$ and only observations centred on 4200 Å were obtained.

2.1.3 Reduction

Preliminary reductions of the spectroscopic data were made using the STARLINK software package FIGARO (Shortridge 1986) for bias subtraction, flat-fielding, sky background subtraction, and removal of cosmic ray events. The resulting data were converted into a one-dimensional form for processing with the spectroscopic image-processing package REDUCE (Hill, Fisher, & Poeckert 1982a). This was used to linearize, rectify, and finally log-linearize the spectra, so that, in the case of the 4200 Å observations, the spectra were in a form suitable for cross-correlation analysis.

All the spectroscopic FITS data frames were read into the the University of St Andrews MicroVAX II computer using the FIGARO FITS routine, to create DST format files which were corrected for floating point notation.

The bias frames from an observing run (more than 40 frames) were averaged, to form a low readout noise bias frame for that run. This was then subtracted from all other data frames read from tape, to remove any electrical offset in the CCD detector. No significant night to night variations in the bias level were detected. (Jorden & Lupton 1984).

Next the flat-field data frames, at both wavelengths, were reduced, to form average flat-fields at 4200 Å and 6563 Å for each night of observation. Before these flat-fields could be used to divide out any non-uniform detector response, any spectral response due to the flat-field lamp was removed. (Shortridge 1986).

This was achieved by fitting a smooth, low order, polynomial to the spectral response from the lamp, obtained by collapsing the flat-field in y, and then multiplying by the fitted value, before dividing by the flat-field to normalize the pixel values.

All reference arc and stellar observations were divided by the appropriate flat-field.

Having been bias-subtracted and flat-fielded, the reference Cu-Ar data frames were simply summed over a given y range, to produce standard two-dimensional arc spectra. This y range was typically pixel row 150 to 180, chosen to correspond with the detector area across which the stellar spectra fell.

Before stellar data frames were reduced to the two-dimensional form, each frame was displayed, and cosmic ray events removed using the FIGARO CLEAN routine. Each stellar spectrum was then summed over its y range (typically y=160 to 180), and the sky background subtracted. The sky background was obtained by summing an equal y range of sky above each stellar spectrum (typically y=260 to 280).

The two-dimensional arc and stellar spectra were converted from DST file format to FITS file format, to allow final reduction of the stellar spectra to be made using the software package REDUCE.

This conversion was achieved using the STARLINK SPICA package. This was used to first convert the DST files into a one-dimensional memory file, which could then be converted into FITS files using another routine called SPICON (Hill 1983).

SPICON requires the pixel size of the detector (22 μm for the CCD), and a central feature in each arc spectrum, which is manually identified. For the 4200 Å spectra, the 4237.220 Å feature was used for this identification, and the 6604.853 Å feature used for the 6563 Å arc spectra. Using the arc reference point identified for each arc/stellar data pair, SPICON outputs pixel calibrated "S" and "F" FITS files containing the stellar and arc data respectively.

REDUCE was used to measure each arc spectrum, and thus linearize each corresponding stellar spectrum in wavelength.

Initially a "Standard Plate" was constructed for the Cu-Ar spectrum at each wavelength region (Aitken 1935). The Standard Plate predicts the position of lines in the spectrum, based on known spectrograph constants, such as grating equations and Hartmann constants. The Standard Plates for 4200 Å and 6563 Å were created using the program STDPLATE (Hill & Fisher 1982), which generates these coefficients given manual identification of a relatively small number of widely-distributed features across a representative arc spectrum. STDPLATE measures line positions by fitting parabolae to the peak of each profile.

REDUCE measures each arc spectrum and uses it to wavelength linearize the accompanying stellar spectrum. Positions of selected arc lines are automatically measured, and compared with predicted positions from the Standard Plate. Figures 2.1

and 2.2 show a typical 4200 Å and 6563 Å Cu-Ar comparison arc spectrum respectively, with the lines selected for measurement shown. The residuals of the measured compared with the predicted line positions are fitted with a polynomial which serves as a correction to the Standard Plate. Any mis-identified lines can be removed by preselecting a rejection limit. Using this technique it was found that the RMS error in each measured arc was typically less than 1 μm.

At this stage, the Earth Correction for each observation, due to the motion of the observer, was also calculated and corrected for. Hence final radial velocities from the 4200 Å spectra are "true" velocities in the heliocentric system.

The stellar spectra thus linearized are output as REDUCE "W-files". A typical "W-file" at both 4200 Å and 6563 Å is shown in Figures 2.3 and 2.4.

Finally the 4200 Å radial velocity stellar spectra were rectified and log-linearized using REDUCE, producing "R-files" and "U-files" respectively.

For rectification, a fit was made to each stellar continuum by manually selecting a number of small wavelength ranges across each spectrum. For each range, the local stellar continuum is calculated, and a fit through these points made using the interpolation routine INTEP (Hill 1982c). This routine has the advantage of drawing smooth, stable curves through the points, rather than the usual oscillating curves of a typical polynomial fit. This continuum can than be divided from the stellar spectrum to produce rectified data.

The 6563 Å stellar spectra were also rectified using the above technique to produce "R-files" for final analysis.

2.1.4 Analysis

2.1.4.1 6563 Å *H-α* Spectra

The *H-α* spectra in rectified R-file format were examined using the the stack plotting routine TSTACK (Hill 1986).

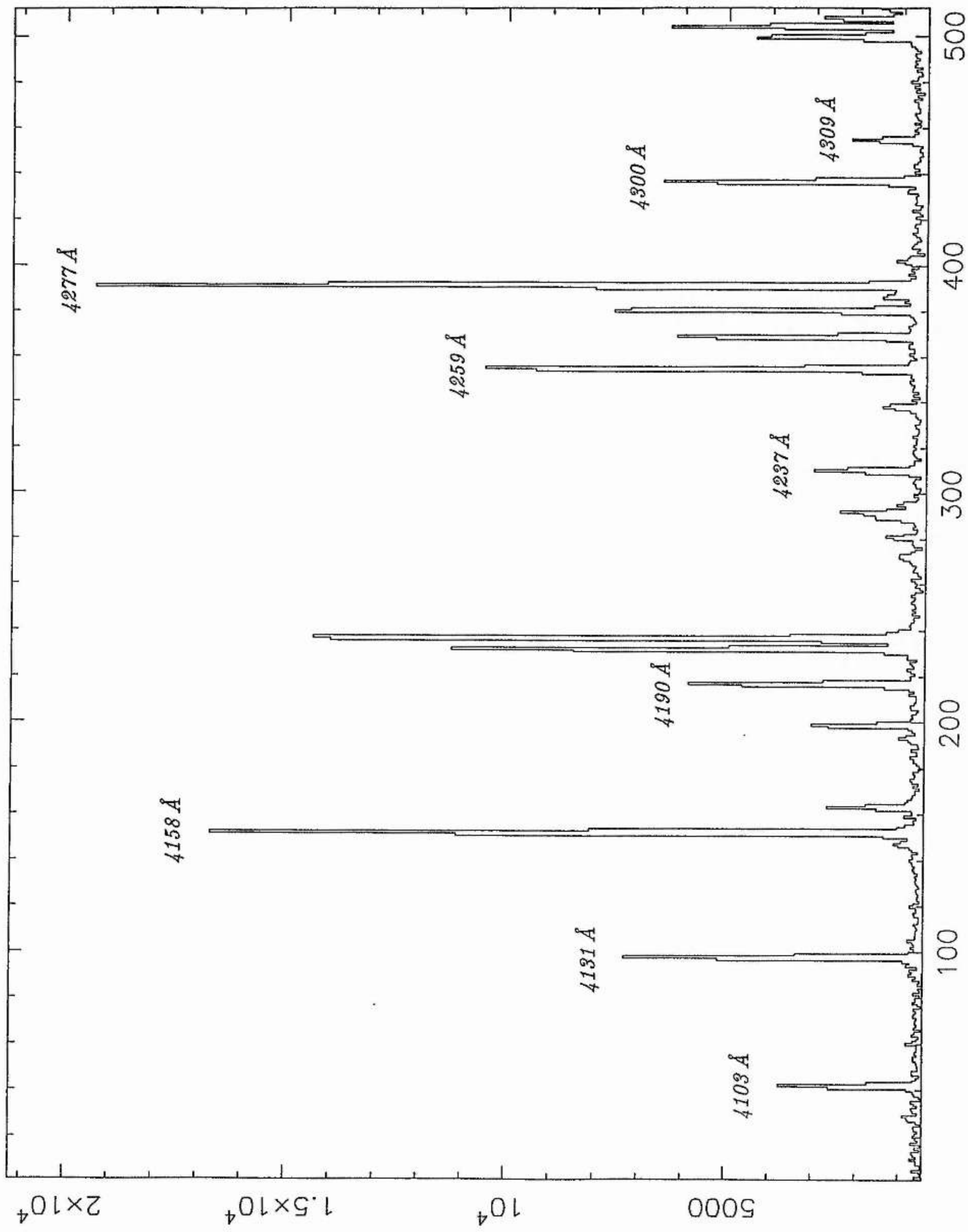

Figure 2.1: Cu-Ar Comparison Spectrum at 4200 Å. The identified lines were used for automatic measuring by REDUCE.

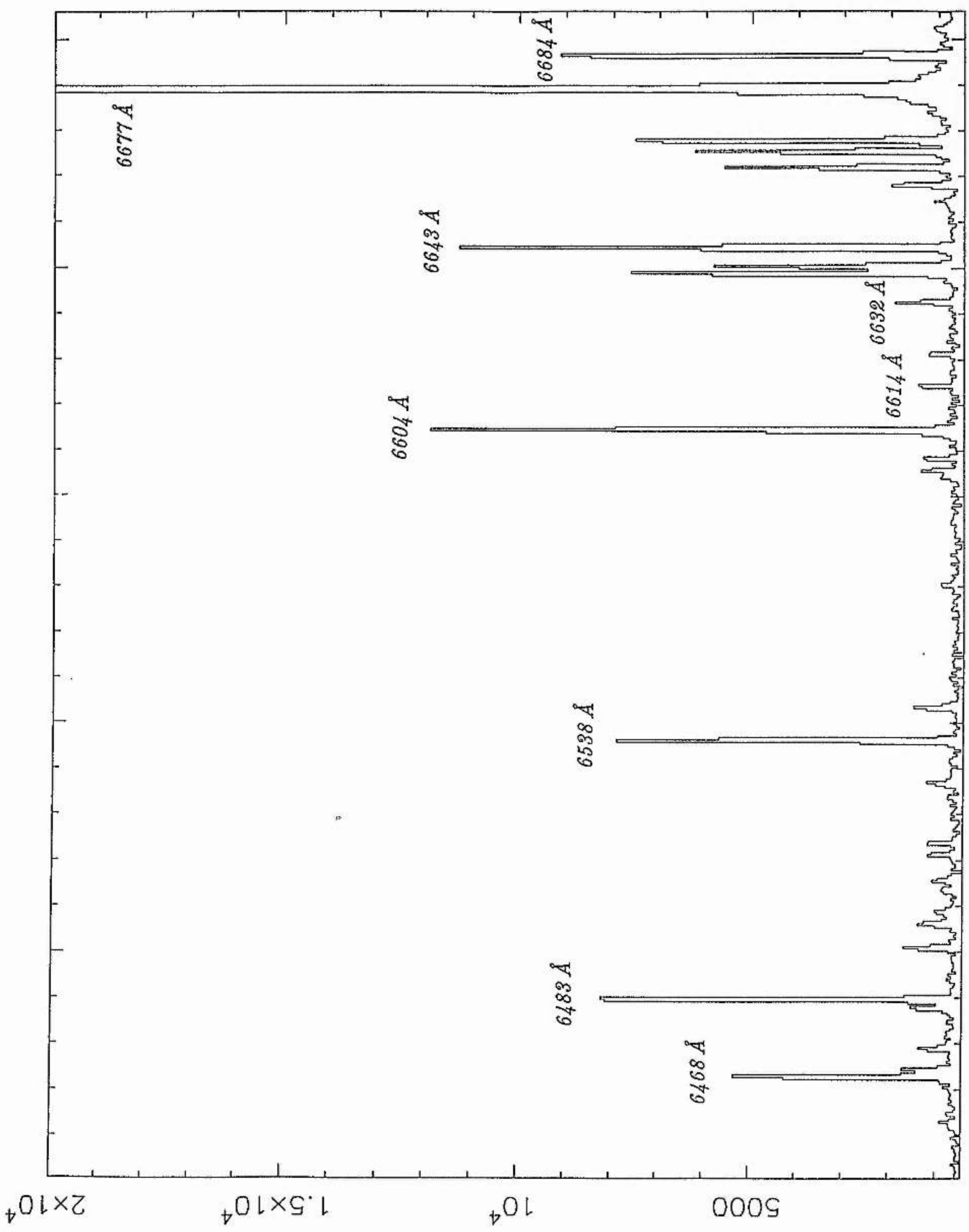

Figure 2.2: Cu-Ar Comparison Spectrum at 6563 Å. The identified lines were used for automatic measuring by REDUCE.

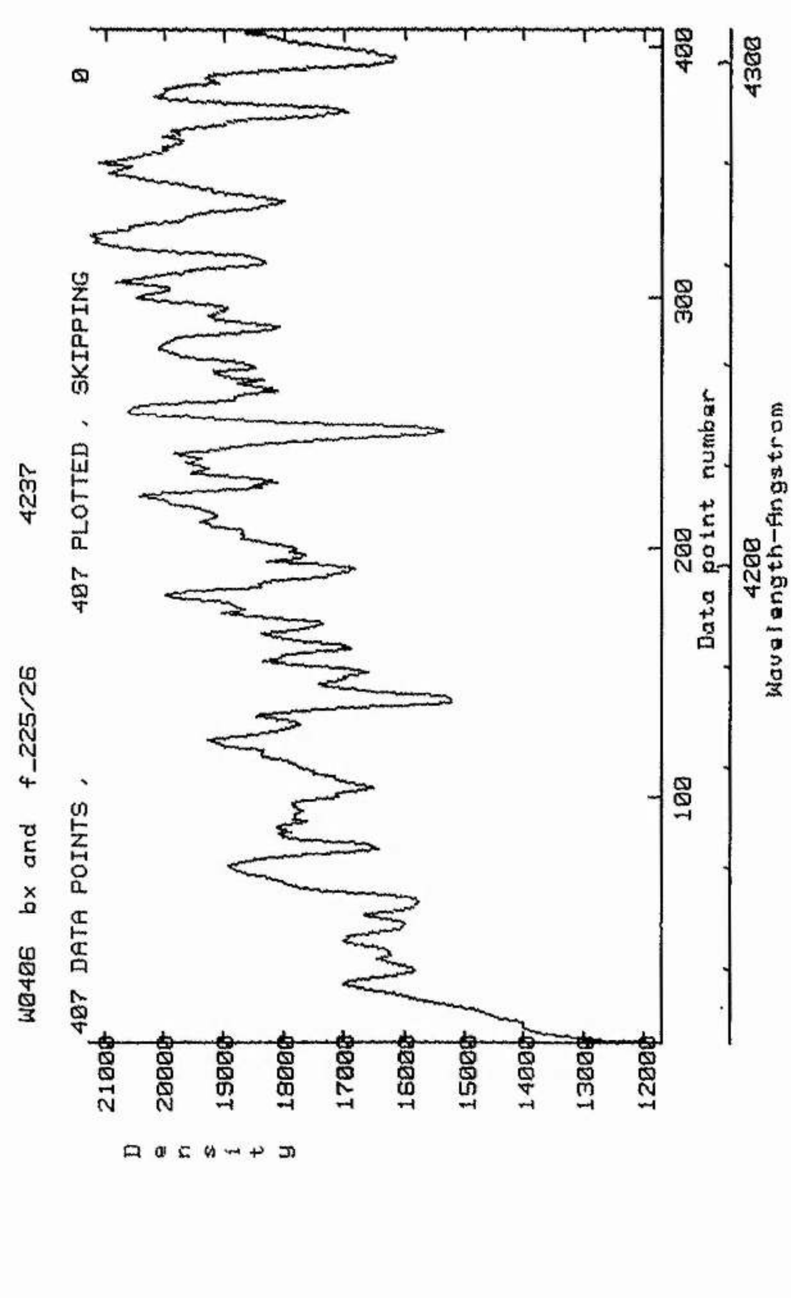

Figure 2.3: A typical 4200 Å stellar spectrum. (A W-file of BX And).

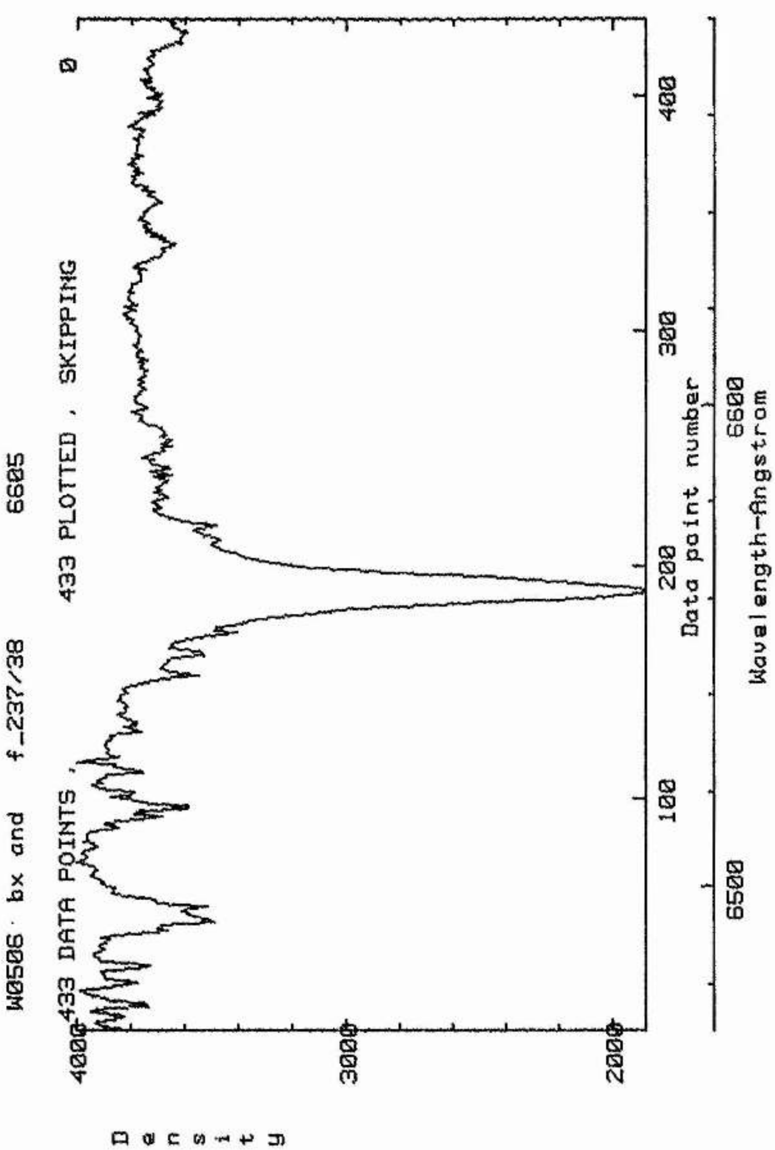

Figure 2.4: A typical 6563 Å stellar spectrum. (A W-file of BX And).

TSTACK allows single or multiple spectra to be plotted, and also enables simple arithmetic functions to be performed. The specific wavelength range around the *H-α* profile was plotted to enable detailed examination of each line profile, both with and without smoothing. The spectra of each binary, taken throughout the orbital phase of the system, were also shifted to a common zero velocity, and then a "template" spectrum of the binary, taken at either $0^{p}\!.0$ or $0^{p}\!.5$ when only one component is visible, was subtracted from the other spectra of that system. However, for the reasons outlined in Section 1.5.3.2, neither these "residual" images, or the detailed profiles themselves revealed any "bump like" features attributable to starspots. Hence, the 6563 Å spectra briefly noted in Chapter 8 are simply presented by TSTACK plotted in orbital phase order without any smoothing.

2.1.4.2 4200 Å Radial Velocity Spectra

Relative radial velocities from the log-linearized stellar spectra (U-files) were obtained using cross-correlation techniques in the program VCROSS (Hill 1982b).

VCROSS calculates the Fourier transform of a known comparison star spectrum, and multiplies it with the conjugate Fourier transform of the programme star spectrum. The inverse Fourier transform of this product, suitable normalized, yields the desired cross-correlation function (CCF), whose peak corresponds to the relative radial velocity between the comparison and programme stars. VCROSS applies the Fast Fourier Transform (FFT) techniques of Cooley and Tukey (1965) to the digitised stellar spectra obtained from REDUCE, and uses the subroutine FOURT (Brenner 1970) to obtain the necessary FFTs.

All stellar radial velocity determinations presented here were carried out using VCROSS. The CCFs for each binary were optimised to produce the sharpest and best defined peaks in the CCFs in two ways.

(i) Windows across the useful range of the spectra, defining the spectral regions to be used for cross-correlation, were set up to omit any 'gross' spectral features which would dominate the CCFs, producing wide central peaks. In practise this meant omitting the broad *Ca-I* feature at 4226 Å.

(ii) Each binary was cross-correlated against the various standard stars, of similar spectral type, observed during observations of the binary (see table 2.3), and the standard which produced the best defined peaks in the CCFs was used for the velocity measurements. The standards thus used for cross-correlation with each binary are listed in Table 2.4.

Object	Standard used for Cross-Correlation
TZ Boo	HD140913
BX And	HD36673
SS Ari	HD693
SV Cam	HD84441
XY UMa	HD84441
AG Vir	HD89449
VW Boo	HD145001
TY Boo	HD122693

Table 2.4: Radial Velocity Standards used for Cross-Correlation with Binaries

The resultant CCFs took one of two forms :-

(i) If the contribution of the secondary component to the spectrum of the binary is weak, either because there is a large magnitude difference between the components, or because the Doppler shift between components is not large enough to be noticeable (for example, around primary and secondary minima), then only a single peak due to the primary component will appear in the CCF, as illustrated in Figure 2.5.

(ii) If the contribution from the secondary is noticeable, for example when the Doppler shift between components is large (around first and second quadratures), then a double peak should be evident in the CCF, as illustrated in Figure 2.6.

The position of the peak/s in each CCF were measured within VCROSS by fitting a single-Gaussian profile when only a single peak was visible, and a double-

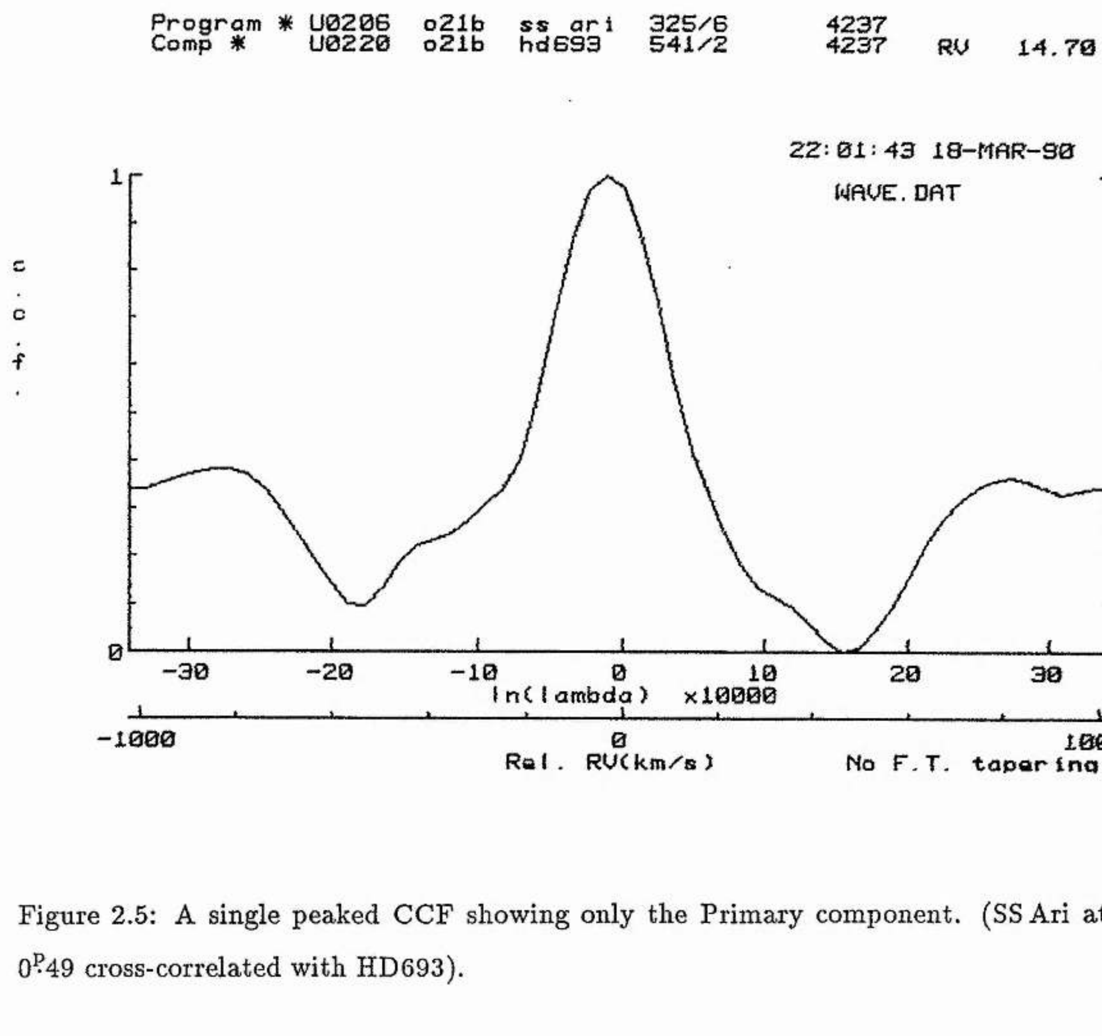

Figure 2.5: A single peaked CCF showing only the Primary component. (SS Ari at $0\overset{\mathrm{P}}{.}49$ cross-correlated with HD693).

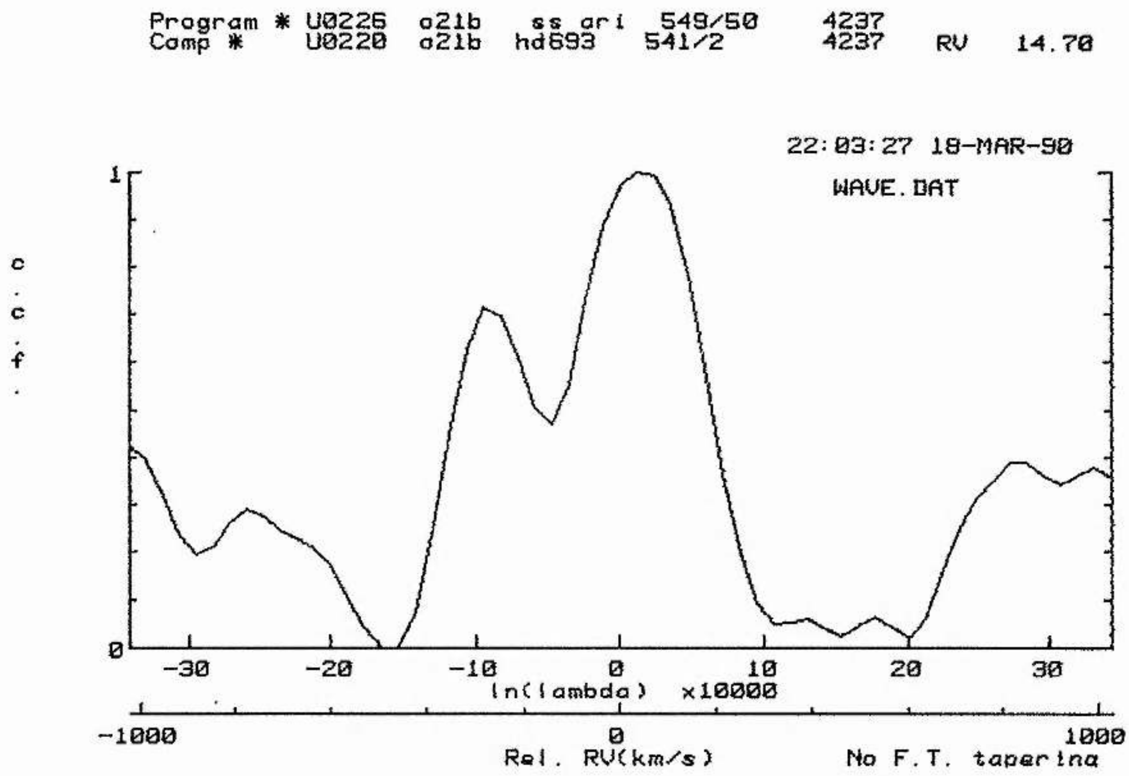

Figure 2.6: A double peaked CCF showing Primary and Secondary components. (SS Ari at $0^{P}.26$ cross-correlated with HD693).

Gaussian profile when twin peaks were evident. As the program is given the known radial velocity of the standard star used for the cross-correlation of each binary, and the stellar spectra had been reduced to the heliocentric system, then the velocities measured from the positions of the CCF peaks represent the true radial velocities of the binary components.

Finally, as a check that observations were compatible with the standard system, and that no hour-angle dependences, or other unforseen errors, were present during observations, the standard star spectra were cross-correlated against each other.

All the standard star spectra recorded whilst observing a given binary system were cross-correlated against each other, and a single-Gaussian profile fitted to the resultant single, sharp peaked CCFs. Since the velocities of the standard stars are known, the expected CCF velocity peak, due to the cross-correlation of any two standard star spectra could be calculated. The residual between the measured and calculated velocity peak for each cross-correlation was thus found (an O-C), and the mean residual and standard deviation for the set of standard star spectra recorded whilst observing each binary was calculated. These mean residuals and their standard deviations are listed in Table 2.5.

The standard star residuals indicate that the observations show no systematic deviations from the standard system outwith the intrinsic observational errors.

Having obtained stellar radial velocities from VCROSS, the data for each binary was plotted against orbital phase (calculated from the best ephemerides available), to yield radial velocity curves for each binary component.

Each radial velocity curve was fitted with a sine wave, using the least squares analysis program PULSAR (Skillen 1985). These sine wave fits enable the radial velocity semi-amplitudes for the primary and secondary components (K_1 and K_2 respectively) and the systemic velocity (V_0) for each binary to be found, and thus the mass functions and projected semi-major axes of the orbits, with their standard errors, can be derived.

The sine waves were fitted to the radial velocity curves on the assumption of circular orbits, given that all the systems presented here show no indications of orbital eccentricity either in the radial velocity data itself, or in the photoelectric data data. Furthermore, there is theoretical support that such contact and near-contact systems

Object	Standard Star Residual/ km s^{-1}
TZ Boo	-0.52 ± 5.03
BX And	-0.83 ± 4.14
SS Ari	-0.48 ± 6.80
SV Cam	-0.08 ± 6.80
	+0.54 ± 3.97 †
XY UMa	+0.54 ± 3.97 †
AG Vir	-1.70 ± 7.00
VW Boo	-0.76 ± 8.80
TY Boo	-0.76 ± 8.80

Table 2.5: Mean Residuals and Standard Deviations from Cross-Correlation of Standard Star observed with each Binary System

† — residuals for those observations made with the JKT.

are almost certain to have circular orbits, since the strong tidal forces present in such systems would act quickly to dampen any orbital eccentricity.

2.2 Optical Photometry

2.2.1 Introduction

The systems observed spectroscopically in this work have all had at least one photoelectric light-curve previously published. Ideally we would have liked to have obtained new photoelectric photometry on all these systems, to analyse with our spectroscopic mass ratios. This would also have enabled comparisons to be made with previously published data.

Of the contact binaries, three of the systems (SS Ari, TY Boo, and VW Boo) were too faint to be observed from St. Andrews University Observatory, so previously published photoelectric data have been re-analysed here, using the now known mass ratios.

However, new photoelectric photometry in the V-band was obtained by the author and Dr.S.A.Bell for BX And and AG Vir, using the St. Andrews Twin Photometric Telescope.

2.2.2 The Twin Photometric Telescope and Data Reduction

The Twin Photometric Telescope (TPT) utilizes two 40 cm, $f/15$, Ritchey Chretien reflecting telescopes mounted on a single fork, to obtain single-band, simultaneous, two-star photometry.

The advantage of simultaneous two-star photometry is illustrated is Figure 2.7. This Figure shows one night's observations of the binary system TT Aurigae, going through primary minimum, made using the TPT (Bell & Hilditch 1984). The variable and comparison star counts from each photometer show the effects of thin mist towards the end of the night, which would have stopped single star photometry. However, the simultaneous variable-comparison ratio clearly shows that the two-star photometric system remains unaffected.

The TPT allows one telescope to be offset by up to five degrees with respect to the second fixed telescope, enabling the programme binary, and a nearby comparison star to be observed simultaneously. The photometers employed are a matched pair of

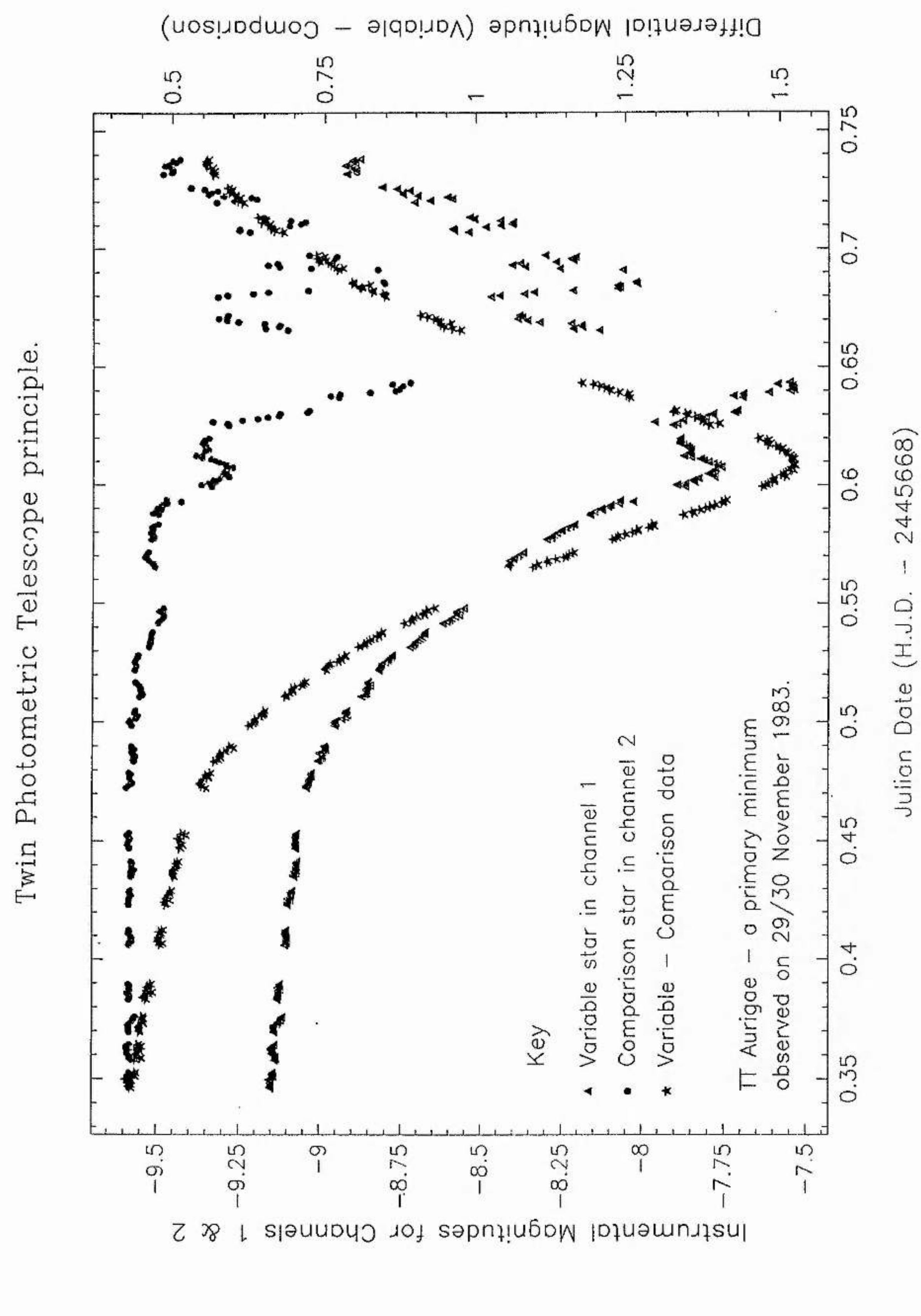

Figure 2.7: Observations of TT Aurigae illustrating the TPT principle

S-20 response EMI 9863A/350 photomultipliers, driven by a single EHT power supply, and housed in thermoelectrically controlled cold boxes. No significant relative drift between the photometer zero-points (in excess of $0^{m}_{\cdot}003$) has yet been recorded during an observing season.

The observing technique, data acquisition, and reduction systems used with the TPT, and outlined here, have been described in detail elsewhere (Bell 1987).

Data acquisition is controlled by a BBC microcomputer employing a FORTH ROM, and using an acquisition program written at St. Andrews by Mr. J.A. Stapleton. This program allows the observer to record the four types of observations required for the simultaneous monitoring of a variable and comparison star in one of four 'modes' labelled 0,1,2, and 3. The observer can define the type of observation recorded in each mode. Table 2.6 shows the mode definitions used for the observations presented here.

Mode	Type of Observation
0	Sky background measurements in both telescopes.
1	Comparison star measurements in both telescopes (to give zero-point differences between the two channels).
2	Comparison star measurements in Reference telescope, and check star measurements in the Offset telescope (to monitor the stability of the comparison star).
3	Comparison star measurements in Reference telescope, and variable star measurements in the Offset telescope.

Table 2.6: Definition of Data Acquisition Modes used for TPT Observations

The data is written in ASCII format on to floppy disk, allowing simple file transfer to be made to the St. Andrews' MicroVAXII computer. Each observation record contains the observation label, mode, filter used, end time of integration (in seconds since the previous midnight), the truncated Julian Date at the start of observations, the integration time, and the counts from each photometer.

TPT data were reduced using two programs, SIMPHOT and SIMPLOT, written by Dr. S.A. Bell, designed specifically to reduce TPT format data. SIMPHOT reads and reduces TPT data transferred from floppy disc, and outputs files in a format suitable for the plotting and data manipulation routine, SIMPLOT. This self-contained reduction system enables a simple flow of data through the reduction stages, allowing a night's data to be reduced straight from the telescope within a matter of hours.

To reduce the TPT data, it is run through SIMPHOT twice. Each run of SIMPHOT reads in the data, corrects the counts for dead-time effects, performs sky background subtraction (described below), corrects for extinction in both channels, and outputs the differential magnitudes for the modes of observations made, (ie. variable minus comparison (V-C), check minus comparison (K-C), and comparison (channel 1) minus comparison (channel 2) (C_1-C_2) observations) against time, orbital phase, and airmass.

SIMPHOT plots the sky background measurements against time for both channels, and offers the choice of two fits for the modelled sky background subtraction :-

(i) L2FRES (Powell 1967) fits a least-squares cubic-spline to the data points.

(ii) INTEP (Hill 1982c) fits an hermite-polynomial.

The user can then select the most plausible fit (L2FRES or INTEP) for the sky background subtraction.

The first run of the raw TPT data through SIMPHOT allows the extinction and zero-point difference between channels to be evaluated. These are both initially set to zero, and the reduced output plotted using SIMPLOT (described below). The extinction is evaluated by determining the slope of the comparison magnitude against airmass plot, and the zero-point difference found from the mean of the (C_1-C_2) observations.

The raw data can then be finally reduced by re-running through SIMPHOT, using the figures for the extinction and zero-point difference thus evaluated, or by adopting standard extinction values for the site.

The SIMPHOT output files are plotted using SIMPLOT, which allows either the differential magnitudes, or the individual channel magnitudes to be plotted against time, phase, or airmass. It allows 'windowing' on areas of interest, and individual or group removal of points. Data plots can be fitted with splines or polynomials up to the ninth order (eg. for extinction and zero-point evaluations). Also time of minimum determinations for the final differential magnitude (V-C) data can be calculated within SIMPLOT, employing the method of Kwee and van Woerden (1956).

2.2.3 BX And - Observations and Analysis

Photoelectric photometry of BX And was obtained by the author and Dr. S.A. Bell using the TPT during 1985 November, 1986 September to October, and 1988 October to November.

The filter used for all these observations was comparable to the Johnson V-filter, and integration times were fixed at 60 s. A $27''$ aperture was employed to exclude the 11^{th} magnitude visual companion of BX And which lies some $20''$ away at a position angle of 59° (Hall & Weedman 1971). Frequent monitoring of the position of BX And in the photometer diaphragm ensured that light from the visual companion did not contaminate the BX And data.

The comparison star used in all of these observations was BD+39° 476, and the check star used was BD+39° 484. One, or both, of these stars have been used in previous studies of BX And by Svolopoulous (1957), Castelaz (1979), Rovithis & Rovithis-Livaniou (1984), and Samec *et al.* (1989). No variability in either the comparison or check star has been noted in these studies, and the differential magnitudes, in the sense of check minus comparison, calculated from our observations were stable to better than $0^{\rm m}\!\!.01$. The typical error in the differential magnitudes for our light curves of BX And are $\approx 0^{\rm m}\!\!.006$.

The first attempts at solving the light curves of BX And were made using the light curve synthesis program WUMA5 which implements the method of Rucinski (1976a,b,c). The analysis procedure has been described in detail elsewhere (Bell & Malcolm 1987), and brief details of the routine are given in the Appendix to this Chapter. The WUMA5 code was used whilst awaiting a working version of LIGHT2.

The main light curve analysis program used in this work, for BX And and indeed all the other photoelectric data, was LIGHT2 (Hill 1989). LIGHT2 is an expanded version of LIGHT (Hill 1979) which incorporates analytical techniques for contact as well as detached systems, as well as allowing cool or hot spot regions to be included in the model. Again the analysis procedure has been described in detail elsewhere (Hilditch & King 1988), and brief details of the routine are given in the Appendix to this Chapter.

2.2.4 AG Vir - Observations and Analysis

Photoelectric photometry of AG Vir was obtained by the author and Dr. S.A. Bell using the TPT on 1989 March 7/8, 10/11, and 15/16.

The filter used for all these observations was comparable to the Johnson V-filter, and integration times were fixed at 60 s, with a $40''$ diaphragm employed throughout the observing run.

The comparison and check stars used in these observations were BD+13° 2485, and BD+13° 2482, respectively. The comparison star has been used extensively in the majority of studies of AG Vir, but for convenience of observing with the TPT, BD+13° 2482 was used as the check star in place of BD+13° 2405 which had been employed in previous studies. No variability in the comparison had been found in previous studies, and the differential magnitudes, in the sense of check minus comparison, calculated for this study were stable to better than $0^{m}_{\cdot}01$. The typical error in the differential magnitudes for our light curve of AG Vir is $\approx 0^{m}_{\cdot}006$.

As for BX And and the other systems presented here, analysis of the AG Vir light curve was attempted using the light curve synthesis program LIGHT2 (Section 2.2.3 and 2.5).

2.3 Infra-Red Photometry

2.3.1 Introduction

Two of the systems presented here (BX And and SS Ari) were also observed in the infra-red by Dr.R.W.Hilditch.

Visual and infra-red photoelectric observations were made simultaneously in either the V and K bands, or the B and J bands, with the intention of forming the colours V-K and B-J (see section 1.5.3.3).

Unfortunately the VISPHOT photometer used for the visual band photometry, and on its commissioning run during our observations, was found to have a temporary fault. A misalignment of the primary mirror image on the photomultiplier's Lyot stop caused zero-point shifts in the visual data. Comparison star observations were found not to follow these drifts with sufficient accuracy to allow a reduction to the standard system (Adams 1988).

Although it was not possible to reduce the visual photometry to data coherent enough to warrant analysis, the infra-red photometric data could be reduced independently, to produce infra-red light curves for the two binaries.

2.3.2 Observations

The simultaneous infrared and optical photometry was obtained during 1987 November 17-21 using the United Kingdom Infrared Telescope (UKIRT) with the UKT6 and VISPHOT photometers respectively to make simultaneous J B and K V filter observations. Integration times for both systems were fixed at 80 s, and a diaphragm of 19.6″ employed throughout the observing run. Several infrared and optical standard stars were observed during each night to allow transformation to the standard system.

BX And was observed during November 17-19, employing the comparison star BD+39° 484 for these measurements. SS Ari was observed during November 19-21, and the comparison star BD+23° 277 employed.

Since the UKIRT photometer defines the standard system, the infrared observations were reduced as outlined in Section 2.3.3, with standard star measurements allowing zero-point determinations to be made for transformation to the standard system. These observations showed a scatter of approximately $0^{m}.02$ about the standard system. There was no evidence for variability in the comparison stars within this limit, and the typical scatter in the differential magnitudes of the infrared light curves of BX And and SS Ari was $\approx 0^{m}.03$.

2.3.3 Reduction and Analysis

The infra-red photoelectric data were reduced to a differential magnitude, in the sense of variable minus comparison, by fitting a least-squares polynomial to the comparison observations for each night. The comparison star fits were produced using the computer routine SIMPLOT (see section 2.2.2).

The data were manipulated using a simple FORTRAN routine written by the author. This routine reads in data from the "Observation Summary" output files produced at the telescope, performs the required reduction for the object of interest, and outputs data in a format suitable for the SIMPLOT plotting and manipulation program.

For each J/B or K/V observation pair, the telescope's output file records the object name, the aperture and filters used, start time (in UT), airmass, integration time, and the counts from the visual and infra-red photometer, along with their corresponding instrumental magnitudes (in the sense of $-2.5\,log_{10}(counts)$), and their associated errors.

Since the UKIRT photometers define the standard system, the instrumental magnitudes logged at the telescope were simply corrected for extinction. The values used for infra-red atmospheric extinction at the Mauna Kea site were the median values determined by Krisciunas *et al.* (1987) ; namely 0.1 and 0.07 magnitudes/airmass for J and K respectively.

Standard star observations showed a scatter of $\pm 0^{m}.02$ about the standard system, and allowed zero-points for each night to be found. The scatter compares favourably with the instrument performance measured by previous observers (Williams 1988).

The comparison star data were reduced, using these values of extinction and zero-points, following the equation :-

$$M_{std} = \text{instrumental magnitude} + \text{zero point} - (\text{extinction} \times \text{airmass})$$

and a least-squares polynomial fitted to the comparison star data for each night using SIMPLOT.

The BX And and SS Ari data were finally reduced using the same reduction equation to form the binary's magnitude, interpolating the comparison star magnitude to the time of binary observation, and forming the resultant differential magnitude (variable minus comparison).

For the analysis of the infrared photometry, times of minimum for the BX And and SS Ari were calculated, as for the optical data, within the SIMPLOT program (Section 2.2.2). Similarly the light curve analysis employed the synthesis program LIGHT2 (Section 2.2.3 and 2.5).

2.4 References

Adams, D., 1988. *Private communication*, Draft copy of VISPHOT Users Handbook.

Aitken, R.G., 1935. *The Binary Stars*, McGraw-Hill, New York.

Bell, S.A., 1987. *PhD thesis*, University of St. Andrews.

Bell, S.A., & Hilditch, R.W., 1984. *Mon. Not. R. astr. Soc.*, **211**, 229.

Bell, S.A., & Malcolm, G.J., 1987. *Mon. Not. R. astr. Soc.*, **226**, 899.

Bevington, P.R., 1969. *Data Reduction and Error Analysis for the Physical Sciences*, McGraw-Hill, New York.

Brenner, N.M., 1970. *"Fourt", Cosmic/Share*, University of Georgia.

Castelaz, M., 1979. *Inf. Bull. Var. Stars*, No. 1554.

Cooley, J.W., & Tukey, J.W., 1965. *Mathematical Computing*, **19**, 297.

Edwin, R.P., 1989. *The Observatory*, **1092**, 173.

Hilditch, R.W., & King, D.J., 1988. *Mon. Not. R. astr. Soc.*, **231**, 397.

Hall, D., & Weedman, S.L., 1971. *Publs astr. Soc. Pacif.*, **83**, 69.

Hill, G., 1979. *Publs Dom. astrophys. Obs.*, **15**, 297.

Hill, G., 1982b. *Publs Dom. astrophys. Obs.*, **16**, 67.

Hill, G., 1982c. *Publs Dom. astrophys. Obs.*, **16**, 59.

Hill, G., 1983. *Private Communication.*

Hill, G., 1986. *Private Communication.*

Hill, G., 1987. *Private Communication.*

Hill, G., & Fisher, W.A., 1982. *Publs Dom. astrophys. Obs.*, **16**, 159.

Hill, G., Fisher, W.A., & Poeckert, R., 1982a. *Publs Dom. astrophys. Obs.*, **16**, 27.

Jorden, P., & Lupton, W., 1984. *Spectroscopy with the CCD on the INT - A User Guide*, Royal Greenwich Observatory.

Krisciunas, K., Sinton, W., Tholen, D., Tokunaga, A., Golisch, W., Griep, D., Kaminski, C., Impey, C., & Christian, C., 1987. *Publs astr. Soc. Pacif.*, **99**, 887.

Kwee, K.K., & van Woerden, H., 1956. *Bull. Astr. Inst. Neth.*, **12**, 327.

Mochnacki, S.W., 1984. *Astrophys. J. Suppl.*, **55**, 551.

Powell, M.J.D., 1967. *Report No. HL67/5309*, AERE Harwell.

Rovithis, P., & Rovithis-Livaniou, H., 1984. *Astrophys. Space Sci.*, **105**, 171.

Rucinski, S.M., 1973a. *Acta Astr.*, **23**, 79.

Rucinski, S.M., 1973b. *Acta Astr.*, **24**, 119.

Rucinski, S.M., 1976a. *Publs astr. Soc. Pacif.*, **88**, 224.

Rucinski, S.M., 1976b. *Acta Astr.*, **26**, 227.

Rucinski, S.M., 1976c. *Publs astr. Soc. Pacif.*, **88**, 777.

Samec, R.G., Fuller, R.E., & Kaitchuck, R.H., 1989. *Astr. J.*, **97**, 1159.

Shortridge, K., 1986. *Figaro Users Manual*, Starlink Project.

Skillen, W.J., 1985. *PhD Thesis*, University of St. Andrews.

Smart, W.M., 1977. *A Textbook on Spherical Astronomy*, Cambridge University Press.

Svolopoulous, S.N., 1957. *Astr. J.*, **62**, 330.

Wells, D.C., Greisen, E.W., & Harten, R.H., 1981. *Astrophys. J. Suppl.*, 44, 363.

Williams, P.W., 1988. *Private communication.*

2.5 Appendix - Light Curve Analysis Programs

Two separate light curve synthesis programs are used in the analysis presented here (see Section 2.2.3), the bulk of the modelling being done using LIGHT2, an expanded version of LIGHT, to include hot spots in the basic contact binary model. Only a brief description is provided here as both programs have been described in detail elsewhere.

The light curve generation code for "over-contact" systems which forms the basis of the WUMA5 program was written and discussed by Rucinski (1973a,b and 1976a,b,c).

The "surface" of a common envelope of an over-contact system may be assumed to follow an equipotential surface lying between the inner and outer critical surfaces. Rucinski (1973a) defined a "fill-out factor" (f), which effectively measures the degree of contact in a system, such that f=1 when the envelope's surface is coincident with the inner critical surface (marginal contact), and f=0 for coincident with the outer critical surface (deep contact).

Using a given fill-out factor and mass ratio, a binary's common envelope "surface" can then be defined, and Rucinski's code generates a light curve on this basis, including the inclination of the orbit and the relative increase of the local temperature of the less massive component. WUMA5 allows five fluxes and limb-darkening coefficients to be specified for the desired central wavelength around the primary's (reference) temperature. The program then calculates the emergent flux from the visible portions of the common envelope at each orbital phase step, taking into account limb and gravity darkening. (The reflection effect is negligible for these systems when the temperature difference between components is small).

Solutions were made for fill-out, inclination and relative temperature difference, fixing the mass ratio (at the spectroscopically derived value) and the primary temperature. The component radii can then be calculated from the mass ratio and fill-out factor solution from the tabulations presented by Mochnacki (1984).

The majority of light curve analyses presented here were made using LIGHT2, an expanded version of LIGHT (Hill 1979).

LIGHT generates light curves for detached binary systems by employing Roche geometry, and using the radii, component temperatures, mass ratio and system inclination. It also treats heating and scattering effects in a realistic manner, and offers theoretical or observed limb-darkening coefficients, and black-body or model atmospheres for up to 90 wavelengths. The light curve is solved by means of CURFIT (Bevington 1969). (LIGHT can also treat eccentric orbits, the presence of a third body, and non-synchronous rotation if required).

LIGHT2 has been expanded to incorporate Rucinski's code, described above, so that contact systems can also be analysed. Further, the new program allows "starspots" to be added to the contact systems, with up to ten spots on each component (although only two spots may be included in the unknowns when solving a light curve). Each spot may be non-circular, of different temperature, and an absorption or emission region. Each spot is also subject to limb and gravity darkening. In total then, each spot may be defined by up to seventeen parameters if required, although the program's author does give a timely reminder that, given enough parameters, it is possible to fit anything.

A full description of the use of the program in the analysis of the systems presented here is given in the relevant Chapters. For most of the work, LIGHT2 was used in the Rucinski "over-contact" mode, with the mass ratio and primary component temperatures fixed, and solutions for the secondary temperature, fill-out and inclination sought. Some simple spot models were also investigated, mostly with a single circular spot in the system, defined simply by position, size by radius, and temperature.

Chapter 3

The Binary System TY Bootis

3.1 Introduction

The variability and W Ursae Majoris classification of TY Boo was discovered by Guthnick & Prager (1926), who derived a period of 0.31730 day.

A long-term visual study by Szafraniec (1953) determined a period of $0^{d}.317146$, and noted a possible cyclic period variation on the scale of 400 orbital cycles (127 days).

Carr (1972) published the first UBV photoelectric light curves of TY Boo, and found the period derived from his four times of primary minimum to be in agreement with Szafraniec's visual determination. Carr's light curve solution was of limited accuracy due to non-rectifiable distortions, but suggested that TY Boo was an A-type system consisting of two main-sequence (G3 and G7) components. Assuming a contact configuration, Carr's solution leads to a mass ratio of 0.88 (Kopal 1978), implying that TY Boo is an A-type binary with W-type characteristics.

Niarchos (1978) re-analysed Carr's data using frequency domain techniques, and suggested that TY Boo was a W-type with a very small mass ratio of 0.22.

Samec & Bookmyer (1987) published new BV photometry, and concluded that the system as a whole had undergone a slight reddening since Carr's observations (due at least in part to the different response curves of the two instruments used), but noted no apparent changes in the depths of the eclipse curves.

They derived a new ephemeris from the seven photoelectric times of minima available, but using 91 visual estimates, could not find evidence of the cyclic variation suggested by Szafraniec. They did conclude however that two period changes had occurred in a 19 year interval around 1945, but more recent photoelectric observations were insufficient to establish the nature of any current period variations in the system.

A light curve analysis of Samec &Bookmyer's data is, the author understands, in the process of being published.

Groisman *et al.* (1987) also report new VBI light curves for TY Boo, and Milone *et al.* (1987) report spectroscopic observations, but again the author understands that the analysis of these data is still to be published.

Here we present spectroscopic radial velocity data for TY Boo, and use the mass ratio thus derived to analyse the light curve data published by Samec & Bookmyer, and obtain accurate system elements.

3.2 Spectroscopy

Radial velocity spectra of TY Boo, centred on 4200 Å were obtained and reduced as detailed in Chapter 2.

Using the F8 radial velocity standard star HD122693 for cross-correlation, the radial velocity measurements listed in Table 3.1 were obtained. The corresponding orbital phases of these measurements were derived using the ephemeris in Section 3.3.

H.J.D.	Phase	V_1 $km\,s^{-1}$	(O-C) $km\,s^{-1}$	V_2 $km\,s^{-1}$	(O-C) $km\,s^{-1}$
2447281.42069	0.7690	−134	+3.1	+180	−3.9
2447281.43596	0.8171	−132	−1.9	+164	−4.3
2447281.56317	0.2182	+58	−4.5	−272	+1.2
2447281.57782	0.2644	+62	−3.2	−280	−0.1
2447281.59247	0.3106	+59	−0.5	−265	+2.3
2447281.67493	0.5706	−75	+1.0	——	——
2447281.70486	0.6650	−123	−1.7	+152	+5.5
2447281.71965	0.7116	−137	−3.5	+179	+4.0
2447281.73434	0.7579	−138	−0.5	+185	+0.5
2447282.48686	0.1307	+40	+4.5	−209	+1.4
2447282.58000	0.4244	+19	+5.2	−170	−6.4
2447283.68401	0.9054	−94	+2.0	+91	−0.1

Table 3.1: Radial Velocity data for TY Boo

The sine wave fits to the radial velocity data are shown in Figure 3.1. The resulting radial velocity semi-amplitudes for the primary and secondary components (K_1 and K_2 respectively), and the systemic velocity (V_0) are given in Table 3.2, along with the derived mass function, projected semi-major axes of the orbits, and their standard errors.

The values of V_{0_1} and V_{0_2} differ by 11.8 $km\,s^{-1}$ almost certainly due to under-sampling of the radial velocity curves. However, this difference does not significantly affect the determination of the mass ratio, or other parameters in Table 3.2.

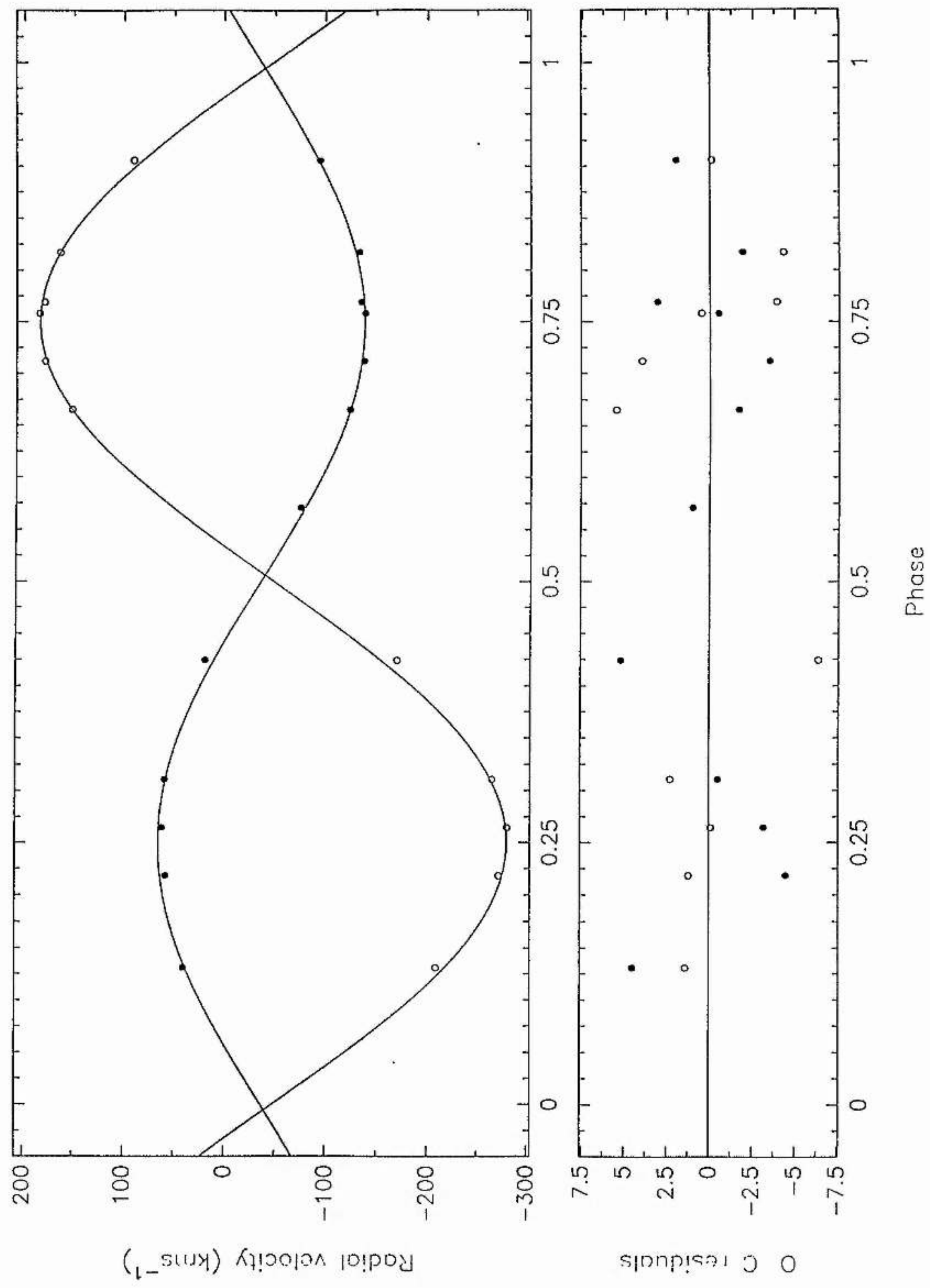

Figure 3.1: Radial Velocities of the Primary and Secondary Components of TY Boo (closed and open circles respectively), plotted together with their Orbital Solutions.

$K_1\,(\mathrm{km\,s^{-1}})$	=	101.4 ± 1.2
$K_2\,(\mathrm{km\,s^{-1}})$	=	232.2 ± 2.4
$V_{0_1}\,(\mathrm{km\,s^{-1}})$	=	-36.0 ± 1.0
$V_{0_2}\,(\mathrm{km\,s^{-1}})$	=	-47.8 ± 2.1
$\sigma_1\,(\mathrm{km\,s^{-1}})$ †	=	3.2
$\sigma_2\,(\mathrm{km\,s^{-1}})$ †	=	3.6
$\mathrm{q}\ (\mathrm{m_2/m_1})$	=	0.437 ± 0.007
e	=	0 (adopted)
$\mathrm{a_1 \cdot \sin i\ (R_\odot)}$	=	0.635 ± 0.008
$\mathrm{a_2 \cdot \sin i\ (R_\odot)}$	=	1.455 ± 0.015
$\mathrm{a \cdot \sin i\ (R_\odot)}$	=	2.090 ± 0.017
$\mathrm{m_1 \cdot \sin^3 i\ (M_\odot)}$	=	0.851 ± 0.016
$\mathrm{m_2 \cdot \sin^3 i\ (M_\odot)}$	=	0.372 ± 0.007

Table 3.2: Orbital Elements for TY Boo

† — r.m.s. scatter of a single observation.

3.3 Ephemeris

The period study presented by Samec & Bookmyer (1987), comprised largely of visual data, indicated that two period changes had occurred in a 19 year interval, whilst the newer photoelectric data suggested that the system was now more stable.

The author has compiled published times of minimum for TY Boo, starting with the latter visual data used by Samec & Bookmyer (starting at approximately -35000 cycles), and including new visual and photoelectric estimates published since their study. These data are shown in Table 3.3.

Residuals to the data were calculated with respect to the photoelectric ephemeris determined by Samec & Bookmyer :-

$$\mathrm{HJD}\ 2446589.7906(\pm 4) + 0.3\dot{1}714964(\pm 3)E$$

These residuals, plotted in Figure 3.2, show the second of the two period changes noted by Samec & Bookmyer (at -35000 to -25000 cycles). The newer photoelectric data indicates that little overall period change is currently occurring. However the lack of photoelectric data, and the scatter in the visual data, make it impossible to determine whether these general trends are due to abrupt or continuous changes.

A least-squares analysis of the photoelectric data yields a period of 0.31714968 day, in good agreement with that of Samec & Bookmyer. The fit to the photoelectric data show in Figure 3.2 indicates the current stable nature of the system, although the photoelectric data does hint at a possible small scale sinusoidal or parabolic variation. Clearly more photoelectric observations are needed to determine the true nature of any such variations.

Given the current stability of the system's period, the photoelectric ephemeris derived by Samec & Bookmyer was used to determine all the orbital phases presented in this study.

Table 3.3: Times of minima for TY Boo.

H.J.D.	Cycle	Method	Reference
2435217.498	-35858	VIS	Szafraniec, 1956
2435240.478	-35785.5	VIS	Szafraniec, 1956
2435603.440	-34641	VIS	Szafraniec, 1957
2435903.469	-33695	VIS	Szafraniec, 1958
2435933.442	-33600.5	VIS	Szafraniec, 1958
2436074.408	-33156	VIS	Szafraniec, 1958
2436361.431	-32251	VIS	Szafraniec, 1959
2436727.410	-31097	VIS	Szafraniec, 1960
2436728.373	-31094	VIS	Szafraniec, 1960
2437015.380	-30189	VIS	Szafraniec, 1963
2437027.428	-30151	VIS	Szafraniec, 1963
2438882.428	-24302	VIS	Szafraniec, 1966
2438961.403	-24052	VIS	Szafraniec, 1966
2440367.7906	-19618.5	PE	Carr, 1972
2440367.9487	-19618	PE	Carr, 1972
2440368.7419	-19615.5	PE	Carr, 1972
2440368.9003	-19615	PE	Carr, 1972
2440369.6936	-19612.5	PE	Carr, 1972
2440369.8517	-19612	PE	Carr, 1972
2440370.8030	-19609	PE	Carr, 1972
2443360.400	-10182.5	VIS	Locher, 1977
2445102.368	-4690	PG	Braune *et al.*, 1983
2445120.4393	-4633	PE	Braune & Mundry, 1982
2445815.474	-2441.5	VIS	Hübscher & Mundry, 1984
2445816.432	-2438.5	VIS	Isles, 1985
2445911.4057	-2139	PE	Hübscher *et al.*, 1985
2445934.402	-2066	VIS	Isles, 1985
2446230.7751	-1132	PE	Groisman *et al.*, 1987
2446587.7281	-6.5	PE	Samec & Bookmyer, 1987
2446588.8392	-3	PE	Samec & Bookmyer, 1987
2446589.7908	0	PE	Samec & Bookmyer, 1987
2446590.7428	3	PE	Samec & Bookmyer, 1987
2446591.8510	6.5	PE	Samec & Bookmyer, 1987

Table 3.3: Times of minima for TY Boo — *continued.*

H.J.D.	Cycle	Method	Reference
2446925.498	1058.5	PG	Hübscher & Lichtenknecker, 1988
2447205.5406	1941.5	PE	Hübscher & Lichtenknecker, 1988
2447263.394	2124	VIS	Locher, 1988a
2447263.5774	2124.5	PE	Hübscher & Lichtenknecker, 1988
2447263.5781	2124.5	PE	Hübscher & Lichtenknecker, 1988
2447269.414	2143	VIS	Locher, 1988a
2447273.401	2155.5	VIS	Locher, 1988a
2447276.424	2165	VIS	Locher, 1988a
2447303.386	2250	VIS	Locher, 1988a
2447349.372	2395	VIS	Locher, 1988b
2447353.484	2408	VIS	Locher, 1988b
2447368.400	2455	VIS	Locher, 1988b
2447374.421	2474	VIS	Locher, 1988b
2447381.407	2496	VIS	Locher, 1988b
2447388.382	2518	VIS	Locher, 1988b
2447612.442	3224.5	VIS	Locher, 1989

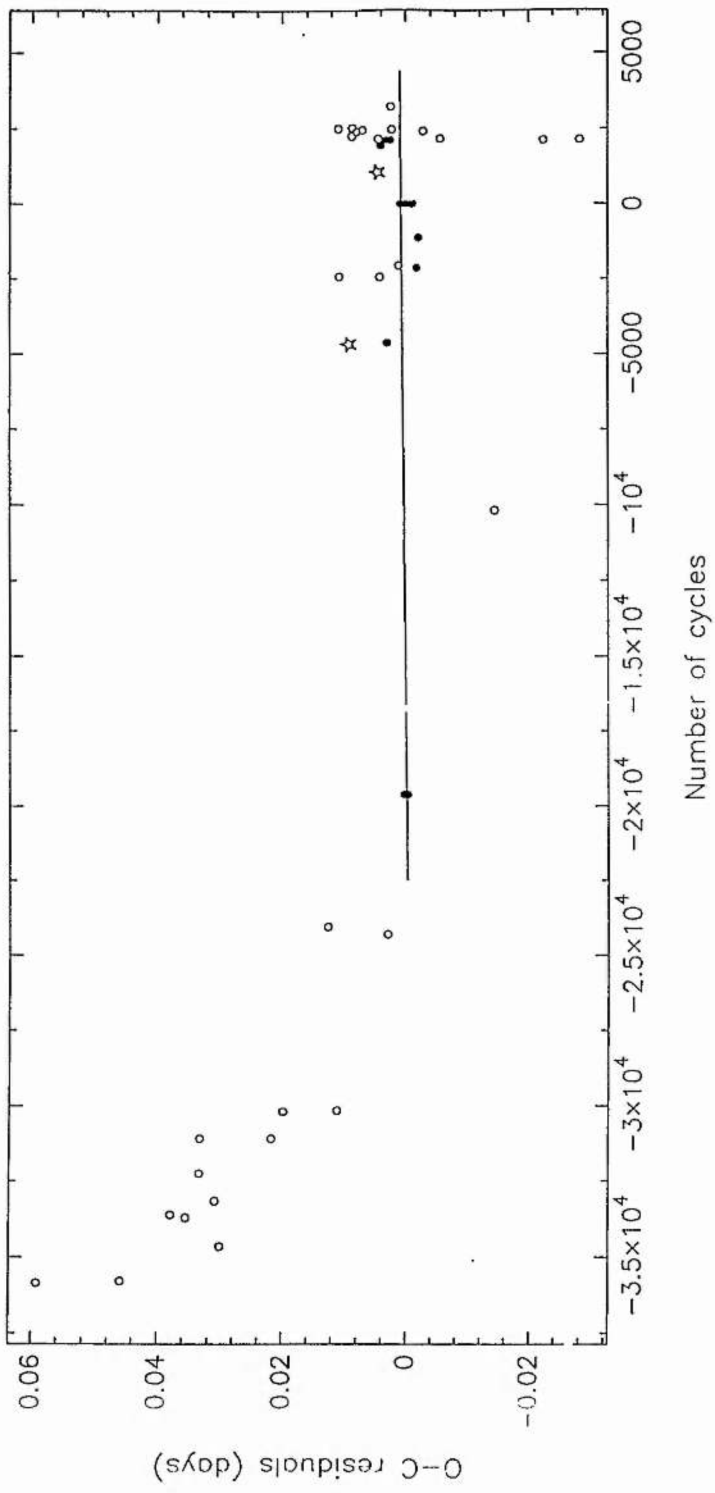

Figure 3.2: The Period behaviour of TY Boo over the last 35 years. (Open Circles represent visual times of minima; Open Stars represent photographic minima; and Filled Circles represent photoelectric minima). The fit shown to the photoelectric data indicates the current stable nature of the system.

3.4 Photometric Analysis

Light curve analysis of TY Boo was carried out using the B-filter observations published by Samec & Bookmyer (1987). This consisted of 348 observations, reduced to a differential magnitude, with a probable error in a single observation of $0^{m}\!.009$. The data were phased using the ephemeris given in Section 3.3, and are shown plotted in Figure 3.3. The analysis was performed using the light curve synthesis program LIGHT2 (described in Chapter 2).

The analysis by Carr (1972) gave a spectral type of G3 to the primary component of TY Boo, implying a temperature of some 5800 ± 200 K (Popper 1980) which was adopted for this analysis.

Carr's published colour index of (B-V) = $+0^{m}\!.71$ implies a slightly later spectral type at some 5600 K or 5500 K (Popper 1980 and Böhm-Vitense 1981 respectively), but the colour excess for the system is unknown. The most well defined cross-correlation functions (Section 3.2) were obtained with an F8 rather than a G5 standard star template, thus supporting a slightly earlier spectral type. The adopted temperature reflects a spectral range of some F8 to G5 (Popper 1980).

With the mass ratio fixed at the spectroscopic value, the gravity darkening exponents for both components ($\beta_{1,2}$) were fixed at the convective value of 0.08. The bolometric albedo for both components ($\alpha_{1,2}$) was fixed at 0.5, and the "fill-out" factor (f), secondary component temperature (T_2), and system inclination (i) were solved for.

The light curve solution obtained is shown plotted with the data, and the corresponding O-C's, in Figure 3.3. Table 3.4 lists the solution parameters. The errors quoted for f, i and T_2 are the standard deviations in each quantity, and the errors in the component volume radii r_1 and r_2 have been evaluated using the tabulation of Mochnacki (1984), combining the errors in the system mass ratio and fill-out factor.

Within the limits of the observational scatter in the data, the light curve solution for TY Boo shown in Figure 3.3 cannot be refined further. Within these limits the system does not seem to exhibit any regions of "excess" luminosity.

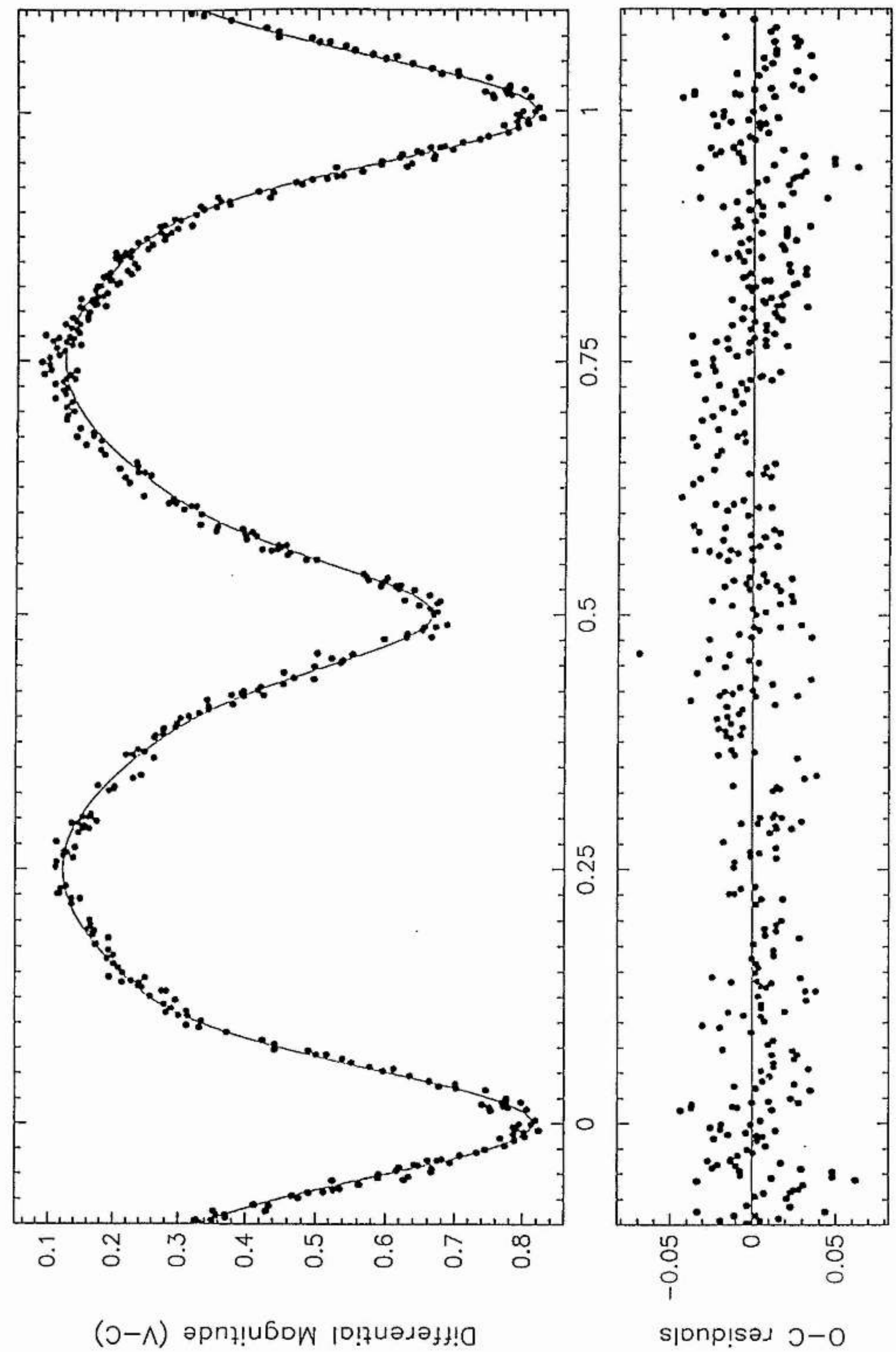

Figure 3.3: 1986 *B*-filter light curve of TY Boo (Samec & Bookmyer 1987), with light curve solution (solid line), and corresponding O-C's (lower plot).

q	=	0.437 (fixed)
T_1 (K)	=	5800 (fixed)
$\alpha_{1,2}$	=	0.5 (fixed)
$\beta_{1,2}$	=	0.08 (fixed)
f	=	0.871 ± 0.021
i (°)	=	76.59 ± 0.16
r_1 (mean)	=	0.463 ± 0.002
r_2 (mean)	=	0.319 ± 0.002
T_2 (K)	=	6185 ± 12
χ^2	=	2.69×10^{-4}

Table 3.4: Light Curve Solution for TY Boo (with standard errors).

In Chapter 1 it was described how systems which do show regions of excess luminosity have been fitted by allowing the secondary component's albedo (α_2) to go free (eg. McFarlane *et al.* 1986). This technique produces secondary albedos greater than unity, which although of little physical meaning, does facilitate a crude method of synthesizing a region of enhanced brightness on the secondary component.

As a small, but by no means exhaustive test of this technique, the same method of solution was applied to TY Boo, a system which does not show signs of excess luminosity regions. For this second solution, the starting value of α_2 was set to 1.0, and the parameter was added to the list of solution variables to be solved. The solution obtained for TY Boo with the secondary albedo free is listed in Table 3.5.

It is encouraging that the difference between the two fits was negligible, and that the secondary albedo found its way back to the region of 0.5. It is also worth noting that there is very little information content in a single light curve for the secondary albedo.

q	=	0.437 (fixed)
T_1 (K)	=	5800 (fixed)
α_1	=	0.5 (fixed)
α_2	=	0.301 $\pm$ 0.047
$\beta_{1,2}$	=	0.08 (fixed)
f	=	0.870 $\pm$ 0.081
i (°)	=	76.86 $\pm$ 0.17
r_1 (mean)	=	0.463 $\pm$ 0.002
r_2 (mean)	=	0.319 $\pm$ 0.002
T_2 (K)	=	6177 $\pm$ 11
χ^2	=	2.37 $\times 10^{-4}$

Table 3.5: Light Curve Solution for TY Boo (with standard errors), allowing the secondary albedo to go free.

3.5 Discussion

The spectroscopic mass ratio and light curve analysis of the binary system TY Boo indicates that this system is a well behaved, normal looking W-type contact binary.

Comparison with future photoelectric light curves, and further photoelectric times of minimum are required to determine the nature of any current small period changes, and to show whether this system exhibits the type of erratic light curve changes usually seen in W-type systems, indicating the presence of large-scale dark starspots.

The astrophysical data for TY Boo, derived from this analysis, are given in Table 3.6. An error of 200 K has been adopted in the secondary component temperature, as the analysis standard error is certainly an underestimate, and takes no account of the uncertainty in the primary component temperature. The bolometric corrections have been taken from the compilation of Popper (1980). Since the colour excess is unknown, a value of zero has been used to calculate an upper limit for the distance estimate.

Figure 3.4 shows a schematic diagram of the TY Boo system configuration.

Absolute dimensions	Primary	Secondary
$M\,(M_\odot)$	0.92 ± 0.02	0.40 ± 0.01
$R\,(R_\odot)$	1.00 ± 0.01	0.69 ± 0.01
$log\,g$ (cgs)	4.41 ± 0.01	4.37 ± 0.01
T_{eff} (K)	5800 ± 200	6180 ± 200
$log\,L/L_\odot$	$+0.01 \pm 0.06$	-0.21 ± 0.06
M_{bol}	$4^{m}.75 \pm 0^{m}.15$	$5^{m}.28 \pm 0^{m}.14$
B.C.	$-0^{m}.14$	$-0^{m}.06$
M_V	$4^{m}.89 \pm 0^{m}.15$	$5^{m}.34 \pm 0^{m}.07$
$E_{(B-V)}$	0	(unknown)
Distance (pc)	270 ± 60	(upper limit)

Table 3.6: Astrophysical Data for TY Boo.

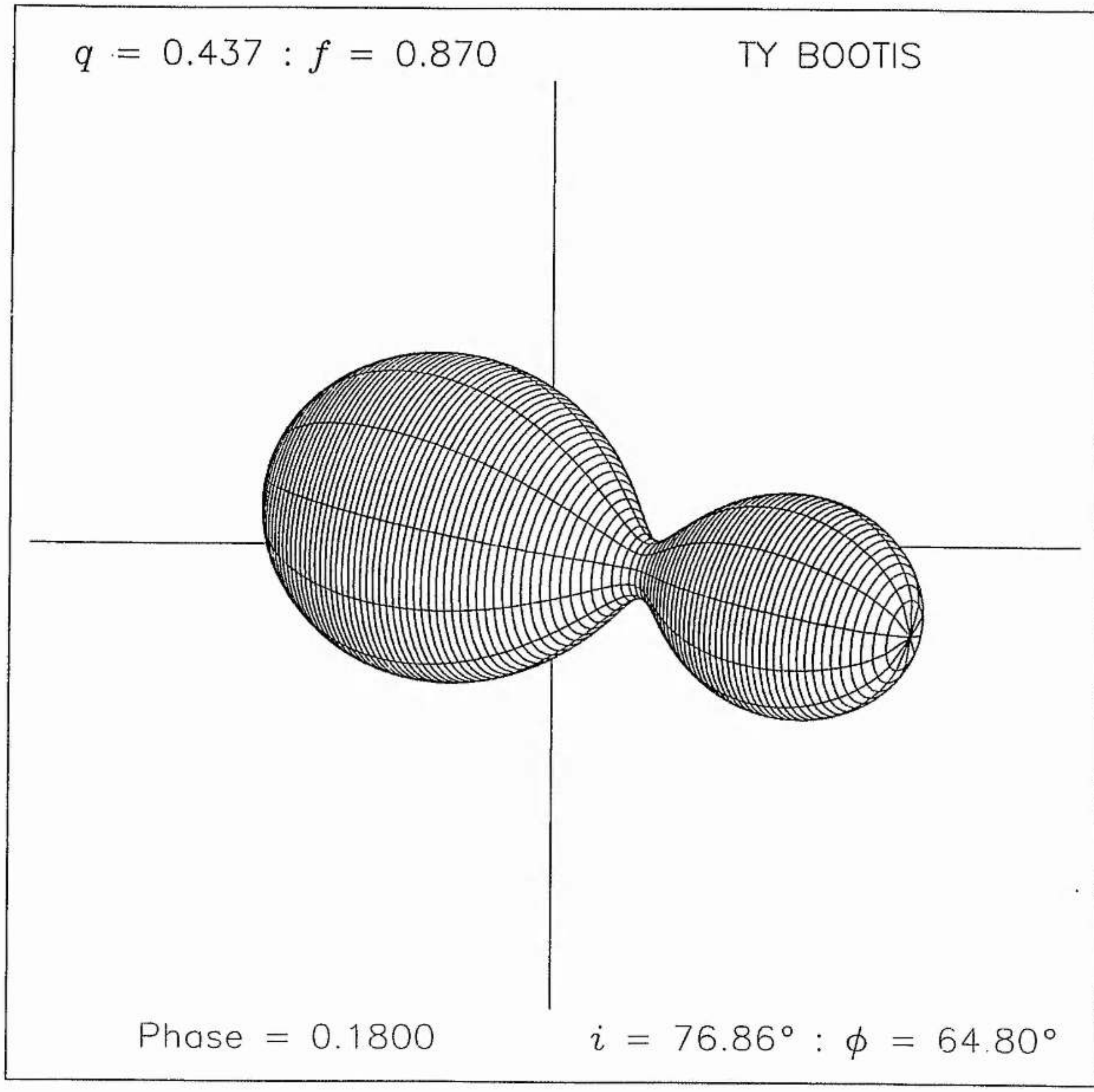

Figure 3.4: A schematic diagram of TY Boo at $0^{\mathrm{P}}\!.18$, based on this analysis.

A comparison of the masses, radii, temperatures, and luminosities of the components of TY Boo (see Chapter 9), with those of other marginal-contact and contact binaries, complied by Hilditch *et al.* (1988) shows that both the primary and secondary components occupy the same regions in the M-R, M-L, and HR diagrams as other W-type contact binary components.

The primary component lies within the main-sequence band whilst the secondary component is $\approx$1.4 times larger than expected (adopting the low-mass, main-sequence, M-R relationship of Patterson 1984), showing the expected substantial over-luminosity in the M-L plane, and a location to the left of the main-sequence band in the HR diagram (below the ZAMS line).

3.6 References

Böhm-Vitense, E., 1981. *Ann. Rev. Astr. Astrophys.*, **19**, 295.

Braune, W., & Mundry, E., 1982. *BAV Bull.*, No. 34.

Braune, W., Hübscher, J., & Mundry, E., 1983. *BAV Bull.*, No. 36.

Carr, R.B., 1972. *Astr. J.*, **77**, 155.

Groisman, G., Milone, E.F., & VanLeeuwen, J.A., 1987. *Bull. am. astr. Soc.*, **19** 954.

Guthnick, P., & Prager, R., 1926. *Astr. Nachr.*, **228**, 99.

Hilditch, R.W., King, D.J., & McFarlane, T.M., 1988. *Mon. Not. R. astr. Soc.*, **231**, 341.

Hübscher, J., & Lichtenknecker, D., 1988. *BAV Bull.*, No. 50.

Hübscher, J., & Mundry, E., 1984. *BAV Bull.*, No. 38.

Hübscher, J., Lichtenknecker, D., & Mundry, E., 1985. *BAV Bull.*, No. 39.

Isles, J.E., 1985. *BAA Var. Star Section Circ.*, No. 61.

Kopal, Z., 1978. *Dynamics of Binary Systems*, Reidel.

Locher, K., 1977. *BBSAG Bull.*, No. 34.

Locher, K., 1988a. *BBSAG Bull.*, No. 88.

Locher, K., 1988b. *BBSAG Bull.*, No. 89.

Locher, K., 1989. *BBSAG Bull.*, No. 91.

McFarlane, T.M., Hilditch, R.W., & King, D.J., 1986. *Mon. Not. R. astr. Soc.*, **223**, 595.

Milone, E.F, Fry, D.J.I., & Grillmair, C., 1987. *Bull. am. astr. Soc.*, **19**, 643.

Mochnacki, S.W., 1984. *Astrophys. J. Suppl.*, **55**, 551.

Niarchos, P.G., 1978. *Astrophys. Space Sci.*, **58**, 301.

Patterson, J., 1984. *Astrophys. J. Suppl.*, **54**, 443.

Popper, D.M., 1980. *Ann. Rev. Astr. Astrophys.*, **18**, 115.

Samec, R.G., & Bookmyer, B.B., 1987. *Publs astr. Soc. Pacif.*, **99**, 842.

Szafraniec, R., 1953. *Acta Astr.*, **2**, 101.

Szafraniec, R., 1956. *Acta Astr.*, **6**, 141.

Szafraniec, R., 1957. *Acta Astr.*, **7**, 188.

Szafraniec, R., 1958. *Acta Astr.*, **8**, 58.

Szafraniec, R., 1959. *Acta Astr.*, **9**, 48.

Szafraniec, R., 1960. *Acta Astr.*, **10**, 69.

Szafraniec, R., 1963. *Acta Astr.*, **13**, 63.

Szafraniec, R., 1966. *Acta Astr.*, **16**, 158.

Chapter 4

The Binary System VW Bootis

4.1 Introduction

The variability of VW Boo was discovered by Hoffmeister (1935). Visual observations by Zessewitsch (1944, 1954) determined its W Ursae Majoris-type nature. Binnendijk (1973) published the first, and so far only, photoelectric light curves for VW Boo, in the B and V wavelengths. These light curves were characteristic of a contact configuration system, but with unequal depth minima, indicative of components which are not in thermal equilibrium.

Binnendijk's solution of his light curve was based upon the technique of rectification and the Russell-Merrill method, and resulted in an orbital inclination and relative radii of the components not too far removed from the final solution presented here. Binnendijk noted that his theoretical light curve deviated significantly from his observed curve only at the ingress and egress of the secondary eclipse.

Niarchos (1978) re-analysed Binnendijk's data using frequency domain techniques, and obtained a mass ratio estimate of $q = 0.3$ for the system.

4.2 Spectroscopy

Radial velocity spectra of VW Boo, centred on 4200 Å were obtained and reduced as detailed in Chapter 2.

Using the G8 radial velocity standard star HD145001 for cross-correlation, the radial velocity measurements listed in Table 4.1 were obtained. The corresponding orbital phases of these measurements were derived with the revised ephemeris in Section 4.3. Although this ephemeris works well for the secondary component data, the fit to the primary data exhibits a shift of some $0^{P}.027$, this difference between the two almost certainly being due to under-sampling of the radial velocity curves, and remains unaltered if the two spectra obtained near the mid-eclipses are omitted from the analysis.

H.J.D.	Phase	V_1 $km\,s^{-1}$	(O-C) $km\,s^{-1}$	V_2 $km\,s^{-1}$	(O-C) $km\,s^{-1}$
2447280.39284	0.6749	+118	+1.6	−177	−1.2
2447280.42575	0.7711	+123	+6.9	−192	+10.6
2447280.49845	0.9835	+12	−2.5	——	——
2447280.54530	0.1204	−55	+3.0	+173	−6.7
2447280.57596	0.2100	−74	+3.4	+232	−15.5
2447280.62195	0.3444	−54	−4.2	+223	+2.6
2447280.63726	0.3892	−32	−4.1	+189	+10.5
2447280.66867	0.4810	+32	+5.0	——	——
2447280.70618	0.5906	+82	−6.7	−112	−19.5
2447281.48591	0.8692	+74	−7.4	−142	+4.4
2447281.62704	0.2816	−69	+1.8	+267	+14.0
2447282.44367	0.6680	+118	+3.0	−170	+0.9

Table 4.1: Radial Velocity data for VW Boo

The sine wave fits to the radial velocity data are shown in Figure 4.1. The resulting radial velocity semi-amplitudes for the primary and secondary components (K_1 and K_2 respectively), and the systemic velocity (V_0) are given in Table 4.3, along with the derived mass function, projected semi-major axes of the orbits, and their standard errors. Again as in Section 3.2, there is a small difference between V_{0_1} and V_{0_2} due to undersampling and uncertainty, particularly in the secondary component orbit.

To check if the phase shift or differences in the systemic velocity, due to undersampling, introduced an additional error, the mass ratio was calculated from the ratio of the radial velocity semi-amplitudes, and from the average of the mass ratio values obtained from the data point pairs, using the systemic velocity defined by the primary and secondary component data respectively. These analyses give the values for the mass ratio listed in Table 4.2. Clearly from Table 4.2 the uncertainty in the sine wave fit phasing, due to data under-sampling, does introduce a small, but not significant, additional uncertainty in the determination of the mass ratio, and hence the value of q given in Table 4.3 was adopted for this analysis.

Method of Determination	Mass Ratio
Ratio of Semi-Amplitudes	0.431 ± 0.01
V_0 from Primary	0.426 ± 0.02
V_0 from Secondary	0.425 ± 0.02

Table 4.2: Determinations of Mass Ratio for VW Boo

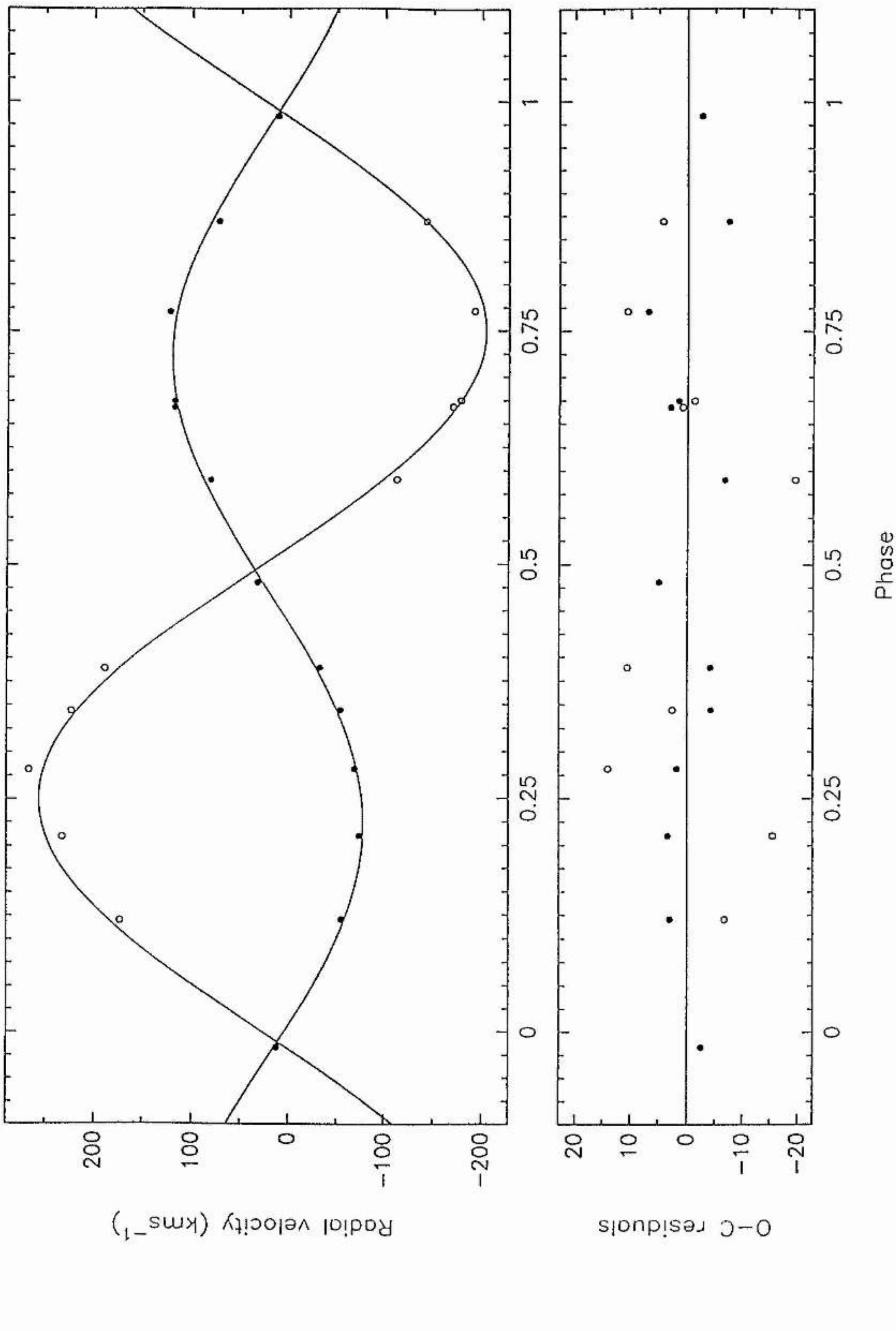

Figure 4.1: Radial Velocities of the Primary and Secondary Components of VW Boo (closed and open circles respectively), plotted together with their Orbital Solutions.

$K_1\,(\mathrm{km\,s^{-1}})$	=	99.2 ± 2.1
$K_2\,(\mathrm{km\,s^{-1}})$	=	230.1 ± 5.4
$V_{0_1}\,(\mathrm{km\,s^{-1}})$	=	21.5 ± 1.5
$V_{0_2}\,(\mathrm{km\,s^{-1}})$	=	26.3 ± 4.2
$\sigma_1\,(\mathrm{km\,s^{-1}})$ †	=	4.8
$\sigma_2\,(\mathrm{km\,s^{-1}})$ †	=	11.1
$\mathrm{q}\ (\mathrm{m_2/m_1})$	=	0.428 ± 0.03
e	=	0 (adopted)
$\mathrm{a_1 \cdot sin\,i}\ (\mathrm{R_\odot})$	=	0.671 ± 0.014
$\mathrm{a_2 \cdot sin\,i}\ (\mathrm{R_\odot})$	=	1.556 ± 0.037
$\mathrm{a \cdot sin\,i}\ (\mathrm{R_\odot})$	=	2.226 ± 0.039
$\mathrm{m_1 \cdot sin^3\,i}\ (\mathrm{M_\odot})$	=	0.887 ± 0.038
$\mathrm{m_2 \cdot sin^3\,i}\ (\mathrm{M_\odot})$	=	0.382 ± 0.016

Table 4.3: Orbital Elements for VW Boo

† — r.m.s. scatter of a single observation.

4.3 Ephemeris

The study by Binnendijk (1973) derived an ephemeris for VW Boo from the three photoelectric times of minima obtained from Binnendijk's data, plus two photographic and five visual times of minima previously published. This produced the ephemeris (with no errors stated) :-

HJD 2441091.8840 + 0.3421934E

A literature search by the author revealed a further seven visual times of minima published before Binnendijk's study, plus one photoelectric, four photographic, and nine visual times of minima which have been published by amateur astronomers since Binnendijk's study.

These data are listed in Table 4.4. Residuals to the data were calculated with respect to Binnendijk's ephemeris given above, and are shown in Figure 4.2.

Although there is a chronic lack of photoelectric data, and the visual data exhibits a large scatter, Figure 4.2 indicates that the period of VW Boo could currently be increasing, after a past duration of stability. Uncertainty in the system's period may also be involved, and further photoelectric data are required to determine accurately both the period and the nature of any changes occurring.

Using Binnendijk's ephemeris to phase the spectroscopic data given in Section 4.2, was found to produce a substantial error in the orbital phasing, indicative of an O-C of the magnitude shown in Figure 4.2. This is supported by an amateur photoelectric time of minimum from the same epoch, which also indicates a similar value of O-C with respect to Binnendijk's ephemeris.

A revised ephemeris (indicated by the second line in Figure 4.2) based only on the photoelectric data yields :-

HJD 2441091.8840 + 0.34219634E

and this revised ephemeris was used to phase the spectroscopic data presented in Section 4.2. Since three of the four photoelectrically observed minima occurred within three

Table 4.4: Times of minima for VW Boo.

H.J.D.	Cycle	Method	Reference
2431173.406	-28985	VIS	Zessewitsch, 1954
2435127.609	-17429.5	VIS	Szafraniec, 1956
2435151.570	-17359.5	VIS	Szafraniec, 1956
2435168.505	-17310	VIS	Szafraniec, 1956
2435197.434	-17225.5	VIS	Szafraniec, 1956
2435223.439	-17149.5	VIS	Szafraniec, 1956
2435228.423	-17135	VIS	Szafraniec, 1956
2435244.498	-17088	VIS	Szafraniec, 1956
2435576.371	-16118	VIS	Szafraniec, 1957
2435933.431	-15074.5	VIS	Szafraniec, 1958
2435976.378	-14949	PG	Huth, 1964
2436339.482	-13888	VIS	Szafraniec, 1959
2436631.422	-13035	VIS	Szafraniec, 1960
2436672.483	-12915	PG	Huth, 1964
2441090.8574	-3	PE	Binnendijk, 1973
2441091.7137	-0.5	PE	Binnendijk, 1973
2441091.8840	0.0	PE	Binnendijk, 1973
2443358.390	6623.5	VIS	Locher, 1977
2445120.433	11772.5	VIS	Isles, 1985
2445441.400	12710.5	PG	Hübscher & Mundry, 1984
2445492.387	12859.5	PG	Hübscher & Mundry, 1984
2445494.435	12865.5	PG	Hübscher & Mundry, 1984
2445740.586	13585	VIS	Hübscher & Mundry, 1984
2445742.643	13591	VIS	Hübscher & Mundry, 1984
2445808.365	13783	PG	Hübscher & Mundry, 1984
2445814.366	13800.5	VIS	Locher, 1984
2446952.399	17126.5	VIS	Locher, 1987
2446962.317	17155.5	VIS	Locher, 1987
2446963.359	17158.5	VIS	Locher, 1987
2446964.374	17161.5	VIS	Locher, 1987
2447276.3988	18073	PE	Locher, 1988

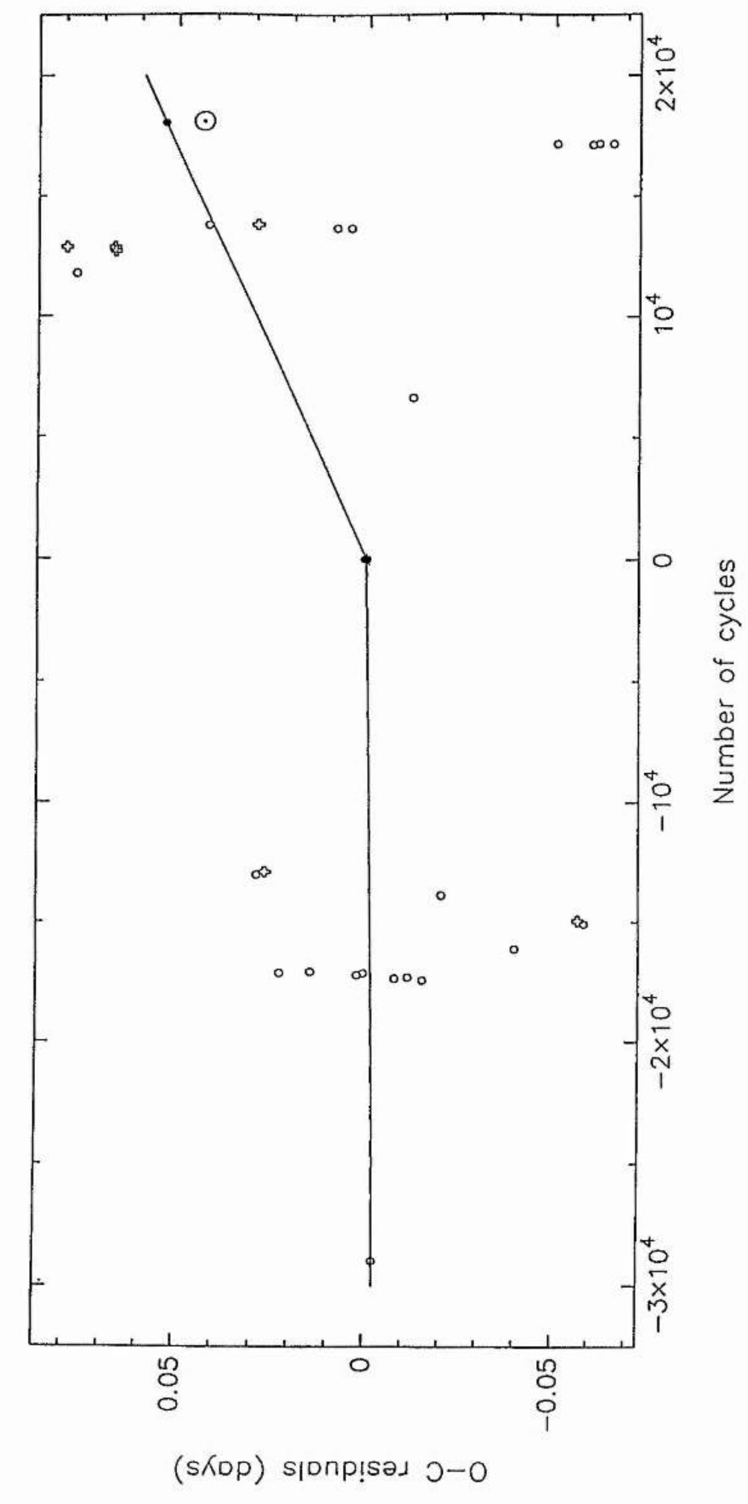

(Open circles represent visual times of minima ; open crosses represents photographic minima ; and filled circles represent photoelectric minima).

Figure 4.2: The Period behaviour of VW Boo. The large Circle with Dot is an estimated value of O-C obtained from the author's spectroscopic data. The first line indicates possible past stability, whilst the second line indicates that the period could now be increasing.

orbital cycles, and the fourth (an amateur determination) some 18000 cycles later, the formal error on the revised linear ephemeris above is extremely small and meaningless. It is noticed in Figure 4.2, that even with this revised ephemeris, the spectroscopic data exhibit a phase shift of some -0.01 day with respect to this revised ephemeris based on an amateur photoelectric determination. On the basis of such limited data, it is not possible to resolve this discrepancy, but it should be noted that it represents a change in orbital period of just 0.05 s and has no effect upon the derived values of the semi-amplitudes of the velocity curves.

4.4 Photometric Analysis

A light curve analysis of VW Boo was obtained using the B-filter observations published by Binnendijk (1973). These data consisted of 290 observations, reduced to a differential magnitude, with a probable error in a single observation of $0^{\text{m}}\!.007$. The data were phased using Binnendijk's ephemeris given in Section 4.3.

The analysis was performed using the light curve synthesis program LIGHT2 (as described in Chapter 2).

Kholopov *et al.* (1985) reported a spectral type of G5 for the primary component of VW Boo, which implies a primary temperature of some 5800K (Popper 1980).

Hilditch & Hill (1975) published one Stromgren four-colour observation of VW Boo, at an orbital phase of $0^{\text{P}}\!.3003$, which supports a primary temperature in this region, suggesting a value of some 5400K (Olsen 1984). Also the best cross-correlation functions (Section 4.2) were produced using a G8 standard star template.

Hence for this analysis, a primary temperature of 5700 ± 200 K was adopted, the mass ratio fixed at the spectroscopic value, and the gravity darkening exponents for both components ($\beta_{1,2}$) fixed at the convective value of 0.08.

The first solution attempted using LIGHT2 solved for a "standard" contact solution, with the bolometric albedo for both components ($\alpha_{1,2}$) fixed at 0.5, and the "fill-out" factor (f), secondary component temperature (T_2), and system inclination (i) as free parameters.

The light curve parameters obtained from this solution are listed in Table 4.5, and the theoretical fit is shown plotted, with the data, and corresponding O-Cs, in Figure 4.3. The solution is similar to that of Binnendijk (1973), and the same standard errors are quoted as in the analysis of TY Boo (Section 3.4).

Although this "standard" contact solution fits the shape of primary minimum, it clearly fails to match the secondary minimum, exhibiting the significant deviations in the wings of the eclipse curve, noted by Binnendijk (1973).

Following recent techniques used to obtain more accurate fits for objects exhibiting such B-type light curves, (described in Chapter 1, and eg. McFarlane *et al.* 1986),

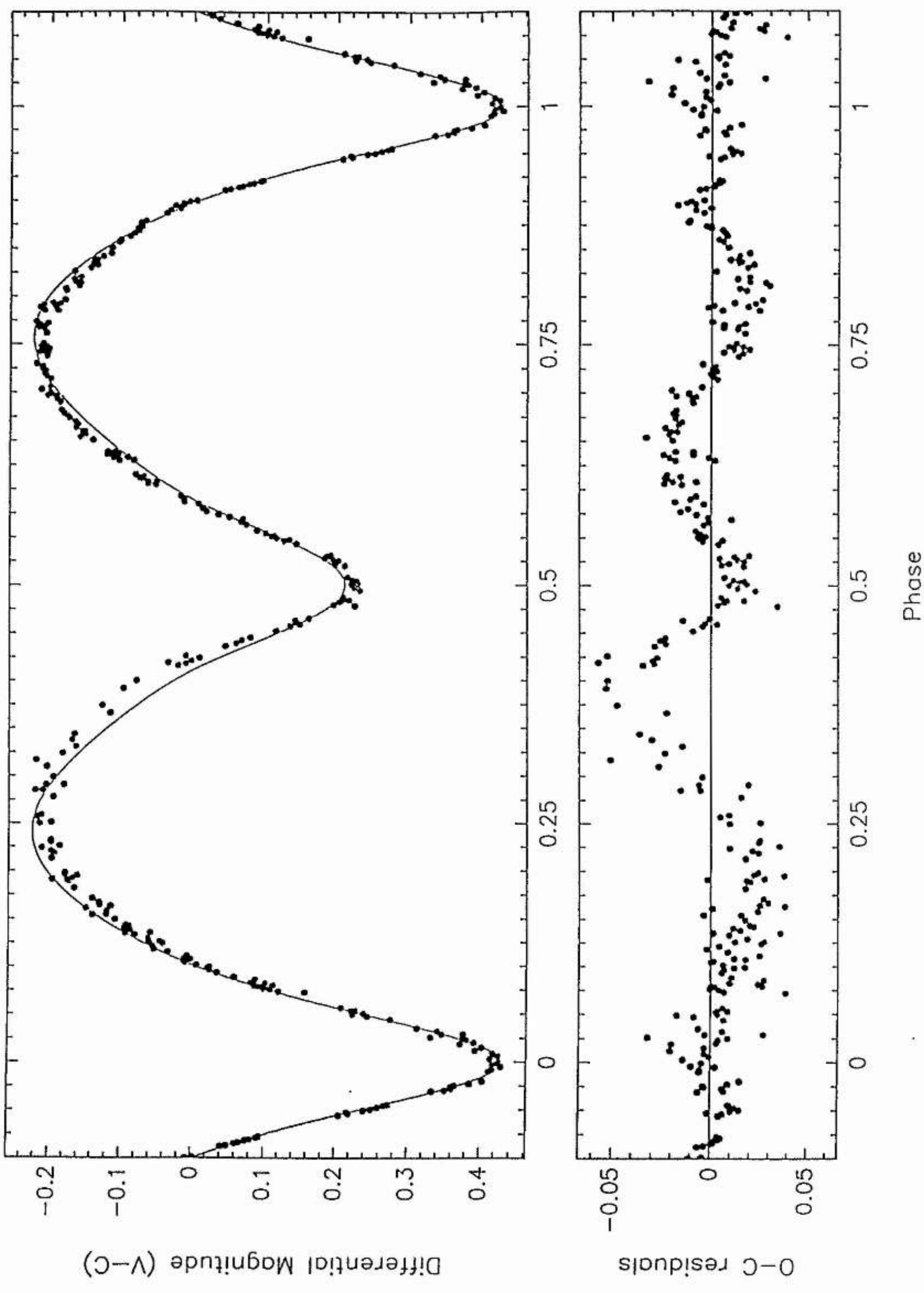

Figure 4.3: 1986 B-filter light curve of VW Boo (Binnendijk 1973), with "standard" light curve solution (solid line), and corresponding O-C's (lower plot).

q	=	0.428 (fixed)
T_1 (K)	=	5700 (fixed)
$\alpha_{1,2}$	=	0.5 (fixed)
$\beta_{1,2}$	=	0.08 (fixed)
f	=	0.716 ± 0.028
i (°)	=	76.19 ± 0.24
r_1 (mean)	=	0.477 ± 0.006
r_2 (mean)	=	0.329 ± 0.005
T_2 (K)	=	5221 ± 16
χ^2	=	3.20×10^{-4}

Table 4.5: "Standard" Light Curve Solution for VW Boo (with standard errors).

a second LIGHT2 solution was attempted, allowing the secondary albedo (α_2) to be treated as a fourth free parameter.

This solution produced the parameters listed in Table 4.6, with a theoretical fit, as shown with the data and corresponding O-Cs, in Figure 4.4.

Although a secondary albedo of greater than unity has little physical meaning, it does allow for a crude synthesis of a region of enhanced brightness on one hemisphere of the secondary component. Comparison of the fits shown in Figure 4.3 and Figure 4.4 indicates that this synthesis technique provides an improved fit to the observed light curve. Such analysis leads to the suggestion that there is some area of anomalous luminosity which resides (from geometric considerations) at, or near, the neck of the secondary component.

4.4.1 Modelling a Hot Spot

LIGHT2 provides the facility for a number of hot/cool spots to be added to either binary components (as described in Chapter 2). Hence the author was able to attempt a further solution of the VW Boo light curve, modelling a discrete region of enhanced luminosity (hot spot) on the secondary component, rather than treating the entire secondary albedo as a free parameter.

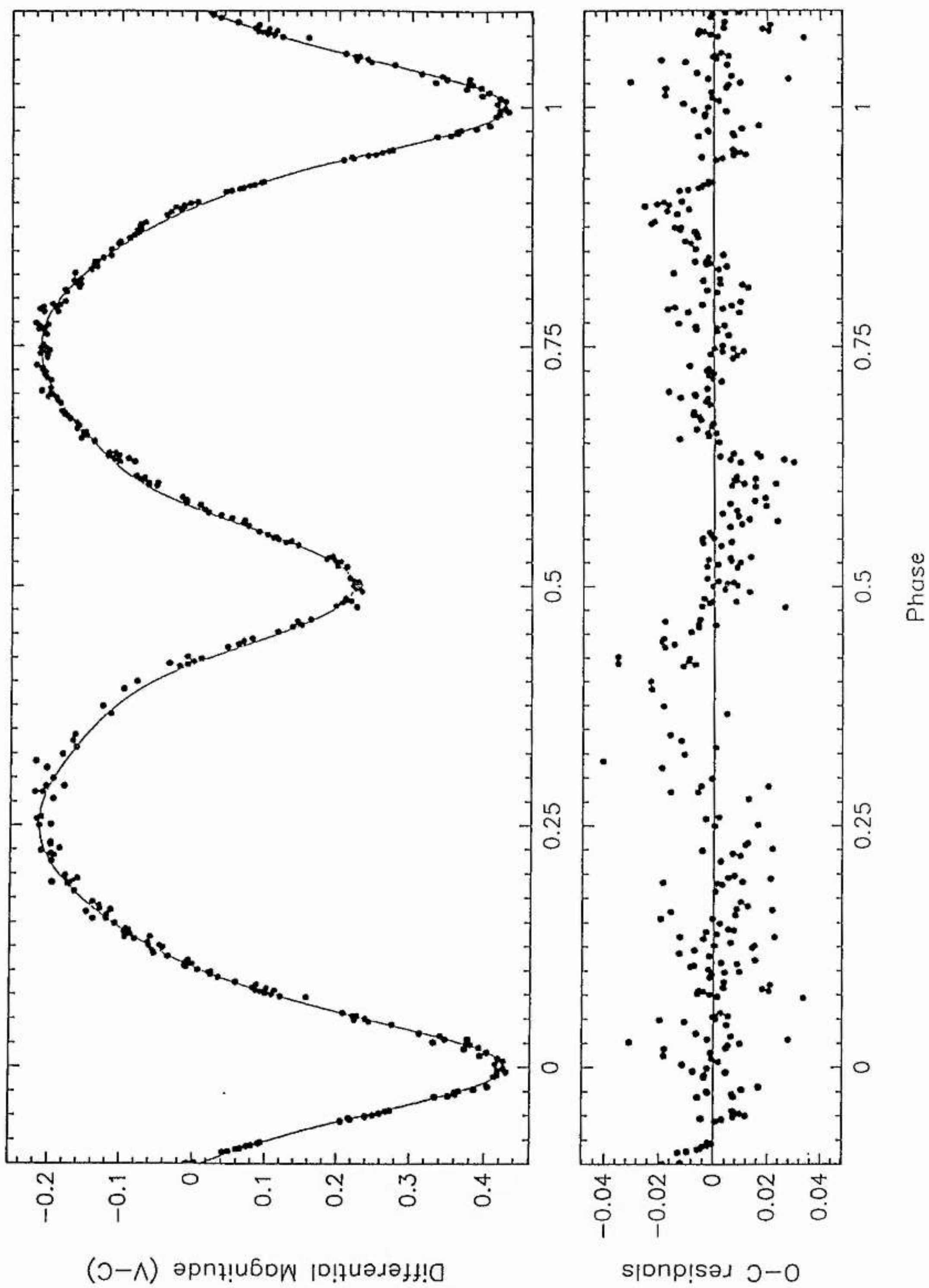

Figure 4.4: 1986 B-filter light curve of VW Boo (Binnendijk 1973), with light curve solution allowing the secondary albedo to be a free parameter (solid line), and corresponding O-C's (lower plot).

q	=	0.428 (fixed)
T_1 (K)	=	5700 (fixed)
α_1	=	0.5 (fixed)
α_2	=	1.695 ± 0.086
$\beta_{1,2}$	=	0.08 (fixed)
f	=	0.810 ± 0.017
i (°)	=	75.63 ± 0.15
r_1 (mean)	=	0.470 ± 0.006
r_2 (mean)	=	0.322 ± 0.005
T_2 (K)	=	5216 ± 10
χ^2	=	1.17 $\times 10^{-4}$

Table 4.6: Light Curve Solution for VW Boo (with standard errors), allowing the secondary albedo to be a free parameter.

Geometric considerations of the fit shown in Figure 4.3 suggest that a hot spot would be centred at the sub-stellar point. A circular shape was assumed for the analysis, but only simple boundary conditions employed, using a step function for the temperature change from the photosphere to hot spot.

For this "hot spot" analysis, LIGHT2 solved for the spot radius, r_s (in degrees of arc), spot "over"-temperature, T_s (ie. temperature over that of the surrounding photosphere), and the secondary component temperature, T_2. The values of inclination (i), and fill-out (f), were fixed at the values found from the solution which treated the secondary albedo as a free parameter (listed in Table 4.6).

The secondary component temperature must be included in the solution since the spot is likely to be considerably smaller than one hemisphere of the star, whereas the values of i and f are mainly defined by the primary eclipse, where the enhanced secondary albedo has no affect. To verify this method of solution, a test solution for r_s, T_s, f, i and T_2 was also made, yielding results in excellent agreement with the solution for r_s, T_s, T_2, and the adopted values for i and f found from the free secondary albedo solution.

Using this "hot spot" model, the parameters listed in Table 4.7 were obtained, producing the theoretical fit shown, with the observed data and corresponding O-Cs, in Figure 4.5.

q	=	0.428 (fixed)
T_1 (K)	=	5700 (fixed)
$\alpha_{1,2}$	=	0.5 (fixed)
$\beta_{1,2}$	=	0.08 (fixed)
f	=	0.810 (fixed)
i (°)	=	75.63 (fixed)
r_1 (mean)	=	0.470 (fixed)
r_2 (mean)	=	0.322 (fixed)
T_2 (K)	=	5190 ± 12
χ^2	=	1.43×10^{-4}
Spot Parameters		
r_s (degrees)	=	36.6 ± 1.4
T_s (above T_2)	=	634 ± 59

Table 4.7: "Hot Spot" Light Curve Solution for VW Boo (with standard errors).

Bearing in mind the problems of solution nonuniqueness, and the strong interdependence of r_s and T_s, it would appear from comparing Figure 4.3 and Figure 4.5, that a hot spot, modelled on simple mass transfer through the inner Lagrangian point, resulting in enhanced luminosity on the cooler component, can adequately explain the observed deviations from the "standard" contact solution.

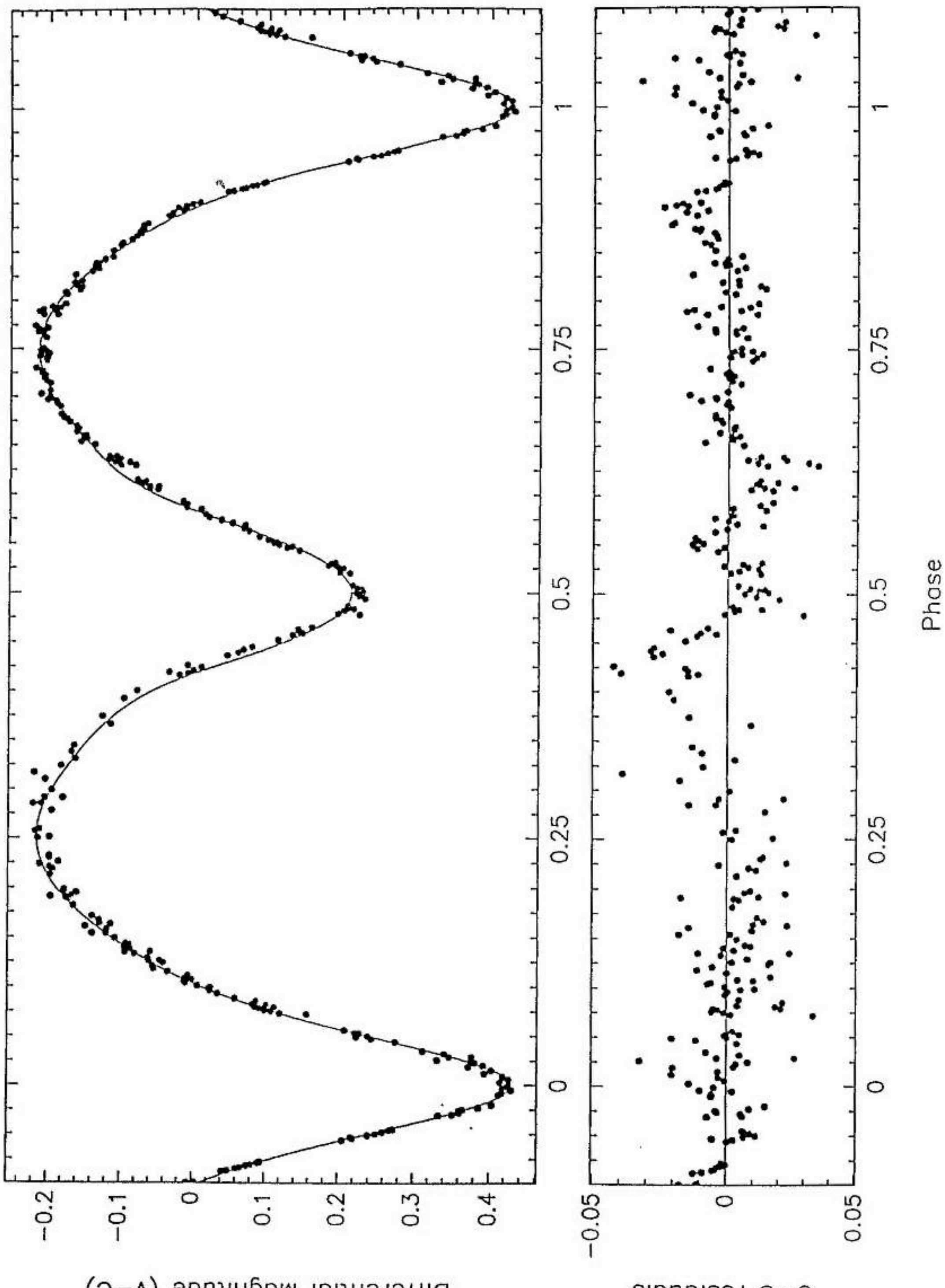

Figure 4.5: 1986 B-filter light curve of VW Boo (Binnendijk 1973), with "hot spot" light curve solution (solid line), and corresponding O-C's (lower plot).

4.5 Discussion

The light curve analysis of the binary system VW Boo presented here indicates that this system is one of the small, but growing number of B-type binaries whose observed light curves can be explained in terms of the normal transfer of energy between two components which are not in thermodynamic equilibrium.

McFarlane *et al.* (1986) quite rightly point out that such conclusions based only on light curve analysis could not easily distinguish between the suggested hot spot, and an equal but opposite cool region on the averted hemisphere of the secondary, due perhaps to extensive starspot activity. However, the hot spot scenario does have the advantage of appearing to be a natural consequence of the thermodynamic environment in which these binaries find themselves.

The chronic lack of photoelectric times of minimum for VW Boo make it very difficult to determine the nature and character of any orbital period changes occuring now. Further photoelectric light curves would also be useful to investigate if any changes in the apparent hot spot could be determined over a long time base.

The astrophysical data for VW Boo, derived from this analysis, are given in Table 4.8. As in Section 3.5, an error of 200 K has been adopted in the secondary component temperature, and the bolometric corrections have been taken from the compilation of Popper (1980). Since the colour excess is unknown, a value of zero has been used to calculate an upper limit for the distance estimate.

Figure 4.6 shows a schematic diagram of the VW Boo system configuration, indicating the location of the proposed hot spot on the neck of the secondary component.

A comparison of the masses, radii, temperatures, and luminosities of the components of VW Boo (see Chapter 9), with those of other marginal-contact and contact binaries, complied by Hilditch *et al.* (1988) indicates that the primary and secondary components occupy similar regions in the M-R and M-L diagrams, allowing for the smaller mass of VW Boo, as other B-type binary components.

The primary component lies on the main-sequence band, whilst the secondary component is over-sized and over-luminous compared with a standard low mass, main-sequence star (Patterson 1984).

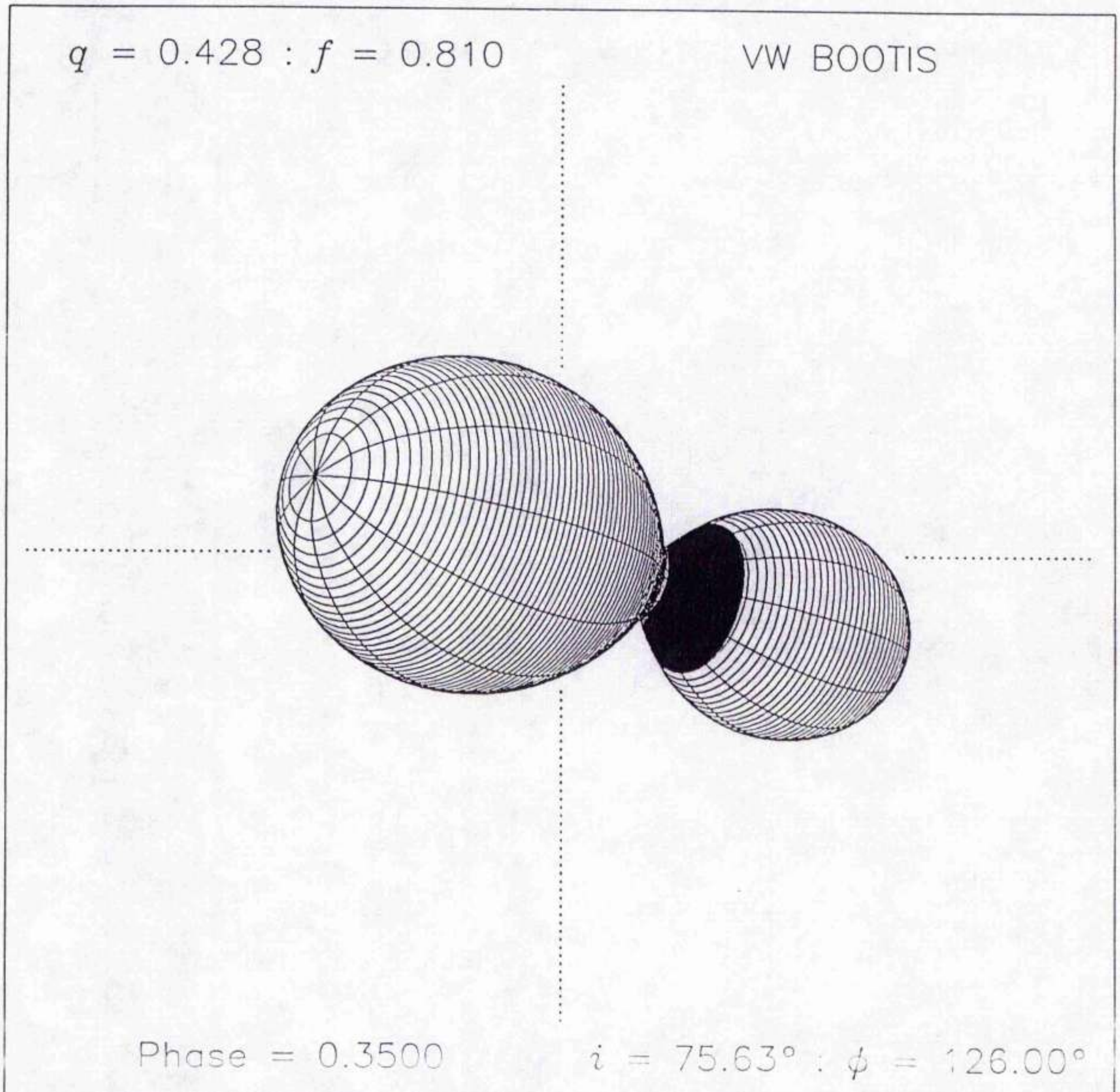

Figure 4.6: A schematic diagram of VW Boo at $0^{P}.35$, based on this analysis, showing the proposed hot spot on the neck of the secondary component.

Absolute dimensions	Primary	Secondary
$M\,(M_\odot)$	0.98 ± 0.04	0.42 ± 0.02
$R\,(R_\odot)$	1.08 ± 0.02	0.74 ± 0.01
$log\,g\,(cgs)$	4.36 ± 0.03	4.32 ± 0.03
T_{eff} (K)	5700 ± 200	5190 ± 200
$log\,L/L_\odot$	0.05 ± 0.06	-0.45 ± 0.07
M_{bol}	$4^m\!.65 \pm 0^m\!.16$	$5^m\!.87 \pm 0^m\!.17$
B.C.	$-0^m\!.16$	$-0^m\!.24$
M_V	$4^m\!.81 \pm 0^m\!.16$	$6^m\!.11 \pm 0^m\!.18$
$E_{(B-V)}$	0	(unknown)
Distance (pc)	160 ± 20	(upper limit)

Table 4.8: Astrophysical Data for VW Boo.

The secondary component is also found to occupy an interesting position on the HR diagram, lying near the ZAMS line, to the left of the other B-type secondary components, and to the right of the W-type secondary components, which lie above and below the ZAMS line respectively. VW Boo then is the first such system to be found in this "gap" between the two types, appearing to be further "into" contact on the possible evolutionary path from B-type to W-type system. Whether this evolution from "first contact" or a cycle on some TRO path is difficult to distinguish (see Chapter 9). The fact that this is the first object to be found in this region suggests that whatever evolutionary process is occurring may well be a rapid phenomenon. It should also be noted that the difference could simply be due to the uncertainty in assigning an effective temperature to the primary component.

4.6 References

Binnendijk, L., 1973. *Astr. J.*, **78**, 103.

Hilditch, R.W., & Hill, G., 1975. *Mem. R. astr. Soc.*, **79**, 101.

Hilditch, R.W., King, D.J., & McFarlane, T.M., 1988. *Mon. Not. R. astr. Soc.*, **231**, 341.

Hoffmeister, C., 1935. *Astr. Nachr.*, **255**, 401.

Hübscher, J., & Mundry, E., 1984. *BAV Bull.*, No. 38.

Huth, H., 1964. *Mitt. Sonneberg*, **2**, 112.

Isles, J.E., 1985. *BAA Var. Star Section Circ.*, No. 60.

Kholopov, P.N., Samus, N.N., Frolov, M.S., Goranskij, V.P., Gorynya, N.A., Kireeva, N.N., Kukarkin, N.P., Kurochkin, N.E., Medvedeva, G.I., Perova, N.B., & Shugarov, S.Yu., 1985. *General Catalogue of Variable Stars*, Vol 1, Nauka Publishing House, Moscow.

Locher, K., 1977. *BBSAG Bull.*, No. 34.

Locher, K., 1984. *BBSAG Bull.*, No. 71.

Locher, K., 1987. *BBSAG Bull.*, No. 84.

Locher, K., 1988. *BBSAG Bull.*, No. 88.

McFarlane, T.M., Hilditch, R.W., & King, D.J., 1986. *Mon. Not. R. astr. Soc.*, **223**, 595.

Niarchos, P.G., 1978. *Astrophys. Space Sci.*, **58**, 301.

Olsen, E.H., 1984. *Astr. Astrophys. Suppl.*, **57**, 443.

Patterson, J., 1984. *Astrophys. J. Suppl.*, **54**, 443.

Popper, D.M., 1980. *Ann. Rev. Astr. Astrophys.*, **18**, 115.

Szafraniec, R., 1956. *Acta Astr.*, **6**, 141.

Szafraniec, R., 1957. *Acta Astr.*, **7**, 188.

Szafraniec, R., 1958. *Acta Astr.*, **8**, 189.

Szafraniec, R., 1959. *Acta Astr.*, **9**, 48.

Szafraniec, R., 1960. *Acta Astr.*, **10**, 69.

Zessewitsch, W.P., 1944. *Kazan Astronomical Circ.*, **No. 32**, 6.

Zessewitsch, W.P., 1954. *Odessa Izv.*, **4**, 133.

Chapter 5

The Binary System BX Andromedae

5.1 Introduction

The short-period eclipsing binary BX And (HD 130878, SAO 37805, SVS 995) is the brighter component of the visual binary ADS 1671 (Σ 215). Soloviev (1945) discovered its variability and noted that the light curve displayed Algol-like behaviour. A photographic study by Ashbrook (1951) using 200 Harvard patrol plates confirmed the binary nature of BX And and showed it to be a variable of the β-Lyrae type. He also determined 25 times of minima from which an ephemeris was derived for the system.

Svolopoulos (1957) published the first photoelectric observations of BX And using yellow (5150 Å) and blue (4450 Å) filters. He attempted to analyse the light curves with the Russell-Merrill (1952) method but this proved unsuccessful. Todoran (1965), however, succeeded in obtaining orbital elements for BX And which suggested that the system was of moderate inclination and composed of two stars of quite different temperatures. A study of the times of minima by Chou (1959) suggested that the period of BX And had lengthened by approximately 0.3 s around 1952.

Castelaz (1979) obtained *UBV* observations of BX And showing variations in the magnitude of the system at maximum brightness. Anomalous "spikes" in the light curve were reported near primary minimum for which no satisfactory explanation was given. Castelaz also suggested that a period change took place between 1924 and 1936 and that there was also evidence of a period variation around 1950.

Further photoelectric data in the *B* and *V* passbands were obtained by Rovithis & Rovithis-Livaniou (1984), hereafter RRL, during 1981-82 showing evidence of small night to night variations in the light curve and displaying clearly-defined shoulders evocative of a detached or semi-detached system. More recently Samec *et al.* (1989), hereafter SFK, have published *UBV* data on BX And obtained during 1976. Their light curve is indicative of a contact system in which both components are considerably distorted. Derman *et al.* (1989) have also published *UBV* light curves of BX And obtained during 1987 which are similar in appearance to those of SFK.

Gülmen *et al.* (1988) published a period analysis summarizing the times of minima observed by many authors. Their analysis confirms the occurrence of a period change between 1945 and 1950 and suggests another change around 1981. The period determined before 1945 and after 1981 was found to be 0.25 s shorter than that between 1945 and 1981.

The changing shape of the light curve, the period variations and the large temperature difference between the components which appear to be in contact make this an interesting system to study. The lack of a spectroscopically-derived mass ratio makes the analysis of the light curve and the subsequent interpretation of the configuration of the system uncertain. The light curve variations could be explained in terms of either hot or cool spots on one or both of the components and evidence to support this contention may be forthcoming from simultaneous infrared and visual photometry.

5.2 Spectroscopy

Radial velocity spectra of BX And, centred on 4200 Å were obtained and reduced as detailed in Chapter 2.

The spectra were cross-correlated against the F0Ib standard star HD 36673. The resulting radial velocity measurements, with their corresponding orbital phases, are given in Table 5.1. The observations were phased using the ephemeris given in Section 5.3. One radial velocity measurement for the primary component made at $0^{p}.06$ was omitted from the analysis because the rotational velocity of the star may have contaminated the measurement.

H.J.D.	Phase	V_1 $km\,s^{-1}$	(O-C) $km\,s^{-1}$	V_2 $km\,s^{-1}$	(O-C) $km\,s^{-1}$
2447107.39044	0.7257	+59	+1.9	−241	+11.8
2447107.42852	0.7881	+56	+0.7	−245	+4.2
2447107.47221	0.8597	+34	−0.2	−223	−16.2
2447107.48745	0.8847	+26	+3.3	−187	−3.3
2447107.59661	0.0636	†)−107	——	——	——
2447107.62919	0.1170	−127	−9.0	——	——
2447107.69113	0.2185	−150	+0.7	+161	−4.1
2447107.71673	0.2605	−153	−0.5	+163	−5.8
2447108.34498	0.2902	−145	+4.4	+160	−2.5
2447108.39626	0.3743	−116	+6.2	+126	+18.2
2447108.51847	0.5746	−10	−10.4	——	——
2447108.54999	0.6262	+27	−1.0	−203	−8.7
2447108.57808	0.6723	+50	+4.0	−224	+6.5

Table 5.1: Radial Velocity data for BX And

† — This radial velocity measurement was omitted from the analysis (see Section 5.2).

The sine wave fits to the radial velocity data are shown in Figure 5.1. The resulting radial velocity semi-amplitudes for the primary and secondary, K_1 and K_2

respectively, the systemic velocity V_0, the derived mass function and projected semi-major axes of the orbits, with their standard errors are given in Table 5.2.

$K_1\,(\mathrm{km\,s^{-1}})$	=	105.5 ± 1.9
$K_2\,(\mathrm{km\,s^{-1}})$	=	212.3 ± 4.0
$V_{0_1}\,(\mathrm{km\,s^{-1}})$	=	-47.2 ± 1.5
$V_{0_2}\,(\mathrm{km\,s^{-1}})$	=	-43.0 ± 3.5
$\sigma_1\,(\mathrm{km\,s^{-1}})$ †	=	5.3
$\sigma_2\,(\mathrm{km\,s^{-1}})$ †	=	10.8
$\mathrm{q}\ (\mathrm{m_2/m_1})$	=	0.497 ± 0.013
e	=	0 (adopted)
$\mathrm{a_1 \cdot sin\,i}\ (\mathrm{R_\odot})$	=	1.272 ± 0.022
$\mathrm{a_2 \cdot sin\,i}\ (\mathrm{R_\odot})$	=	2.559 ± 0.048
$\mathrm{a \cdot sin\,i}\ (\mathrm{R_\odot})$	=	3.831 ± 0.053
$\mathrm{m_1 \cdot sin^3\,i}\ (\mathrm{M_\odot})$	=	1.358 ± 0.045
$\mathrm{m_2 \cdot sin^3\,i}\ (\mathrm{M_\odot})$	=	0.675 ± 0.022

Table 5.2: Orbital Elements for BX And

† — r.m.s. error in an observation.

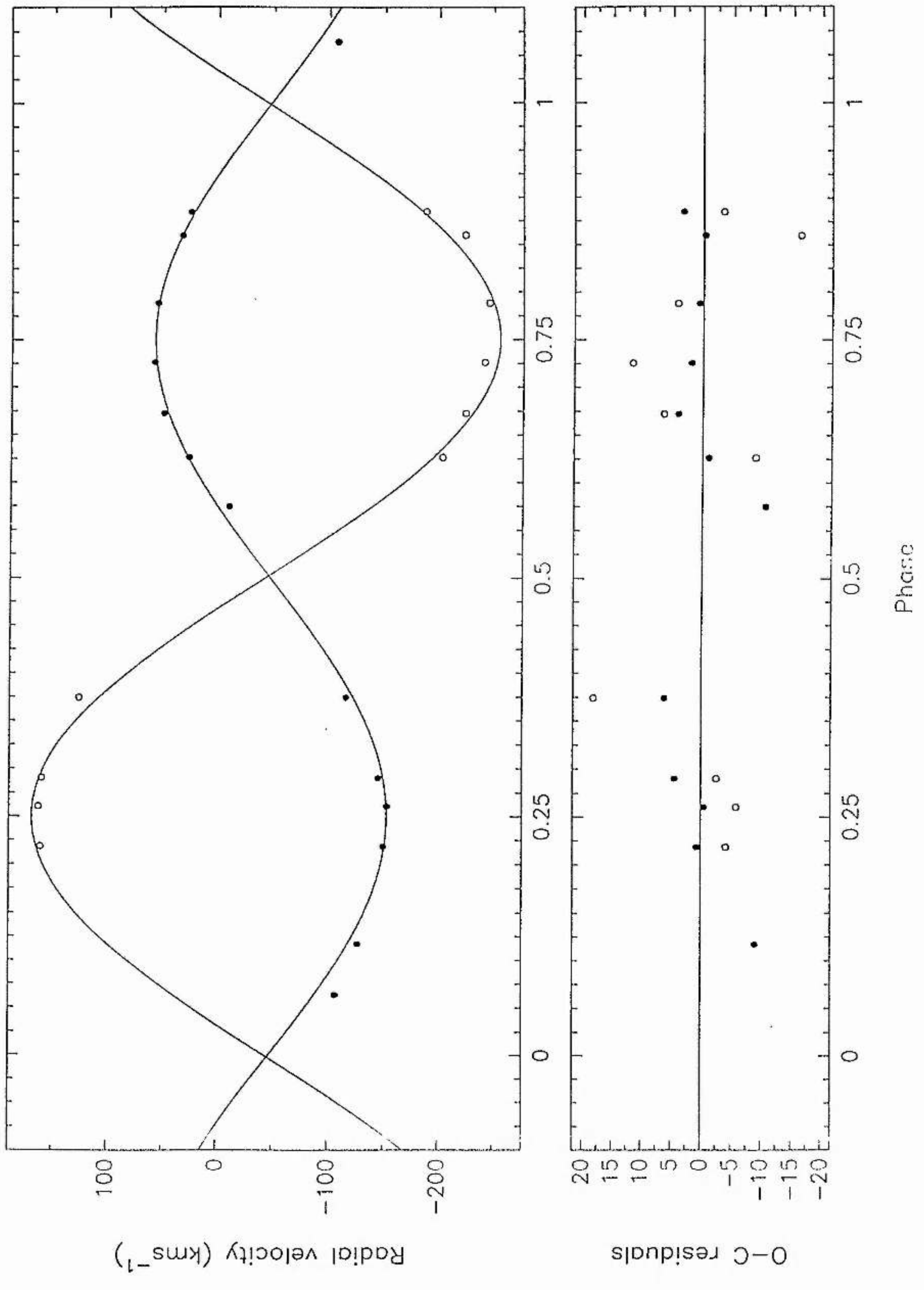

Figure 5.1: Radial Velocities of the Primary and Secondary Components of BX And (closed and open circles respectively), plotted together with their Orbital Solutions.

5.3 Ephemeris

Gülmen *et al.* (1988) have presented a period analysis for BX And which shows two clear period changes around 1950 and 1981. The scatter in the pre-1950 photographic determinations is approximately $0^{d}.02$ and becomes somewhat larger around 1950 making estimates of the period within that interval less accurate. However, the periods determined for the pre-1950 and post-1981 data are very the nearly the same whereas the period calculated for 1950 to 1981 is approximately 3×10^{-6} day longer.

A total of ten times of minima, seven primary and three secondary, have been calculated from the new data presented in this study (Section 5.4) using the method of Kwee and van Woerden (1956). These are listed in Table 5.3, along with the other available times of minima for BX And.

In view of the behaviour of the $O-C$ diagram presented by Gülmen *et al.* (1988), linear ephemerides have been evaluated for each observing season based on the best defined time of minimum for each light curve and a period determined using a least-squares analysis of 24 times of minima (denoted by † in Table 5.3) since 1985. The period calculated and subsequently adopted for this study is $0.61011258 \pm 0.00000034$ day and the residuals for this determination are plotted in Figure 5.2. The same ephemeris has been adopted for the INT spectroscopic observations and the UKIRT infrared photometry as they were obtained within two weeks of each other. The ephemerides used to phase the photometric and spectroscopic data presented in this study are as follows:

1985 TPT data	$2446372.37192 \pm 0.00009 + E \cdot 0.61011258$
1986 TPT data	$2446705.49310 \pm 0.00012 + E \cdot 0.61011258$
1987 INT/UKIRT data	$2447117.92790 \pm 0.00010 + E \cdot 0.61011258$
1988 TPT data	$2447465.69309 \pm 0.00006 + E \cdot 0.61011258$

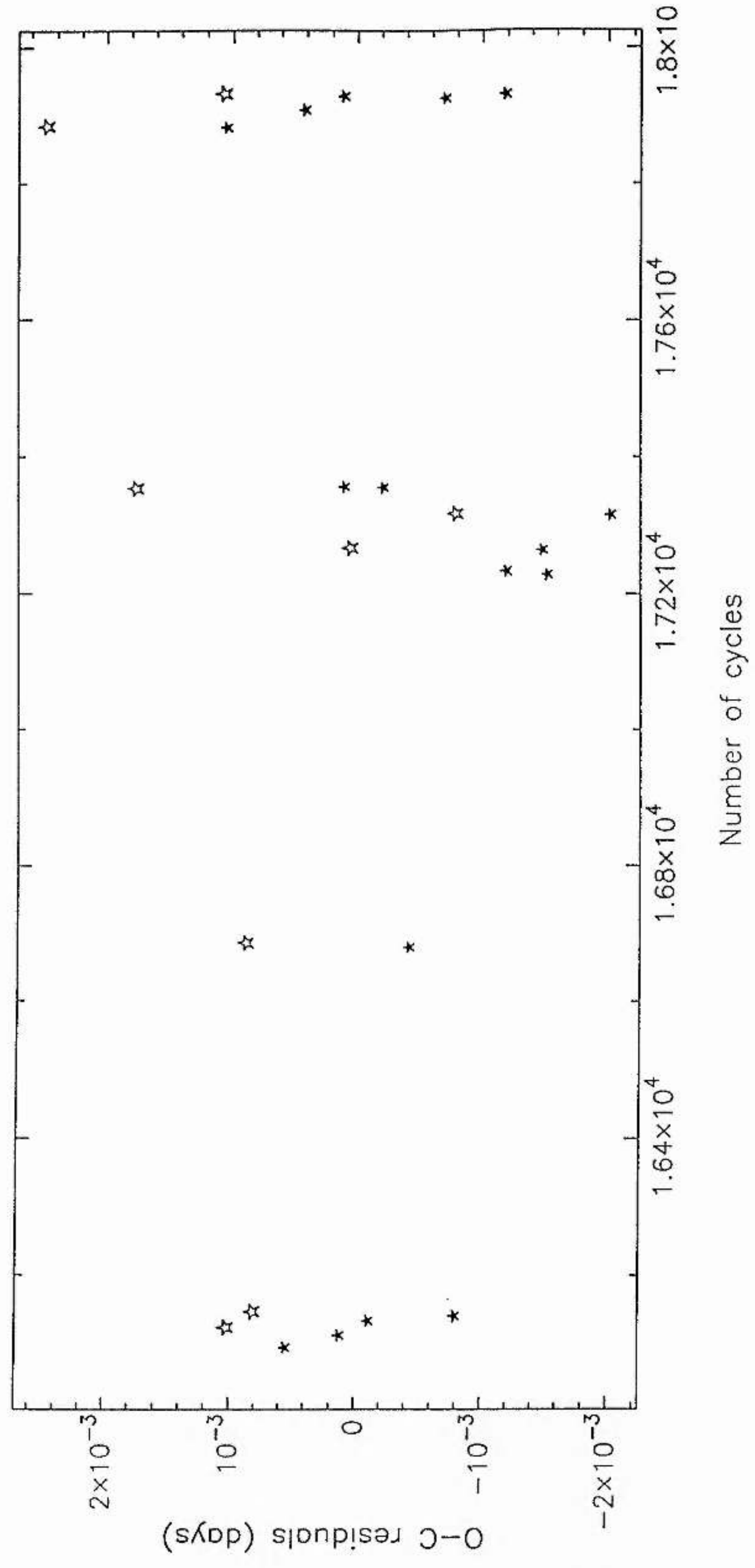

(Filled symbols represent primary minima and open circles represent secondary minima).

Figure 5.2: Recent observed minus calculated times of minima for BX And, based on the period determined from 24 new photoelectric times of minima denoted by † in Table 5.3. Cycle numbers are based on the ephemeris computed by Chou (1959).

Table 5.3: Times of minima for BX And.

H.J.D.	Cycle	Method	Reference
2414688.54	−35797	PG	Ashbrook, 1951
2414966.78	−35341	PG	Ashbrook, 1951
2415282.80	−34823	PG	Ashbrook, 1951
2416371.88	−33038	PG	Ashbrook, 1951
2416860.55	−32237	PG	Ashbrook, 1951
2417168.67	−31732	PG	Ashbrook, 1951
2418542.70	−29480	PG	Ashbrook, 1951
2420751.89	−25859	PG	Ashbrook, 1951
2420803.74	−25774	PG	Ashbrook, 1951
2421089.86	−25305	PG	Ashbrook, 1951
2422942.79	−22268	PG	Ashbrook, 1951
2423019.65	−22142	PG	Ashbrook, 1951
2424064.77	−20429	PG	Ashbrook, 1951
2427357.88	−15031.5	PG	Ashbrook, 1951
2428502.68	−13155	PG	Ashbrook, 1951
2429274.51	−11890	PG	Ashbrook, 1951
2430306.79	−10198	PG	Ashbrook, 1951
2430324.54	−10169	PG	Ashbrook, 1951
2430339.17	−10145	VIS	Ashbrook, 1951
2430594.82	−9726	PG	Ashbrook, 1951
2430597.83	−9721	PG	Ashbrook, 1951
2430647.25:	−9640	VIS	Ashbrook, 1951
2430996.25:	−9068	VIS	Ashbrook, 1951
2431076.52	−8936.5	PG	Ashbrook, 1951
2431438.60	−8343	PG	Ashbrook, 1951
2433541.65	−4896	VIS	Ashbrook, 1951
2433571.57	−4847	VIS	Ashbrook, 1951
2433582.54	−4829	VIS	Ashbrook, 1951
2434242.672	−3747	VIS	Ashbrook, 1952
2434261.59	−3716	VIS	Ashbrook, 1953
2434699.652	−2998	PE	Svolopoulos, 1957
2434710.6338	−2980	PE	Svolopoulos, 1957
2434735.6485	−2939	PE	Svolopoulos, 1957
2434743.5798	−2926	PE	Svolopoulos, 1957

Table 5.3: Times of minima for BX And — *continued.*

H.J.D.	Cycle	Method	Reference
2436528.7777	0	PE	Chou, 1959
2436538.54	16	PE	Chou, 1959
2437180.688	1068.5	VIS	Robinson, 1965
2438269.447	2853	PG	Oburka, 1965
2439352.363	4628	VIS	Braune *et al.*, 1970
2440100.398	5854	PE	Pohl & Kizilirmak, 1970
2440103.448	5859	PE	Pohl & Kizilirmak, 1970
2440133.344	5908	PE	Pohl & Kizilirmak, 1970
2440496.363:	6503	PE	Pohl & Kizilirmak, 1970
2441186.4006	7634	PE	Pohl & Kizilirmak, 1972
2441210.805	7674	PE	Meyer, 1972
2441213.858	7679	PE	Meyer, 1972
2441276.697	7782	PE	Meyer, 1972
2441618.3634	8342	PE	Kizilirmak & Pohl, 1974
2441679.371	8442	PE	Kizilirmak & Pohl, 1974
2441900.538	8804.5	PE	Kizilirmak & Pohl, 1974
2441951.485:	8888	PE	Kizilirmak & Pohl, 1974
2443012.4755	10627	PE	Pohl & Kizilirmak, 1977
2443033.8307	10662	PE	Faulkner & Kaitchuck, 1983
2443034.7460	10663.5	PE	Faulkner & Kaitchuck, 1983
2443086.294	10748	VIS	Locher, 1977a
2443098.8043	10768.5	PE	Faulkner & Kaitchuck, 1983
2443099.7228	10770	PE	Faulkner & Kaitchuck, 1983
2443142.434	10840	VIS	Braune *et al.*, 1979
2443175.344	10894	VIS	Braune *et al.*, 1979
2443405.401	11271	VIS	Braune *et al.*, 1981
2443430.406	11312	VIS	Locher, 1977b
2443446.286	11338	VIS	Locher, 1978a
2443456.338	11354.5	VIS	Locher, 1978a
2443457.261	11356	VIS	Locher, 1978a
2443488.361	11387	VIS	Locher, 1978a
2443510.339	11409	VIS	Locher, 1978a
2443776.343	11845	VIS	Locher, 1978b
2443793.416	11873	VIS	Locher, 1978b

Table 5.3: Times of minima for BX And — *continued.*

H.J.D.	Cycle	Method	Reference
2443809.279	11933	VIS	Locher, 1978b
2443809.8924	11934	PE	Castelaz, 1979
2443837.346	11979	VIS	Locher, 1978c
2443848.339	11997	VIS	Braune *et al.*, 1981
2443876.3917	12043	VIS	Isles, 1985
2444140.573	12476	VIS	Isles, 1985
2444167.431	12520	VIS	Isles, 1985
2444868.4446	13669	PE	Rovithis & Rovithis-Livaniou, 1982
2445213.4622	14234.5	PE	Rovithis & Rovithis-Livaniou, 1983
2445217.4266	14241	PE	Rovithis & Rovithis-Livaniou, 1983
2445218.3475	14242.5	PE	Rovithis & Rovithis-Livaniou, 1983
2445220.4784	14246	PE	Rovithis & Rovithis-Livaniou, 1983
2445576.484	14829.5	PE	Pohl *et al.*, 1985
2445638.411	14931	PE	Pohl *et al.*, 1985
2446348.5782	16095	PE	Pohl *et al.*, 1986 (†
2446359.5598	16113	PE	Pohl *et al.*, 1986 (†
2446366.577	16124.5	PE	Pohl *et al.*, 1986 (†
2446372.37193	16134	PE	TPT — this paper (†
2446376.64203	16141	PE	TPT — this paper (†
2446380.60937	16147.5	PE	TPT — this paper (†
2446705.49310	16680	PE	TPT — this paper (†
2446709.46013	16686.5	PE	TPT — this paper (†
2446718.31	16701	VIS	Locher, 1987
2447040.4438	17229	PE	Gülmen *et al.*, 1988 (†
2447043.4947	17234	PE	Gülmen *et al.*, 1988 (†
2447051.431	17247	VIS	Locher, 1988a
2447062.4079	17265	PE	Gülmen *et al.*, 1988 (†
2447063.3246	17266.5	PE	Gülmen *et al.*, 1988 (†
2447092.293	17314	VIS	Locher, 1988a
2447093.5231	17316	PE	Derman *et al.*, 1989 (†
2447094.4395	17317.5	PE	Derman *et al.*, 1989 (†
2447106.352	17337	VIS	Locher, 1988a
2447114.270	17350	VIS	Locher, 1988b
2447116.4061	17353.5	PE	Derman *et al.*, 1989 (†

Table 5.3: Times of minima for BX And — *continued.*

H.J.D.	Cycle	Method	Reference
2447117.3193	17355	PE	Derman *et al.*, 1989 (†
2447117.92972	17356	PE	UKIRT — this paper (†
2447153.299	17414	VIS	Hübscher & Lichtenknecker, 1988
2447439.460:	17883	PE	Gülmen *et al.*, 1988 (†
2447440.3766	17884.5	PE	Gülmen *et al.*, 1988 (†
2447455.3223	17909	PE	Gülmen *et al.*, 1988 (†
2447465.69309	17926	PE	TPT — this paper (†
2447467.52424	17929	PE	TPT — this paper (†
2447469.35329	17932	PE	TPT — this paper (†
2447469.66060	17932.5	PE	TPT — this paper (†
2447524.207	18022	VIS	Locher, 1989

† — Times of minima used in the period determination for this paper.

The residuals to the times of minima presented in Table 5.3 were calculated with respect to the ephemeris given by Chou (1959), and are shown plotted in Figure 5.3. Several interpretations of the data can be made other than that put forward by Gülmen *et al.* (1988). If the visual data are omitted from the analysis on the grounds that they cover more or less the same time interval as the photoelectric data but with a considerably enhanced scatter, an alternative interpretation can be put forward for the photographic and photoelectric data. Although a rigorous analysis cannot be justified due to the scatter in the photographic data, a sine wave can be fitted to these data with a period of approximately 78 yr and an amplitude of around 0.015 day. This sinusoidal variation is plotted in Figure 5.3. However, if the photoelectric data are examined in isolation, a quadratic function can be fitted to the residuals with respect to the ephemeris of Chou (1959) which could be ascribed to a mass transfer rate of about $-4.3\times10^{-8}\,M_{\odot}\,yr^{-1}$. These residuals and the quadratic function are plotted in Figure 5.4.

If the assumption is made that the sinusoidal variation in the $O-C$ residuals is the result of the motion of a third body whose orbit is coplanar with that of BX And, then the total mass of the system can be estimated as approximately $2\times10^{-3}\,M_{\odot}$. Unless the orbit of the third body is nearly perpendicular to that of BX And, this explanation can be rejected as the total mass of BX And is approximately $2\,M_{\odot}$. However, if the sinusoidal variation is real and there is mass transfer in the system then the suggestion can be made that there appears to be cyclic behaviour in the mass transfer rate with a period of around 80 yr. Figures 5.3 and 5.4 also show quite a noticeable scatter in the photoelectrically measured time of minimum residuals. The observed small-scale departures from the calculated ephemeris may be due to either fluctuations in the mass transfer rate from the primary to the secondary component or systematic measurement errors in times of minima which have been distorted by the presence of hot or cool spots on one or both of the stars.

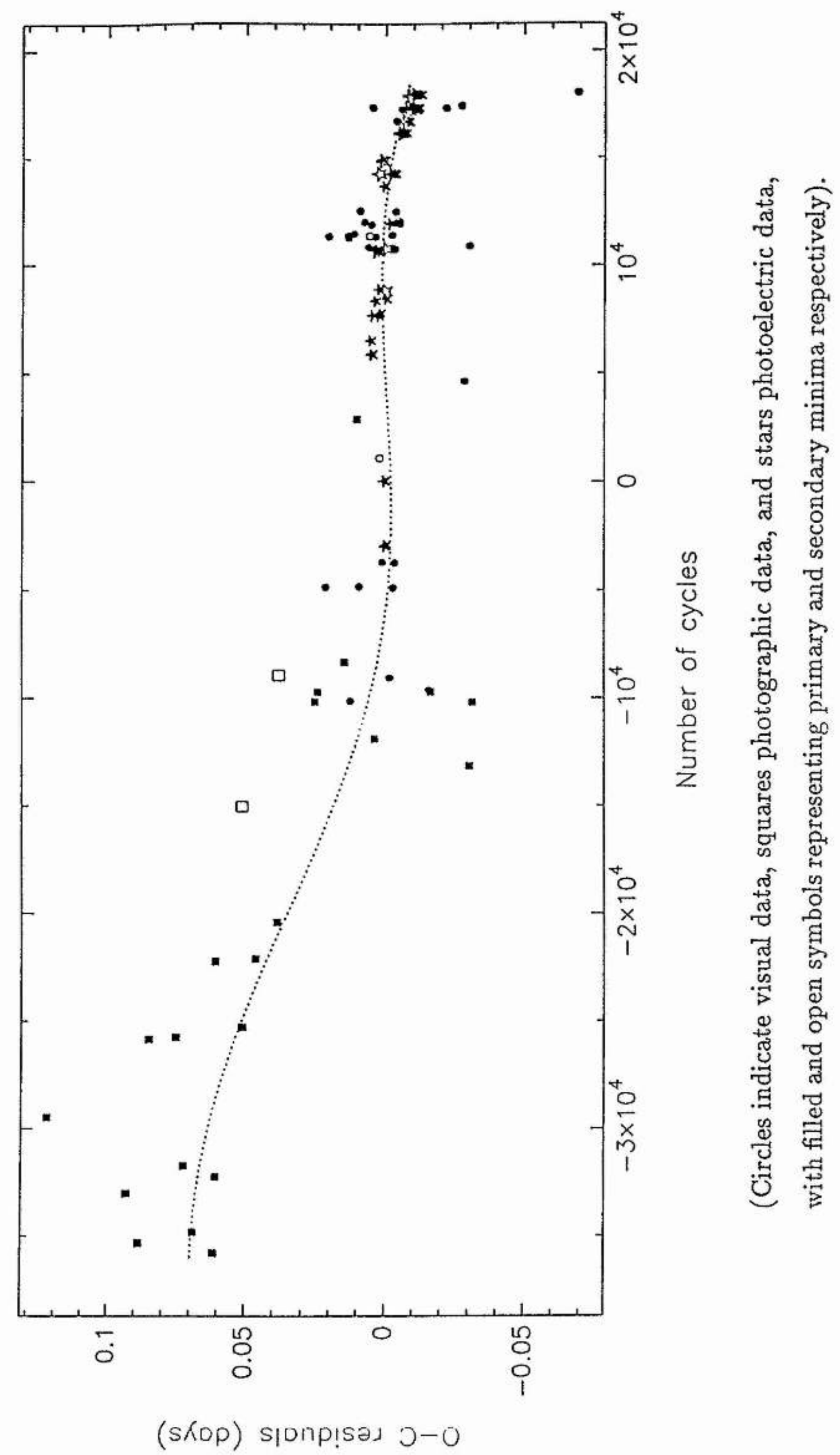

Figure 5.3: Period behaviour of BX And based on the ephemeris computed by Chou (1959), using all the available times of minima. The dotted line is a sine wave with a period of 78yr and amplitude 0.015 day.

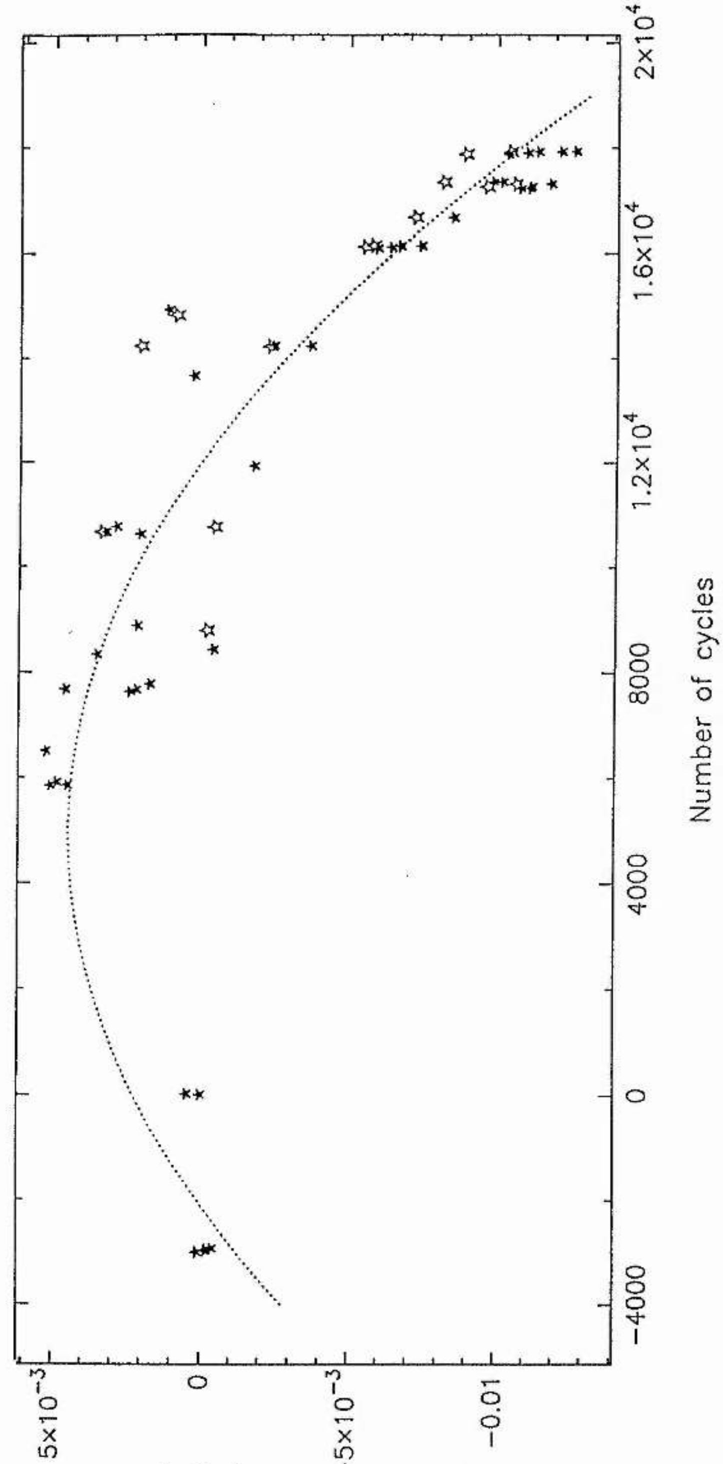

(Filled and open symbols represent primary and secondary minima respectively).

Figure 5.4: Period behaviour of BX And based on the ephemeris computed by Chou (1959), using only photoelectric data. The quadratic function fitted implies a mass transfer of some $-4.3\times10^{-8}\,M_{\odot}\,yr^{-1}$.

5.4 Photometric Analysis

5.4.1 Optical Observations

New photoelectric photometry of BX And in 1985, 1986, and 1988, was obtained and reduced to a differential magnitude as outlined in Chapter 2. Observations were made in the V passband, with typical error in the differential magnitudes of $0^{m}.006$. The data were phased using the ephemerides given in Section 5.3. The 1985 data consisting of 380 observations, the 1986 data consisting of 602 observations and the 1988 data consisting of 1959 observations are listed in the Appendix to this Chapter, and are shown plotted in Figures 5.5, 5.6, and 5.7, respectively.

Although somewhat incomplete, the 1985 TPT data are similar to that of 1986, the only difference being an anomalous brightening of the system during the egress from secondary minimum in the 1986 data. Both of these curves are similar in appearance to the V light curve of SFK. With the exception of the 1985 data where the coverage is poor, the remaining TPT data and that of SFK show that the phases of maximum light for the system are displaced by about $0^{P}.02$ towards secondary minimum. The 1988 TPT curve also shows a clear disparity ($\approx 0^{m}.02$) between first and second quadrature which is not seen in the other curves. The depth of primary minimum of the 1988 TPT data shows a variation of approximately $0^{m}.03$. The primary minima obtained on HJD 2447465 and 2447467 are deeper than that observed on HJD 2447469, the latter showing good agreement with previous light curves. All the TPT and SFK secondary minima have depths to within $0^{m}.01$ of each other.

The major discrepancies between the available light curves arise when the V observations obtained by RRL during 1981/1982 are compared with existing published data and that presented in this study. The depth of 1981/1982 primary minimum is the same as that of the deeper 1988 TPT minima but the phases of maximum brightness are displaced by $0^{P}.08$ towards secondary minimum. Secondary eclipse is approximately $0^{m}.05$ shallower than has been found by other observers and both primary and secondary minima appear to be noticeably asymmetric. It should also be noted that the appearance of the 1981/1982 data are quite different from that of SFK and that presented here — not only are the quadratures flatter making the shoulders more clearly defined, but the individual nights of data show no appreciable scatter and give the appearance of smoothed data. Such matters are not discussed by RRL. A more detailed comparison with the light curves obtained by Castelaz (1979) and Derman *et al.* (1989) cannot be made as the individual observations are not available to the author.

5.4.2 Infrared Observations

Simultaneous infrared and optical photometry of BX And was obtained and reduced as described in Chapter 2. The J and K data were reduced to differential magnitudes with an accuracy of approximately $0^{\rm m}\!.02$, and phased using the ephemeris given in Section 5.3. The J and K observations are listed in the Appendix to this Chapter and are shown plotted in Figures 5.8 and 5.9, respectively.

The overall scatter in the J light curve is approximately $0^{\rm m}\!.02$ whereas that for the K light curve is $0^{\rm m}\!.03$. The increased scatter in the data for both light curves around first quadrature makes it difficult to assess the relative brightnesses of both quadratures but first quadrature appears to be approximately $0^{\rm m}\!.03$ brighter than second quadrature. The depth of primary and secondary minima are $0^{\rm m}\!.59$ and $0^{\rm m}\!.34$ in J respectively and $0^{\rm m}\!.54$ and $0^{\rm m}\!.39$ in K. Both light curves appear to be quite symmetrical and similar in shape to the majority of the UBV data.

5.4.3 Colour Indices

Eggen (1967) published a colour index $(B-V) = 0^{\rm m}\!.44$ for BX And at maximum light and a colour excess $E_{(B-V)} = +0^{\rm m}\!.04$ based on the colours of two nearby field stars. He also noted that BX And shows slight reddening at both eclipses indicative of a contact configuration and that the common proper motion companion of BX And (ADS 1671B) has an $E_{(B-V)} = 0^{\rm m}\!.24$ suggesting that there is no physical connection with BX And. The period-colour relation plotted by Eggen showed that BX And lies in an area between regions occupied by detached and contact systems at an age of about 10^9 yr.

SFK obtained $(B-V)$ colour indices for BX And at primary and secondary minimum of $0^{m}_{\cdot}484$ and $0^{m}_{\cdot}426$ respectively and mean value of $0^{m}_{\cdot}450$ for both quadratures. These observations show slight reddening at primary minimum and a slight decrease in $(B-V)$ at secondary minimum. Assuming that the contribution of the secondary component to the total light of the system is of the order of a few percent at secondary minimum and that the colour excess is $0^{m}_{\cdot}04$ then a temperature estimate can be made for the primary component. Using the $(B-V)_0$-temperature tabulation given by Popper (1980) a mean temperature of 6600 K can be inferred. This estimate is supported by the Strömgren colour indices obtained by Hilditch & Hill (1975) at $0^{p}_{\cdot}58$. If $E_{(b-y)} = 0.74\,E_{(B-V)}$, then the $(b-y)_0$-temperature tabulation of Popper would also suggest a temperature for the primary component of 6600 K. These estimates indicate that the primary component should have a spectral type of about F3. This is in good agreement with the classification of F3 given by Kholopov *et al.* (1985) and F2V given by Hill *et al.* (1975). Also the best cross-correlation function (Section 5.2) was produced using an F0 standard star template. However, as the secondary eclipse is not total this temperature estimate must be regarded as a lower limit. The $(B-V)_0$-effective temperature calibration of Böhm-Vitense (1981) suggests a temperature for the primary component of 6900 ± 200 K. According to Böhm-Vitense this estimate places the primary component below the limiting temperature for which models incorporating radiative equilibrium are required. A temperature estimate for the primary component of 6800 ± 200 K has been adopted for this analysis and gravity darkening exponents for both components have been fixed at their convective values of 0.08.

5.4.4 Light curve analysis

For the analysis presented here, not only were the three new optical and two new infrared light curves analyzed, but the previously published V data of SFK and RRL were also re-analyzed.

The first attempt at solving the light curves of BX And was made using the light curve synthesis program WUMA5 (see Chapter 2).

The solution was initiated with an inclination i of 75°, a "fill-out" factor f as defined by Rucinski (1973) of 1.0 (denoting marginal contact), the mass ratio q fixed at that derived spectroscopically and a fractional temperature difference $x = \frac{(T_2 - T_1)}{T_1}$ of -0.2 where T_1 and T_2 are the primary and secondary component temperatures respectively. The bolometric albedos α_1 and α_2 for the primary and secondary components respectively were both fixed at 0.5 and the gravity darkening exponents β_1 and β_2 for the primary and secondary components respectively were fixed at 0.08.

The results of the analyses for the 1985, 1986, and 1988 TPT data are given in Table 5.4 and are plotted in Figures 5.5, 5.6 and 5.7 respectively. Similarly, the solutions to the UKIRT J and K data are given in Table 5.4 and plotted in Figures 5.8 and 5.9 respectively and the V data of SFK and RRL are also given in Table 5.4 and plotted in Figures 5.10 and 5.11 respectively. Clearly, the RRL data is unlikely to be fitted well by a contact solution because of the pronounced shoulders in the light curve and is presented here only for completeness. The most notable feature of these solutions is the poor fitting between $0\overset{p}{.}25$ and $0\overset{p}{.}75$. In particular, this inadequacy becomes most pronounced at around $0\overset{p}{.}38$ and $0\overset{p}{.}62$. The size of the departure at these phases is clearly visible in the 1985 and 1986 TPT data where the fit is underluminous by approximately $0\overset{m}{.}04$ but somewhat less so in the 1988 TPT data. The departure of the fit from the data of RRL is at maximum at the phases already noted at a level of around $0\overset{m}{.}08$. All of the TPT solutions and also that of SFK suggest a mean fill-out factor of 0.79 indicating a substantial degree of contact. However, the fractional temperature difference x is between -0.31 and -0.38 suggesting a secondary component temperature of around 4400 K. It is difficult to see how such a large temperature difference between the two components can be sustained in a system with such a high degree of contact. However, the UKIRT data suggests a somewhat higher secondary component temperature of 4600 K with a much shallower degree of contact ($f = 0.93$). The solutions all suggest a mean inclination for the system of $75\overset{\circ}{.}3$.

Following the analysis in Section 4.4, the light curve synthesis program LIGHT2 (see Chapter 2), was used to analyse the seven sets of data, treating the secondary albedo α_2 as an additional free parameter. The details of these solutions are given in Table 5.5 and are shown plotted in Figures 5.5, 5.6, 5.7, 5.8, 5.9, 5.10, and 5.11.

The solutions to the TPT and SFK data suggest a shallower contact configuration ($f = 0.88$) with a secondary component temperature of around 4600 K and a secondary

Light curve	x	i	f	σ (mmag.)
TPT V 1985	-0.363 ± 0.016	73.78 ± 0.42	0.763 ± 0.023	15.2
TPT V 1986	-0.377 ± 0.014	73.59 ± 0.39	0.802 ± 0.021	13.6
TPT V 1988	-0.314 ± 0.008	76.16 ± 0.29	0.803 ± 0.017	9.3
UKIRT J 1987	-0.304 ± 0.011	76.27 ± 0.36	0.935 ± 0.018	13.3
UKIRT K 1987	-0.335 ± 0.045	75.82 ± 0.34	0.930 ± 0.017	11.1
SFK V 1976	-0.325 ± 0.010	74.85 ± 0.31	0.806 ± 0.018	10.4
RRL V 1981/82	-0.399 ± 0.037	76.46 ± 1.03	1.305 ± 0.083	32.8

Table 5.4: WUMA5 solutions for BX And.

All the above fits are based on spline fits to the original data evaluated every $0\overset{\mathrm{P}}{.}01$ with the exception of the 1987 infrared data where the original data were used.

albedo of between 3.5 and 6.0. Once again, the UKIRT data indicate a slightly hotter secondary in a very marginal-contact configuration ($f = 0.98$). The inclination of the system ranged from $74\overset{\circ}{.}0$ to $74\overset{\circ}{.}9$ with the 1988 TPT data giving an inclination of $75\overset{\circ}{.}4$ based on the deeper primary eclipse. Once again, the data of RRL yielded a very poor solution which featured a detached system with a secondary component whose temperature is 3360 K with and albedo of nearly 26!

Light curve	T_2	i	f	α_2	χ^2
TPT V 1985	4513 ± 21	74.00 ± 0.04	0.878 ± 0.008	5.67 ± 0.20	2.662×10^{-5}
TPT V 1986	4472 ± 21	73.98 ± 0.04	0.882 ± 0.008	4.82 ± 0.16	2.392×10^{-5}
TPT V 1988	4640 ± 31	75.41 ± 0.07	0.865 ± 0.014	4.05 ± 0.24	7.183×10^{-5}
UKIRT J 1987	4674 ± 38	74.86 ± 0.10	0.985 ± 0.017	5.33 ± 0.54	8.528×10^{-5}
UKIRT K 1987	4786 ± 68	74.36 ± 0.13	0.981 ± 0.020	5.99 ± 0.89	1.463×10^{-4}
SFK V 1976	4598 ± 16	74.67 ± 0.04	0.908 ± 0.007	3.46 ± 0.11	1.852×10^{-5}
RRL V 1981/82	3357 ± 375	74.16 ± 0.26	1.022 ± 0.023	25.7 ± 12.4	3.854×10^{-4}

Table 5.5: LIGHT2 solutions for BX And.

All the above fits are based on spline fits to the original data evaluated every $0\overset{\mathrm{P}}{.}01$ with the exception of the 1987 infrared data where the original data were used.

As discussed in Chapter 4, although solutions involving a secondary albedo of greater than unity have little physical meaning, the technique does facilitate a crude method of synthesizing a hemisphere of enhanced brightness on the secondary component. This leads to the suggestion that there is some source of anomalous luminosity at or near the neck of the system which resides on the secondary component. The poor fit to secondary minimum using the albedo models would suggest that there is a discrete hot spot on the secondary component which does not get eclipsed totally at secondary minimum.

As in Section 4.4, LIGHT2 was employed to model a hot spot close to the sub-stellar point on the secondary component. The spot parameters solved for were the spot radius r_s (in degrees of arc) and the spot over-temperature, T_s which is the excess temperature of the spot over that of the surrounding photosphere. The symmetrical nature of secondary minimum suggests that the spot is centred at the sub-stellar point and initial solutions confirmed this, allowing the spot position to be fixed. The spot has been assumed to be circular for this analysis. It should be pointed out that the spot has very sharply defined edges in the temperature domain and that across the boundary of the spot the temperature increases as a step function from that of the photosphere to that of the spot itself.

Solutions were made for r_s, T_s and T_2 for all seven light curves adopting the values of i and f found from the solutions with free secondary albedos. The secondary temperature must be included in the solution since the spot is likely to be considerably smaller than one hemisphere of the star whereas i and f are mainly defined by the primary eclipse where the enhanced secondary albedo has no effect.

The details of the solutions are given in Table 5.6 and are again plotted in Figures 5.5, 5.6, 5.7, 5.8, 5.9, 5.10, and 5.11.

A test solution for r_s, T_s, f, i and T_2 was also made to verify the method of solution for the spot parameters. This yielded results in excellent agreement with the adopted i and f found from the free secondary albedo solutions and the solutions for r_s, T_s and T_2.

With the exception of the data of RRL, the spot size ranges from 30° to 38° and the spot over-temperature from 1100 K to 2200 K. The solutions for the 1985 TPT data and the UKIRT data should be regarded with some caution as the light curves are not well defined on either side of secondary minimum, but the 1986 and 1988 TPT data

Light curve	T_2	r_s	T_s	χ^2
TPT V 1985	4335 ± 22	29.7 ± 0.5	2215 ± 47	2.763×10^{-5}
TPT V 1986	4381 ± 21	37.9 ± 0.8	1394 ± 55	2.603×10^{-5}
TPT V 1988	4563 ± 28	35.0 ± 1.3	1420 ± 75	7.472×10^{-5}
UKIRT J 1987	4593 ± 40	35.6 ± 1.9	1967 ± 142	8.760×10^{-5}
UKIRT K 1987	4664 ± 69	31.9 ± 3.5	2186 ± 246	1.434×10^{-4}
SFK V 1976	4540 ± 16	36.8 ± 0.9	1105 ± 48	2.026×10^{-5}
RRL V 1981/82	3277 ± 263	44.1 ± 2.6	2662 ± 317	3.737×10^{-4}

Table 5.6: LIGHT2 spot solutions for BX And.

All the above fits are based on spline fits to the original data evaluated every $0^{\mathrm{P}}.01$ with the exception of the 1987 infrared data where the original data were used.

and that of SFK do show good agreement.

However, it has proved impossible to obtain a satisfactory solution to the data of RRL which reflects a larger anomalous luminosity in the ingress to and egress from secondary minimum. This could be interpreted as a larger and / or hotter spot caused by enhanced mass transfer, an explanation which may be supported by the scatter in the $O - C$ residuals in Figure 5.4 at around 14 000 cycles.

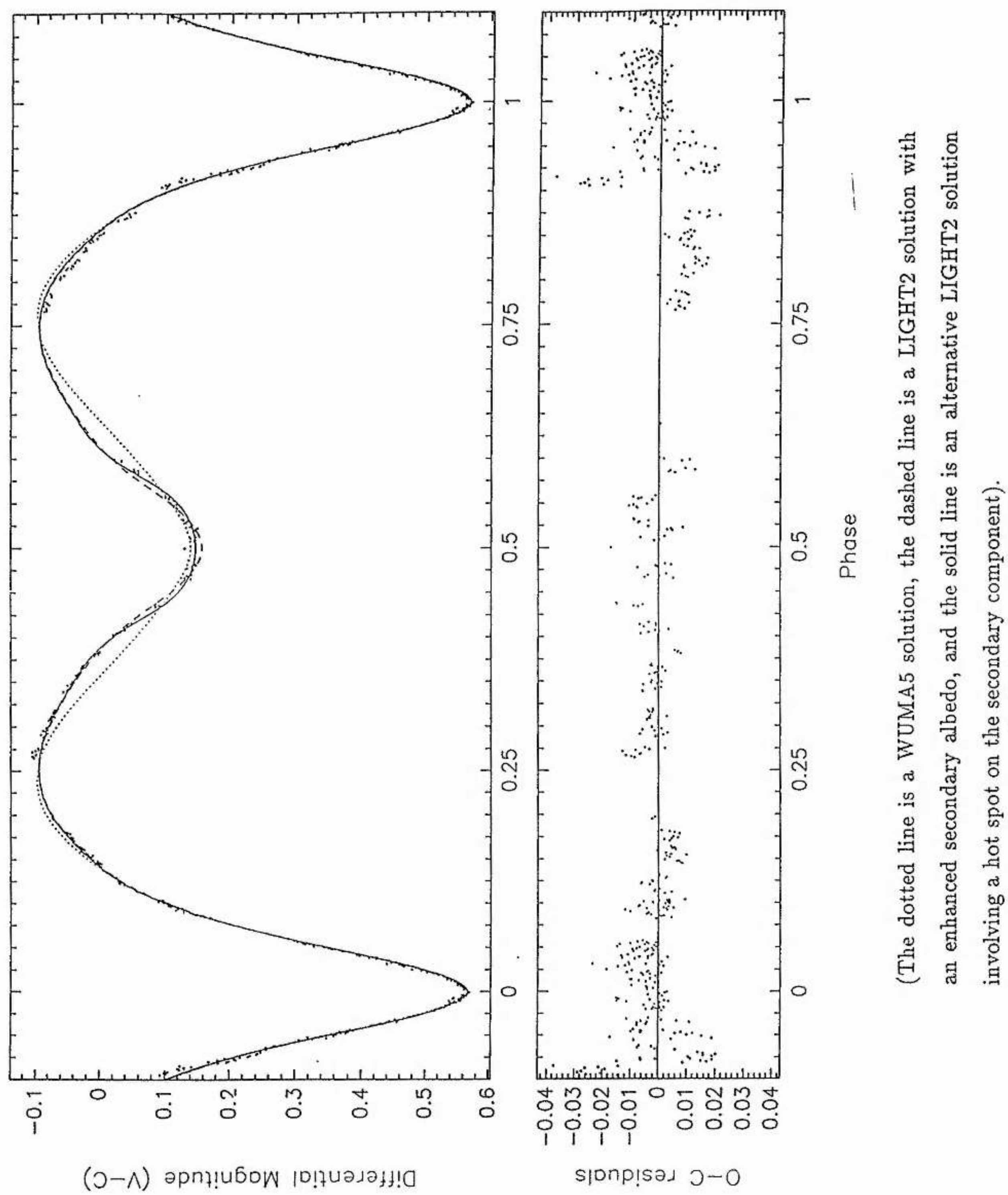

Figure 5.5: 1985 TPT *V* light curve of BX And. The three lines represent different types of contact solutions of these data. The lower plot shows the residuals of the these observations from the spot solution.

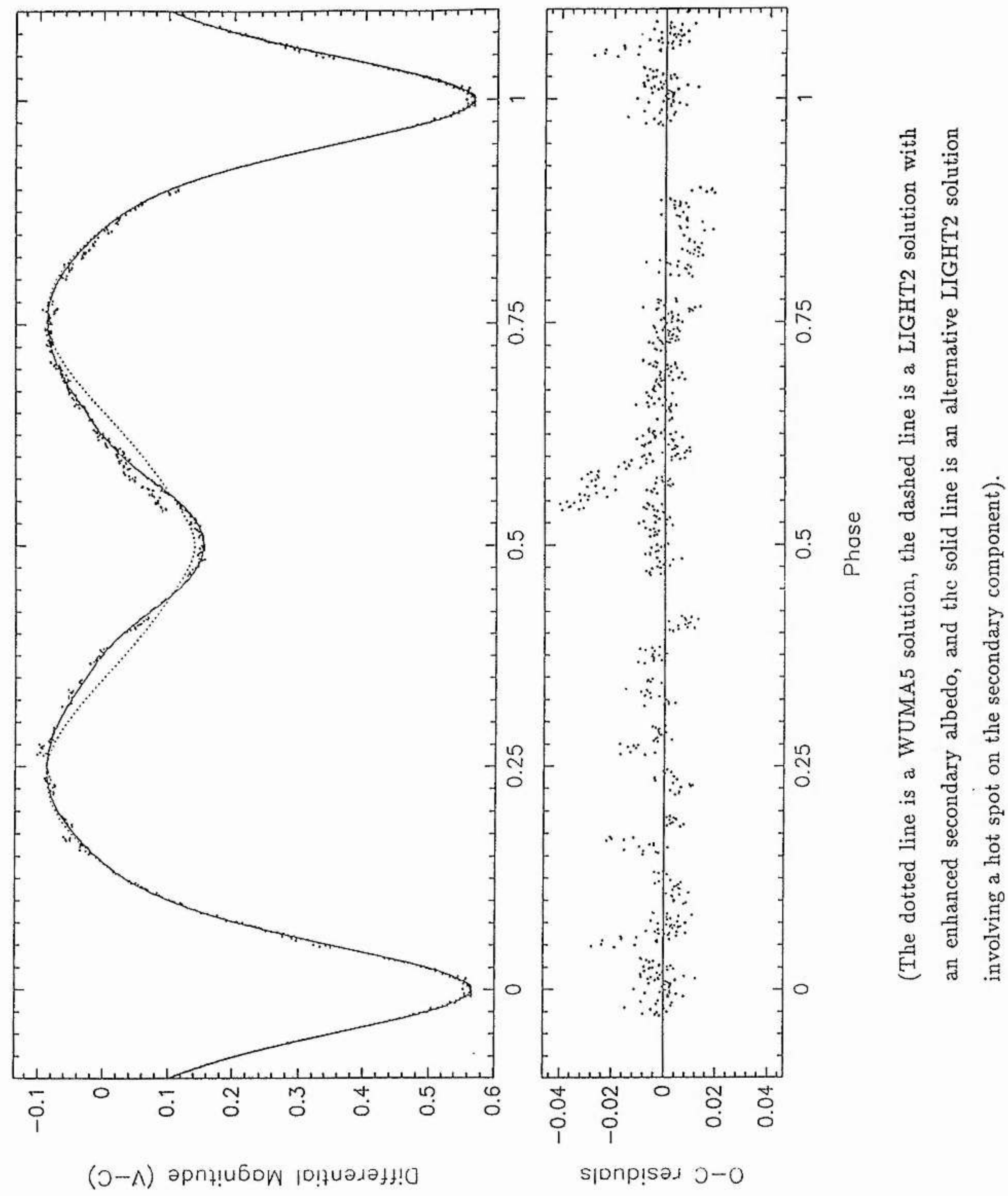

Figure 5.6: 1986 TPT *V* light curve of BX And. The three lines represent different types of contact solutions of these data. The lower plot shows the residuals of the these observations from the spot solution.

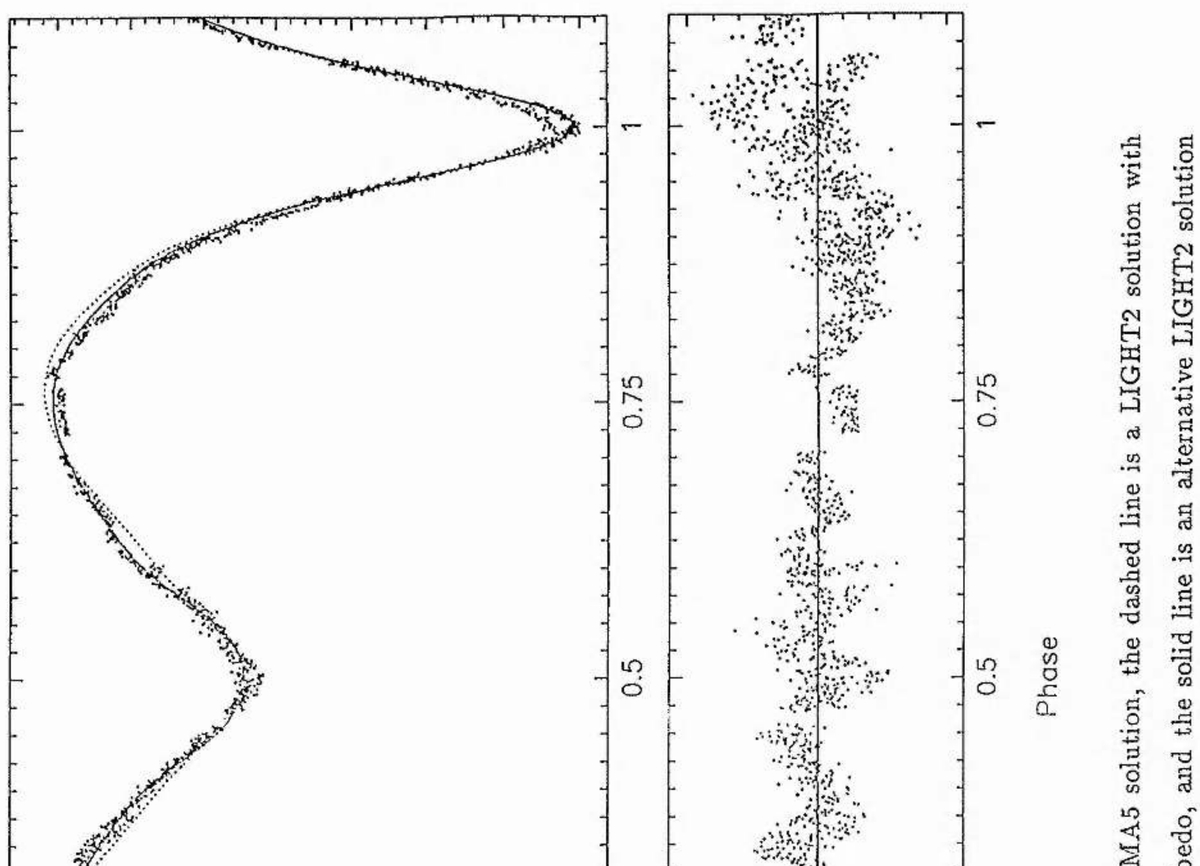

Figure 5.7: 1988 TPT *V* light curve of BX And. The three lines represent different types of contact solutions of these data. The lower plot shows the residuals of the these observations from the spot solution.

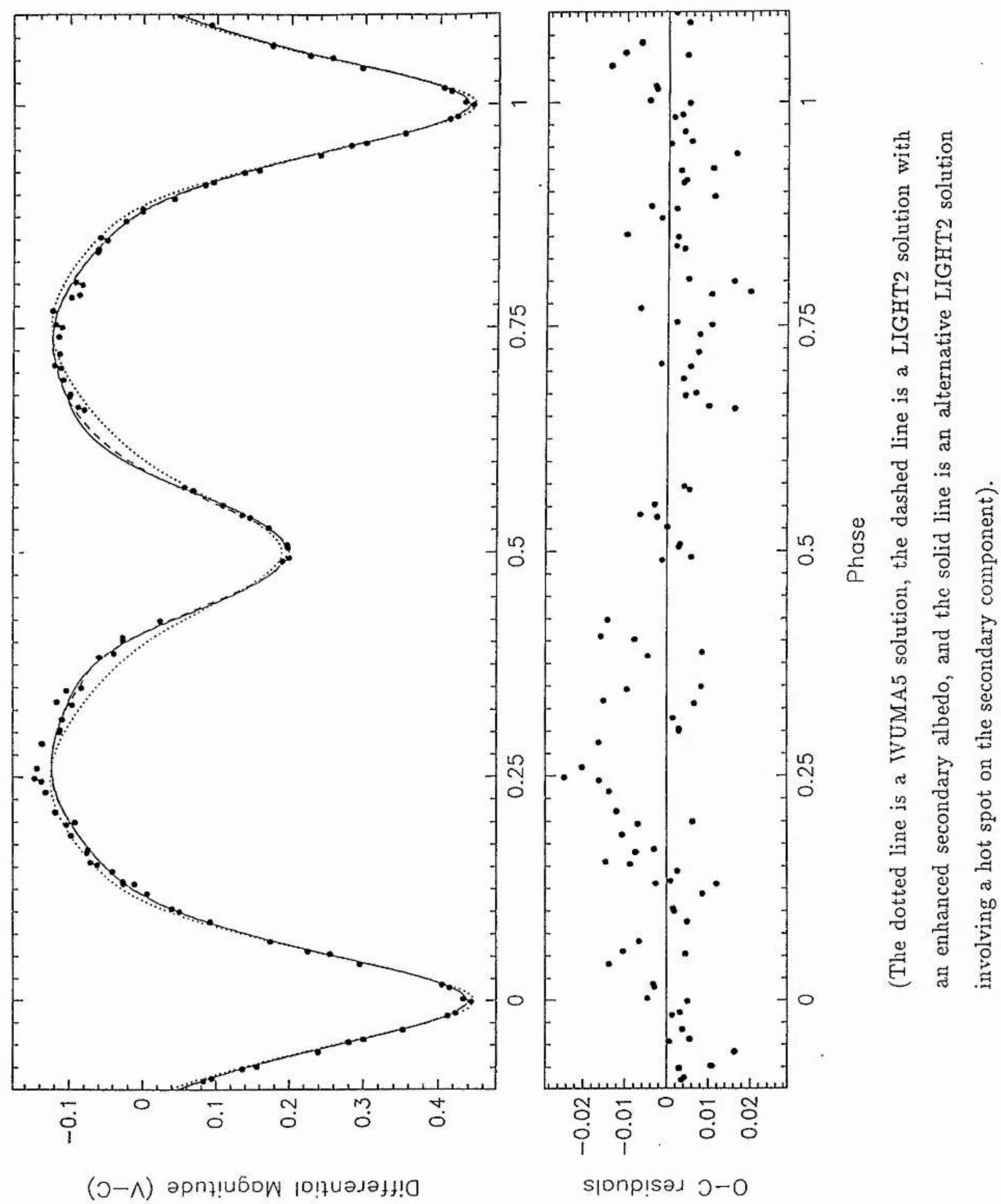

Figure 5.8: 1987 UKIRT J light curve of BX And. The three lines represent different types of contact solutions of these data. The lower plot shows the residuals of the these observations from the spot solution.

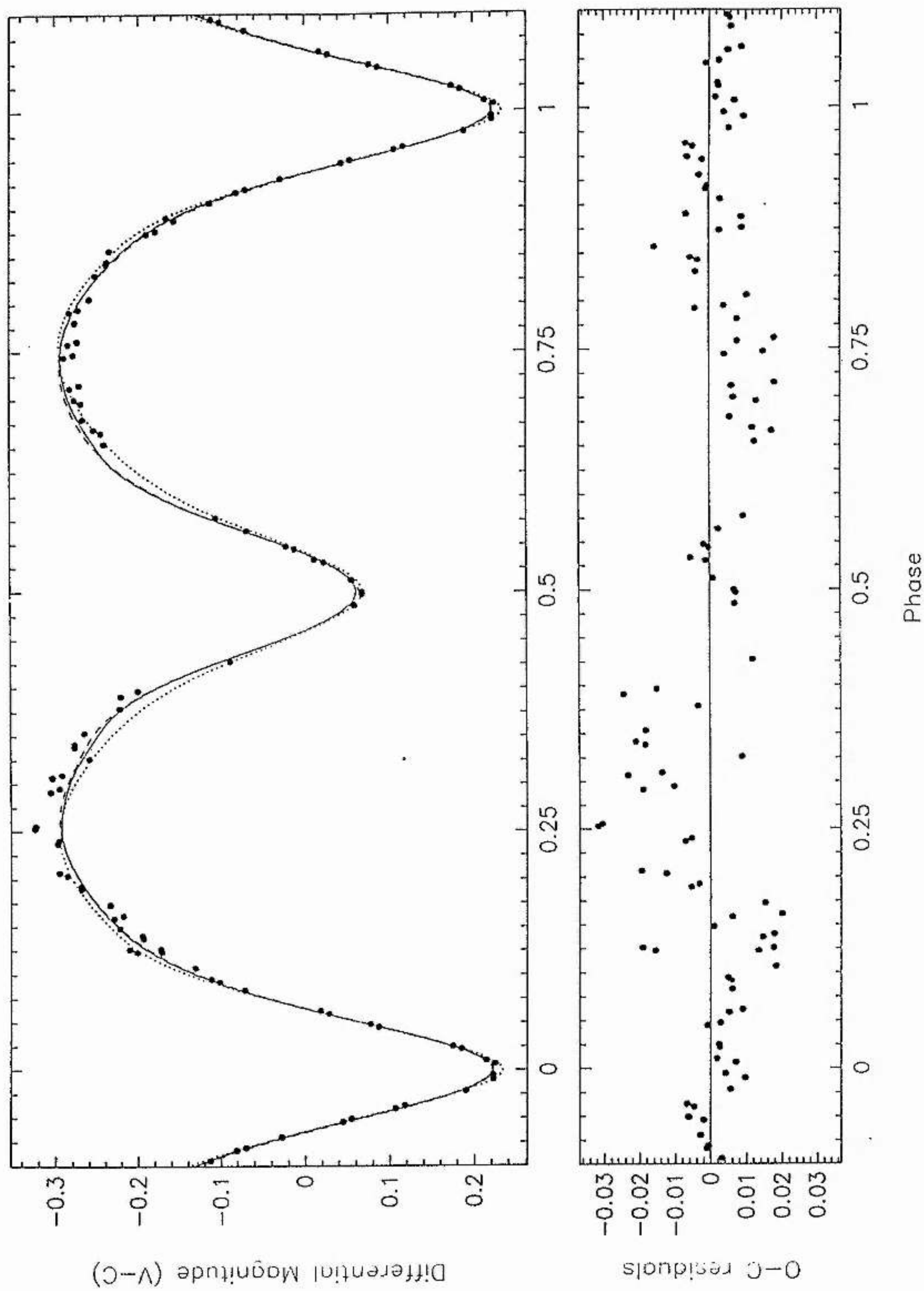

(The dotted line is a WUMA5 solution, the dashed line is a LIGHT2 solution with an enhanced secondary albedo, and the solid line is an alternative LIGHT2 solution involving a hot spot on the secondary component).

Figure 5.9: 1987 UKIRT *K* light curve of BX And. The three lines represent different types of contact solutions of these data. The lower plot shows the residuals of the these observations from the spot solution.

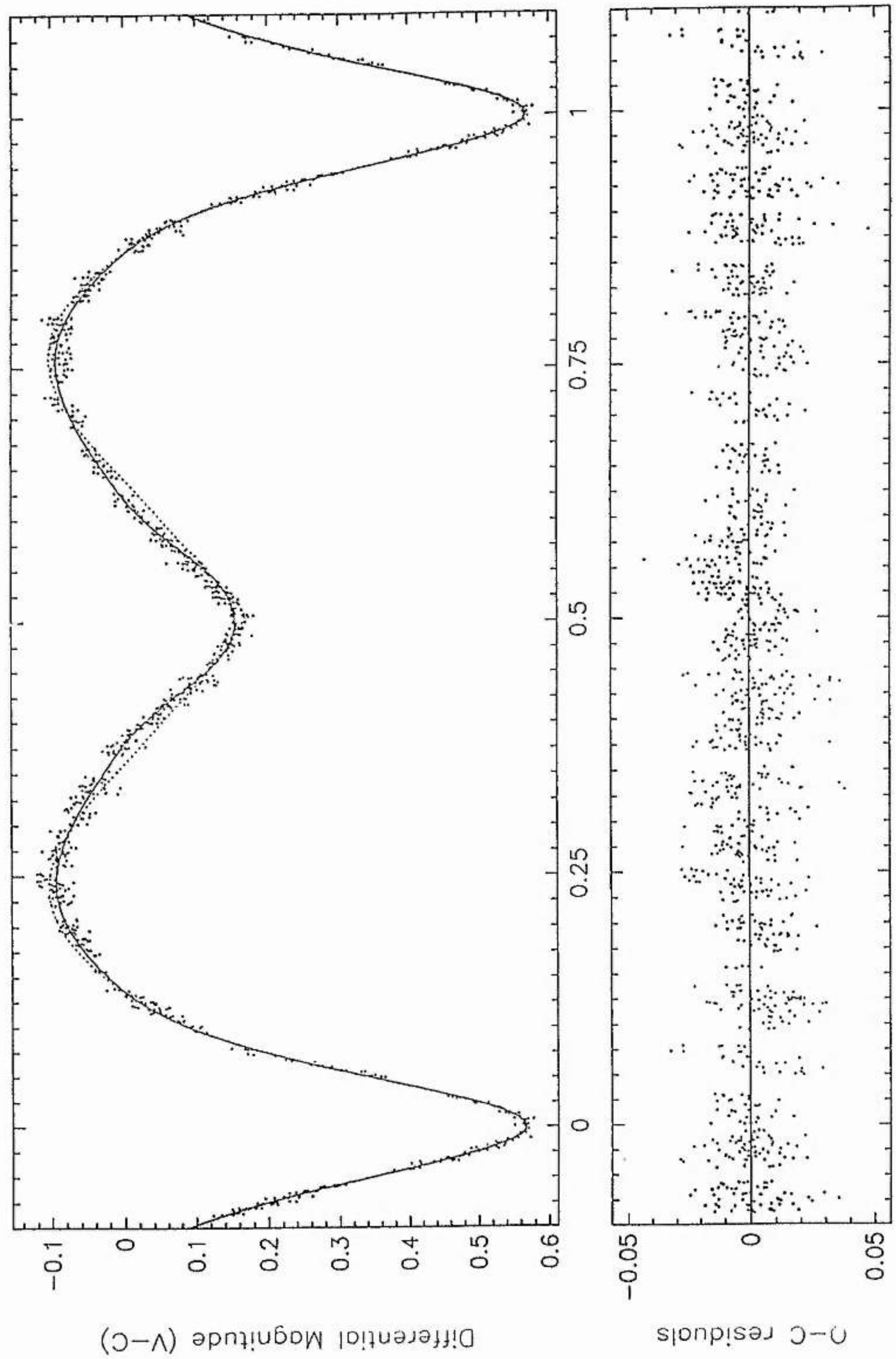

(The dotted line is a WUMA5 solution, the dashed line is a LIGHT2 solution with an enhanced secondary albedo, and the solid line is an alternative LIGHT2 solution involving a hot spot on the secondary component).

Figure 5.10: The *V* light curve of Samec *et al.* (1989) of BX And. The three lines represent different types of contact solutions of these data. The lower plot shows the residuals of the these observations from the spot solution.

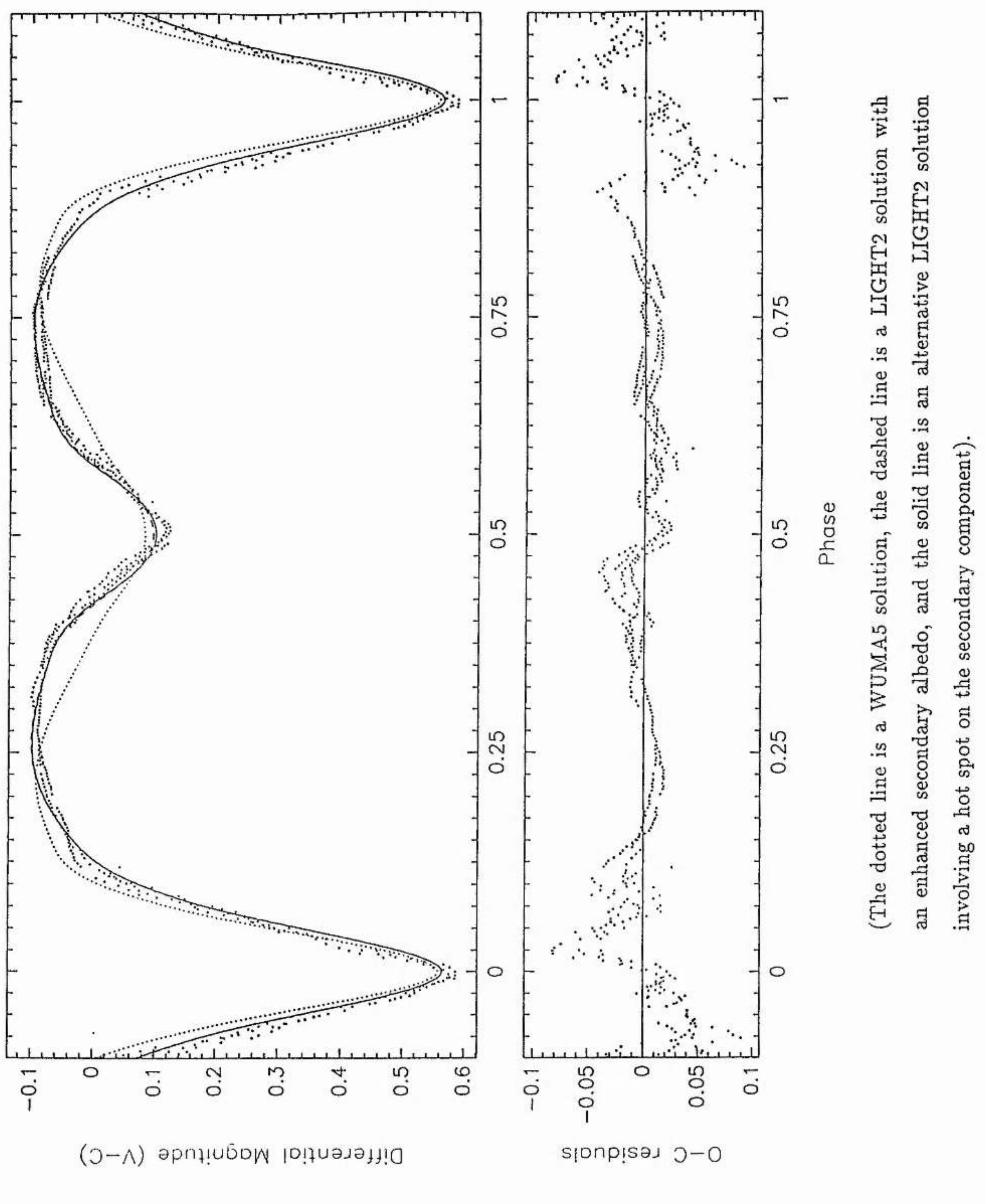

Figure 5.11: The *V* light curve of Rovithis & Rovithis-Livaniou (1984) of BX And. The three lines represent different types of contact solutions of these data. The lower plot shows the residuals of the these observations from the spot solution.

5.5 Discussion

The adopted photometric solution for BX And from this analysis is given in Table 5.7. This represents the mean fill-out factor, inclination and secondary component temperature for all the light curve solutions with the exception of the data of RRL. The errors quoted for f, i and T_2 are the standard deviations in each quantity. The volume radii of the primary component r_1 and the secondary component r_2 have been evaluated using the tabulation of Mochnacki (1984). The corresponding errors in the volume radii have been estimated by combining the errors in the determinations of the mass ratio and the fill-out factor.

$\alpha_{1,2}$	=	0.5 (fixed)
$\beta_{1,2}$	=	0.08 (fixed)
f	=	0.917 ± 0.049
$i\,(^\circ)$	=	74.55 ± 0.50
r_1	=	0.4484 ± 0.005
r_2	=	0.3264 ± 0.005
$T_2\,(\mathrm{K})$	=	4500 ± 120

Table 5.7: Adopted light curve solution for BX And.

The resulting astrophysical data for BX And are given in Table 5.8. An error of 200 K has been adopted in the secondary component temperature as the error of 120 K given in Table 5.7 is probably an underestimate, and takes no account of the uncertainty in the primary component temperature. The bolometric corrections employed in the calculation of absolute magnitudes and the distance have been taken from the compilation of Popper (1980).

A schematic diagram of BX And is given in Figure 5.12 based on the adopted light curve solution and including a spot of radius $36^\circ\!.5$ centred on the sub-stellar point on the secondary component.

A comparison of the masses, radii, temperatures and luminosities of the components of BX And (see Chapter 9) with those of other marginal-contact and contact binaries compiled by Hilditch *et al.* (1988), shows that the primary component is close to

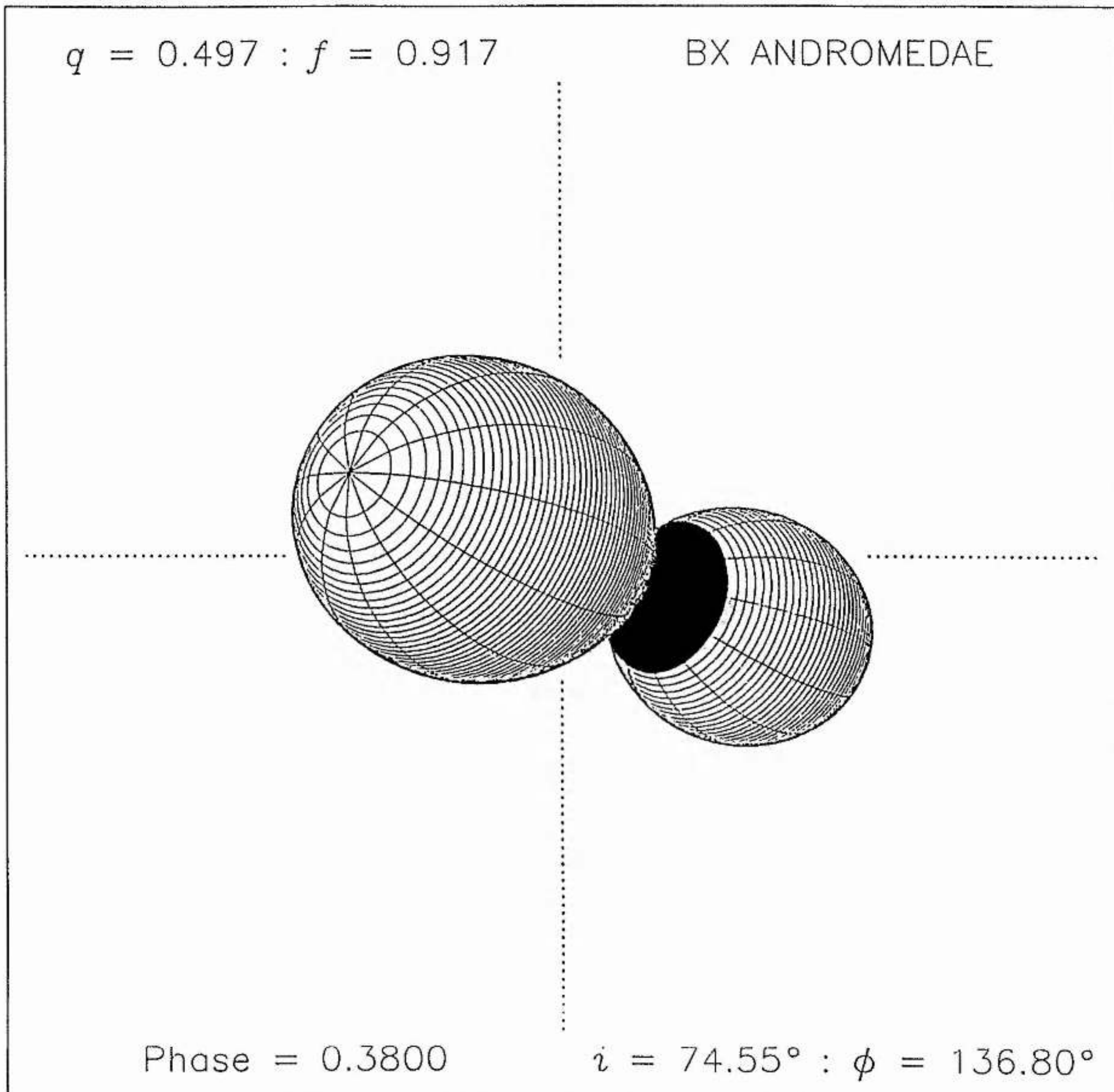

Figure 5.12: A schematic diagram of BX And at $0^{\mathrm{P}}.38$ based on this analysis. (A hot spot of radius $36^{\circ}.5$ centred on the sub-stellar point on the secondary component is also shown).

Absolute dimensions	Primary	Secondary
$M\,(M_\odot)$	1.52 ± 0.05	0.75 ± 0.03
$R\,(R_\odot)$	1.78 ± 0.03	1.30 ± 0.03
$log\,g$ (cgs)	4.12 ± 0.02	4.09 ± 0.02
T_{eff} (K)	6800 ± 200	4500 ± 200
$log\,L/L_\odot$	0.79 ± 0.05	-0.20 ± 0.08
M_{bol}	$2^{m}\!.79 \pm 0^{m}\!.13$	$5^{m}\!.26 \pm 0^{m}\!.20$
B.C.	$-0^{m}\!.02$	$-0^{m}\!.52$
M_V	$2^{m}\!.81 \pm 0^{m}\!.13$	$5^{m}\!.79 \pm 0^{m}\!.22$
$E_{(B-V)}$	$+0^{m}\!.04$	
Distance (pc)	160 ± 20	

Table 5.8: Astrophysical data for BX And.

the TAMS relationship of Vandenberg (1985) and has properties similar to the A-type contact binaries and the B-type marginal-contact systems. The secondary component is 2-3 times larger than expected for its ZAMS mass and occupies the same region in the M-R and M-L diagrams as other B-type secondaries like RT Scl and RS Ind, or the secondaries of W-type contact systems. Thus, although BX And is in a shallow contact state (like the W-type contact systems), luminosity transfer is incomplete, or indeed not yet established. Hence the secondary component (just like those of RT Scl and RS Ind) lies upwards and to the right of the ZAMS line in the HR diagram, as expected for its increased radius, and not to the left of the ZAMS line as for the secondaries of W-type contact systems.

BX And is therefore another example of the increasing number of shallow-contact / marginal-contact binaries displaying evidence of mass transfer between the two components, but not (yet) (see Chapter 9), the thermal contact achieved in a common convective envelope (Hilditch 1989).

5.6 References

Ashbrook, J., 1951. *Astr. J.*, **56**, 54.

Ashbrook, J., 1952. *Astr. J.*, **57**, 259.

Ashbrook, J., 1953. *Astr. J.*, **58**, 171.

Böhm-Vitense, E., 1981. *Ann. Rev. Astr. Astrophys.*, **19**, 295.

Braune, W., Hübscher, J. & Mundy, E., 1970. *Astr. Nachr.*, **292**, 185.

Braune, W., Hübscher, J. & Mundy, E., 1979. *Astr. Nachr.*, **300**, 165.

Braune, W., Hübscher, J. & Mundy, E., 1981. *Astr. Nachr.*, **302**, 53.

Castelaz, M., 1979. *Inf. Bull. Var. Stars*, No. 1554.

Chou, K.C., 1959. *Astr. J.*, **64**, 468.

Derman, E., Akalin, A. & Demircan, O., 1989. *Inf. Bull. Var. Stars*, No. 3325.

Eggen, O.J., 1967. *Mem. R. astr. Soc.*, **70**, 111.

Faulkner, D.R. & Kaitchuck, R.H., 1983. *Inf. Bull. Var. Stars*, No. 2321.

Gülmen, Ö., Güdür, N., Sezer, C., Eker, Z., Keskin, V. & Kilinc, B., 1988. *Inf. Bull. Var. Stars*, No. 3266.

Hilditch, R.W., 1989. In: *Algols, IAU Coll. No. 107*, p. 283, ed Batten, A.H., Kluwer, Dordrecht, Holland.

Hilditch, R.W. & Hill, G., 1975. *Mem. R. astr. Soc.*, **79**, 101.

Hilditch, R.W., King, D.J. & McFarlane, T.M., 1988. *Mon. Not. R. astr. Soc.*, **231**, 341.

Hill, G., Hilditch, R.W., Younger, F. & Fisher, W.A., 1975. *Mem. R. astr. Soc.*, **79**, 131.

Hübscher, J. & Lichtenknecker, D., 1988. *BAV*, No. 50.

Isles, J.E., 1985. *BAA Var. Star Section circ.*, No. 59.

Kizilirmak, A. & Pohl, E., 1974. *Inf. Bull. Var. Stars*, No. 937.

Kholopov, P.N., Samus, N.N., Frolov, M.S., Goranskij, V.P., Gorynya, N.A., Kireeva, N.N., Kukarkina, N.P., Kurochkin, N.E., Medvedeva, G.I., Perova, N.B., Shugarov, S.Yu., 1985. *General Catalogue of Variable Stars*, Vol. 1, Nauka Publishing House, Moscow.

Kwee, K.K. & van Woerden, H., 1956. *Bull. Astr. Inst. Neth.*, **12**, 327.

Locher, K., 1977a. *BBSAG Bull.*, No. 31.

Locher, K., 1977b. *BBSAG Bull.*, No. 35.

Locher, K., 1978a. *BBSAG Bull.*, No. 36.

Locher, K., 1978b. *BBSAG Bull.*, No. 39.

Locher, K., 1978c. *BBSAG Bull.*, No. 40.

Locher, K., 1987. *BBSAG Bull.*, No. 82.

Locher, K., 1988a. *BBSAG Bull.*, No. 86.

Locher, K., 1988b. *BBSAG Bull.*, No. 88.

Locher, K., 1989. *BBSAG Bull.*, No. 91.

Meyer, A., 1972. *Inf. Bull. Var. Stars*, No. 648.

Mochnacki, S.W., 1984. *Astrophys. J. Suppl.*, **55**, 551.

Oburka, O., 1965. *Bull. Astr. Inst. Czech.*, **16**, 212.

Pohl, E. & Kizilirmak, A., 1970. *Inf. Bull. Var. Stars*, No. 456.

Pohl, E. & Kizilirmak, A., 1972. *Inf. Bull. Var. Stars*, No. 647.

Pohl, E. & Kizilirmak, A., 1977. *Inf. Bull. Var. Stars*, No. 1358.

Pohl, E., Tunka, Z., Gülman, S. & Evren, S., 1985. *Inf. Bull. Var. Stars*, No. 2793.

Pohl, E., Akan, M.C., Ibanoglu, C., Sezer, C. & Güdür, N., 1986. *Inf. Bull. Var. Stars*, No. 3078.

Popper, D.M., 1980. *Ann. Rev. Astr. Astrophys.*, **18**, 115.

Robinson, L.J., 1965. *Inf. Bull. Var. Stars*, No. 119.

Rovithis, P. & Rovithis-Livaniou, H., 1982. *Inf. Bull. Var. Stars*, No. 2094.

Rovithis, P. & Rovithis-Livaniou, H., 1983. *Inf. Bull. Var. Stars*, No. 2424.

Rovithis, P. & Rovithis-Livaniou, H., 1984. *Astrophys. Space Sci.*, **105**, 171.

Russell, H.N. & Merrill, J.E., 1952. *Contr. Princeton Univ. Obs.*, No. 26.

Samec, R.G., Fuller, R.E. & Kaitchuck, R.H., 1989. *Astr. J.*, **97**, 1159.

Soloviev, A., 1945. *Astr. Circ. Acad. Sci. U.S.S.R.*, No. 44, 3.

Svolopoulos, S.N., 1957. *Astr. J.*, **62**, 330.

Todoran, I., 1965. *St. Cerc. Astron. Obs.*, **10**, 71.

Vandenburg, D.A., 1985. *Astrophys. J. Suppl.*, **58**, 711.

5.7 Appendix - New Photoelectric Data

This appendix tabulates the new photoelectric data for BX And presented in this study.

Tables 5.9, 5.10, and 5.11 list the V filter observations obtained with the Twin Photometric Telescope at St. Andrews during 1985 November, 1986 September - October, and 1988 October - November respectively.

Tables 5.12 and 5.13 give the J and K filter observations respectively, obtained with the United Kingdom Infrared Telescope during 1987 November.

Table 5.9: 1985 TPT V observations.

H.J.D.	Phase	(V-C)	H.J.D.	Phase	(V-C)	H.J.D.	Phase	(V-C)
2446372.31338	0.9040	+0.100	2446372.37878	0.0112	+0.547	2446372.45146	0.1304	+0.020
2446372.31407	0.9052	+0.093	2446372.37948	0.0124	+0.541	2446372.45216	0.1315	+0.018
2446372.31477	0.9063	+0.102	2446372.38017	0.0135	+0.535	2446372.45284	0.1326	+0.016
2446372.31546	0.9074	+0.099	2446372.38087	0.0147	+0.538	2446372.46019	0.1447	+0.003
2446372.31615	0.9086	+0.105	2446372.38258	0.0175	+0.530	2446372.46089	0.1458	+0.001
2446372.31761	0.9110	+0.123	2446372.38327	0.0186	+0.522	2446372.46158	0.1469	−0.002
2446372.31831	0.9121	+0.120	2446372.38397	0.0197	+0.520	2446372.46228	0.1481	−0.003
2446372.31900	0.9132	+0.130	2446372.38466	0.0209	+0.518	2446372.46297	0.1492	−0.010
2446372.31971	0.9144	+0.142	2446372.38537	0.0220	+0.509	2446372.46471	0.1521	−0.013
2446372.32039	0.9155	+0.124	2446372.38950	0.0288	+0.481	2446372.46540	0.1532	−0.016
2446372.32335	0.9204	+0.169	2446372.39021	0.0300	+0.473	2446372.46610	0.1543	−0.010
2446372.32405	0.9215	+0.182	2446372.39089	0.0311	+0.462	2446372.46679	0.1555	−0.018
2446372.32474	0.9227	+0.193	2446372.39158	0.0322	+0.460	2446372.46749	0.1566	−0.021
2446372.32544	0.9238	+0.193	2446372.39228	0.0334	+0.454	2446372.46927	0.1595	−0.029
2446372.32613	0.9249	+0.217	2446372.39486	0.0376	+0.424	2446372.46996	0.1607	−0.023
2446372.33128	0.9334	+0.256	2446372.39556	0.0387	+0.424	2446372.47066	0.1618	−0.026
2446372.33198	0.9345	+0.255	2446372.39625	0.0399	+0.410	2446372.47135	0.1630	−0.027
2446372.33267	0.9357	+0.256	2446372.39694	0.0410	+0.405	2446372.47205	0.1641	−0.030
2446372.33337	0.9368	+0.268	2446372.39765	0.0422	+0.398	2446372.47607	0.1707	−0.039
2446372.33406	0.9379	+0.269	2446372.39971	0.0455	+0.374	2446372.47677	0.1718	−0.043
2446372.33797	0.9443	+0.307	2446372.40040	0.0467	+0.368	2446372.47746	0.1730	−0.042
2446372.33867	0.9455	+0.327	2446372.40111	0.0478	+0.361	2446372.47816	0.1741	−0.041
2446372.33936	0.9466	+0.348	2446372.40179	0.0489	+0.355	2446372.47885	0.1752	−0.044
2446372.34006	0.9478	+0.319	2446372.40249	0.0501	+0.349	2446372.48088	0.1786	−0.046
2446372.34075	0.9489	+0.359	2446372.40418	0.0529	+0.328	2446372.48157	0.1797	−0.049
2446372.34262	0.9520	+0.369	2446372.40487	0.0540	+0.322	2446372.48227	0.1809	−0.052
2446372.34331	0.9531	+0.364	2446372.40556	0.0551	+0.318	2446372.48296	0.1820	−0.056
2446372.34400	0.9542	+0.367	2446372.40626	0.0563	+0.304	2446372.49083	0.1949	−0.073
2446372.34470	0.9554	+0.378	2446372.40695	0.0574	+0.299	2446372.49223	0.1972	−0.074
2446372.34539	0.9565	+0.383	2446372.42213	0.0823	+0.170	2446376.49981	0.7658	−0.087
2446372.34848	0.9616	+0.416	2446372.42282	0.0834	+0.170	2446376.50050	0.7669	−0.084
2446372.34918	0.9627	+0.426	2446372.42352	0.0846	+0.162	2446376.50120	0.7680	−0.083
2446372.34987	0.9638	+0.430	2446372.42421	0.0857	+0.156	2446376.50189	0.7692	−0.085
2446372.35056	0.9650	+0.440	2446372.42490	0.0868	+0.147	2446376.50260	0.7703	−0.085
2446372.35126	0.9661	+0.444	2446372.42740	0.0909	+0.134	2446376.50401	0.7727	−0.088
2446372.35870	0.9783	+0.515	2446372.42809	0.0920	+0.132	2446376.50470	0.7738	−0.080
2446372.35940	0.9795	+0.517	2446372.42878	0.0932	+0.128	2446376.50540	0.7749	−0.083
2446372.36009	0.9806	+0.523	2446372.42948	0.0943	+0.126	2446376.50609	0.7761	−0.082
2446372.36080	0.9818	+0.531	2446372.43017	0.0955	+0.119	2446376.50679	0.7772	−0.085
2446372.36148	0.9829	+0.533	2446372.43232	0.0990	+0.106	2446376.51000	0.7825	−0.076
2446372.36301	0.9854	+0.540	2446372.43302	0.1001	+0.103	2446376.51070	0.7836	−0.076
2446372.36370	0.9865	+0.545	2446372.43372	0.1013	+0.100	2446376.51140	0.7848	−0.076
2446372.36440	0.9877	+0.549	2446372.43441	0.1024	+0.092	2446376.51209	0.7859	−0.077
2446372.36509	0.9888	+0.555	2446372.43510	0.1035	+0.092	2446376.51278	0.7870	−0.078
2446372.36578	0.9899	+0.556	2446372.43952	0.1108	+0.068	2446376.52223	0.8025	−0.063
2446372.36884	0.9949	+0.565	2446372.44022	0.1119	+0.068	2446376.52292	0.8036	−0.063
2446372.36953	0.9961	+0.551	2446372.44092	0.1131	+0.058	2446376.52363	0.8048	−0.072
2446372.37024	0.9972	+0.566	2446372.44161	0.1142	+0.056	2446376.52431	0.8059	−0.062
2446372.37092	0.9983	+0.569	2446372.44230	0.1153	+0.054	2446376.52500	0.8071	−0.057
2446372.37162	0.9995	+0.570	2446372.44556	0.1207	+0.038	2446376.52909	0.8138	−0.053
2446372.37335	0.0023	+0.562	2446372.44626	0.1218	+0.032	2446376.52978	0.8149	−0.046
2446372.37405	0.0035	+0.563	2446372.44695	0.1230	+0.030	2446376.53048	0.8160	−0.051
2446372.37474	0.0046	+0.560	2446372.44765	0.1241	+0.031	2446376.53117	0.8172	−0.042
2446372.37544	0.0058	+0.558	2446372.44834	0.1252	+0.028	2446376.53187	0.8183	−0.044
2446372.37613	0.0069	+0.551	2446372.45007	0.1281	+0.027	2446376.53331	0.8207	−0.040
2446372.37809	0.0101	+0.553	2446372.45076	0.1292	+0.025	2446376.53401	0.8218	−0.039

Table 5.9: 1985 TPT *V* observations — *continued.*

H.J.D.	Phase	(V-C)	H.J.D.	Phase	(V-C)	H.J.D.	Phase	(V-C)
2446376.53470	0.8230	−0.039	2446376.65116	0.0138	+0.535	2446380.48171	0.2923	−0.081
2446376.53540	0.8241	−0.033	2446376.65186	0.0150	+0.540	2446380.48315	0.2946	−0.084
2446376.53609	0.8252	−0.036	2446376.65528	0.0206	+0.513	2446380.48384	0.2958	−0.088
2446376.54136	0.8339	−0.025	2446376.65597	0.0217	+0.503	2446380.48453	0.2969	−0.081
2446376.54205	0.8350	−0.022	2446376.65666	0.0229	+0.505	2446380.48523	0.2980	−0.083
2446376.54275	0.8361	−0.022	2446376.65735	0.0240	+0.494	2446380.48592	0.2992	−0.083
2446376.54344	0.8373	−0.023	2446376.65805	0.0251	+0.479	2446380.49081	0.3072	−0.079
2446376.54414	0.8384	−0.023	2446376.65992	0.0282	+0.468	2446380.49150	0.3083	−0.078
2446376.54749	0.8439	−0.016	2446376.66062	0.0293	+0.464	2446380.49220	0.3095	−0.077
2446376.54819	0.8451	−0.011	2446376.66131	0.0305	+0.459	2446380.49289	0.3106	−0.070
2446376.54888	0.8462	−0.012	2446376.66201	0.0316	+0.440	2446380.49359	0.3117	−0.075
2446376.54958	0.8473	−0.015	2446376.66270	0.0328	+0.447	2446380.49547	0.3148	−0.072
2446376.55028	0.8485	−0.005	2446376.66534	0.0371	+0.423	2446380.49617	0.3160	−0.072
2446376.55158	0.8506	−0.011	2446376.66605	0.0382	+0.412	2446380.49686	0.3171	−0.070
2446376.55227	0.8518	−0.002	2446376.66673	0.0394	+0.411	2446380.49756	0.3182	−0.071
2446376.55297	0.8529	+0.001	2446376.66742	0.0405	+0.397	2446380.49825	0.3194	−0.068
2446376.55366	0.8540	+0.005	2446376.66812	0.0416	+0.393	2446380.50974	0.3382	−0.056
2446376.55436	0.8552	+0.005	2446376.67044	0.0454	+0.371	2446380.51044	0.3394	−0.056
2446376.56200	0.8677	+0.026	2446376.67114	0.0466	+0.370	2446380.51113	0.3405	−0.050
2446376.56269	0.8688	+0.027	2446376.67183	0.0477	+0.356	2446380.51183	0.3416	−0.049
2446376.56338	0.8700	+0.037	2446376.67253	0.0489	+0.350	2446380.51252	0.3428	−0.046
2446376.56408	0.8711	+0.040	2446376.67323	0.0500	+0.344	2446380.51430	0.3457	−0.050
2446376.56477	0.8722	+0.046	2446376.67392	0.0511	+0.329	2446380.51500	0.3468	−0.044
2446376.56644	0.8750	+0.045	2446376.67461	0.0523	+0.335	2446380.51569	0.3480	−0.045
2446376.56713	0.8761	+0.044	2446376.67531	0.0534	+0.315	2446380.51639	0.3491	−0.040
2446376.56783	0.8773	+0.053	2446376.67600	0.0546	+0.312	2446380.51708	0.3502	−0.043
2446376.59298	0.9185	+0.183	2446376.67669	0.0557	+0.311	2446380.52149	0.3575	−0.037
2446376.59367	0.9196	+0.197	2446376.69476	0.0853	+0.159	2446380.52220	0.3586	−0.034
2446376.59437	0.9208	+0.200	2446376.69546	0.0864	+0.150	2446380.52288	0.3597	−0.033
2446376.59506	0.9219	+0.210	2446376.69615	0.0876	+0.144	2446380.52357	0.3609	−0.028
2446376.59576	0.9230	+0.207	2446376.69684	0.0887	+0.139	2446380.52573	0.3644	−0.028
2446376.59747	0.9258	+0.229	2446376.69754	0.0899	+0.128	2446380.52642	0.3655	−0.025
2446376.59816	0.9270	+0.232	2446376.69895	0.0922	+0.117	2446380.52712	0.3667	−0.027
2446376.59886	0.9281	+0.242	2446376.69965	0.0933	+0.120	2446380.52781	0.3678	−0.027
2446376.59955	0.9292	+0.243	2446376.70034	0.0944	+0.122	2446380.52852	0.3690	−0.025
2446376.60026	0.9304	+0.248	2446376.70103	0.0956	+0.109	2446380.53593	0.3811	−0.001
2446376.61241	0.9503	+0.363	2446376.70173	0.0967	+0.105	2446380.53663	0.3823	−0.001
2446376.61358	0.9522	+0.377	2446376.70319	0.0991	+0.107	2446380.53732	0.3834	+0.001
2446376.61428	0.9534	+0.380	2446376.70388	0.1002	+0.097	2446380.53802	0.3846	+0.001
2446376.61498	0.9545	+0.373	2446376.70458	0.1014	+0.090	2446380.54963	0.4036	+0.020
2446376.61566	0.9557	+0.388	2446376.70527	0.1025	+0.094	2446380.55033	0.4047	+0.025
2446376.62140	0.9651	+0.455	2446376.70597	0.1037	+0.097	2446380.55102	0.4059	+0.031
2446376.62210	0.9662	+0.457	2446380.46475	0.2645	−0.103	2446380.55171	0.4070	+0.032
2446376.62279	0.9673	+0.458	2446380.46545	0.2656	−0.104	2446380.55240	0.4081	+0.039
2446376.62349	0.9685	+0.453	2446380.46614	0.2667	−0.105	2446380.55435	0.4113	+0.037
2446376.62418	0.9696	+0.467	2446380.46684	0.2679	−0.100	2446380.55506	0.4125	+0.044
2446376.63032	0.9797	+0.516	2446380.46753	0.2690	−0.099	2446380.55574	0.4136	+0.041
2446376.63101	0.9808	+0.525	2446380.46904	0.2715	−0.105	2446380.55643	0.4147	+0.049
2446376.63171	0.9820	+0.527	2446380.46973	0.2726	−0.100	2446380.55713	0.4159	+0.049
2446376.63240	0.9831	+0.534	2446380.47043	0.2738	−0.095	2446380.56788	0.4335	+0.085
2446376.63309	0.9842	+0.532	2446380.47112	0.2749	−0.089	2446380.56857	0.4346	+0.086
2446376.63558	0.9883	+0.539	2446380.47181	0.2760	−0.096	2446380.56927	0.4358	+0.091
2446376.63628	0.9894	+0.538	2446380.47892	0.2877	−0.087	2446380.56996	0.4369	+0.084
2446376.63697	0.9906	+0.553	2446380.47962	0.2888	−0.087	2446380.57066	0.4381	+0.086
2446376.63767	0.9917	+0.544	2446380.48031	0.2900	−0.084	2446380.58723	0.4652	+0.140
2446376.63836	0.9929	+0.545	2446380.48100	0.2911	−0.091	2446380.58793	0.4664	+0.131

Table 5.9: 1985 TPT *V* observations — *continued.*

H.J.D.	Phase	(V-C)	H.J.D.	Phase	(V-C)	H.J.D.	Phase	(V-C)
2446380.58862	0.4675	+0.137	2446380.62142	0.5213	+0.147	2446380.64240	0.5556	+0.105
2446380.58931	0.4686	+0.134	2446380.62212	0.5224	+0.151	2446380.64310	0.5568	+0.101
2446380.59002	0.4698	+0.141	2446380.62281	0.5235	+0.138	2446380.64379	0.5579	+0.107
2446380.59443	0.4770	+0.135	2446380.62540	0.5278	+0.132	2446380.65946	0.5836	+0.060
2446380.59512	0.4782	+0.142	2446380.62610	0.5289	+0.132	2446380.66016	0.5848	+0.055
2446380.59582	0.4793	+0.142	2446380.62679	0.5301	+0.135	2446380.66085	0.5859	+0.053
2446380.59651	0.4804	+0.148	2446380.62749	0.5312	+0.129	2446380.66155	0.5870	+0.059
2446380.59721	0.4816	+0.146	2446380.62818	0.5323	+0.128	2446380.66225	0.5882	+0.053
2446380.60831	0.4998	+0.130	2446380.63541	0.5442	+0.119	2446380.66768	0.5971	+0.033
2446380.61317	0.5077	+0.145	2446380.63611	0.5453	+0.117	2446380.66837	0.5982	+0.034
2446380.61386	0.5089	+0.147	2446380.63680	0.5465	+0.113	2446380.66906	0.5993	+0.023
2446380.61525	0.5111	+0.140	2446380.63750	0.5476	+0.113	2446380.66975	0.6005	+0.019
2446380.61595	0.5123	+0.148	2446380.63819	0.5487	+0.117	2446380.69282	0.6383	−0.030
2446380.62003	0.5190	+0.149	2446380.64102	0.5534	+0.113	2446380.69352	0.6394	−0.031
2446380.62073	0.5201	+0.146	2446380.64102	0.5534	+0.113			

Table 5.10: 1986 TPT V observations.

H.J.D.	Phase	(V-C)	H.J.D.	Phase	(V-C)	H.J.D.	Phase	(V-C)
2446688.40730	0.9957	+0.556	2446688.48325	0.1201	+0.050	2446688.57208	0.2657	−0.098
2446688.40799	0.9968	+0.563	2446688.48394	0.1213	+0.039	2446688.57486	0.2703	−0.095
2446688.40870	0.9980	+0.567	2446688.48464	0.1224	+0.041	2446688.57554	0.2714	−0.098
2446688.40938	0.9991	+0.566	2446688.48885	0.1293	+0.025	2446688.57623	0.2725	−0.095
2446688.41008	0.0002	+0.554	2446688.48954	0.1305	+0.020	2446688.57693	0.2737	−0.093
2446688.41189	0.0032	+0.564	2446688.49024	0.1316	+0.016	2446688.57762	0.2748	−0.099
2446688.41259	0.0043	+0.566	2446688.49093	0.1327	+0.017	2446688.57922	0.2774	−0.084
2446688.41328	0.0055	+0.564	2446688.49162	0.1339	+0.015	2446688.57990	0.2786	−0.085
2446688.41398	0.0066	+0.563	2446688.50263	0.1519	−0.022	2446688.58060	0.2797	−0.078
2446688.41467	0.0077	+0.560	2446688.50333	0.1531	−0.018	2446688.58129	0.2808	−0.083
2446688.41641	0.0106	+0.556	2446688.50401	0.1542	−0.021	2446688.58199	0.2820	−0.082
2446688.41709	0.0117	+0.543	2446688.50471	0.1553	−0.027	2446688.58343	0.2843	−0.080
2446688.41778	0.0128	+0.558	2446688.50540	0.1565	−0.036	2446688.58412	0.2855	−0.079
2446688.41848	0.0140	+0.534	2446688.50710	0.1592	−0.023	2446688.58481	0.2866	−0.079
2446688.41916	0.0151	+0.547	2446688.50780	0.1604	−0.036	2446688.58550	0.2877	−0.076
2446688.42341	0.0221	+0.513	2446688.50848	0.1615	−0.032	2446688.58620	0.2889	−0.078
2446688.42410	0.0232	+0.510	2446688.50917	0.1626	−0.035	2446688.58752	0.2910	−0.077
2446688.42480	0.0243	+0.496	2446688.50987	0.1638	−0.035	2446688.58819	0.2921	−0.076
2446688.42549	0.0255	+0.496	2446688.51173	0.1668	−0.057	2446688.58888	0.2933	−0.077
2446688.42619	0.0266	+0.488	2446688.51241	0.1679	−0.052	2446688.58958	0.2944	−0.078
2446688.43871	0.0471	+0.349	2446688.51311	0.1691	−0.058	2446688.59027	0.2956	−0.072
2446688.43941	0.0483	+0.333	2446688.51381	0.1702	−0.051	2446688.60368	0.3175	−0.065
2446688.44011	0.0494	+0.343	2446688.51450	0.1714	−0.062	2446688.60437	0.3187	−0.056
2446688.44078	0.0505	+0.323	2446688.52136	0.1826	−0.048	2446688.60506	0.3198	−0.054
2446688.44341	0.0548	+0.297	2446688.52206	0.1838	−0.055	2446688.60575	0.3209	−0.050
2446688.44410	0.0560	+0.296	2446688.52275	0.1849	−0.049	2446688.60644	0.3221	−0.052
2446688.44480	0.0571	+0.290	2446688.52344	0.1860	−0.056	2446688.60803	0.3247	−0.050
2446688.44548	0.0582	+0.289	2446688.52414	0.1872	−0.056	2446688.60941	0.3269	−0.054
2446688.44619	0.0594	+0.276	2446688.52569	0.1897	−0.060	2446688.61010	0.3281	−0.050
2446688.44787	0.0622	+0.274	2446688.52638	0.1908	−0.058	2446688.61079	0.3292	−0.054
2446688.44857	0.0633	+0.278	2446688.52708	0.1920	−0.060	2446688.61259	0.3321	−0.050
2446688.44924	0.0644	+0.260	2446688.52778	0.1931	−0.064	2446688.61328	0.3333	−0.052
2446688.44994	0.0655	+0.250	2446688.52847	0.1943	−0.064	2446688.61397	0.3344	−0.049
2446688.45063	0.0667	+0.248	2446688.54294	0.2180	−0.078	2446688.61466	0.3355	−0.048
2446688.45288	0.0704	+0.232	2446688.54363	0.2191	−0.077	2446688.61535	0.3367	−0.055
2446688.45356	0.0715	+0.228	2446688.54432	0.2202	−0.077	2446688.61938	0.3433	−0.035
2446688.45425	0.0726	+0.219	2446688.54502	0.2214	−0.078	2446688.62008	0.3444	−0.038
2446688.45495	0.0738	+0.210	2446688.54571	0.2225	−0.081	2446688.62077	0.3455	−0.038
2446688.45564	0.0749	+0.215	2446688.54784	0.2260	−0.079	2446688.62147	0.3467	−0.036
2446688.46861	0.0962	+0.122	2446688.54854	0.2272	−0.075	2446688.62215	0.3478	−0.034
2446688.46931	0.0973	+0.119	2446688.54923	0.2283	−0.075	2446688.63297	0.3655	−0.020
2446688.46998	0.0984	+0.111	2446688.54993	0.2294	−0.076	2446688.63366	0.3667	−0.022
2446688.47068	0.0995	+0.107	2446688.55061	0.2306	−0.083	2446688.63436	0.3678	−0.015
2446688.47137	0.1007	+0.102	2446688.55250	0.2336	−0.090	2446688.63504	0.3689	−0.010
2446688.47343	0.1041	+0.091	2446688.55319	0.2348	−0.082	2446688.63574	0.3701	−0.012
2446688.47412	0.1052	+0.087	2446688.55388	0.2359	−0.091	2446688.63688	0.3720	−0.010
2446688.47481	0.1063	+0.087	2446688.55457	0.2370	−0.091	2446688.63756	0.3731	−0.010
2446688.47550	0.1074	+0.078	2446688.55526	0.2382	−0.084	2446688.63826	0.3742	−0.006
2446688.47620	0.1086	+0.083	2446688.55746	0.2418	−0.088	2446688.63894	0.3753	−0.007
2446688.47797	0.1115	+0.069	2446688.55816	0.2429	−0.085	2446688.63964	0.3765	−0.001
2446688.47865	0.1126	+0.068	2446688.55884	0.2440	−0.089	2446688.64133	0.3792	−0.003
2446688.47935	0.1138	+0.065	2446688.55953	0.2452	−0.087	2446688.64202	0.3804	−0.005
2446688.48004	0.1149	+0.060	2446688.56023	0.2463	−0.087	2446688.64272	0.3815	−0.006
2446688.48074	0.1160	+0.058	2446688.57001	0.2623	−0.094	2446688.64340	0.3826	+0.000
2446688.48187	0.1179	+0.055	2446688.57070	0.2635	−0.103	2446688.64409	0.3838	+0.004
2446688.48255	0.1190	+0.043	2446688.57138	0.2646	−0.089	2446688.65533	0.4022	+0.035

Table 5.10: 1986 TPT *V* observations — *continued.*

H.J.D.	Phase	(V-C)	H.J.D.	Phase	(V-C)	H.J.D.	Phase	(V-C)
2446688.65601	0.4033	+0.035	2446705.51319	0.0329	+0.449	2446709.46594	0.5117	+0.148
2446688.65671	0.4045	+0.041	2446705.51389	0.0341	+0.440	2446709.46664	0.5128	+0.152
2446688.65740	0.4056	+0.049	2446705.51458	0.0352	+0.433	2446709.46774	0.5146	+0.147
2446688.65810	0.4067	+0.048	2446705.52531	0.0528	+0.331	2446709.46842	0.5157	+0.147
2446688.65914	0.4084	+0.047	2446705.52600	0.0539	+0.323	2446709.46912	0.5169	+0.144
2446688.65985	0.4096	+0.052	2446705.52670	0.0551	+0.316	2446709.46981	0.5180	+0.144
2446688.66052	0.4107	+0.055	2446705.52739	0.0562	+0.314	2446709.47050	0.5191	+0.141
2446688.66121	0.4118	+0.058	2446705.52809	0.0574	+0.305	2446709.47231	0.5221	+0.149
2446688.66191	0.4130	+0.051	2446705.52974	0.0601	+0.293	2446709.47298	0.5232	+0.146
2446688.66295	0.4147	+0.061	2446705.53044	0.0612	+0.284	2446709.47368	0.5243	+0.134
2446688.66364	0.4158	+0.068	2446705.53113	0.0623	+0.276	2446709.47437	0.5255	+0.140
2446688.66432	0.4169	+0.064	2446705.53183	0.0635	+0.271	2446709.47506	0.5266	+0.135
2446688.66502	0.4181	+0.069	2446705.53251	0.0646	+0.267	2446709.47619	0.5285	+0.142
2446688.66571	0.4192	+0.067	2446705.53424	0.0674	+0.244	2446709.47687	0.5296	+0.138
2446705.47494	0.9702	+0.472	2446705.53494	0.0686	+0.243	2446709.47756	0.5307	+0.141
2446705.47563	0.9714	+0.476	2446705.53563	0.0697	+0.240	2446709.47826	0.5318	+0.135
2446705.47633	0.9725	+0.477	2446705.53633	0.0709	+0.234	2446709.47895	0.5330	+0.133
2446705.47702	0.9736	+0.489	2446705.53701	0.0720	+0.225	2446709.48085	0.5361	+0.133
2446705.47771	0.9748	+0.498	2446705.53883	0.0750	+0.215	2446709.48153	0.5372	+0.131
2446705.47919	0.9772	+0.504	2446705.53952	0.0761	+0.206	2446709.48223	0.5384	+0.128
2446705.47988	0.9783	+0.514	2446705.54022	0.0772	+0.191	2446709.48294	0.5395	+0.125
2446705.48058	0.9795	+0.504	2446705.54090	0.0783	+0.192	2446709.48362	0.5406	+0.121
2446705.48127	0.9806	+0.523	2446705.54159	0.0795	+0.187	2446709.48468	0.5424	+0.118
2446705.48195	0.9817	+0.530	2446705.54273	0.0813	+0.177	2446709.48537	0.5435	+0.120
2446705.48318	0.9837	+0.532	2446705.54342	0.0825	+0.177	2446709.48606	0.5446	+0.116
2446705.48387	0.9849	+0.542	2446705.54412	0.0836	+0.177	2446709.48675	0.5458	+0.120
2446705.48457	0.9860	+0.534	2446705.54481	0.0848	+0.162	2446709.48745	0.5469	+0.113
2446705.48526	0.9871	+0.544	2446705.54549	0.0859	+0.152	2446709.49442	0.5583	+0.098
2446705.48595	0.9883	+0.549	2446709.43784	0.4656	+0.129	2446709.49511	0.5595	+0.094
2446705.48788	0.9914	+0.558	2446709.43855	0.4668	+0.134	2446709.49581	0.5606	+0.091
2446705.48857	0.9926	+0.566	2446709.43922	0.4679	+0.131	2446709.49650	0.5617	+0.088
2446705.48927	0.9937	+0.562	2446709.43991	0.4690	+0.133	2446709.49719	0.5629	+0.089
2446705.48996	0.9949	+0.567	2446709.44062	0.4702	+0.132	2446709.49919	0.5661	+0.089
2446705.49065	0.9960	+0.566	2446709.44239	0.4731	+0.137	2446709.49988	0.5673	+0.086
2446705.49431	0.0020	+0.567	2446709.44307	0.4742	+0.141	2446709.50057	0.5684	+0.086
2446705.49500	0.0031	+0.564	2446709.44377	0.4753	+0.141	2446709.50127	0.5696	+0.077
2446705.49569	0.0042	+0.566	2446709.44446	0.4764	+0.147	2446709.50196	0.5707	+0.078
2446705.49639	0.0054	+0.562	2446709.44517	0.4776	+0.145	2446709.50265	0.5718	+0.076
2446705.49708	0.0065	+0.555	2446709.44706	0.4807	+0.146	2446709.50334	0.5730	+0.073
2446705.49870	0.0092	+0.556	2446709.44774	0.4818	+0.148	2446709.50403	0.5741	+0.074
2446705.49940	0.0103	+0.549	2446709.44843	0.4830	+0.152	2446709.50473	0.5752	+0.067
2446705.50009	0.0115	+0.548	2446709.44913	0.4841	+0.156	2446709.50542	0.5764	+0.067
2446705.50078	0.0126	+0.545	2446709.44982	0.4852	+0.147	2446709.51708	0.5955	+0.036
2446705.50148	0.0137	+0.539	2446709.45180	0.4885	+0.146	2446709.51777	0.5966	+0.039
2446705.50295	0.0161	+0.534	2446709.45250	0.4896	+0.144	2446709.51848	0.5978	+0.040
2446705.50364	0.0173	+0.522	2446709.45319	0.4908	+0.146	2446709.51915	0.5989	+0.033
2446705.50431	0.0184	+0.525	2446709.45388	0.4919	+0.149	2446709.51984	0.6000	+0.033
2446705.50503	0.0196	+0.522	2446709.45458	0.4930	+0.150	2446709.52143	0.6026	+0.030
2446705.50573	0.0207	+0.511	2446709.45671	0.4965	+0.148	2446709.52213	0.6037	+0.031
2446705.50726	0.0232	+0.501	2446709.45740	0.4977	+0.152	2446709.52282	0.6049	+0.031
2446705.50797	0.0244	+0.497	2446709.45810	0.4988	+0.153	2446709.52351	0.6060	+0.028
2446705.50867	0.0255	+0.488	2446709.45879	0.4999	+0.151	2446709.52420	0.6071	+0.021
2446705.50936	0.0267	+0.492	2446709.45949	0.5011	+0.155	2446709.52489	0.6083	+0.021
2446705.51007	0.0278	+0.482	2446709.46387	0.5083	+0.153	2446709.52559	0.6094	+0.025
2446705.51180	0.0307	+0.463	2446709.46456	0.5094	+0.147	2446709.52629	0.6106	+0.019
2446705.51250	0.0318	+0.458	2446709.46526	0.5105	+0.148	2446709.52697	0.6117	+0.016

Table 5.10: 1986 TPT *V* observations — *continued.*

H.J.D.	Phase	(V-C)	H.J.D.	Phase	(V-C)	H.J.D.	Phase	(V-C)
2446709.52766	0.6128	+0.012	2446709.60810	0.7447	−0.088	2446714.40110	0.6006	+0.020
2446709.52990	0.6165	+0.009	2446709.60879	0.7458	−0.088	2446714.40178	0.6017	+0.020
2446709.53059	0.6176	+0.008	2446709.61018	0.7481	−0.087	2446714.40247	0.6028	+0.019
2446709.53128	0.6187	+0.006	2446709.61088	0.7492	−0.087	2446714.40317	0.6040	+0.022
2446709.53196	0.6199	+0.002	2446709.61157	0.7503	−0.082	2446714.40749	0.6111	+0.005
2446709.53266	0.6210	+0.008	2446709.61225	0.7515	−0.083	2446714.40818	0.6122	+0.003
2446709.53487	0.6246	−0.001	2446709.61296	0.7526	−0.090	2446714.40887	0.6133	+0.003
2446709.53556	0.6258	−0.006	2446709.61364	0.7537	−0.089	2446714.40957	0.6145	+0.003
2446709.53625	0.6269	−0.001	2446709.61434	0.7549	−0.088	2446714.41025	0.6156	+0.002
2446709.53694	0.6280	−0.011	2446709.61503	0.7560	−0.085	2446714.41262	0.6195	−0.008
2446709.53763	0.6292	−0.008	2446709.61853	0.7618	−0.079	2446714.41332	0.6206	−0.002
2446709.54439	0.6402	−0.017	2446709.61922	0.7629	−0.077	2446714.41401	0.6217	−0.003
2446709.54509	0.6414	−0.023	2446709.61991	0.7640	−0.078	2446714.41470	0.6229	−0.009
2446709.54578	0.6425	−0.018	2446709.62060	0.7651	−0.078	2446714.41539	0.6240	−0.007
2446709.55003	0.6495	−0.025	2446709.62129	0.7663	−0.076	2446714.41668	0.6261	−0.010
2446709.55074	0.6506	−0.027	2446709.62199	0.7674	−0.073	2446714.41737	0.6273	−0.012
2446709.55142	0.6518	−0.027	2446714.36381	0.5395	+0.090	2446714.41806	0.6284	−0.011
2446709.55211	0.6529	−0.029	2446714.36450	0.5406	+0.095	2446714.41875	0.6295	−0.015
2446709.55280	0.6540	−0.030	2446714.36519	0.5417	+0.095	2446714.41944	0.6306	−0.015
2446709.55349	0.6551	−0.031	2446714.36589	0.5429	+0.088	2446714.43465	0.6556	−0.039
2446709.55420	0.6563	−0.031	2446714.36658	0.5440	+0.087	2446714.43534	0.6567	−0.035
2446709.55488	0.6574	−0.030	2446714.36812	0.5465	+0.080	2446714.43603	0.6578	−0.046
2446709.55557	0.6586	−0.033	2446714.36882	0.5477	+0.083	2446714.43672	0.6590	−0.040
2446709.57134	0.6844	−0.060	2446714.36951	0.5488	+0.079	2446714.43742	0.6601	−0.044
2446709.57203	0.6855	−0.057	2446714.37021	0.5500	+0.082	2446714.43921	0.6630	−0.039
2446709.57273	0.6867	−0.053	2446714.37090	0.5511	+0.083	2446714.43989	0.6642	−0.043
2446709.57343	0.6878	−0.056	2446714.37268	0.5540	+0.086	2446714.44059	0.6653	−0.047
2446709.57410	0.6889	−0.057	2446714.37338	0.5551	+0.077	2446714.44128	0.6664	−0.043
2446709.57480	0.6901	−0.062	2446714.37407	0.5563	+0.074	2446714.44198	0.6676	−0.050
2446709.57549	0.6912	−0.066	2446714.37477	0.5574	+0.070	2446714.44381	0.6706	−0.044
2446709.57619	0.6924	−0.065	2446714.37546	0.5586	+0.074	2446714.44449	0.6717	−0.055
2446709.57688	0.6935	−0.059	2446714.37760	0.5621	+0.075	2446714.44518	0.6728	−0.053
2446709.57758	0.6946	−0.064	2446714.37830	0.5632	+0.069	2446714.44588	0.6740	−0.054
2446709.58032	0.6991	−0.065	2446714.37898	0.5643	+0.067	2446714.44657	0.6751	−0.056
2446709.58101	0.7003	−0.073	2446714.37967	0.5655	+0.058	2446714.44751	0.6767	−0.056
2446709.58171	0.7014	−0.075	2446714.38037	0.5666	+0.059	2446714.44819	0.6778	−0.055
2446709.58240	0.7025	−0.068	2446714.38392	0.5724	+0.047	2446714.44887	0.6789	−0.058
2446709.58309	0.7037	−0.078	2446714.38462	0.5736	+0.047	2446714.44957	0.6800	−0.057
2446709.58378	0.7048	−0.076	2446714.38530	0.5747	+0.039	2446714.45026	0.6812	−0.059
2446709.58447	0.7059	−0.077	2446714.38600	0.5758	+0.044	2446714.45206	0.6841	−0.062
2446709.58518	0.7071	−0.083	2446714.38669	0.5770	+0.048	2446714.45274	0.6852	−0.060
2446709.58586	0.7082	−0.083	2446714.38767	0.5786	+0.038	2446714.45344	0.6864	−0.063
2446709.59674	0.7260	−0.084	2446714.38837	0.5797	+0.032	2446714.45413	0.6875	−0.063
2446709.59744	0.7272	−0.082	2446714.38974	0.5820	+0.030	2446714.45482	0.6886	−0.062
2446709.59813	0.7283	−0.083	2446714.39044	0.5831	+0.030	2446714.45804	0.6939	−0.067
2446709.59883	0.7295	−0.080	2446714.39210	0.5858	+0.036	2446714.45874	0.6951	−0.069
2446709.59951	0.7306	−0.079	2446714.39280	0.5870	+0.040	2446714.45943	0.6962	−0.067
2446709.60020	0.7317	−0.082	2446714.39348	0.5881	+0.030	2446714.46014	0.6974	−0.067
2446709.60090	0.7329	−0.088	2446714.39418	0.5892	+0.032	2446714.46082	0.6985	−0.068
2446709.60159	0.7340	−0.081	2446714.39488	0.5904	+0.030	2446714.46217	0.7007	−0.068
2446709.60229	0.7351	−0.083	2446714.39574	0.5918	+0.034	2446714.46287	0.7018	−0.070
2446709.60298	0.7363	−0.083	2446714.39642	0.5929	+0.024	2446714.46356	0.7030	−0.071
2446709.60533	0.7401	−0.081	2446714.39712	0.5941	+0.033	2446714.46426	0.7041	−0.078
2446709.60603	0.7413	−0.086	2446714.39780	0.5952	+0.023	2446714.46495	0.7052	−0.069
2446709.60672	0.7424	−0.084	2446714.39850	0.5963	+0.027	2446714.47230	0.7173	−0.079
2446709.60741	0.7435	−0.083	2446714.40040	0.5994	+0.021	2446714.47300	0.7184	−0.082

Table 5.10: 1986 TPT *V* observations — *continued.*

H.J.D.	Phase	(V-C)	H.J.D.	Phase	(V-C)	H.J.D.	Phase	(V-C)
2446714.47368	0.7195	−0.083	2446714.50548	0.7717	−0.088	2446714.54849	0.8422	−0.014
2446714.47437	0.7207	−0.084	2446714.50618	0.7728	−0.081	2446714.55129	0.8468	−0.009
2446714.47507	0.7218	−0.081	2446714.50687	0.7739	−0.087	2446714.55448	0.8520	+0.007
2446714.47793	0.7265	−0.088	2446714.50756	0.7751	−0.087	2446714.55517	0.8531	+0.012
2446714.47862	0.7276	−0.090	2446714.50825	0.7762	−0.080	2446714.55587	0.8543	+0.001
2446714.47931	0.7288	−0.085	2446714.52315	0.8006	−0.060	2446714.55656	0.8554	+0.005
2446714.48001	0.7299	−0.086	2446714.52384	0.8018	−0.064	2446714.55725	0.8565	+0.004
2446714.48070	0.7311	−0.083	2446714.52452	0.8029	−0.067	2446714.56032	0.8616	+0.021
2446714.48330	0.7353	−0.084	2446714.52522	0.8040	−0.058	2446714.56102	0.8627	+0.018
2446714.48400	0.7365	−0.083	2446714.52591	0.8052	−0.069	2446714.56171	0.8638	+0.019
2446714.48469	0.7376	−0.085	2446714.52812	0.8088	−0.055	2446714.56240	0.8650	+0.021
2446714.48538	0.7387	−0.090	2446714.52879	0.8099	−0.055	2446714.56309	0.8661	+0.023
2446714.48607	0.7399	−0.085	2446714.52949	0.8110	−0.051	2446714.56394	0.8675	+0.023
2446714.48698	0.7413	−0.088	2446714.53018	0.8122	−0.055	2446714.56464	0.8686	+0.024
2446714.48767	0.7425	−0.082	2446714.53088	0.8133	−0.050	2446714.56533	0.8698	+0.021
2446714.48837	0.7436	−0.091	2446714.53157	0.8144	−0.056	2446714.56671	0.8720	+0.034
2446714.48906	0.7448	−0.088	2446714.53227	0.8156	−0.056	2446714.56969	0.8769	+0.040
2446714.48977	0.7459	−0.092	2446714.53295	0.8167	−0.063	2446714.57038	0.8780	+0.048
2446714.49256	0.7505	−0.086	2446714.53364	0.8178	−0.049	2446714.57106	0.8792	+0.047
2446714.49325	0.7516	−0.083	2446714.53434	0.8190	−0.055	2446714.57176	0.8803	+0.048
2446714.49396	0.7528	−0.083	2446714.53695	0.8232	−0.035	2446714.57245	0.8814	+0.053
2446714.49464	0.7539	−0.086	2446714.53764	0.8244	−0.032	2446714.57315	0.8826	+0.058
2446714.49533	0.7550	−0.089	2446714.53833	0.8255	−0.034	2446714.57384	0.8837	+0.059
2446714.49639	0.7568	−0.085	2446714.53903	0.8267	−0.034	2446714.57453	0.8848	+0.059
2446714.49708	0.7579	−0.083	2446714.53972	0.8278	−0.030	2446714.57522	0.8860	+0.057
2446714.49778	0.7590	−0.087	2446714.54041	0.8289	−0.032	2446714.57591	0.8871	+0.064
2446714.49847	0.7602	−0.085	2446714.54111	0.8301	−0.028	2446714.58026	0.8942	+0.101
2446714.49916	0.7613	−0.085	2446714.54180	0.8312	−0.032	2446714.58096	0.8954	+0.101
2446714.50103	0.7644	−0.091	2446714.54249	0.8323	−0.023	2446714.58165	0.8965	+0.100
2446714.50172	0.7655	−0.090	2446714.54318	0.8335	−0.023	2446714.58235	0.8977	+0.111
2446714.50242	0.7667	−0.095	2446714.54573	0.8376	−0.015	2446714.58304	0.8988	+0.115
2446714.50311	0.7678	−0.087	2446714.54641	0.8388	−0.017	2446714.58372	0.8999	+0.114
2446714.50379	0.7689	−0.087	2446714.54641	0.8388	−0.017			

Table 5.11: 1988 TPT V observations.

H.J.D.	Phase	(V-C)	H.J.D.	Phase	(V-C)	H.J.D.	Phase	(V-C)
2447465.43857	0.5828	+0.050	2447465.46675	0.6290	−0.030	2447465.49064	0.6682	−0.049
2447465.43890	0.5834	+0.046	2447465.46710	0.6296	−0.024	2447465.49099	0.6687	−0.065
2447465.43925	0.5839	+0.039	2447465.46744	0.6302	−0.029	2447465.49133	0.6693	−0.068
2447465.43960	0.5845	+0.045	2447465.46819	0.6314	−0.026	2447465.49168	0.6699	−0.075
2447465.43994	0.5851	+0.043	2447465.46852	0.6319	−0.025	2447465.49203	0.6705	−0.065
2447465.44030	0.5857	+0.039	2447465.46887	0.6325	−0.034	2447465.49238	0.6710	−0.060
2447465.44064	0.5862	+0.043	2447465.46922	0.6331	−0.024	2447465.49272	0.6716	−0.070
2447465.44099	0.5868	+0.036	2447465.46956	0.6336	−0.028	2447465.49540	0.6760	−0.079
2447465.44133	0.5874	+0.032	2447465.46991	0.6342	−0.030	2447465.49574	0.6765	−0.070
2447465.44168	0.5879	+0.030	2447465.47027	0.6348	−0.034	2447465.49609	0.6771	−0.074
2447465.44451	0.5926	+0.031	2447465.47060	0.6353	−0.029	2447465.49644	0.6777	−0.065
2447465.44486	0.5931	+0.026	2447465.47095	0.6359	−0.026	2447465.49679	0.6783	−0.070
2447465.44521	0.5937	+0.020	2447465.47131	0.6365	−0.032	2447465.49713	0.6788	−0.075
2447465.44555	0.5943	+0.023	2447465.47322	0.6396	−0.029	2447465.49748	0.6794	−0.072
2447465.44589	0.5948	+0.020	2447465.47356	0.6402	−0.030	2447465.49783	0.6800	−0.071
2447465.44624	0.5954	+0.023	2447465.47390	0.6407	−0.029	2447465.49817	0.6805	−0.075
2447465.44659	0.5960	+0.021	2447465.47425	0.6413	−0.027	2447465.49853	0.6811	−0.075
2447465.44694	0.5965	+0.023	2447465.47460	0.6419	−0.035	2447465.49888	0.6817	−0.077
2447465.44728	0.5971	+0.023	2447465.47494	0.6424	−0.032	2447465.49923	0.6823	−0.074
2447465.44763	0.5977	+0.012	2447465.47529	0.6430	−0.034	2447465.49956	0.6828	−0.072
2447465.44832	0.5988	+0.013	2447465.47564	0.6436	−0.026	2447465.49991	0.6834	−0.083
2447465.44867	0.5994	+0.009	2447465.47599	0.6442	−0.034	2447465.50026	0.6839	−0.078
2447465.44902	0.6000	+0.015	2447465.47633	0.6447	−0.036	2447465.50060	0.6845	−0.084
2447465.44937	0.6005	+0.018	2447465.47707	0.6459	−0.031	2447465.50095	0.6851	−0.081
2447465.44971	0.6011	+0.018	2447465.47742	0.6465	−0.031	2447465.50130	0.6856	−0.085
2447465.45006	0.6017	+0.009	2447465.47777	0.6471	−0.029	2447465.50166	0.6862	−0.083
2447465.45041	0.6022	+0.016	2447465.47812	0.6477	−0.035	2447465.50201	0.6868	−0.087
2447465.45076	0.6028	+0.014	2447465.47848	0.6482	−0.041	2447465.50652	0.6942	−0.085
2447465.45110	0.6034	+0.012	2447465.47881	0.6488	−0.038	2447465.50687	0.6948	−0.088
2447465.45145	0.6039	+0.005	2447465.47916	0.6494	−0.041	2447465.50721	0.6953	−0.088
2447465.45299	0.6065	+0.004	2447465.47951	0.6499	−0.033	2447465.50756	0.6959	−0.093
2447465.45334	0.6070	−0.002	2447465.47985	0.6505	−0.045	2447465.50791	0.6965	−0.090
2447465.45368	0.6076	+0.003	2447465.48020	0.6511	−0.043	2447465.50826	0.6971	−0.089
2447465.45403	0.6082	+0.002	2447465.48126	0.6528	−0.048	2447465.50860	0.6976	−0.093
2447465.45473	0.6093	−0.005	2447465.48161	0.6534	−0.039	2447465.50895	0.6982	−0.087
2447465.45507	0.6099	−0.004	2447465.48196	0.6539	−0.044	2447465.50930	0.6988	−0.088
2447465.45542	0.6104	−0.007	2447465.48231	0.6545	−0.051	2447465.50964	0.6993	−0.091
2447465.45577	0.6110	−0.002	2447465.48265	0.6551	−0.049	2447465.50999	0.6999	−0.093
2447465.45611	0.6116	−0.013	2447465.48300	0.6557	−0.044	2447465.51034	0.7005	−0.093
2447465.45681	0.6127	−0.008	2447465.48335	0.6562	−0.050	2447465.51069	0.7010	−0.094
2447465.45716	0.6133	−0.002	2447465.48369	0.6568	−0.054	2447465.51103	0.7016	−0.097
2447465.45750	0.6139	+0.000	2447465.48404	0.6574	−0.042	2447465.51138	0.7022	−0.094
2447465.45785	0.6144	−0.016	2447465.48439	0.6579	−0.053	2447465.51173	0.7027	−0.097
2447465.45820	0.6150	−0.015	2447465.48550	0.6598	−0.050	2447465.51207	0.7033	−0.097
2447465.45854	0.6156	−0.012	2447465.48585	0.6603	−0.047	2447465.51242	0.7039	−0.088
2447465.45889	0.6161	−0.005	2447465.48619	0.6609	−0.056	2447465.51277	0.7044	−0.094
2447465.45924	0.6167	−0.018	2447465.48654	0.6615	−0.054	2447465.51312	0.7050	−0.091
2447465.45959	0.6173	−0.013	2447465.48690	0.6620	−0.047	2447465.52344	0.7219	−0.091
2447465.45994	0.6179	−0.015	2447465.48724	0.6626	−0.058	2447465.52379	0.7225	−0.086
2447465.46432	0.6250	−0.022	2447465.48758	0.6632	−0.061	2447465.52413	0.7231	−0.088
2447465.46467	0.6256	−0.033	2447465.48793	0.6637	−0.062	2447465.52448	0.7236	−0.087
2447465.46501	0.6262	−0.018	2447465.48828	0.6643	−0.058	2447465.52483	0.7242	−0.092
2447465.46536	0.6267	−0.026	2447465.48863	0.6649	−0.051	2447465.52518	0.7248	−0.093
2447465.46571	0.6273	−0.030	2447465.48960	0.6665	−0.052	2447465.52554	0.7254	−0.089
2447465.46606	0.6279	−0.022	2447465.48994	0.6670	−0.061	2447465.52587	0.7259	−0.091
2447465.46640	0.6284	−0.026	2447465.49029	0.6676	−0.060	2447465.52622	0.7265	−0.093

Table 5.11: 1988 TPT *V* observations — *continued.*

H.J.D.	Phase	(V-C)	H.J.D.	Phase	(V-C)	H.J.D.	Phase	(V-C)
2447465.52657	0.7271	−0.087	2447465.55572	0.7748	−0.101	2447465.58688	0.8259	−0.041
2447465.52691	0.7276	−0.093	2447465.55607	0.7754	−0.115	2447465.58723	0.8265	−0.048
2447465.52726	0.7282	−0.088	2447465.55641	0.7760	−0.107	2447465.58757	0.8270	−0.045
2447465.52761	0.7288	−0.089	2447465.55676	0.7765	−0.105	2447465.58792	0.8276	−0.033
2447465.52795	0.7293	−0.093	2447465.55711	0.7771	−0.109	2447465.58827	0.8282	−0.043
2447465.52830	0.7299	−0.090	2447465.55746	0.7777	−0.106	2447465.58861	0.8288	−0.038
2447465.52865	0.7305	−0.098	2447465.55780	0.7783	−0.112	2447465.58896	0.8293	−0.035
2447465.52969	0.7322	−0.091	2447465.55815	0.7788	−0.107	2447465.58931	0.8299	−0.036
2447465.53004	0.7328	−0.092	2447465.55850	0.7794	−0.109	2447465.58966	0.8305	−0.040
2447465.53052	0.7335	−0.090	2447465.55885	0.7800	−0.109	2447465.59000	0.8310	−0.032
2447465.53087	0.7341	−0.090	2447465.55919	0.7805	−0.103	2447465.59035	0.8316	−0.025
2447465.53122	0.7347	−0.092	2447465.55954	0.7811	−0.108	2447465.59070	0.8322	−0.028
2447465.53157	0.7353	−0.099	2447465.55989	0.7817	−0.102	2447465.59106	0.8328	−0.034
2447465.53191	0.7358	−0.090	2447465.56023	0.7822	−0.104	2447465.59139	0.8333	−0.038
2447465.53226	0.7364	−0.092	2447465.56058	0.7828	−0.100	2447465.59449	0.8384	−0.033
2447465.53261	0.7370	−0.094	2447465.56093	0.7834	−0.108	2447465.59484	0.8390	−0.030
2447465.53295	0.7375	−0.097	2447465.56356	0.7877	−0.097	2447465.59519	0.8395	−0.030
2447465.53330	0.7381	−0.093	2447465.56390	0.7883	−0.094	2447465.59554	0.8401	−0.028
2447465.53365	0.7387	−0.094	2447465.56425	0.7888	−0.098	2447465.59988	0.8472	−0.011
2447465.53400	0.7392	−0.096	2447465.56460	0.7894	−0.091	2447465.60022	0.8478	−0.018
2447465.53434	0.7398	−0.094	2447465.56494	0.7900	−0.098	2447465.60057	0.8484	−0.010
2447465.53469	0.7404	−0.097	2447465.56529	0.7905	−0.099	2447465.60092	0.8489	−0.011
2447465.53540	0.7415	−0.097	2447465.56564	0.7911	−0.095	2447465.60126	0.8495	−0.021
2447465.53573	0.7421	−0.093	2447465.56599	0.7917	−0.086	2447465.60187	0.8505	−0.004
2447465.53608	0.7427	−0.094	2447465.56633	0.7922	−0.086	2447465.60221	0.8510	−0.019
2447465.53643	0.7432	−0.092	2447465.56668	0.7928	−0.093	2447465.60257	0.8516	−0.007
2447465.53677	0.7438	−0.100	2447465.56703	0.7934	−0.086	2447465.60291	0.8522	−0.002
2447465.53712	0.7444	−0.097	2447465.56738	0.7940	−0.091	2447465.60326	0.8528	−0.007
2447465.53986	0.7488	−0.103	2447465.56772	0.7945	−0.083	2447465.60387	0.8538	−0.013
2447465.54022	0.7494	−0.093	2447465.56807	0.7951	−0.083	2447465.60422	0.8543	−0.007
2447465.54059	0.7500	−0.107	2447465.56842	0.7957	−0.081	2447465.60456	0.8549	−0.007
2447465.54154	0.7516	−0.100	2447465.56876	0.7962	−0.083	2447465.60491	0.8555	−0.004
2447465.54235	0.7529	−0.094	2447465.56911	0.7968	−0.086	2447465.60526	0.8560	−0.007
2447465.54270	0.7535	−0.097	2447465.56946	0.7974	−0.087	2447465.60560	0.8566	+0.000
2447465.54305	0.7541	−0.095	2447465.56981	0.7979	−0.082	2447465.60595	0.8572	−0.001
2447465.54339	0.7546	−0.093	2447465.57015	0.7985	−0.082	2447465.60630	0.8577	−0.001
2447465.54374	0.7552	−0.100	2447465.57338	0.8038	−0.072	2447465.60665	0.8583	−0.005
2447465.54409	0.7558	−0.093	2447465.57373	0.8044	−0.075	2447465.60699	0.8589	−0.005
2447465.54444	0.7564	−0.099	2447465.57408	0.8049	−0.072	2447465.61623	0.8740	+0.022
2447465.54478	0.7569	−0.102	2447465.57442	0.8055	−0.069	2447465.61658	0.8746	+0.040
2447465.54513	0.7575	−0.095	2447465.57477	0.8061	−0.076	2447465.61692	0.8752	+0.031
2447465.54548	0.7581	−0.098	2447465.57512	0.8066	−0.070	2447465.61728	0.8757	+0.028
2447465.54582	0.7586	−0.101	2447465.57547	0.8072	−0.067	2447465.61762	0.8763	+0.040
2447465.54617	0.7592	−0.092	2447465.57581	0.8078	−0.069	2447465.61797	0.8769	+0.030
2447465.54652	0.7598	−0.101	2447465.57616	0.8083	−0.067	2447465.61831	0.8774	+0.041
2447465.54687	0.7603	−0.108	2447465.57651	0.8089	−0.073	2447465.61866	0.8780	+0.029
2447465.54721	0.7609	−0.099	2447465.57685	0.8095	−0.075	2447465.61902	0.8786	+0.039
2447465.54756	0.7615	−0.100	2447465.57720	0.8101	−0.067	2447465.61935	0.8791	+0.030
2447465.54791	0.7620	−0.098	2447465.57755	0.8106	−0.066	2447465.62138	0.8825	+0.058
2447465.54826	0.7626	−0.108	2447465.57790	0.8112	−0.072	2447465.62172	0.8830	+0.054
2447465.54860	0.7632	−0.095	2447465.57824	0.8118	−0.065	2447465.62206	0.8836	+0.046
2447465.54895	0.7637	−0.097	2447465.57859	0.8123	−0.065	2447465.62241	0.8842	+0.065
2447465.55433	0.7726	−0.106	2447465.57894	0.8129	−0.064	2447465.62276	0.8847	+0.055
2447465.55468	0.7731	−0.103	2447465.57963	0.8140	−0.064	2447465.62310	0.8853	+0.060
2447465.55503	0.7737	−0.101	2447465.57998	0.8146	−0.063	2447465.62483	0.8881	+0.072
2447465.55537	0.7743	−0.100	2447465.58653	0.8253	−0.040	2447465.62518	0.8887	+0.081

Table 5.11: 1988 TPT *V* observations — *continued.*

H.J.D.	Phase	(V-C)	H.J.D.	Phase	(V-C)	H.J.D.	Phase	(V-C)
2447465.62552	0.8892	+0.078	2447465.65508	0.9377	+0.287	2447465.68905	0.9934	+0.590
2447465.62587	0.8898	+0.077	2447465.65542	0.9383	+0.277	2447465.68940	0.9940	+0.592
2447465.62622	0.8904	+0.079	2447465.65651	0.9400	+0.298	2447465.68975	0.9945	+0.600
2447465.62657	0.8910	+0.078	2447465.65685	0.9406	+0.302	2447465.69010	0.9951	+0.583
2447465.62691	0.8915	+0.084	2447465.65720	0.9412	+0.306	2447465.69044	0.9957	+0.599
2447465.62726	0.8921	+0.082	2447465.65755	0.9417	+0.308	2447465.69079	0.9962	+0.592
2447465.62761	0.8927	+0.082	2447465.65790	0.9423	+0.314	2447465.69168	0.9977	+0.591
2447465.62795	0.8932	+0.088	2447465.65824	0.9429	+0.323	2447465.69203	0.9983	+0.598
2447465.63062	0.8976	+0.122	2447465.65859	0.9435	+0.329	2447465.69238	0.9988	+0.594
2447465.63096	0.8982	+0.113	2447465.65894	0.9440	+0.328	2447465.69272	0.9994	+0.590
2447465.63131	0.8987	+0.111	2447465.65929	0.9446	+0.323	2447465.69307	0.0000	+0.585
2447465.63166	0.8993	+0.110	2447465.65963	0.9452	+0.336	2447465.69342	0.0005	+0.594
2447465.63201	0.8999	+0.120	2447465.66182	0.9487	+0.355	2447465.69376	0.0011	+0.595
2447465.63235	0.9004	+0.118	2447465.66217	0.9493	+0.363	2447465.69411	0.0017	+0.591
2447465.63270	0.9010	+0.115	2447465.66253	0.9499	+0.356	2447465.69446	0.0022	+0.592
2447465.63305	0.9016	+0.118	2447465.66286	0.9505	+0.362	2447465.69481	0.0028	+0.599
2447465.63339	0.9021	+0.129	2447465.66321	0.9510	+0.369	2447465.69527	0.0036	+0.590
2447465.63374	0.9027	+0.128	2447465.66356	0.9516	+0.367	2447465.69562	0.0041	+0.589
2447465.63424	0.9035	+0.132	2447465.66390	0.9522	+0.369	2447465.69596	0.0047	+0.592
2447465.63459	0.9041	+0.137	2447465.66425	0.9527	+0.382	2447465.69631	0.0053	+0.594
2447465.63493	0.9047	+0.136	2447465.66460	0.9533	+0.376	2447465.69666	0.0059	+0.591
2447465.63528	0.9052	+0.148	2447465.66494	0.9539	+0.381	2447465.69701	0.0064	+0.581
2447465.63563	0.9058	+0.133	2447465.66721	0.9576	+0.417	2447465.69735	0.0070	+0.576
2447465.63598	0.9064	+0.140	2447465.66756	0.9582	+0.407	2447465.69770	0.0076	+0.588
2447465.63632	0.9070	+0.146	2447465.66791	0.9587	+0.419	2447465.69805	0.0081	+0.583
2447465.63667	0.9075	+0.147	2447465.66827	0.9593	+0.423	2447465.69839	0.0087	+0.584
2447465.63702	0.9081	+0.144	2447465.66860	0.9599	+0.418	2447465.69971	0.0109	+0.578
2447465.63736	0.9087	+0.165	2447465.66896	0.9604	+0.431	2447465.70006	0.0114	+0.578
2447465.64021	0.9133	+0.171	2447465.66930	0.9610	+0.428	2447465.70041	0.0120	+0.571
2447465.64056	0.9139	+0.180	2447465.66964	0.9616	+0.439	2447465.70076	0.0126	+0.568
2447465.64091	0.9145	+0.165	2447465.66999	0.9621	+0.438	2447465.70110	0.0131	+0.558
2447465.64125	0.9150	+0.172	2447465.67034	0.9627	+0.456	2447465.70145	0.0137	+0.556
2447465.64160	0.9156	+0.177	2447465.67743	0.9743	+0.507	2447465.70180	0.0143	+0.568
2447465.64195	0.9162	+0.183	2447465.67778	0.9749	+0.520	2447465.70214	0.0148	+0.558
2447465.64229	0.9167	+0.182	2447465.67813	0.9755	+0.529	2447465.70249	0.0154	+0.571
2447465.64264	0.9173	+0.180	2447465.67848	0.9761	+0.534	2447465.70284	0.0160	+0.564
2447465.64299	0.9179	+0.187	2447465.67882	0.9766	+0.528	2447465.70334	0.0168	+0.561
2447465.64334	0.9185	+0.201	2447465.67917	0.9772	+0.556	2447465.70368	0.0174	+0.565
2447465.64382	0.9192	+0.196	2447465.67952	0.9778	+0.539	2447465.70403	0.0179	+0.557
2447465.64417	0.9198	+0.192	2447465.67986	0.9783	+0.533	2447465.70438	0.0185	+0.535
2447465.64452	0.9204	+0.214	2447465.68021	0.9789	+0.548	2447465.70473	0.0191	+0.552
2447465.64486	0.9209	+0.207	2447465.68056	0.9795	+0.530	2447465.70507	0.0196	+0.551
2447465.64521	0.9215	+0.206	2447465.68141	0.9809	+0.549	2447465.70542	0.0202	+0.542
2447465.64556	0.9221	+0.212	2447465.68176	0.9814	+0.556	2447465.70577	0.0208	+0.546
2447465.64591	0.9227	+0.209	2447465.68211	0.9820	+0.566	2447465.70611	0.0213	+0.540
2447465.64625	0.9232	+0.217	2447465.68246	0.9826	+0.563	2447465.70646	0.0219	+0.542
2447465.64660	0.9238	+0.216	2447465.68280	0.9831	+0.566	2447465.71221	0.0313	+0.486
2447465.64695	0.9244	+0.221	2447465.68315	0.9837	+0.564	2447465.71256	0.0319	+0.488
2447465.65229	0.9331	+0.257	2447465.68350	0.9843	+0.566	2447465.71291	0.0325	+0.468
2447465.65264	0.9337	+0.260	2447465.68385	0.9849	+0.556	2447465.71326	0.0331	+0.473
2447465.65299	0.9343	+0.273	2447465.68419	0.9854	+0.576	2447465.71360	0.0336	+0.476
2447465.65334	0.9348	+0.270	2447465.68454	0.9860	+0.575	2447465.71396	0.0342	+0.469
2447465.65368	0.9354	+0.268	2447465.68766	0.9911	+0.580	2447465.71430	0.0348	+0.452
2447465.65403	0.9360	+0.271	2447465.68801	0.9917	+0.583	2447465.71464	0.0353	+0.456
2447465.65438	0.9366	+0.276	2447465.68837	0.9923	+0.595	2447465.71499	0.0359	+0.455
2447465.65473	0.9371	+0.282	2447465.68871	0.9928	+0.589	2447465.71534	0.0365	+0.446

Table 5.11: 1988 TPT *V* observations — *continued.*

H.J.D.	Phase	(V-C)	H.J.D.	Phase	(V-C)	H.J.D.	Phase	(V-C)
2447465:71580	0.0372	+0.440	2447466.48322	0.2951	−0.096	2447466.50773	0.3352	−0.059
2447465.71615	0.0378	+0.444	2447466.48356	0.2956	−0.088	2447466.50808	0.3358	−0.065
2447465.71650	0.0384	+0.441	2447466.48391	0.2962	−0.099	2447466.50843	0.3364	−0.062
2447465.71684	0.0389	+0.435	2447466.48538	0.2986	−0.093	2447466.50877	0.3369	−0.065
2447465.71719	0.0395	+0.431	2447466.48573	0.2992	−0.098	2447466.50912	0.3375	−0.070
2447465.71754	0.0401	+0.436	2447466.48608	0.2997	−0.097	2447466.50947	0.3381	−0.062
2447465.71788	0.0406	+0.428	2447466.48642	0.3003	−0.105	2447466.50981	0.3386	−0.067
2447465.71823	0.0412	+0.412	2447466.48677	0.3009	−0.091	2447466.51385	0.3453	−0.052
2447465.71858	0.0418	+0.404	2447466.48712	0.3014	−0.086	2447466.51421	0.3458	−0.048
2447465.71893	0.0424	+0.426	2447466.48748	0.3020	−0.083	2447466.51455	0.3464	−0.054
2447465.72074	0.0453	+0.393	2447466.48782	0.3026	−0.087	2447466.51489	0.3470	−0.040
2447465.72109	0.0459	+0.399	2447466.48816	0.3032	−0.094	2447466.51524	0.3475	−0.043
2447465.72144	0.0465	+0.393	2447466.48851	0.3037	−0.090	2447466.51559	0.3481	−0.045
2447465.72179	0.0470	+0.381	2447466.48900	0.3045	−0.090	2447466.51594	0.3487	−0.047
2447465.72213	0.0476	+0.377	2447466.48935	0.3051	−0.086	2447466.51628	0.3492	−0.048
2447465.72248	0.0482	+0.381	2447466.48970	0.3057	−0.097	2447466.51663	0.3498	−0.049
2447465.72283	0.0487	+0.370	2447466.49005	0.3063	−0.086	2447466.51698	0.3504	−0.051
2447465.72317	0.0493	+0.375	2447466.49039	0.3068	−0.087	2447466.51733	0.3510	−0.054
2447465.72352	0.0499	+0.362	2447466.49074	0.3074	−0.090	2447466.51767	0.3515	−0.042
2447465.72387	0.0504	+0.368	2447466.49109	0.3080	−0.088	2447466.51802	0.3521	−0.055
2447465.72434	0.0512	+0.364	2447466.49143	0.3085	−0.080	2447466.51837	0.3527	−0.048
2447465.72469	0.0518	+0.360	2447466.49178	0.3091	−0.097	2447466.51871	0.3532	−0.043
2447465.72504	0.0524	+0.359	2447466.49213	0.3097	−0.080	2447466.51906	0.3538	−0.031
2447465.72538	0.0529	+0.345	2447466.49418	0.3130	−0.083	2447466.51941	0.3544	−0.038
2447465.72573	0.0535	+0.337	2447466.49452	0.3136	−0.083	2447466.51976	0.3549	−0.030
2447465.72608	0.0541	+0.343	2447466.49487	0.3142	−0.073	2447466.52010	0.3555	−0.028
2447465.72643	0.0546	+0.337	2447466.49522	0.3147	−0.085	2447466.52045	0.3561	−0.030
2447465.72679	0.0552	+0.334	2447466.49557	0.3153	−0.088	2447466.52218	0.3589	−0.022
2447465.72712	0.0558	+0.335	2447466.49591	0.3159	−0.077	2447466.52252	0.3595	−0.029
2447465.72748	0.0564	+0.327	2447466.49626	0.3164	−0.080	2447466.52287	0.3600	−0.022
2447465.72883	0.0586	+0.310	2447466.49661	0.3170	−0.073	2447466.52322	0.3606	−0.017
2447465.72918	0.0592	+0.308	2447466.49697	0.3176	−0.076	2447466.52356	0.3612	−0.031
2447465.72953	0.0597	+0.309	2447466.49730	0.3181	−0.075	2447466.52391	0.3617	−0.031
2447465.72988	0.0603	+0.302	2447466.49765	0.3187	−0.068	2447466.52426	0.3623	−0.022
2447465.73023	0.0609	+0.308	2447466.49800	0.3193	−0.072	2447466.52461	0.3629	−0.019
2447465.73057	0.0614	+0.295	2447466.49834	0.3198	−0.073	2447466.52495	0.3635	−0.023
2447465.73092	0.0620	+0.290	2447466.49869	0.3204	−0.081	2447466.52530	0.3640	−0.019
2447465.73126	0.0626	+0.290	2447466.49904	0.3210	−0.077	2447466.52565	0.3646	−0.024
2447465.73161	0.0631	+0.291	2447466.49939	0.3216	−0.083	2447466.52599	0.3652	−0.014
2447466.47716	0.2851	−0.098	2447466.49973	0.3221	−0.079	2447466.52634	0.3657	−0.032
2447466.47751	0.2857	−0.100	2447466.50008	0.3227	−0.068	2447466.52669	0.3663	−0.024
2447466.47786	0.2863	−0.107	2447466.50043	0.3233	−0.075	2447466.52704	0.3669	−0.015
2447466.47821	0.2868	−0.102	2447466.50077	0.3238	−0.074	2447466.52738	0.3674	−0.025
2447466.47855	0.2874	−0.097	2447466.50322	0.3278	−0.068	2447466.52773	0.3680	−0.024
2447466.47890	0.2880	−0.095	2447466.50356	0.3284	−0.067	2447466.52808	0.3686	−0.025
2447466.47925	0.2885	−0.107	2447466.50391	0.3290	−0.068	2447466.52843	0.3692	−0.015
2447466.47959	0.2891	−0.096	2447466.50426	0.3295	−0.066	2447466.52877	0.3697	−0.008
2447466.47995	0.2897	−0.097	2447466.50461	0.3301	−0.069	2447466.53110	0.3735	−0.004
2447466.48029	0.2903	−0.094	2447466.50495	0.3307	−0.060	2447466.53145	0.3741	+0.001
2447466.48079	0.2911	−0.097	2447466.50530	0.3312	−0.068	2447466.53179	0.3747	−0.005
2447466.48113	0.2916	−0.105	2447466.50566	0.3318	−0.067	2447466.53214	0.3752	−0.006
2447466.48148	0.2922	−0.095	2447466.50599	0.3324	−0.058	2447466.53249	0.3758	−0.012
2447466.48183	0.2928	−0.090	2447466.50634	0.3330	−0.068	2447466.53283	0.3764	+0.003
2447466.48218	0.2934	−0.093	2447466.50669	0.3335	−0.069	2447466.53318	0.3769	−0.006
2447466.48252	0.2939	−0.097	2447466.50704	0.3341	−0.059	2447466.53353	0.3775	−0.005
2447466.48287	0.2945	−0.095	2447466.50738	0.3347	−0.068	2447466.53388	0.3781	−0.008

Table 5.11: 1988 TPT *V* observations — *continued.*

H.J.D.	Phase	(V-C)	H.J.D.	Phase	(V-C)	H.J.D.	Phase	(V-C)
2447466.53422	0.3786	−0.009	2447466.57139	0.4396	+0.091	2447466.59930	0.4853	+0.154
2447466.53457	0.3792	−0.012	2447466.57172	0.4401	+0.085	2447466.59965	0.4859	+0.169
2447466.53492	0.3798	−0.012	2447466.57207	0.4407	+0.086	2447466.60000	0.4865	+0.173
2447466.53527	0.3804	−0.004	2447466.57243	0.4413	+0.101	2447466.60069	0.4876	+0.148
2447466.53561	0.3809	−0.007	2447466.57277	0.4418	+0.091	2447466.60104	0.4882	+0.159
2447466.53631	0.3821	−0.012	2447466.57311	0.4424	+0.097	2447466.60139	0.4887	+0.164
2447466.53665	0.3826	−0.007	2447466.57346	0.4430	+0.087	2447466.60174	0.4893	+0.160
2447466.53735	0.3838	−0.005	2447466.57381	0.4435	+0.091	2447466.60208	0.4899	+0.157
2447466.53770	0.3844	−0.008	2447466.57605	0.4472	+0.102	2447466.60243	0.4904	+0.161
2447466.54950	0.4037	+0.026	2447466.57640	0.4478	+0.096	2447466.60278	0.4910	+0.173
2447466.54985	0.4043	+0.027	2447466.57675	0.4484	+0.103	2447466.60314	0.4916	+0.157
2447466.55020	0.4048	+0.029	2447466.57709	0.4489	+0.104	2447466.60483	0.4944	+0.169
2447466.55054	0.4054	+0.022	2447466.57744	0.4495	+0.107	2447466.60517	0.4949	+0.164
2447466.55089	0.4060	+0.032	2447466.57780	0.4501	+0.094	2447466.60552	0.4955	+0.174
2447466.55124	0.4065	+0.036	2447466.57814	0.4506	+0.102	2447466.60587	0.4961	+0.177
2447466.55158	0.4071	+0.030	2447466.57848	0.4512	+0.099	2447466.60621	0.4966	+0.173
2447466.55193	0.4077	+0.032	2447466.57883	0.4518	+0.104	2447466.60656	0.4972	+0.179
2447466.55228	0.4082	+0.027	2447466.57918	0.4523	+0.104	2447466.60691	0.4978	+0.161
2447466.55263	0.4088	+0.040	2447466.57952	0.4529	+0.114	2447466.60726	0.4984	+0.177
2447466.55297	0.4094	+0.032	2447466.57987	0.4535	+0.115	2447466.60760	0.4989	+0.158
2447466.55332	0.4100	+0.049	2447466.58022	0.4540	+0.115	2447466.60795	0.4995	+0.164
2447466.55367	0.4105	+0.037	2447466.58057	0.4546	+0.125	2447466.60830	0.5001	+0.168
2447466.55402	0.4111	+0.043	2447466.58091	0.4552	+0.115	2447466.60864	0.5006	+0.175
2447466.55436	0.4117	+0.046	2447466.58126	0.4557	+0.123	2447466.60899	0.5012	+0.174
2447466.55560	0.4137	+0.050	2447466.58161	0.4563	+0.117	2447466.60934	0.5018	+0.175
2447466.55596	0.4143	+0.045	2447466.58196	0.4569	+0.115	2447466.60969	0.5023	+0.177
2447466.55630	0.4148	+0.044	2447466.58230	0.4575	+0.119	2447466.61003	0.5029	+0.178
2447466.55664	0.4154	+0.048	2447466.58266	0.4580	+0.112	2447466.61038	0.5035	+0.181
2447466.55699	0.4160	+0.054	2447466.58944	0.4692	+0.132	2447466.61073	0.5041	+0.177
2447466.55734	0.4165	+0.050	2447466.58979	0.4697	+0.136	2447466.61108	0.5046	+0.175
2447466.55770	0.4171	+0.050	2447466.59014	0.4703	+0.138	2447466.61142	0.5052	+0.181
2447466.55803	0.4177	+0.048	2447466.59049	0.4709	+0.132	2447466.61347	0.5085	+0.161
2447466.55839	0.4183	+0.049	2447466.59083	0.4714	+0.140	2447466.61382	0.5091	+0.158
2447466.55873	0.4188	+0.054	2447466.59118	0.4720	+0.130	2447466.61417	0.5097	+0.155
2447466.55907	0.4194	+0.045	2447466.59153	0.4726	+0.129	2447466.61451	0.5102	+0.169
2447466.55942	0.4200	+0.057	2447466.59187	0.4731	+0.133	2447466.61486	0.5108	+0.163
2447466.55977	0.4205	+0.052	2447466.59222	0.4737	+0.143	2447466.61521	0.5114	+0.155
2447466.56011	0.4211	+0.058	2447466.59257	0.4743	+0.141	2447466.61555	0.5120	+0.164
2447466.56046	0.4217	+0.058	2447466.59292	0.4749	+0.135	2447466.61590	0.5125	+0.171
2447466.56081	0.4222	+0.070	2447466.59327	0.4754	+0.139	2447466.61625	0.5131	+0.165
2447466.56116	0.4228	+0.059	2447466.59361	0.4760	+0.138	2447466.61660	0.5137	+0.164
2447466.56150	0.4234	+0.063	2447466.59396	0.4766	+0.139	2447466.61694	0.5142	+0.160
2447466.56185	0.4239	+0.063	2447466.59432	0.4772	+0.151	2447466.61729	0.5148	+0.162
2447466.56220	0.4245	+0.065	2447466.59465	0.4777	+0.139	2447466.61764	0.5154	+0.159
2447466.56721	0.4327	+0.078	2447466.59500	0.4783	+0.141	2447466.61799	0.5159	+0.166
2447466.56756	0.4333	+0.081	2447466.59535	0.4788	+0.144	2447466.61833	0.5165	+0.157
2447466.56790	0.4339	+0.074	2447466.59569	0.4794	+0.153	2447466.61868	0.5171	+0.165
2447466.56825	0.4344	+0.080	2447466.59604	0.4800	+0.149	2447466.61903	0.5177	+0.156
2447466.56860	0.4350	+0.084	2447466.59653	0.4808	+0.143	2447466.61937	0.5182	+0.156
2447466.56895	0.4356	+0.085	2447466.59689	0.4814	+0.147	2447466.61972	0.5188	+0.159
2447466.56929	0.4361	+0.087	2447466.59722	0.4819	+0.145	2447466.62007	0.5194	+0.155
2447466.56964	0.4367	+0.090	2447466.59757	0.4825	+0.142	2447467.40830	0.8113	−0.073
2447466.56999	0.4373	+0.082	2447466.59792	0.4831	+0.151	2447467.40864	0.8119	−0.061
2447466.57033	0.4378	+0.094	2447466.59826	0.4836	+0.160	2447467.40899	0.8124	−0.068
2447466.57068	0.4384	+0.088	2447466.59861	0.4842	+0.154	2447467.40933	0.8130	−0.074
2447466.57103	0.4390	+0.086	2447466.59896	0.4848	+0.154	2447467.40968	0.8136	−0.066

Table 5.11: 1988 TPT *V* observations — *continued.*

H.J.D.	Phase	(V-C)	H.J.D.	Phase	(V-C)	H.J.D.	Phase	(V-C)
2447467.41003	0.8141	−0.079	2447467.43690	0.8582	+0.010	2447467.46313	0.9012	+0.107
2447467.41038	0.8147	−0.068	2447467.43725	0.8588	−0.001	2447467.47435	0.9196	+0.198
2447467.41072	0.8153	−0.062	2447467.43760	0.8593	+0.001	2447467.47469	0.9201	+0.196
2447467.41107	0.8158	−0.064	2447467.43795	0.8599	+0.005	2447467.47504	0.9207	+0.203
2447467.41142	0.8164	−0.060	2447467.43829	0.8605	+0.015	2447467.47539	0.9213	+0.200
2447467.41270	0.8185	−0.068	2447467.43865	0.8610	+0.005	2447467.47573	0.9218	+0.211
2447467.41306	0.8191	−0.064	2447467.43899	0.8616	+0.005	2447467.47608	0.9224	+0.206
2447467.41340	0.8197	−0.062	2447467.43933	0.8622	+0.010	2447467.47643	0.9230	+0.207
2447467.41374	0.8202	−0.064	2447467.43968	0.8627	+0.006	2447467.47678	0.9235	+0.219
2447467.41409	0.8208	−0.064	2447467.44003	0.8633	+0.015	2447467.47712	0.9241	+0.222
2447467.41444	0.8214	−0.058	2447467.44038	0.8639	+0.020	2447467.47747	0.9247	+0.220
2447467.41479	0.8219	−0.057	2447467.44072	0.8644	+0.021	2447467.47782	0.9252	+0.230
2447467.41513	0.8225	−0.048	2447467.44107	0.8650	+0.021	2447467.47818	0.9258	+0.227
2447467.41548	0.8231	−0.059	2447467.44142	0.8656	+0.017	2447467.47851	0.9264	+0.237
2447467.41583	0.8236	−0.051	2447467.44176	0.8661	+0.019	2447467.47886	0.9270	+0.242
2447467.41628	0.8244	−0.042	2447467.44211	0.8667	+0.021	2447467.47921	0.9275	+0.242
2447467.41663	0.8250	−0.042	2447467.44247	0.8673	+0.028	2447467.47955	0.9281	+0.238
2447467.41697	0.8255	−0.048	2447467.44791	0.8762	+0.042	2447467.47990	0.9287	+0.247
2447467.41732	0.8261	−0.047	2447467.44826	0.8768	+0.030	2447467.48026	0.9292	+0.252
2447467.41767	0.8267	−0.040	2447467.44860	0.8774	+0.029	2447467.48061	0.9298	+0.248
2447467.41801	0.8272	−0.053	2447467.44895	0.8779	+0.035	2447467.48095	0.9304	+0.255
2447467.41836	0.8278	−0.045	2447467.44930	0.8785	+0.042	2447467.48297	0.9337	+0.267
2447467.41871	0.8284	−0.048	2447467.44965	0.8791	+0.041	2447467.48332	0.9343	+0.271
2447467.41906	0.8289	−0.039	2447467.44999	0.8796	+0.032	2447467.48366	0.9348	+0.287
2447467.41940	0.8295	−0.043	2447467.45034	0.8802	+0.041	2447467.48401	0.9354	+0.278
2447467.42341	0.8361	−0.029	2447467.45069	0.8808	+0.046	2447467.48436	0.9360	+0.282
2447467.42376	0.8366	−0.023	2447467.45104	0.8814	+0.048	2447467.48470	0.9365	+0.284
2447467.42411	0.8372	−0.023	2447467.45138	0.8819	+0.043	2447467.48505	0.9371	+0.298
2447467.42445	0.8378	−0.021	2447467.45173	0.8825	+0.050	2447467.48540	0.9377	+0.291
2447467.42514	0.8389	−0.022	2447467.45208	0.8831	+0.054	2447467.48575	0.9382	+0.300
2447467.42550	0.8395	−0.028	2447467.45242	0.8836	+0.052	2447467.48609	0.9388	+0.295
2447467.42619	0.8406	−0.024	2447467.45277	0.8842	+0.048	2447467.48644	0.9394	+0.293
2447467.42653	0.8412	−0.021	2447467.45312	0.8848	+0.054	2447467.48679	0.9399	+0.313
2447467.42789	0.8434	−0.029	2447467.45347	0.8853	+0.056	2447467.48713	0.9405	+0.299
2447467.42823	0.8440	−0.023	2447467.45381	0.8859	+0.064	2447467.48748	0.9411	+0.297
2447467.42858	0.8445	−0.022	2447467.45416	0.8865	+0.062	2447467.48783	0.9417	+0.308
2447467.42893	0.8451	−0.017	2447467.45452	0.8871	+0.059	2447467.48818	0.9422	+0.315
2447467.42928	0.8457	−0.019	2447467.45653	0.8904	+0.069	2447467.48852	0.9428	+0.310
2447467.42962	0.8462	−0.016	2447467.45688	0.8909	+0.071	2447467.48887	0.9434	+0.316
2447467.42997	0.8468	−0.018	2447467.45723	0.8915	+0.071	2447467.48922	0.9439	+0.317
2447467.43033	0.8474	−0.013	2447467.45757	0.8921	+0.084	2447467.48957	0.9445	+0.326
2447467.43066	0.8479	−0.013	2447467.45792	0.8926	+0.083	2447467.49172	0.9480	+0.348
2447467.43101	0.8485	−0.017	2447467.45827	0.8932	+0.081	2447467.49205	0.9486	+0.355
2447467.43136	0.8491	−0.008	2447467.45862	0.8938	+0.075	2447467.49240	0.9491	+0.365
2447467.43171	0.8497	−0.011	2447467.45896	0.8943	+0.093	2447467.49275	0.9497	+0.360
2447467.43205	0.8502	−0.013	2447467.45931	0.8949	+0.091	2447467.49310	0.9503	+0.370
2447467.43240	0.8508	−0.011	2447467.45966	0.8955	+0.088	2447467.49344	0.9508	+0.375
2447467.43275	0.8514	−0.004	2447467.46001	0.8961	+0.092	2447467.49379	0.9514	+0.377
2447467.43310	0.8519	−0.014	2447467.46035	0.8966	+0.094	2447467.49414	0.9520	+0.384
2447467.43344	0.8525	−0.014	2447467.46070	0.8972	+0.102	2447467.49448	0.9526	+0.380
2447467.43379	0.8531	−0.009	2447467.46105	0.8978	+0.097	2447467.49483	0.9531	+0.392
2447467.43414	0.8537	−0.001	2447467.46139	0.8983	+0.103	2447467.49518	0.9537	+0.401
2447467.43448	0.8542	−0.010	2447467.46174	0.8989	+0.096	2447467.49553	0.9543	+0.394
2447467.43586	0.8565	+0.003	2447467.46209	0.8995	+0.102	2447467.49587	0.9548	+0.398
2447467.43621	0.8570	+0.012	2447467.46244	0.9000	+0.101	2447467.49622	0.9554	+0.410
2447467.43656	0.8576	+0.012	2447467.46278	0.9006	+0.105	2447467.49657	0.9560	+0.405

Table 5.11: 1988 TPT *V* observations — *continued.*

H.J.D.	Phase	(V-C)	H.J.D.	Phase	(V-C)	H.J.D.	Phase	(V-C)
2447467.49691	0.9565	+0.411	2447467.52224	0.9981	+0.586	2447469.28026	0.8795	+0.047
2447467.49726	0.9571	+0.406	2447467.52259	0.9986	+0.587	2447469.28060	0.8801	+0.028
2447467.49761	0.9577	+0.410	2447467.52293	0.9992	+0.598	2447469.28095	0.8807	+0.042
2447467.49796	0.9583	+0.417	2447467.52328	0.9998	+0.589	2447469.28130	0.8812	+0.054
2447467.49830	0.9588	+0.408	2447467.52364	0.0003	+0.597	2447469.28165	0.8818	+0.042
2447467.50231	0.9654	+0.458	2447467.52398	0.0009	+0.590	2447469.28199	0.8824	+0.056
2447467.50266	0.9660	+0.444	2447467.52432	0.0015	+0.588	2447469.28234	0.8829	+0.042
2447467.50300	0.9665	+0.473	2447467.52467	0.0020	+0.592	2447469.28269	0.8835	+0.061
2447467.50335	0.9671	+0.457	2447467.52502	0.0026	+0.593	2447469.28689	0.8904	+0.065
2447467.50370	0.9677	+0.469	2447467.52558	0.0035	+0.591	2447469.28724	0.8910	+0.069
2447467.50404	0.9682	+0.467	2447467.52593	0.0041	+0.595	2447469.28758	0.8915	+0.071
2447467.50439	0.9688	+0.476	2447467.52628	0.0047	+0.590	2447469.28793	0.8921	+0.075
2447467.50474	0.9694	+0.475	2447467.52663	0.0052	+0.593	2447469.28828	0.8927	+0.067
2447467.50509	0.9699	+0.476	2447467.52697	0.0058	+0.587	2447469.28863	0.8932	+0.080
2447467.50543	0.9705	+0.491	2447467.52732	0.0064	+0.584	2447469.28897	0.8938	+0.065
2447467.50578	0.9711	+0.491	2447467.52767	0.0070	+0.581	2447469.28932	0.8944	+0.083
2447467.50614	0.9717	+0.500	2447467.52801	0.0075	+0.580	2447469.28967	0.8949	+0.080
2447467.50648	0.9722	+0.498	2447467.52836	0.0081	+0.577	2447469.29001	0.8955	+0.075
2447467.50682	0.9728	+0.490	2447467.52871	0.0087	+0.580	2447469.29067	0.8966	+0.090
2447467.50717	0.9734	+0.498	2447467.52906	0.0092	+0.582	2447469.29102	0.8972	+0.083
2447467.50752	0.9739	+0.511	2447467.52940	0.0098	+0.590	2447469.29137	0.8977	+0.076
2447467.50786	0.9745	+0.506	2447467.52975	0.0104	+0.581	2447469.29172	0.8983	+0.085
2447467.50821	0.9751	+0.515	2447467.53010	0.0109	+0.582	2447469.29206	0.8989	+0.096
2447467.50856	0.9756	+0.507	2447467.53045	0.0115	+0.571	2447469.29241	0.8994	+0.099
2447467.50891	0.9762	+0.514	2447467.53079	0.0121	+0.574	2447469.29276	0.9000	+0.092
2447467.51090	0.9795	+0.530	2447467.53114	0.0126	+0.567	2447469.29310	0.9006	+0.102
2447467.51123	0.9800	+0.532	2447467.53149	0.0132	+0.567	2447469.29345	0.9011	+0.107
2447467.51158	0.9806	+0.540	2447467.53183	0.0138	+0.577	2447469.29380	0.9017	+0.096
2447467.51193	0.9812	+0.546	2447467.53218	0.0143	+0.574	2447469.29545	0.9044	+0.106
2447467.51227	0.9817	+0.535	2447467.53485	0.0187	+0.549	2447469.29580	0.9050	+0.109
2447467.51262	0.9823	+0.552	2447467.53520	0.0193	+0.552	2447469.29615	0.9056	+0.114
2447467.51297	0.9829	+0.549	2447467.53555	0.0199	+0.549	2447469.29651	0.9062	+0.118
2447467.51332	0.9834	+0.551	2447467.53590	0.0204	+0.536	2447469.29684	0.9067	+0.134
2447467.51366	0.9840	+0.542	2447467.53624	0.0210	+0.542	2447469.29719	0.9073	+0.127
2447467.51401	0.9846	+0.555	2447467.53659	0.0216	+0.538	2447469.29754	0.9078	+0.139
2447467.51437	0.9852	+0.557	2447469.27113	0.8646	+0.006	2447469.29788	0.9084	+0.133
2447467.51470	0.9857	+0.553	2447469.27147	0.8651	−0.002	2447469.29823	0.9090	+0.134
2447467.51505	0.9863	+0.559	2447469.27182	0.8657	+0.004	2447469.29858	0.9095	+0.137
2447467.51540	0.9868	+0.572	2447469.27217	0.8663	+0.011	2447469.29932	0.9108	+0.142
2447467.51575	0.9874	+0.554	2447469.27251	0.8668	+0.003	2447469.29967	0.9113	+0.142
2447467.51609	0.9880	+0.573	2447469.27321	0.8680	+0.007	2447469.30001	0.9119	+0.140
2447467.51645	0.9886	+0.570	2447469.27356	0.8685	+0.023	2447469.30036	0.9125	+0.146
2447467.51679	0.9891	+0.577	2447469.27390	0.8691	+0.002	2447469.30071	0.9130	+0.144
2447467.51713	0.9897	+0.582	2447469.27425	0.8697	+0.010	2447469.30106	0.9136	+0.149
2447467.51748	0.9903	+0.570	2447469.27581	0.8722	+0.005	2447469.30140	0.9142	+0.158
2447467.51842	0.9918	+0.580	2447469.27616	0.8728	+0.020	2447469.30175	0.9147	+0.154
2447467.51878	0.9924	+0.579	2447469.27651	0.8734	+0.017	2447469.30210	0.9153	+0.150
2447467.51911	0.9929	+0.572	2447469.27685	0.8739	+0.032	2447469.30244	0.9159	+0.142
2447467.51946	0.9935	+0.584	2447469.27720	0.8745	+0.019	2447469.30395	0.9184	+0.164
2447467.51981	0.9941	+0.580	2447469.27755	0.8751	+0.023	2447469.30430	0.9189	+0.172
2447467.52016	0.9946	+0.569	2447469.27790	0.8757	+0.022	2447469.30464	0.9195	+0.182
2447467.52050	0.9952	+0.577	2447469.27824	0.8762	+0.033	2447469.30499	0.9201	+0.173
2447467.52085	0.9958	+0.590	2447469.27859	0.8768	+0.030	2447469.30534	0.9206	+0.183
2447467.52120	0.9963	+0.588	2447469.27894	0.8774	+0.037	2447469.30569	0.9212	+0.188
2447467.52154	0.9969	+0.586	2447469.27956	0.8784	+0.026	2447469.30603	0.9218	+0.186
2447467.52189	0.9975	+0.582	2447469.27991	0.8789	+0.052	2447469.30638	0.9223	+0.174

Table 5.11: 1988 TPT *V* observations — *continued.*

H.J.D.	Phase	(V-C)	H.J.D.	Phase	(V-C)	H.J.D.	Phase	(V-C)
2447469.30673	0.9229	+0.192	2447469.34603	0.9873	+0.547	2447469.37607	0.0366	+0.427
2447469.30707	0.9235	+0.189	2447469.34638	0.9879	+0.549	2447469.37643	0.0371	+0.415
2447469.31305	0.9333	+0.237	2447469.34673	0.9885	+0.546	2447469.37676	0.0377	+0.423
2447469.31341	0.9339	+0.243	2447469.34707	0.9890	+0.555	2447469.37712	0.0383	+0.410
2447469.31374	0.9344	+0.239	2447469.34742	0.9896	+0.564	2447469.37746	0.0388	+0.411
2447469.31409	0.9350	+0.259	2447469.35199	0.9971	+0.566	2447469.37780	0.0394	+0.402
2447469.31444	0.9355	+0.251	2447469.35234	0.9977	+0.553	2447469.37842	0.0404	+0.395
2447469.31478	0.9361	+0.248	2447469.35304	0.9988	+0.560	2447469.37875	0.0410	+0.401
2447469.31513	0.9367	+0.255	2447469.35338	0.9994	+0.561	2447469.37910	0.0415	+0.383
2447469.31548	0.9372	+0.259	2447469.35373	0.9999	+0.567	2447469.37945	0.0421	+0.393
2447469.31584	0.9378	+0.253	2447469.35408	0.0005	+0.554	2447469.37979	0.0427	+0.380
2447469.31617	0.9384	+0.255	2447469.35442	0.0011	+0.561	2447469.38014	0.0432	+0.389
2447469.31751	0.9406	+0.289	2447469.35512	0.0022	+0.563	2447469.38049	0.0438	+0.382
2447469.31786	0.9411	+0.277	2447469.35633	0.0042	+0.559	2447469.38084	0.0444	+0.382
2447469.31821	0.9417	+0.285	2447469.35668	0.0048	+0.556	2447469.38118	0.0449	+0.360
2447469.31856	0.9423	+0.302	2447469.35738	0.0059	+0.555	2447469.38153	0.0455	+0.370
2447469.31890	0.9429	+0.297	2447469.35772	0.0065	+0.545	2447469.38323	0.0483	+0.358
2447469.31925	0.9434	+0.296	2447469.35807	0.0071	+0.545	2447469.38358	0.0489	+0.345
2447469.31960	0.9440	+0.301	2447469.35842	0.0076	+0.549	2447469.38393	0.0494	+0.356
2447469.31996	0.9446	+0.304	2447469.35876	0.0082	+0.559	2447469.38427	0.0500	+0.331
2447469.32029	0.9451	+0.319	2447469.35911	0.0088	+0.554	2447469.38462	0.0506	+0.342
2447469.32064	0.9457	+0.297	2447469.35946	0.0093	+0.543	2447469.38497	0.0511	+0.332
2447469.32119	0.9466	+0.322	2447469.36070	0.0114	+0.534	2447469.38532	0.0517	+0.329
2447469.32154	0.9472	+0.323	2447469.36104	0.0119	+0.542	2447469.38566	0.0523	+0.324
2447469.32189	0.9478	+0.332	2447469.36139	0.0125	+0.531	2447469.38601	0.0529	+0.322
2447469.32224	0.9483	+0.337	2447469.36174	0.0131	+0.535	2447469.38636	0.0534	+0.319
2447469.32258	0.9489	+0.335	2447469.36209	0.0136	+0.533	2447469.38683	0.0542	+0.306
2447469.32293	0.9495	+0.350	2447469.36243	0.0142	+0.528	2447469.38717	0.0548	+0.302
2447469.32328	0.9500	+0.350	2447469.36278	0.0148	+0.534	2447469.38751	0.0553	+0.313
2447469.32363	0.9506	+0.346	2447469.36313	0.0153	+0.524	2447469.38786	0.0559	+0.309
2447469.32397	0.9512	+0.346	2447469.36347	0.0159	+0.539	2447469.38821	0.0565	+0.306
2447469.32432	0.9517	+0.350	2447469.36382	0.0165	+0.530	2447469.38856	0.0570	+0.292
2447469.32550	0.9537	+0.356	2447469.36492	0.0183	+0.517	2447469.38890	0.0576	+0.287
2447469.32585	0.9542	+0.376	2447469.36527	0.0189	+0.520	2447469.38926	0.0582	+0.295
2447469.32619	0.9548	+0.380	2447469.36562	0.0194	+0.512	2447469.38960	0.0587	+0.272
2447469.32654	0.9554	+0.375	2447469.36596	0.0200	+0.497	2447469.38994	0.0593	+0.277
2447469.32689	0.9559	+0.378	2447469.36631	0.0206	+0.498	2447469.39785	0.0723	+0.201
2447469.32724	0.9565	+0.384	2447469.36667	0.0212	+0.503	2447469.39820	0.0728	+0.199
2447469.32758	0.9571	+0.389	2447469.36702	0.0217	+0.513	2447469.39854	0.0734	+0.191
2447469.32793	0.9577	+0.388	2447469.36735	0.0223	+0.493	2447469.39889	0.0740	+0.199
2447469.32863	0.9588	+0.389	2447469.36770	0.0228	+0.503	2447469.39924	0.0745	+0.182
2447469.34022	0.9778	+0.504	2447469.36805	0.0234	+0.493	2447469.39959	0.0751	+0.182
2447469.34057	0.9784	+0.512	2447469.36996	0.0265	+0.487	2447469.39993	0.0757	+0.179
2447469.34092	0.9789	+0.521	2447469.37030	0.0271	+0.469	2447469.40028	0.0762	+0.178
2447469.34126	0.9795	+0.515	2447469.37065	0.0277	+0.453	2447469.40063	0.0768	+0.175
2447469.34161	0.9801	+0.534	2447469.37100	0.0282	+0.465	2447469.40097	0.0774	+0.168
2447469.34196	0.9807	+0.519	2447469.37135	0.0288	+0.475	2447469.40144	0.0781	+0.166
2447469.34231	0.9812	+0.526	2447469.37169	0.0294	+0.462	2447469.40179	0.0787	+0.166
2447469.34265	0.9818	+0.525	2447469.37204	0.0300	+0.464	2447469.40213	0.0793	+0.148
2447469.34300	0.9824	+0.533	2447469.37239	0.0305	+0.467	2447469.40248	0.0798	+0.149
2447469.34335	0.9829	+0.537	2447469.37273	0.0311	+0.457	2447469.40283	0.0804	+0.163
2447469.34430	0.9845	+0.546	2447469.37308	0.0317	+0.461	2447469.40319	0.0810	+0.166
2447469.34464	0.9850	+0.546	2447469.37468	0.0343	+0.430	2447469.40352	0.0815	+0.151
2447469.34499	0.9856	+0.553	2447469.37503	0.0349	+0.445	2447469.40387	0.0821	+0.146
2447469.34535	0.9862	+0.535	2447469.37537	0.0354	+0.414	2447469.40423	0.0827	+0.146
2447469.34569	0.9868	+0.549	2447469.37572	0.0360	+0.416	2447469.40456	0.0833	+0.144

Table 5.11: 1988 TPT *V* observations — *continued.*

H.J.D.	Phase	(V-C)	H.J.D.	Phase	(V-C)	H.J.D.	Phase	(V-C)
2447469.40606	0.0857	+0.141	2447469.42740	0.1207	+0.017	2447469.45349	0.1635	−0.064
2447469.40640	0.0863	+0.125	2447469.42775	0.1213	+0.021	2447469.45383	0.1640	−0.049
2447469.40675	0.0868	+0.140	2447469.42809	0.1218	+0.016	2447469.45418	0.1646	−0.063
2447469.40710	0.0874	+0.120	2447469.42844	0.1224	+0.006	2447469.45453	0.1652	−0.051
2447469.40744	0.0880	+0.125	2447469.42988	0.1248	+0.004	2447469.45488	0.1657	−0.062
2447469.40779	0.0885	+0.116	2447469.43022	0.1253	+0.011	2447469.45522	0.1663	−0.060
2447469.40814	0.0891	+0.117	2447469.43057	0.1259	+0.011	2447469.45557	0.1669	−0.059
2447469.40849	0.0897	+0.112	2447469.43092	0.1265	+0.016	2447469.45592	0.1674	−0.072
2447469.40883	0.0903	+0.109	2447469.43126	0.1270	+0.001	2447469.45732	0.1697	−0.064
2447469.40918	0.0908	+0.116	2447469.43161	0.1276	+0.002	2447469.45766	0.1703	−0.068
2447469.40954	0.0914	+0.114	2447469.43196	0.1282	+0.001	2447469.45801	0.1709	−0.064
2447469.40989	0.0920	+0.108	2447469.43231	0.1287	+0.007	2447469.45836	0.1714	−0.057
2447469.41022	0.0925	+0.110	2447469.43265	0.1293	+0.004	2447469.45871	0.1720	−0.073
2447469.41057	0.0931	+0.101	2447469.43300	0.1299	−0.004	2447469.45905	0.1726	−0.074
2447469.41092	0.0937	+0.104	2447469.43335	0.1304	+0.006	2447469.45940	0.1731	−0.069
2447469.41126	0.0942	+0.102	2447469.43369	0.1310	+0.002	2447469.45975	0.1737	−0.067
2447469.41161	0.0948	+0.101	2447469.43404	0.1316	−0.001	2447469.46010	0.1743	−0.067
2447469.41196	0.0954	+0.102	2447469.43439	0.1321	−0.010	2447469.46044	0.1748	−0.053
2447469.41231	0.0960	+0.093	2447469.43474	0.1327	+0.000	2447469.46079	0.1754	−0.067
2447469.41265	0.0965	+0.086	2447469.43508	0.1333	−0.005	2447469.46114	0.1760	−0.067
2447469.41352	0.0979	+0.088	2447469.43543	0.1339	−0.003	2447469.46148	0.1765	−0.061
2447469.41387	0.0985	+0.086	2447469.43578	0.1344	−0.003	2447469.46183	0.1771	−0.068
2447469.41422	0.0991	+0.092	2447469.43613	0.1350	−0.007	2447469.46218	0.1777	−0.069
2447469.41456	0.0996	+0.080	2447469.43647	0.1356	−0.002	2447469.46253	0.1783	−0.069
2447469.41491	0.1002	+0.079	2447469.44036	0.1419	−0.024	2447469.46287	0.1788	−0.070
2447469.41526	0.1008	+0.087	2447469.44071	0.1425	−0.020	2447469.46322	0.1794	−0.069
2447469.41560	0.1013	+0.072	2447469.44106	0.1431	−0.027	2447469.46357	0.1800	−0.075
2447469.41595	0.1019	+0.070	2447469.44140	0.1436	−0.025	2447469.46391	0.1805	−0.078
2447469.41630	0.1025	+0.073	2447469.44175	0.1442	−0.023	2447469.46626	0.1844	−0.084
2447469.41666	0.1031	+0.057	2447469.44210	0.1448	−0.023	2447469.46661	0.1850	−0.085
2447469.41701	0.1037	+0.065	2447469.44244	0.1453	−0.035	2447469.46697	0.1855	−0.079
2447469.41734	0.1042	+0.065	2447469.44279	0.1459	−0.029	2447469.46732	0.1861	−0.074
2447469.41769	0.1048	+0.067	2447469.44314	0.1465	−0.034	2447469.46766	0.1867	−0.077
2447469.41804	0.1053	+0.057	2447469.44349	0.1471	−0.021	2447469.46801	0.1873	−0.070
2447469.41838	0.1059	+0.065	2447469.44383	0.1476	−0.038	2447469.46835	0.1878	−0.078
2447469.41873	0.1065	+0.066	2447469.44418	0.1482	−0.024	2447469.46869	0.1884	−0.075
2447469.41908	0.1071	+0.066	2447469.44453	0.1488	−0.019	2447469.46904	0.1889	−0.077
2447469.41942	0.1076	+0.053	2447469.44488	0.1493	−0.033	2447469.46939	0.1895	−0.072
2447469.41977	0.1082	+0.058	2447469.44522	0.1499	−0.036	2447469.46974	0.1901	−0.080
2447469.42012	0.1088	+0.060	2447469.44557	0.1505	−0.030	2447469.47008	0.1906	−0.076
2447469.42184	0.1116	+0.037	2447469.44592	0.1510	−0.037	2447469.47043	0.1912	−0.069
2447469.42219	0.1122	+0.036	2447469.44626	0.1516	−0.030	2447469.47079	0.1918	−0.084
2447469.42254	0.1127	+0.038	2447469.44661	0.1522	−0.034	2447469.47114	0.1924	−0.078
2447469.42288	0.1133	+0.034	2447469.44696	0.1527	−0.037	2447469.47148	0.1929	−0.078
2447469.42323	0.1139	+0.037	2447469.44932	0.1566	−0.045	2447469.47182	0.1935	−0.077
2447469.42358	0.1144	+0.028	2447469.44967	0.1572	−0.042	2447469.47217	0.1941	−0.081
2447469.42393	0.1150	+0.037	2447469.45001	0.1577	−0.052	2447469.47251	0.1946	−0.070
2447469.42427	0.1156	+0.041	2447469.45037	0.1583	−0.038	2447469.47286	0.1952	−0.081
2447469.42462	0.1161	+0.033	2447469.45072	0.1589	−0.049	2447469.47470	0.1982	−0.088
2447469.42497	0.1167	+0.022	2447469.45106	0.1595	−0.050	2447469.47505	0.1988	−0.083
2447469.42532	0.1173	+0.016	2447469.45140	0.1600	−0.049	2447469.47540	0.1994	−0.080
2447469.42566	0.1178	+0.025	2447469.45175	0.1606	−0.052	2447469.47574	0.1999	−0.089
2447469.42601	0.1184	+0.016	2447469.45210	0.1612	−0.054	2447469.47609	0.2005	−0.097
2447469.42636	0.1190	+0.021	2447469.45244	0.1617	−0.051	2447469.47644	0.2011	−0.096
2447469.42670	0.1195	+0.011	2447469.45280	0.1623	−0.054	2447469.47680	0.2017	−0.098
2447469.42705	0.1201	+0.016	2447469.45314	0.1629	−0.052	2447469.47713	0.2022	−0.089

Table 5.11: 1988 TPT *V* observations — *continued.*

H.J.D.	Phase	(V-C)	H.J.D.	Phase	(V-C)	H.J.D.	Phase	(V-C)
2447469.47748	0.2028	−0.086	2447469.51210	0.2595	−0.120	2447469.53782	0.3017	−0.087
2447469.47783	0.2033	−0.091	2447469.51244	0.2601	−0.126	2447469.53816	0.3022	−0.090
2447469.47817	0.2039	−0.093	2447469.51279	0.2606	−0.118	2447469.53851	0.3028	−0.092
2447469.47852	0.2045	−0.082	2447469.51314	0.2612	−0.120	2447469.53886	0.3034	−0.094
2447469.47887	0.2051	−0.089	2447469.51349	0.2618	−0.120	2447469.53920	0.3039	−0.095
2447469.47922	0.2056	−0.086	2447469.51383	0.2624	−0.126	2447469.53956	0.3045	−0.078
2447469.47956	0.2062	−0.092	2447469.51437	0.2632	−0.128	2447469.53991	0.3051	−0.089
2447469.47991	0.2068	−0.103	2447469.51471	0.2638	−0.113	2447469.54025	0.3057	−0.072
2447469.48026	0.2073	−0.098	2447469.51506	0.2644	−0.126	2447469.54059	0.3062	−0.079
2447469.48060	0.2079	−0.093	2447469.51541	0.2649	−0.108	2447469.54094	0.3068	−0.072
2447469.48095	0.2085	−0.105	2447469.51576	0.2655	−0.115	2447469.55930	0.3369	−0.076
2447469.48130	0.2090	−0.104	2447469.51610	0.2661	−0.119	2447469.55964	0.3374	−0.068
2447469.48345	0.2126	−0.102	2447469.51645	0.2666	−0.111	2447469.55999	0.3380	−0.072
2447469.48380	0.2131	−0.101	2447469.51680	0.2672	−0.118	2447469.56034	0.3386	−0.076
2447469.48415	0.2137	−0.095	2447469.51714	0.2678	−0.118	2447469.56069	0.3392	−0.073
2447469.48449	0.2143	−0.103	2447469.51749	0.2684	−0.109	2447469.56103	0.3397	−0.069
2447469.48484	0.2148	−0.099	2447469.52059	0.2734	−0.117	2447469.56138	0.3403	−0.072
2447469.48519	0.2154	−0.096	2447469.52094	0.2740	−0.102	2447469.56173	0.3409	−0.058
2447469.48554	0.2160	−0.089	2447469.52129	0.2746	−0.117	2447469.56207	0.3414	−0.063
2447469.48588	0.2165	−0.101	2447469.52163	0.2751	−0.107	2447469.56242	0.3420	−0.067
2447469.48623	0.2171	−0.101	2447469.52198	0.2757	−0.113	2447469.56293	0.3428	−0.065
2447469.48658	0.2177	−0.113	2447469.52233	0.2763	−0.120	2447469.56328	0.3434	−0.073
2447469.49180	0.2262	−0.090	2447469.52268	0.2769	−0.117	2447469.56363	0.3440	−0.070
2447469.49214	0.2268	−0.107	2447469.52302	0.2774	−0.102	2447469.56397	0.3445	−0.073
2447469.49249	0.2274	−0.101	2447469.52337	0.2780	−0.111	2447469.56432	0.3451	−0.068
2447469.49284	0.2279	−0.105	2447469.52372	0.2786	−0.108	2447469.56467	0.3457	−0.065
2447469.49319	0.2285	−0.093	2447469.52532	0.2812	−0.106	2447469.56501	0.3462	−0.060
2447469.49353	0.2291	−0.114	2447469.52566	0.2817	−0.116	2447469.56536	0.3468	−0.056
2447469.49388	0.2297	−0.096	2447469.52601	0.2823	−0.102	2447469.56571	0.3474	−0.062
2447469.49423	0.2302	−0.106	2447469.52636	0.2829	−0.097	2447469.56607	0.3480	−0.067
2447469.49457	0.2308	−0.113	2447469.52670	0.2834	−0.098	2447469.56762	0.3505	−0.055
2447469.49492	0.2314	−0.113	2447469.52705	0.2840	−0.107	2447469.56797	0.3511	−0.058
2447469.49617	0.2334	−0.105	2447469.52740	0.2846	−0.101	2447469.56831	0.3516	−0.052
2447469.49652	0.2340	−0.116	2447469.52775	0.2852	−0.095	2447469.56866	0.3522	−0.063
2447469.49687	0.2346	−0.121	2447469.52809	0.2857	−0.088	2447469.56901	0.3528	−0.054
2447469.49721	0.2351	−0.110	2447469.52844	0.2863	−0.096	2447469.56935	0.3534	−0.051
2447469.49756	0.2357	−0.111	2447469.52895	0.2871	−0.099	2447469.56970	0.3539	−0.051
2447469.49792	0.2363	−0.110	2447469.52930	0.2877	−0.094	2447469.57005	0.3545	−0.049
2447469.49826	0.2368	−0.115	2447469.52964	0.2883	−0.100	2447469.57040	0.3551	−0.059
2447469.49860	0.2374	−0.118	2447469.52999	0.2888	−0.099	2447469.57074	0.3556	−0.041
2447469.49895	0.2380	−0.105	2447469.53034	0.2894	−0.093	2447469.57109	0.3562	−0.051
2447469.49930	0.2385	−0.108	2447469.53069	0.2900	−0.095	2447469.57144	0.3568	−0.054
2447469.50247	0.2437	−0.109	2447469.53104	0.2906	−0.101	2447469.57179	0.3574	−0.047
2447469.50282	0.2443	−0.109	2447469.53139	0.2911	−0.086	2447469.57213	0.3579	−0.050
2447469.50316	0.2449	−0.110	2447469.53173	0.2917	−0.088	2447469.57248	0.3585	−0.037
2447469.50351	0.2454	−0.112	2447469.53207	0.2922	−0.098	2447469.57283	0.3591	−0.042
2447469.50386	0.2460	−0.119	2447469.53434	0.2960	−0.086	2447469.57317	0.3596	−0.045
2447469.50420	0.2466	−0.122	2447469.53469	0.2965	−0.089	2447469.57352	0.3602	−0.052
2447469.50455	0.2471	−0.103	2447469.53504	0.2971	−0.087	2447469.57387	0.3608	−0.047
2447469.50490	0.2477	−0.104	2447469.53538	0.2977	−0.091	2447469.57422	0.3613	−0.043
2447469.50525	0.2483	−0.129	2447469.53573	0.2982	−0.103	2447469.57791	0.3674	−0.036
2447469.50559	0.2488	−0.108	2447469.53608	0.2988	−0.094	2447469.57824	0.3679	−0.040
2447469.51071	0.2572	−0.099	2447469.53643	0.2994	−0.087	2447469.57859	0.3685	−0.034
2447469.51106	0.2578	−0.116	2447469.53677	0.3000	−0.090	2447469.57894	0.3691	−0.023
2447469.51140	0.2584	−0.117	2447469.53712	0.3005	−0.093	2447469.57929	0.3696	−0.032
2447469.51175	0.2589	−0.116	2447469.53747	0.3011	−0.082	2447469.57963	0.3702	−0.025

Table 5.11: 1988 TPT *V* observations — *continued.*

H.J.D.	Phase	(V-C)	H.J.D.	Phase	(V-C)	H.J.D.	Phase	(V-C)
2447469.57998	0.3708	−0.030	2447469.61043	0.4207	+0.055	2447469.64836	0.4829	+0.142
2447469.58033	0.3713	−0.031	2447469.61078	0.4213	+0.060	2447469.64931	0.4844	+0.154
2447469.58067	0.3719	−0.023	2447469.61113	0.4218	+0.059	2447469.64966	0.4850	+0.156
2447469.58102	0.3725	−0.025	2447469.61147	0.4224	+0.052	2447469.65000	0.4855	+0.158
2447469.58137	0.3731	−0.021	2447469.61182	0.4230	+0.060	2447469.65035	0.4861	+0.155
2447469.58172	0.3736	−0.026	2447469.61217	0.4235	+0.062	2447469.65070	0.4867	+0.154
2447469.58206	0.3742	−0.025	2447469.61251	0.4241	+0.051	2447469.65104	0.4872	+0.148
2447469.58241	0.3748	−0.024	2447469.61286	0.4247	+0.061	2447469.65139	0.4878	+0.150
2447469.58276	0.3753	−0.021	2447469.61322	0.4253	+0.051	2447469.65174	0.4884	+0.151
2447469.58310	0.3759	−0.013	2447469.61357	0.4258	+0.052	2447469.65209	0.4890	+0.156
2447469.58345	0.3765	−0.020	2447469.61391	0.4264	+0.065	2447469.65243	0.4895	+0.160
2447469.58380	0.3770	−0.007	2447469.61426	0.4270	+0.062	2447469.65278	0.4901	+0.146
2447469.58415	0.3776	−0.005	2447469.61460	0.4275	+0.063	2447469.65313	0.4907	+0.151
2447469.58449	0.3782	−0.011	2447469.61494	0.4281	+0.067	2447469.65347	0.4912	+0.155
2447469.58880	0.3852	+0.013	2447469.61529	0.4286	+0.060	2447469.65382	0.4918	+0.153
2447469.58915	0.3858	+0.003	2447469.61564	0.4292	+0.065	2447469.65417	0.4924	+0.160
2447469.58949	0.3864	+0.012	2447469.61600	0.4298	+0.072	2447469.65486	0.4935	+0.156
2447469.58985	0.3870	+0.003	2447469.61635	0.4304	+0.071	2447469.65521	0.4941	+0.162
2447469.59020	0.3875	+0.004	2447469.62121	0.4384	+0.093	2447469.65556	0.4947	+0.164
2447469.59055	0.3881	+0.004	2447469.62155	0.4389	+0.090	2447469.65591	0.4952	+0.149
2447469.59089	0.3887	+0.009	2447469.62190	0.4395	+0.093	2447469.65710	0.4972	+0.144
2447469.59123	0.3892	+0.009	2447469.62260	0.4406	+0.089	2447469.65744	0.4977	+0.160
2447469.59158	0.3898	+0.000	2447469.62294	0.4412	+0.084	2447469.65779	0.4983	+0.149
2447469.59192	0.3903	+0.009	2447469.62329	0.4418	+0.098	2447469.65814	0.4989	+0.164
2447469.59227	0.3909	+0.012	2447469.62364	0.4423	+0.084	2447469.65849	0.4995	+0.157
2447469.59262	0.3915	+0.010	2447469.62398	0.4429	+0.091	2447469.65883	0.5000	+0.154
2447469.59297	0.3921	+0.008	2447469.62433	0.4435	+0.095	2447469.65953	0.5012	+0.152
2447469.59331	0.3926	+0.009	2447469.62468	0.4440	+0.100	2447469.65988	0.5017	+0.153
2447469.59366	0.3932	+0.015	2447469.62503	0.4446	+0.093	2447469.66022	0.5023	+0.154
2447469.59401	0.3938	+0.009	2447469.62537	0.4452	+0.084	2447469.66057	0.5029	+0.155
2447469.59435	0.3943	+0.002	2447469.62572	0.4457	+0.096	2447469.66092	0.5034	+0.148
2447469.59470	0.3949	+0.023	2447469.62608	0.4463	+0.094	2447469.66126	0.5040	+0.147
2447469.59505	0.3955	+0.012	2447469.62641	0.4469	+0.089	2447469.66196	0.5051	+0.150
2447469.59540	0.3960	+0.019	2447469.62676	0.4474	+0.093	2447469.66231	0.5057	+0.146
2447469.59698	0.3986	+0.029	2447469.62711	0.4480	+0.107	2447469.66265	0.5063	+0.147
2447469.59733	0.3992	+0.012	2447469.62746	0.4486	+0.105	2447469.66300	0.5068	+0.138
2447469.59768	0.3998	+0.022	2447469.62780	0.4492	+0.111	2447469.66335	0.5074	+0.153
2447469.59802	0.4003	+0.031	2447469.64176	0.4720	+0.139	2447469.66369	0.5080	+0.154
2447469.59837	0.4009	+0.032	2447469.64211	0.4726	+0.152	2447469.66798	0.5150	+0.140
2447469.59872	0.4015	+0.020	2447469.64246	0.4732	+0.155	2447469.66832	0.5156	+0.143
2447469.59907	0.4021	+0.027	2447469.64280	0.4737	+0.151	2447469.66867	0.5161	+0.148
2447469.59941	0.4026	+0.024	2447469.64315	0.4743	+0.141	2447469.66902	0.5167	+0.153
2447469.59976	0.4032	+0.029	2447469.64350	0.4749	+0.152	2447469.66937	0.5173	+0.135
2447469.60011	0.4038	+0.010	2447469.64385	0.4755	+0.152	2447469.66971	0.5178	+0.148
2447469.60045	0.4043	+0.031	2447469.64419	0.4760	+0.152	2447469.67006	0.5184	+0.148
2447469.60080	0.4049	+0.024	2447469.64454	0.4766	+0.152	2447469.67041	0.5190	+0.140
2447469.60115	0.4055	+0.034	2447469.64489	0.4772	+0.144	2447469.67076	0.5196	+0.151
2447469.60150	0.4060	+0.028	2447469.64523	0.4777	+0.148	2447469.67110	0.5201	+0.140
2447469.60184	0.4066	+0.036	2447469.64558	0.4783	+0.149	2447469.67145	0.5207	+0.151
2447469.60219	0.4072	+0.034	2447469.64593	0.4789	+0.156	2447469.67180	0.5213	+0.149
2447469.60254	0.4078	+0.032	2447469.64628	0.4794	+0.141	2447469.67214	0.5218	+0.138
2447469.60288	0.4083	+0.033	2447469.64662	0.4800	+0.157	2447469.67249	0.5224	+0.132
2447469.60323	0.4089	+0.032	2447469.64697	0.4806	+0.153	2447469.67284	0.5230	+0.153
2447469.60358	0.4095	+0.025	2447469.64732	0.4811	+0.155	2447469.67319	0.5236	+0.134
2447469.60974	0.4196	+0.045	2447469.64766	0.4817	+0.145	2447469.67353	0.5241	+0.132
2447469.61008	0.4201	+0.050	2447469.64801	0.4823	+0.156	2447469.67388	0.5247	+0.134

Table 5.11: 1988 TPT *V* observations — *continued.*

H.J.D.	Phase	(V-C)	H.J.D.	Phase	(V-C)	H.J.D.	Phase	(V-C)
2447469.67423	0.5253	+0.144	2447469.68868	0.5489	+0.119	2447469.70372	0.5736	+0.071
2447469.67457	0.5258	+0.136	2447469.68903	0.5495	+0.115	2447469.70407	0.5742	+0.080
2447469.67570	0.5277	+0.144	2447469.68937	0.5501	+0.098	2447469.70441	0.5747	+0.079
2447469.67603	0.5282	+0.126	2447469.68971	0.5506	+0.118	2447469.70476	0.5753	+0.059
2447469.67638	0.5288	+0.123	2447469.69006	0.5512	+0.100	2447469.70511	0.5759	+0.064
2447469.67673	0.5294	+0.130	2447469.69159	0.5537	+0.085	2447469.70545	0.5764	+0.049
2447469.67707	0.5299	+0.142	2447469.69194	0.5543	+0.105	2447469.70580	0.5770	+0.074
2447469.67742	0.5305	+0.139	2447469.69228	0.5548	+0.110	2447469.70615	0.5776	+0.066
2447469.67777	0.5311	+0.132	2447469.69263	0.5554	+0.109	2447469.70680	0.5786	+0.061
2447469.67813	0.5316	+0.144	2447469.69298	0.5560	+0.097	2447469.70714	0.5792	+0.076
2447469.67846	0.5322	+0.145	2447469.69332	0.5565	+0.113	2447469.70749	0.5798	+0.069
2447469.67882	0.5328	+0.140	2447469.69367	0.5571	+0.105	2447469.70784	0.5803	+0.059
2447469.67916	0.5333	+0.133	2447469.69402	0.5577	+0.106	2447469.70819	0.5809	+0.056
2447469.67951	0.5339	+0.130	2447469.69437	0.5583	+0.098	2447469.70853	0.5815	+0.066
2447469.67985	0.5345	+0.121	2447469.69471	0.5588	+0.100	2447469.70888	0.5820	+0.067
2447469.68020	0.5350	+0.119	2447469.69506	0.5594	+0.090	2447469.70923	0.5826	+0.071
2447469.68055	0.5356	+0.137	2447469.69541	0.5600	+0.091	2447469.70957	0.5832	+0.049
2447469.68089	0.5362	+0.122	2447469.69576	0.5605	+0.109	2447469.70992	0.5838	+0.078
2447469.68124	0.5367	+0.135	2447469.69610	0.5611	+0.090	2447469.71518	0.5924	+0.024
2447469.68159	0.5373	+0.128	2447469.69645	0.5617	+0.117	2447469.71552	0.5929	+0.036
2447469.68194	0.5379	+0.131	2447469.69680	0.5622	+0.105	2447469.71587	0.5935	+0.033
2447469.68228	0.5384	+0.128	2447469.69714	0.5628	+0.096	2447469.71622	0.5941	+0.027
2447469.68346	0.5404	+0.106	2447469.69749	0.5634	+0.098	2447469.71657	0.5947	+0.037
2447469.68381	0.5410	+0.125	2447469.69784	0.5640	+0.102	2447469.71691	0.5952	+0.030
2447469.68416	0.5415	+0.131	2447469.69819	0.5645	+0.084	2447469.71726	0.5958	+0.029
2447469.68451	0.5421	+0.122	2447469.69955	0.5668	+0.098	2447469.71761	0.5964	+0.014
2447469.68485	0.5427	+0.095	2447469.69990	0.5673	+0.087	2447469.71795	0.5969	+0.029
2447469.68520	0.5432	+0.124	2447469.70025	0.5679	+0.084	2447469.71830	0.5975	+0.038
2447469.68555	0.5438	+0.124	2447469.70059	0.5685	+0.083	2447469.71912	0.5988	+0.027
2447469.68589	0.5444	+0.127	2447469.70094	0.5690	+0.092	2447469.71983	0.6000	+0.032
2447469.68624	0.5449	+0.110	2447469.70129	0.5696	+0.094	2447469.72018	0.6006	+0.041
2447469.68659	0.5455	+0.110	2447469.70163	0.5702	+0.072	2447469.72051	0.6011	+0.032
2447469.68694	0.5461	+0.116	2447469.70198	0.5707	+0.087	2447469.72086	0.6017	+0.039
2447469.68728	0.5466	+0.127	2447469.70233	0.5713	+0.080	2447469.72121	0.6023	+0.027
2447469.68764	0.5472	+0.105	2447469.70268	0.5719	+0.078	2447469.72155	0.6028	+0.016
2447469.68799	0.5478	+0.124	2447469.70302	0.5724	+0.087	2447469.72190	0.6034	+0.044
2447469.68832	0.5483	+0.120	2447469.70337	0.5730	+0.070	2447469.72225	0.6040	+0.030

Table 5.12: 1987 UKIRT J observations.

H.J.D.	Phase	(V-C)	H.J.D.	Phase	(V-C)	H.J.D.	Phase	(V-C)
2447116.78886	0.1301	−0.011	2447117.01913	0.5075	+0.196	2447117.85667	0.8803	−0.002
2447116.80221	0.1520	−0.062	2447117.03072	0.5265	+0.171	2447117.85843	0.8832	−0.002
2447116.80387	0.1547	−0.071	2447117.03756	0.5377	+0.146	2447117.86531	0.8944	+0.041
2447116.81054	0.1656	−0.076	2447117.03931	0.5406	+0.135	2447117.87468	0.9098	+0.083
2447116.81247	0.1688	−0.075	2447117.04613	0.5518	+0.109	2447117.87641	0.9126	+0.094
2447116.82235	0.1850	−0.098	2447117.05626	0.5684	+0.068	2447117.88293	0.9233	+0.136
2447116.82958	0.1968	−0.104	2447117.05849	0.5720	+0.056	2447117.88466	0.9261	+0.156
2447116.83129	0.1996	−0.093	2447117.72119	0.6582	−0.081	2447117.89450	0.9423	+0.239
2447116.83811	0.2108	−0.119	2447117.72290	0.6610	−0.089	2447117.90125	0.9533	+0.280
2447116.85154	0.2328	−0.132	2447117.73013	0.6729	−0.101	2447117.90301	0.9562	+0.300
2447116.85886	0.2448	−0.138	2447117.73193	0.6758	−0.100	2447117.90959	0.9670	+0.352
2447116.86096	0.2483	−0.147	2447117.74162	0.6917	−0.110	2447117.91934	0.9830	+0.413
2447116.86778	0.2594	−0.144	2447117.74967	0.7049	−0.113	2447117.92110	0.9859	+0.423
2447116.88466	0.2871	−0.137	2447117.75154	0.7080	−0.121	2447117.92904	0.9989	+0.444
2447116.89241	0.2998	−0.114	2447117.75941	0.7209	−0.115	2447117.93092	0.0020	+0.434
2447116.89419	0.3027	−0.113	2447117.77133	0.7404	−0.116	2447117.93875	0.0148	+0.415
2447116.90116	0.3141	−0.110	2447117.77779	0.7510	−0.112	2447117.94075	0.0181	+0.405
2447116.91115	0.3305	−0.097	2447117.77965	0.7540	−0.120	2447117.95473	0.0410	+0.295
2447116.91317	0.3338	−0.117	2447117.78911	0.7695	−0.124	2447117.96162	0.0523	+0.255
2447116.92071	0.3462	−0.104	2447117.79853	0.7850	−0.099	2447117.96341	0.0552	+0.225
2447116.92246	0.3491	−0.084	2447117.80026	0.7878	−0.088	2447117.97009	0.0662	+0.174
2447116.94311	0.3829	−0.059	2447117.80731	0.7994	−0.084	2447117.98345	0.0881	+0.092
2447116.94558	0.3870	−0.039	2447117.80899	0.8021	−0.093	2447117.99034	0.0994	+0.050
2447116.95439	0.4014	−0.027	2447117.82960	0.8359	−0.063	2447117.99233	0.1026	+0.040
2447116.95651	0.4049	−0.027	2447117.83130	0.8387	−0.062	2447118.00236	0.1191	+0.006
2447116.96784	0.4234	+0.024	2447117.83740	0.8487	−0.050	2447118.00920	0.1303	−0.026
2447117.00832	0.4898	+0.190	2447117.83911	0.8515	−0.059	2447118.01101	0.1332	−0.027
2447117.01033	0.4931	+0.199	2447117.85022	0.8697	−0.025	2447118.01777	0.1443	−0.041
2447117.01718	0.5043	+0.197						

Table 5.13: 1987 UKIRT *K* observations.

H.J.D.	Phase	(V-C)	H.J.D.	Phase	(V-C)	H.J.D.	Phase	(V-C)
2447116.78446	0.1229	−0.202	2447117.02167	0.5117	+0.056	2447117.86081	0.8871	−0.157
2447116.78631	0.1259	−0.211	2447117.03319	0.5305	+0.023	2447117.86261	0.8900	−0.166
2447116.79974	0.1479	−0.223	2447117.03492	0.5334	+0.012	2447117.87216	0.9057	−0.113
2447116.80619	0.1585	−0.230	2447117.04165	0.5444	−0.012	2447117.87866	0.9163	−0.081
2447116.80791	0.1613	−0.219	2447117.04346	0.5474	−0.022	2447117.88041	0.9192	−0.070
2447116.81492	0.1728	−0.235	2447117.05335	0.5636	−0.069	2447117.88712	0.9302	−0.028
2447116.82529	0.1898	−0.270	2447117.06173	0.5773	−0.106	2447117.89683	0.9461	+0.045
2447116.82707	0.1927	−0.270	2447117.71860	0.6540	−0.241	2447117.89864	0.9491	+0.055
2447116.83370	0.2036	−0.287	2447117.72546	0.6652	−0.245	2447117.90528	0.9599	+0.107
2447116.83557	0.2066	−0.296	2447117.72748	0.6685	−0.253	2447117.90704	0.9628	+0.118
2447116.85407	0.2370	−0.298	2447117.73420	0.6795	−0.267	2447117.91659	0.9785	+0.190
2447116.85596	0.2401	−0.297	2447117.74438	0.6962	−0.269	2447117.92383	0.9903	+0.222
2447116.86358	0.2526	−0.325	2447117.74660	0.6999	−0.277	2447117.92650	0.9947	+0.222
2447116.86526	0.2553	−0.324	2447117.75387	0.7118	−0.282	2447117.93379	0.0067	+0.224
2447116.88729	0.2914	−0.306	2447117.75598	0.7152	−0.271	2447117.93590	0.0101	+0.214
2447116.88942	0.2949	−0.296	2447117.77372	0.7443	−0.289	2447117.94328	0.0222	+0.185
2447116.89649	0.3065	−0.304	2447117.77540	0.7471	−0.278	2447117.94503	0.0251	+0.175
2447116.89827	0.3094	−0.293	2447117.78200	0.7579	−0.284	2447117.95724	0.0451	+0.087
2447116.90852	0.3262	−0.260	2447117.78391	0.7610	−0.273	2447117.95902	0.0480	+0.077
2447116.91595	0.3384	−0.278	2447117.79610	0.7810	−0.276	2447117.96574	0.0590	+0.028
2447116.91789	0.3416	−0.278	2447117.80271	0.7918	−0.282	2447117.96753	0.0620	+0.018
2447116.92500	0.3532	−0.266	2447117.80444	0.7947	−0.272	2447117.98053	0.0833	−0.072
2447116.94042	0.3785	−0.223	2447117.81119	0.8057	−0.258	2447117.98578	0.0919	−0.102
2447116.94798	0.3909	−0.222	2447117.82625	0.8304	−0.251	2447117.98758	0.0948	−0.112
2447116.95137	0.3964	−0.201	2447117.83348	0.8423	−0.238	2447117.99467	0.1065	−0.132
2447116.97018	0.4273	−0.089	2447117.83518	0.8450	−0.237	2447118.00471	0.1229	−0.173
2447117.00571	0.4855	+0.059	2447117.84180	0.8559	−0.234	2447118.00649	0.1258	−0.174
2447117.01273	0.4970	+0.068	2447117.85245	0.8734	−0.190	2447118.01338	0.1371	−0.195
2447117.01451	0.4999	+0.068	2447117.85415	0.8761	−0.179	2447118.01519	0.1401	−0.196

Chapter 6

The Binary System SS Arietis

6.1 Introduction

The W UMa-type short-period eclipsing binary SS Ari (BD+23 279), was discovered by Hoffmeister (1934).

Many times of minima for the system have been determined over the last 20 years, and a study by Kaluzny & Pojmański (1984b) showed that the O-C diagram exhibits a sinusoidal variation.

Zhukov (1975) reported the first *UBV* light curves of SS Ari, with Kaluzny & Pojmański (1984a) having published the only photoelectric data for the system to date. Kaluzny & Pojmański also reported unpublished photoelectric observations of SS Ari, made by Paczyński (in 1965) and Ruciński (in 1966).

The B and V light curves of Kaluzny & Pojmański (1984a) indicate a system which is in contact, whilst exhibiting a difference between depth of minima (of some $0\overset{m}{.}08$). The first quadrature is also found to be approximately $0\overset{m}{.}03$ brighter than the second quadrature. Although the mass ratio was not known, they analysed the light curves using Ruciński's code to produce the best fit for both the A-type and W-type configurations, concluding that the W-type case produced the best solution. This solution employed a mass ratio, $q = 0.27$, with an inclination, $i = 74.9$ deg, and a fill-out,

$f = 0.791$. A systematic difference between this synthetic fit and the observed light curves was found to occur over the phase interval $0^{\mathrm{P}}.25$ to $0^{\mathrm{P}}.50$, which was interpreted as indicating the presence of an over-luminous region on one side of the more massive component, located near the neck between the two stars.

6.2 Spectroscopy

Radial velocity spectra of SS Ari, centred on 4200 Å were obtained and reduced as detailed in Chapter 2.

Using the F6V radial velocity standard star HD693 for cross-correlation, the radial velocity measurements listed in Table 6.1 were obtained. The corresponding orbital phasing of these measurements were calculated using the revised ephemeris in Section 6.3.

H.J.D.	Phase	V_1 $km\,s^{-1}$	(O-C) $km\,s^{-1}$	V_2 $km\,s^{-1}$	(O-C) $km\,s^{-1}$
2447108.61260	0.4900	−19	−0.5	—	—
2447108.67396	0.6411	−85	−3.6	+160	−3.1
2447108.70540	0.7185	−94	+2.4	+212	−1.3
2447110.40186	0.8971	−65	+1.5	+130	+4.9
2447110.51716	0.1811	+42	−5.2	−245	−7.5
2447110.54880	0.2590	+57	+3.5	−258	+2.3
2447110.58641	0.3517	+40	+2.0	−210	+4.7

Table 6.1: Radial Velocity data for SS Ari

The sine wave fits to the radial velocity data are shown in Figure 6.1. The additional primary velocity measurement at phase $0^{\text{P}}\!.49$ may have been contaminated by the rotational velocity of the star, but was in fact found to have no effect on the resulting best fit computed for the primary data. The resulting radial velocity semi-amplitudes for the primary and secondary components (K_1 and K_2 respectively), and the systemic velocity (V_0) are given in Table 6.2, along with the derived mass function, projected semi-major axes of the orbits, and their standard errors.

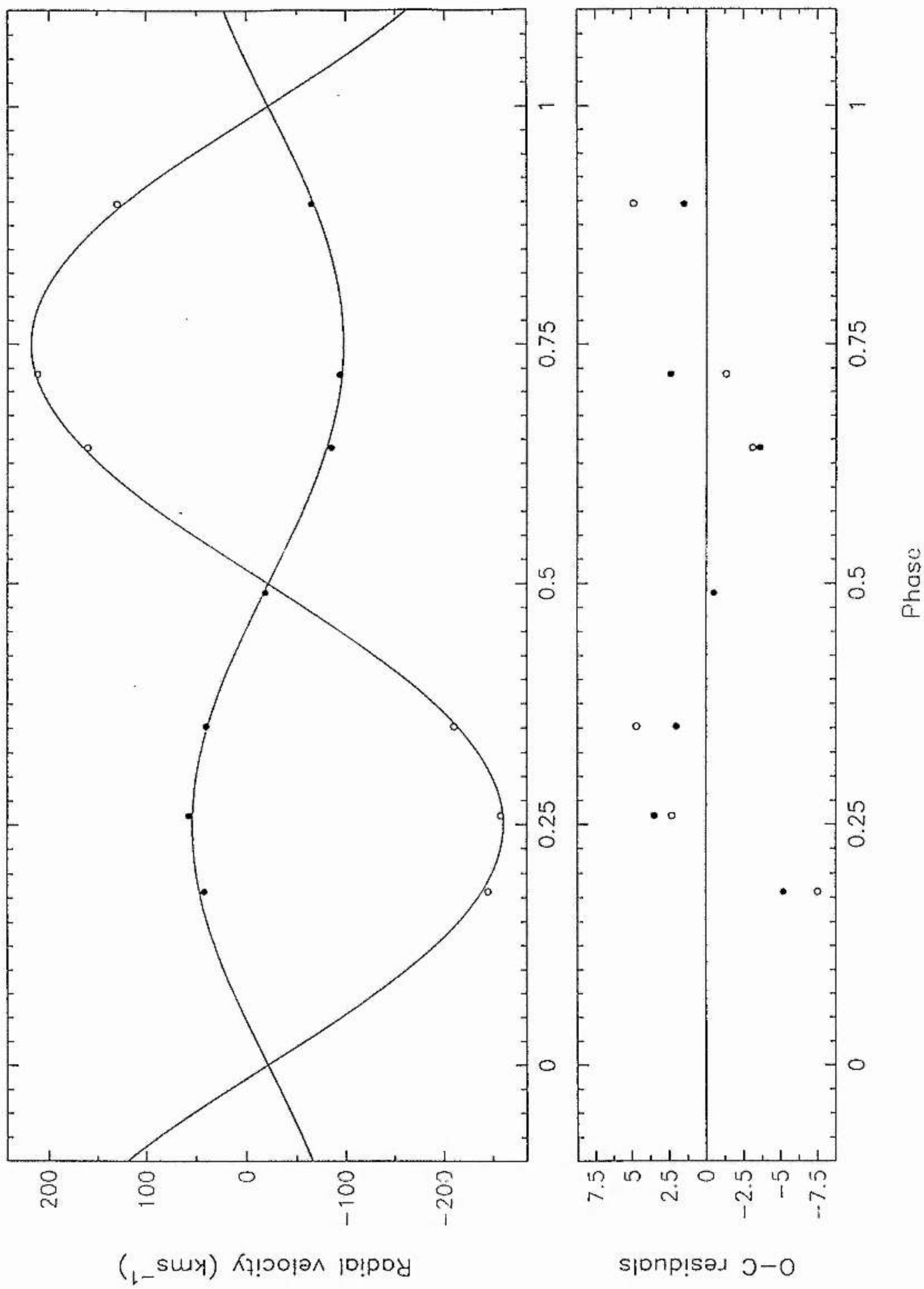

Figure 6.1: Radial Velocities of the Primary and Secondary Components of SS Ari (closed and open circles respectively), plotted together with their Orbital Solutions, and corresponding O-Cs (lower plot).

$K_1\,(\mathrm{km\,s^{-1}})$	=	75.6 ± 1.9
$K_2\,(\mathrm{km\,s^{-1}})$	=	239.5 ± 3.0
$V_{0_1}\,(\mathrm{km\,s^{-1}})$	=	−21.9 ± 1.6
$V_{0_2}\,(\mathrm{km\,s^{-1}})$	=	−21.0 ± 2.6
$\sigma_1\,(\mathrm{km\,s^{-1}})$ †	=	3.0
$\sigma_2\,(\mathrm{km\,s^{-1}})$ †	=	4.9
$\mathrm{q}\ (\mathrm{m_2/m_1})$	=	0.316 ± 0.01
e	=	0 (adopted)
$\mathrm{a_1 \cdot \sin i}\ (\mathrm{R_\odot})$	=	0.606 ± 0.015
$\mathrm{a_2 \cdot \sin i}\ (\mathrm{R_\odot})$	=	1.921 ± 0.024
$\mathrm{a \cdot \sin i}\ (\mathrm{R_\odot})$	=	2.528 ± 0.028
$\mathrm{m_1 \cdot \sin^3 i}\ (\mathrm{M_\odot})$	=	1.003 ± 0.026
$\mathrm{m_2 \cdot \sin^3 i}\ (\mathrm{M_\odot})$	=	0.316 ± 0.011

Table 6.2: Orbital Elements for SS Ari

† — r.m.s. scatter of a single observation.

6.3 Ephemeris

Kaluzny & Pojmański (1984a, 1984b) presented a period analysis for SS Ari which showed that the system exhibited a sine-like period variation, although they could not conclude whether this was due to continuous or random, abrupt changes.

From this analysis, Kaluzny & Pojmański derived the linear ephemeris :-

$$\text{HJD } 2444469.5060(\pm 17) + 0.4059917\text{E}(\pm 26)\text{E}$$

This ephemeris was used to calculate the O-Cs for the period study presented here (Table 6.3, and Figures 6.2 & 6.3).

A literature search by the author revealed several new photoelectric times of minima for the system, including two determinations derived from the new infrared photometry presented here (Section 6.4.2). There is also a large body of mainly visual determinations which have been published, mostly by amateur observers. These data are listed in Table 6.3, and the residuals, calculated with respect to the above ephemeris, are shown in Figure 6.2.

Although the visual data exhibit a large scatter, the period behaviour indicated in Figure 6.2 clearly shows the sine-like variation.

A least squares analysis of just the photoelectric data yields a revised period for SS Ari of 0.4059899 ± 0.0000004 day.

In view of the behaviour of the O-C diagram, two different ephemerides were used to phase the data examined in this analysis.

The *V* light curve of Kaluzny & Pojmański re-analysed here (Section 6.4.1), was phased using an ephemeris based on the period derived from their period analysis (given above), with a minimum taken from their *V* and *B* observations :-

$$\text{HJD } 2445261.5860(\pm 3) + 0.4059917(\pm 26)\text{E}$$

The newer INT spectroscopic observations (Section 6.2) and UKIRT photometry (Section 6.4.2) presented here, both obtained in 1987 November, were phased using the

Table 6.3: Times of minima for SS Ari.

H.J.D.	Cycle	Method	Reference
2430948.329	-33304	VIS	Odynskaya, 1949
2432455.347	-29592	VIS	Kramer, 1948
2432455.552	-29591.5	VIS	Kramer, 1948
2432786.229	-28777	VIS	Kramer, 1948
2432786.43	-28776.5	VIS	Kramer, 1984
2435721.545	-21547	PG	Huth, 1964
2436075.581	-20675	PG	Huth, 1964
2439028.387	-13402	VIS	Braune, 1970
2439029.609	-13399	VIS	Braune, 1970
2439040.5713	-13372	PE	Kaluzny & Pojmański, 1984a
2439053.362	-13340.5	VIS	Braune, 1970
2439055.394	-13335.5	VIS	Braune, 1970
2439068.396	-13303.5	VIS	Braune, 1970
2439184.301	-13018	VIS	Braune, 1970
2439389.5261	-12512.5	PE	Kaluzny & Pojmański, 1984a
2439389.535	-12512.5	VIS	Braune, 1970
2439391.5552	-12507.5	PE	Kaluzny & Pojmański, 1984a
2439403.536	-12478	VIS	Braune, 1970
2439407.593	-12468	VIS	Braune, 1970
2439776.4355	-11559.5	VIS	Braune, 1970
2440065.518	-10847.5	VIS	Braune, 1970
2441249.392	-7931.5	VIS	Braune *et al.*, 1972
2441576.422	-7126	VIS	Braune & Mundry, 1973
2441682.376	-6865	VIS	Braune & Mundry, 1972
2441947.4934	-6212	PE	Zhukov, 1975
2441951.5542	-6202	PE	Zhukov, 1975
2441960.4865	-6180	PE	Zhukov, 1975
2441972.4638	-6150.5	PE	Zhukov, 1975
2441975.5072	-6143	PE	Zhukov, 1975
2442036.2053	-5993.5	PE	Zhukov, 1975
2442037.421	-5990.5	PE	Zhukov, 1975
2442414.201	-5062.5	VIS	Braune *et al.*, 1977
2442664.474	-4446	VIS	Braune *et al.*, 1979
2442840.265	-4013	VIS	Braune *et al.*, 1979

Table 6.3: Times of minima for SS Ari — *continued.*

H.J.D.	Cycle	Method	Reference
2443014.459	-3584	VIS	Braune *et al.*, 1979
2443833.332	-1567	VIS	Braune *et al.*, 1981
2443455.3482	-2498	PE	Kurpiński, 1982
2443790.300	-1673	VIS	Locher, 1978
2443795.573	-1660	VIS	Locher, 1978
2444146.5425	-795.5	PE	Kurpiński, 1982
2444266.318	-500.5	VIS	Locher, 1980a
2444469.5070	0	PE	Kurpiński, 1982
2444539.326	172	VIS	Locher, 1980b
2444602.245	327	VIS	Locher, 1981a
2444605.289	334.5	VIS	Locher, 1981a
2444605.3104	334.5	PE	Kurpiński, 1982
2444629.258	393.5	VIS	Locher, 1981a
2444635.319	408.5	VIS	Locher, 1981a
2444636.342	411	VIS	Locher, 1981a
2444642.2559	425.5	PE	Kurpiński, 1982
2444649.324	443	VIS	Locher, 1981b
2444659.269	467.5	VIS	Locher, 1981b
2444821.456	867	VIS	Locher, 1981c
2444823.5270	872	PE	Kurpiński, 1982
2444831.606	892	VIS	Locher, 1981c
2444879.325	1009.5	VIS	Locher, 1981d
2444883.380	1019.5	VIS	Locher, 1981d
2444911.424	1088.5	PE	Locher, 1981d
2444917.278	1103	VIS	Locher, 1981d
2444919.305	1108	VIS	Locher, 1981d
2444926.235	1125	VIS	Locher, 1981d
2444929.269	1132.5	VIS	Locher, 1981d
2444985.298	1270.5	VIS	Locher, 1982a
2445224.458	1859.5	VIS	Locher, 1982b
2445238.450	1894	PG	Braune *et al.*, 1983
2445261.3848	1950.5	PE	Kaluzny & Pojmański, 1984a
2445261.5860	1951	PE	Kaluzny & Pojmański, 1984a
2445262.3990	1953	PE	Kaluzny & Pojmański, 1984a

Table 6.3: Times of minima for SS Ari — *continued.*

H.J.D.	Cycle	Method	Reference
2445294.476	2032	PG	Braune *et al.*, 1983
2445296.299	2036.5	VIS	Locher, 1983a
2445298.536	2042	PG	Braune *et al.*, 1983
2445323.296	2103	PE	Pohl *et al.*, 1983
2445335.284	2132.5	VIS	Locher, 1983a
2445345.231	2157	VIS	Locher, 1983a
2445346.238	2159.5	VIS	Locher, 1983a
2445359.227	2191.5	VIS	Locher, 1983a
2445388.259	2263	VIS	Locher, 1983b
2445576.445	2726.5	VIS	Isles, 1985a
2445577.458	2729	VIS	Isles, 1985a
2445587.386	2753.5	VIS	Isles, 1985a
2445605.8630	2799	PE	Faulkner, 1986
2445621.289	2837	VIS	Locher, 1983c
2445623.333	2842	VIS	Hübscher & Mundry, 1984
2445635.306	2871.5	VIS	Isles, 1985a
2445635.294	2871.5	VIS	Locher, 1983c
2445641.381	2886.5	VIS	Locher, 1983c
2445651.3318	2911	PE	Pohl *et al.*, 1985
2445674.268	2967.5	VIS	Locher, 1984a
2445681.379	2985	VIS	Isles, 1985a
2445701.265	3034	VIS	Locher, 1984a
2445731.314	3108	VIS	Isles, 1985b
2445772.306	3209	VIS	Locher, 1984b
2445943.8485	3631.5	PE	Faulkner, 1986
2445988.297	3741	VIS	Locher, 1984c
2446001.307	3773	VIS	Isles, 1985b
2446005.352	3783	VIS	Locher, 1984c
2446021.5914	3823	PE	Faulkner, 1986
2446059.365	3916	VIS	Isles, 1985b
2446113.360	4049	VIS	Isles, 1986
2446114.358	4051.5	VIS	Isles, 1986
2446321.621	4562	VIS	Locher, 1985
2446327.4994	4576.5	PE	Pohl *et al.*, 1987

Table 6.3: Times of minima for SS Ari — *continued.*

H.J.D.	Cycle	Method	Reference
2446351.478	4635.5	VIS	Isles, 1986
2446355.328	4645	VIS	Locher, 1985
2446355.307	4645	VIS	Hübscher *et al.*, 1986
2446383.328	4714	VIS	Isles, 1986
2446403.411	4763.5	VIS	Locher, 1986
2446421.297	4807.5	VIS	Locher, 1986
2446422.288	4810	VIS	Hübscher *et al.*, 1986
2446440.5677	4855	PE	Faulkner, 1986
2446688.466	5465.5	VIS	Isles, 1988
2446760.293	5642.5	VIS	Locher, 1987a
2446843.323	5847	VIS	Locher, 1987b
2447068.441	6401.5	VIS	Hübscher & Lichtenknecker, 1988
2447077.366	6423.5	VIS	Hübscher & Lichtenknecker, 1988
2447088.341	6450.5	VIS	Locher, 1988a
2447111.287	6507	VIS	Locher, 1988b
2447113.305	6512	VIS	Locher, 1988c
2447118.364	6524.5	VIS	Locher, 1988a
2447118.7666	6525.5	PE	UKIRT — this paper
2447119.7814	6528	PE	UKIRT — this paper
2447128.345	6549	VIS	Locher, 1988c
2447141.301	6581	VIS	Locher, 1988a
2447145.364	6591	VIS	Locher, 1988a
2447153.278	6610.5	VIS	Locher, 1988a
2447157.354	6620.5	VIS	Locher, 1987b
2447206.253	6741	PE	Keskin & Pohl, 1989
2447207.275	6743.5	VIS	Hübscher & Lichtenknecker, 1988
2447208.292	6746	VIS	Locher, 1988c
2447511.3531	7492.5	PE	Keskin & Pohl, 1989
2447523.379	7522	VIS	Locher, 1989b
2447523.312	7522	VIS	Locher, 1989a
2447524.348	7524.5	VIS	Locher, 1989a
2447525.342	7527	VIS	Locher, 1989a
2447534.301	7549	VIS	Locher, 1989b
2447565.346	7625.5	VIS	Locher, 1989b

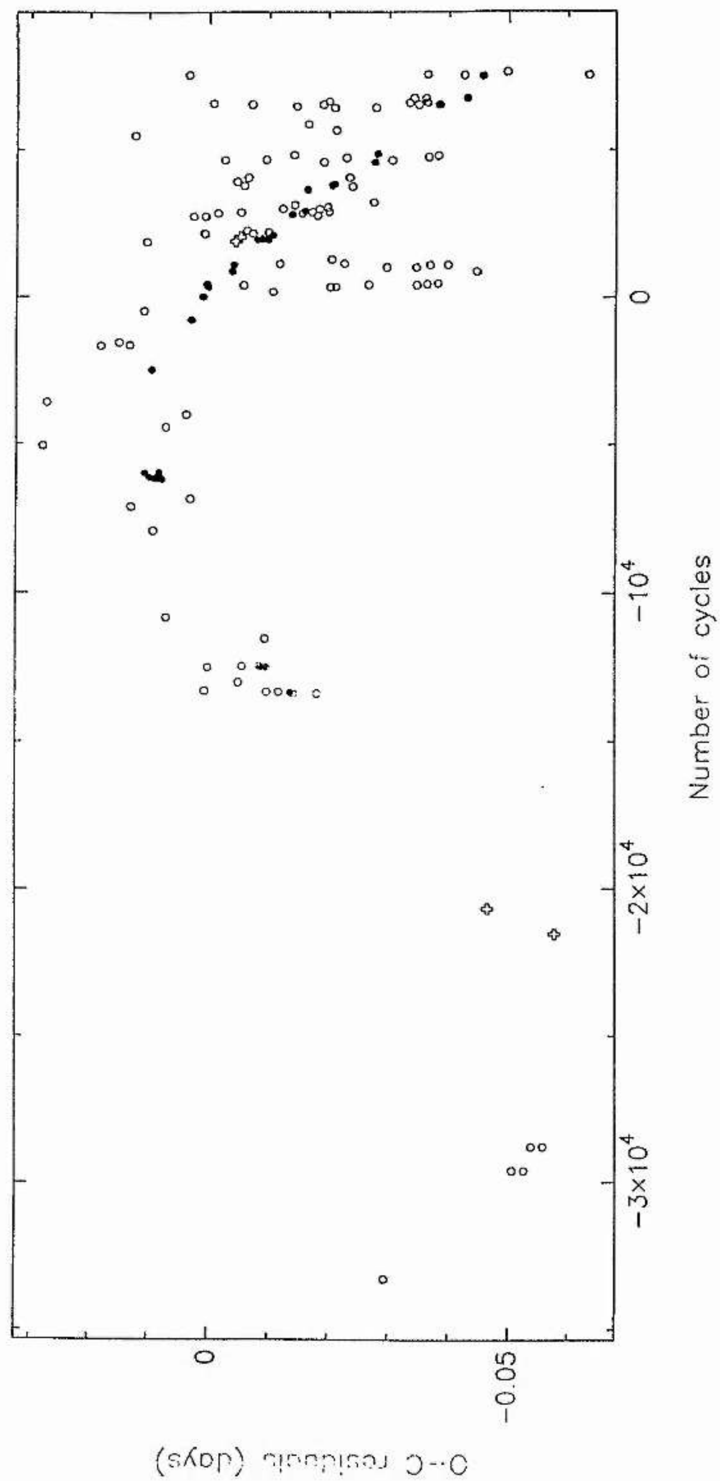

Figure 6.2: The Period behaviour of SS Ari. (Open Circles represent visual times of minima; Open Crosses represent photographic minima; and Filled Circles represent photoelectric minima).

revised period derived above, with a time of minimum taken from the UKIRT data (see Table 6.3) :-

$$\text{HJD } 2447119.7814(\pm 9) + 0.4059899(\pm 4)E$$

The author attempted to fit the O-C data with a sine wave, using only the photoelectric determinations, plus the earliest five visual and two photographic determinations (between -35000 and -20000 cycles), which were included to provide clearer definition of the sinusoidal variation. Although a rigorous analysis cannot be justified due to the scatter in the photographic and visual data, this analysis implied a sine wave fit to the data with a period of approximately 43 years, and an amplitude of around 0.036 day. This fit is shown plotted with the data used for the analysis in Figure 6.3.

If it is assumed that the sinusoidal variation is the result of third body motion, in an orbit coplanar with that of SS Ari, then the total mass of the system can be estimated as approximately $0.132\,M_{\odot}$. As the total mass of SS Ari is approximately $1.5\,M_{\odot}$, this explanation can be rejected, unless the orbit of the third body is nearly perpendicular to that of SS Ari.

Thus if the sinusoidal variation is real, this leads to the possibility that there is mass transfer in the system which exhibits cyclic behaviour with a period of around 43 years. This can be compared with a similar sinusoidal variation in the O-C residuals observed in the binary system BX And (Chapter 5).

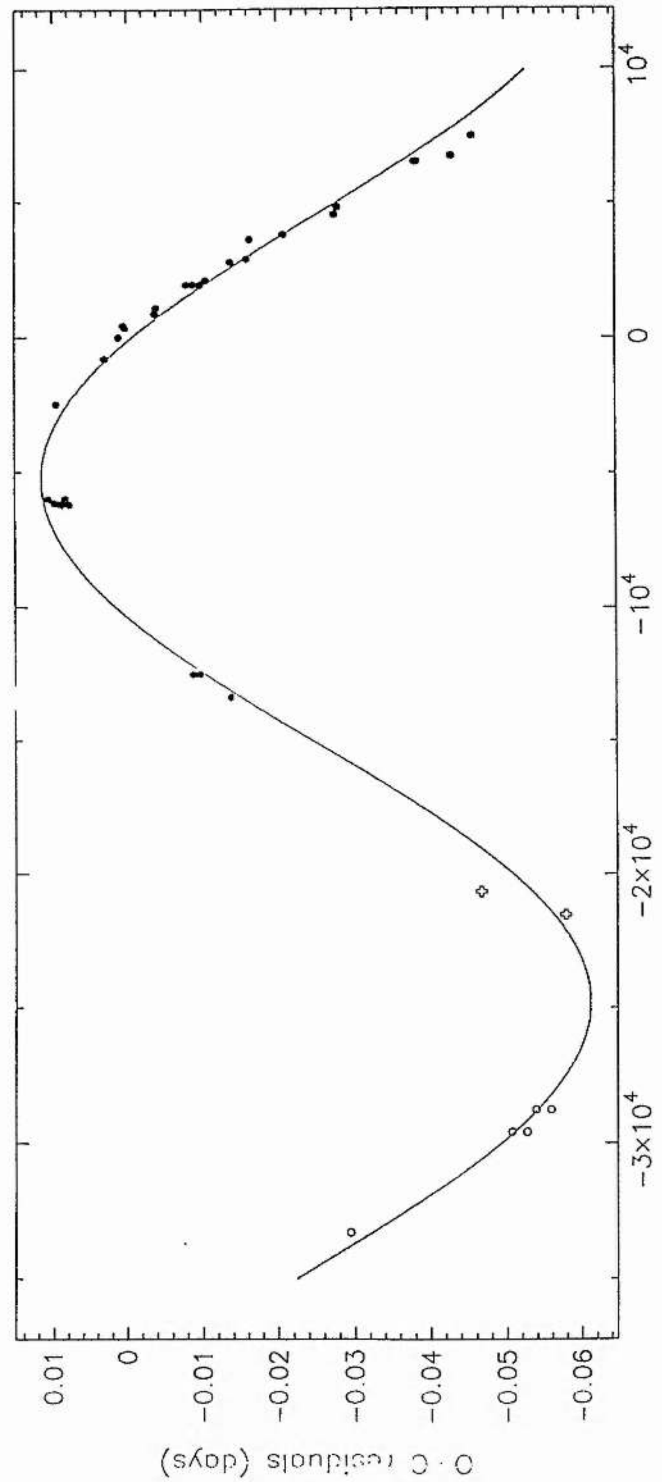

Figure 6.3: The sinusoidal period behaviour of SS Ari. The fit shown is a sine wave with a period of 43yr and amplitude of 0.036 day.
(Open circles represent visual times of minima ; open crosses represent photographic minima ; and filled circles represent photoelectric minima).

6.4 Photometric Analysis

6.4.1 Optical Data

A light curve analysis, using the light curve synthesis program LIGHT2 (Chapter 2), is presented here of the V-filter observations published by Kaluzny & Pojmański (1984a). These data consisted of 318 observations reduced to a differential magnitude, with a probable error in a single observation of approximately $0\overset{m}{.}015$. The data were phased with the ephemeris given in Section 6.3.

These data consist of two nights of observation, made during 1982 October 18/19 and 19/20. When examined, it was found that the last 5/6 observations made at the end of each night exhibited a much larger scatter than the rest of the data, possibly due to the encroaching twilight, an inadequacy at the extremities of the sky fitting algorithm used during data reduction, or similar. Hence for the analysis presented here, these data points were removed from the light curve, the overlap of data ensuring that this did not degrade the orbital phase coverage in any way.

6.4.2 Infrared Observations

Simultaneous infrared and optical photometry of SS Ari was obtained and reduced as described in Chapter 2. The J and K data were reduced to differential magnitudes with an accuracy of $0\overset{m}{.}02$, and phased using the revised ephemeris given in Section 6.3. The J and K observations are listed in the Appendix to this Chapter, and are shown plotted in Figures 6.5 & 6.6 respectively.

The overall scatter in the J light curve is approximately $0\overset{m}{.}02$, whereas that for the K light curve is $0\overset{m}{.}03$. Both light curves appear similar in shape to the visual data, exhibiting a first quadrature approximately $0\overset{m}{.}04$ and $0\overset{m}{.}03$ brighter than the second quadrature in J and K respectively. However, the depth of primary and secondary minima are virtually equal in J, whilst in K the secondary minimum is deeper by approximately $0\overset{m}{.}03$.

6.4.3 Spectral Type

Kholopov *et al.* (1985) give a spectral type of F8 for the primary component of SS Ari, which implies a primary temperature of some 6100K (Popper 1980).

Kaluzny & Pojmański (1984a) adopted a primary temperature of 5600K for their light curve analysis, on the basis of observed colours.

Their observations gave a value of (B-V)=0.63 at primary minimum. The new infrared photometry presented here, although showing some scatter, gives a value of (J-K)$\simeq$0.35 at primary minimum. Both of these colours, if unreddened, imply a spectral type nearer G2. (Popper 1980 and Koornneef 1983 respectively).

However, the spectroscopy presented here (Section 6.2) was cross-correlated with an F6V standard star template, which was found to optimise the cross-correlation functions in preference to a G2V standard star also observed (Chapter 2).

Hilditch & Hill (1975) and Rucinski (1983) have both published Strömgren four-colour observations of SS Ari, which show good agreement. Rucinski's analysis of the observations, based on the standard relations of Crawford (1975) but allowing for evolution away from the zero-age main sequence, gives a reddening for the system of $E_{(B-V)}$ $=0\overset{m}{.}035$ and a spectral type of F8.

If this reddening is taken into account for the observed colours above, (using the relation $E_{(J-K)} = 0.54\, E_{(B-V)}$ for the infrared case), then both also imply a spectral type around F8 (Popper 1980 and Koornneef 1983 respectively).

Hence for the light curve analysis presented here, a temperature for the primary component of 6100±200K, and a colour excess for the system of $E_{(B-V)}$ $=0\overset{m}{.}035$ were adopted.

6.4.4 Light Curve Analysis

Given the non-symmetric shape of the light curves of SS Ari, each half of the *V*, *J*, and *K* curves were analysed separately using LIGHT2.

Fixing the primary component temperature T_1 at 6100K, and the mass ratio at the spectroscopic value, solutions were sought for the "fill-out" factor (f), secondary component temperature (T_2), and system inclination (i). The bolometric albedo for both components ($\alpha_{1,2}$) were fixed at 0.5, and the gravity darkening exponents ($\beta_{1,2}$) were fixed at the convective value of 0.08.

The two analyses for each light curve thus obtained are given in Tables 6.4, 6.5, and 6.6, with the fits, reflected around $0^{\mathrm{P}}.5$ and plotted against the complete data set, are shown in Figures 6.4, 6.5, and 6.6, along with their respective O-C's.

	Data from $0^{\mathrm{P}}.0$ to $0^{\mathrm{P}}.5$	Data from $0^{\mathrm{P}}.5$ to $1^{\mathrm{P}}.0$
q	0.316 (fixed)	0.316 (fixed)
T_1 (K)	6100 (fixed)	6100 (fixed)
$\alpha_{1,2}$	0.5 (fixed)	0.5 (fixed)
$\beta_{1,2}$	0.08 (fixed)	0.08 (fixed)
f	0.822 ± 0.038	0.931 ± 0.022
i (°)	73.61 ± 0.28	74.85 ± 0.17
r_1 (mean)	0.4953 ± 0.003	0.4891 ± 0.003
r_2 (mean)	0.2956 ± 0.001	0.2885 ± 0.001
T_2 (K)	6527 ± 32	6256 ± 17
χ^2	4.39×10^{-4}	1.45×10^{-4}

Table 6.4: Solution for each half of the V light curve of SS Ari (with standard errors).

Unlike the previous binary systems examined, the light curve of SS Ari with unequal quadratures, can only be explained by introducing an anomalous luminosity distribution in the form of either a hot or a cool spot, depending upon which half of the light curve is taken to reflect most accurately the true geometrical configuration of the system. Further, any spot must be displaced to one side of the affected component star, unlike the spots suggested previously on VW Boo and BX And which were formed symmetrically about the neck joining the two stars.

The solutions suggested for the visual and infrared data indicate substantially different geometries, particularly in fill-out and secondary temperature. The decreasing secondary temperature between the J and K curves, apparently contradicting the W-type

	Data from $0^{\mathrm{p}}.0$ to $0^{\mathrm{p}}.5$	Data from $0^{\mathrm{p}}.5$ to $1^{\mathrm{p}}.0$
q	0.316 (fixed)	0.316 (fixed)
T_1 (K)	6100 (fixed)	6100 (fixed)
$\alpha_{1,2}$	0.5 (fixed)	0.5 (fixed)
$\beta_{1,2}$	0.08 (fixed)	0.08 (fixed)
f	0.508 ± 0.032	0.606 ± 0.056
i (°)	76.01 ± 0.15	75.28 ± 0.26
r_1 (mean)	0.5138 ± 0.004	0.5082 ± 0.004
r_2 (mean)	0.3164 ± 0.002	0.3094 ± 0.002
T_2 (K)	6179 ± 49	5972 ± 82
χ^2	1.47×10^{-4}	3.09×10^{-4}

Table 6.5: Solution for each half of the J light curve of SS Ari (with standard errors).

	Data from $0^{\mathrm{p}}.0$ to $0^{\mathrm{p}}.5$	Data from $0^{\mathrm{p}}.5$ to $1^{\mathrm{p}}.0$
q	0.316 (fixed)	0.316 (fixed)
T_1 (K)	6100 (fixed)	6100 (fixed)
$\alpha_{1,2}$	0.5 (fixed)	0.5 (fixed)
$\beta_{1,2}$	0.08 (fixed)	0.08 (fixed)
f	0.417 ± 0.049	0.586 ± 0.055
i (°)	75.72 ± 0.24	74.82 ± 0.27
r_1 (mean)	0.5193 ± 0.004	0.5090 ± 0.004
r_2 (mean)	0.3230 ± 0.002	0.3110 ± 0.002
T_2 (K)	5544 ± 70	5442 ± 67
χ^2	2.35×10^{-4}	2.19×10^{-4}

Table 6.6: Solution for each half of the K light curve of SS Ari (with standard errors).

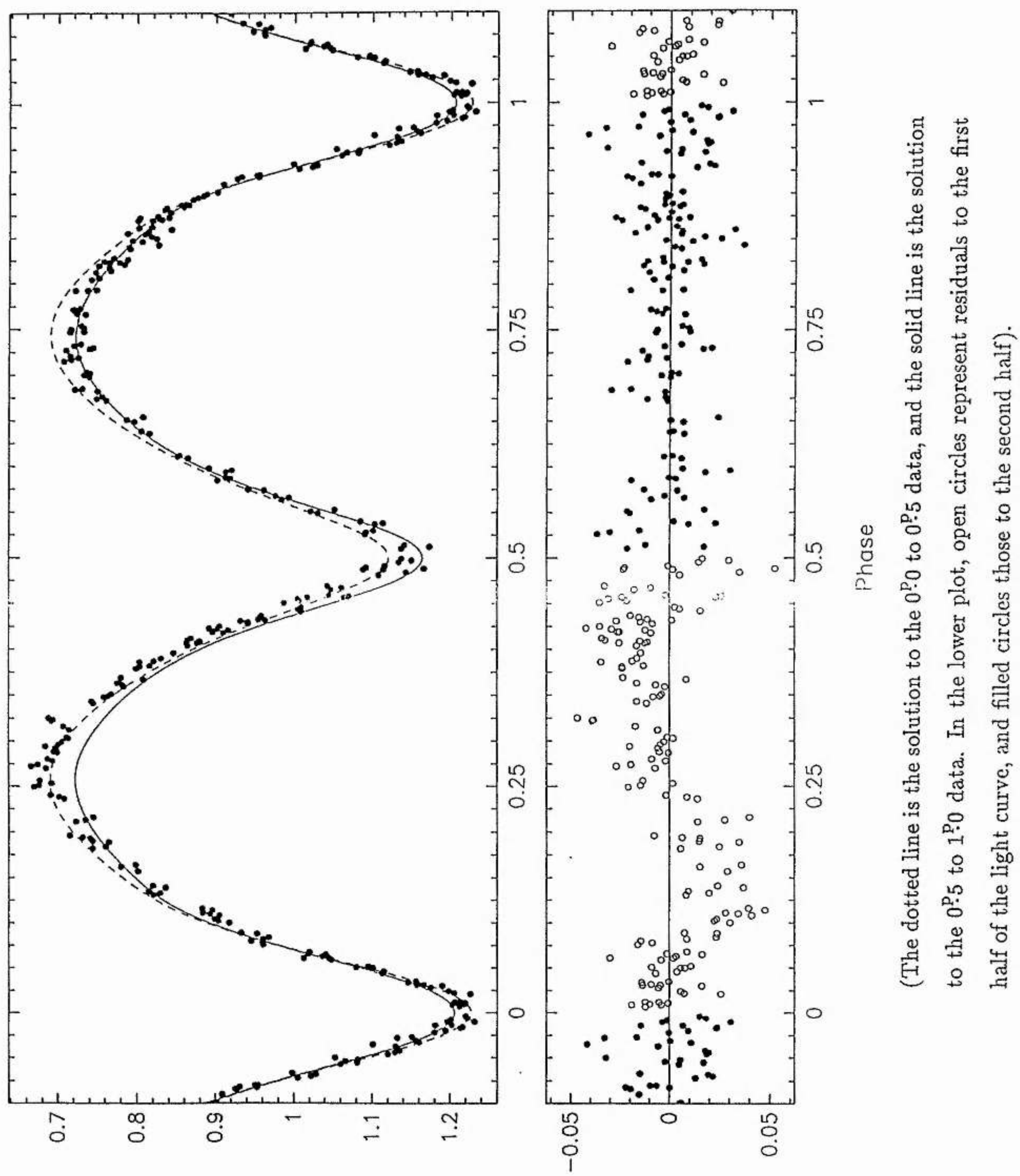

Figure 6.4: *V* observations of SS Ari (Kaluzny & Pojmański (1984a)), with LIGHT2 solutions for each half of the light curve. The lower plot shows the residuals of the data from each half of the light curve and its respective solution.

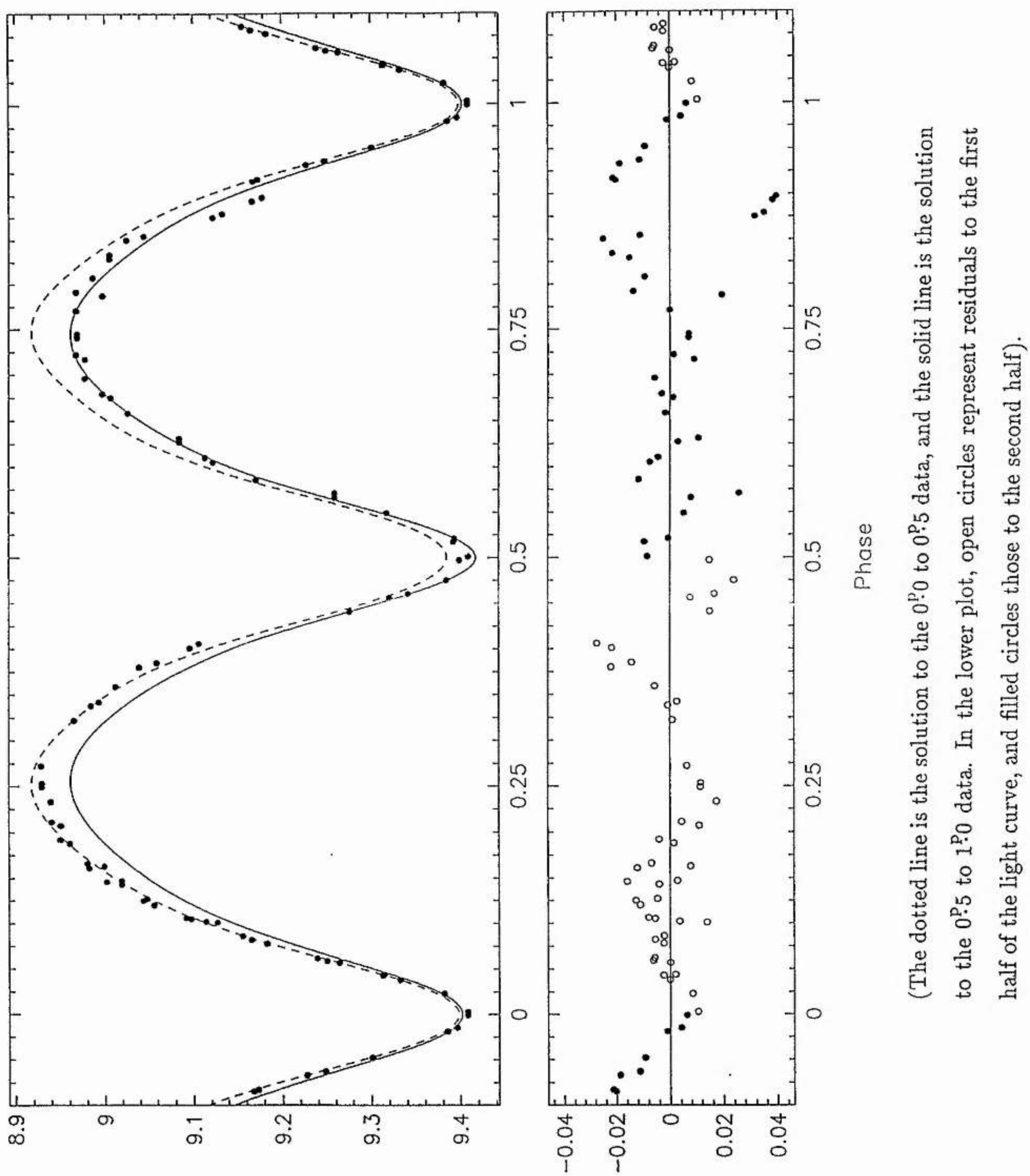

Figure 6.5: *J* observations of SS Ari with LIGHT2 solutions for each half of the light curve. The lower plot shows the residuals of the data from each half of the light curve and its respective solution.

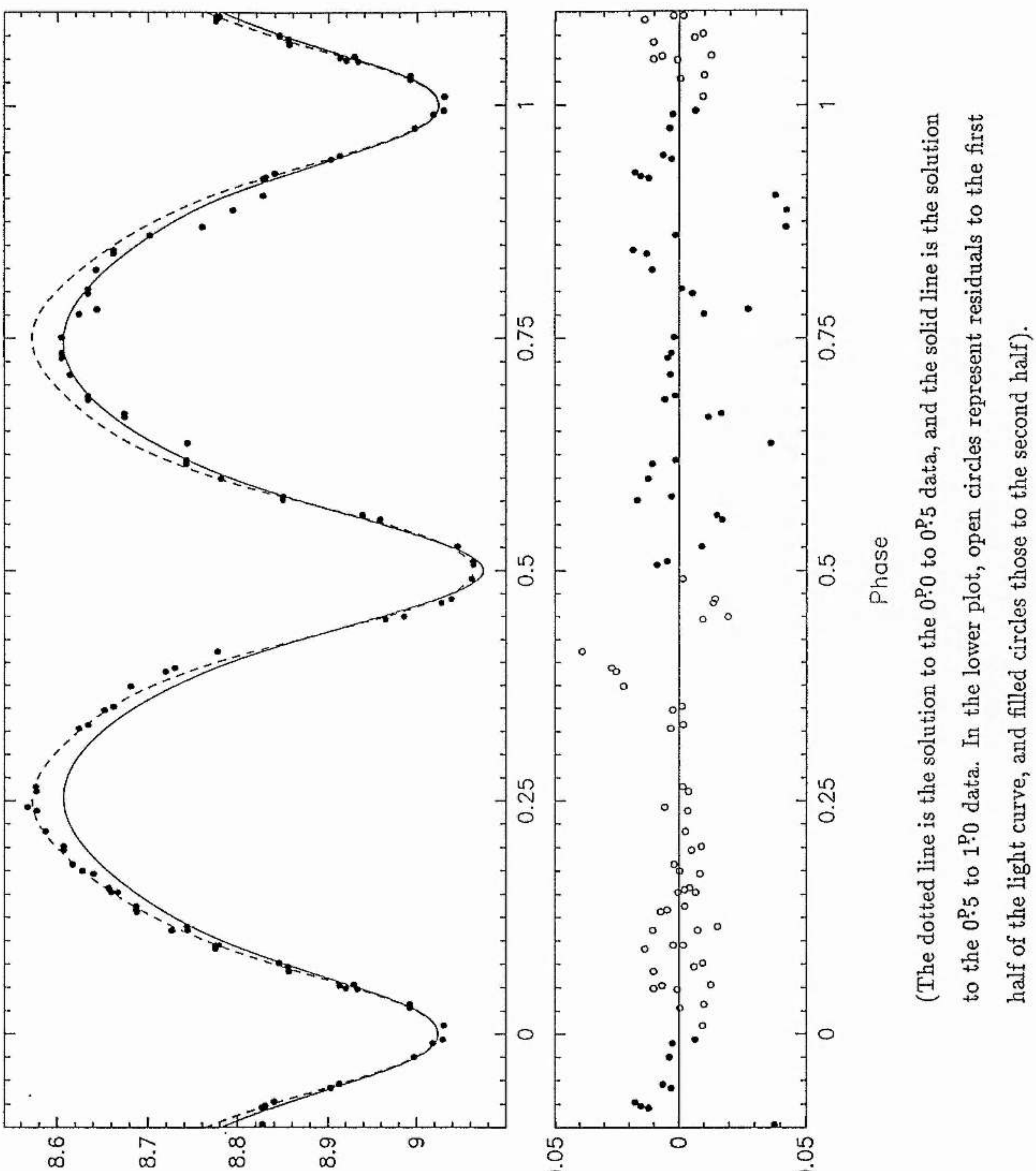

Figure 6.6: *K* observations of SS Ari with LIGHT2 solutions for each half of the light curve. The lower plot shows the residuals of the data from each half of the light curve and its respective solution.

nature of the system indicated by the spectroscopy, have however been misleading, since it is crucially affected by the $0^{\mathrm{m}}.03$ deepening of the secondary minimum in the K light curve, which is within the $0^{\mathrm{m}}.03$ scatter of the data.

On the face of it then the data indicate that SS Ari has moved from a marginal contact system with unequal temperature components (visual data), to a system in deep contact with thermalised components (infrared data). Although the visual and infrared data were obtained in 1983 and 1987 respectively, it is difficult to believe that such a change could occur in just four years.

If the solutions to the first half of the light curve data are taken to represent the true geometry of the system, then a cool spot must be invoked around second quadrature. If the solutions to the second half of the light curve data are taken, then a hot spot around first quadrature is invoked, which is also displaced to one side of the star. If this is the true scenario, then clearly the deep contact, equal temperature solution suggested by the infrared fits cannot be correct, whilst the marginal contact, unequal temperature solution to the visual data does give the type of system configuration needed for such a hot spot to arise, as seen in VW Boo and BX And. This fit to the second half of the visual data (Table 6.4) agrees well with the analysis of Kaluzny & Pojmański (1984a), who also interpreted the discrepancy around first quadrature as indicating the presence of an over-luminous region (Section 6.1).

It must be noted however that deciding the correct geometry of a system which includes some form of spot region from a simple light curve analysis, may well be "contaminated" by the presence of the spot itself. The effects a spot could have on light curve analysis were investigated by Dr S.A.Bell (1990). LIGHT2 was used to generate a light curve at a visual wavelength, with a hot spot around first quadrature. The generated curve was then solved, making no allowance for the presence of a spot. The solution to the distorted first half of the generated light curve yielded consistently smaller fill-out factors ($\simeq 0.5$), denoting larger stars, and a much greater degree of contact than those for the second half of the curve. The inclination and secondary temperature were found to be in good agreement with that used for the generated curve. The second half of the generated curve yielded a fill-out factor and inclination in very good agreement with those values used in the generation process, although the secondary temperature did show a discrepancy of approximately 300K. Similar tests at infrared wavelengths however suggested that the presence of a hot spot had little effect on the solution parameters.

6.4.5 Modelling a Hot Spot

Adopting the solution to the second half of the *V* light curve as the most likely configuration of SS Ari, LIGHT2 was used to try and solve the data with the inclusion of a hot spot around second quadrature on the cooler component. As for previous analyses the spot was assumed to be circular and to have a latitude of 0°.

Geometric considerations of this fit on the visual data indicates that such a spot would have a longitude of approximately 20°, with a radius of some 30°. The spot longitude being defined as the angle between the sub-stellar point and the spot centre, measured anti-clockwise from the sub-stellar point, as seen from the north pole of the star.

Geometric considerations of this fit on the infrared data indicate the spot would have a longitude of approximately 90°, with a radius of some 60°. This of course suggests that the spot has moved round the primary component between 1983 and 1987, possibly indicating that the energy transfer between the components is uneven or indeed that a different phenomenon is responsible for this feature.

Any attempt to use non-simultaneous, single colour light curves to solve for a unique spot radius and temperature will fail unless the radius can be constrained by geometrical considerations, or the spot temperature can be estimated from another source. Unlike VW Boo and BX And, SS Ari with a spot displaced to one side of the star provides far weaker geometrical constraints, and as a result LIGHT2 failed to converge to a solution. However, it was found that reasonable fits to the data could be found by generating light curves using the system configuration indicated by the solution to the second half of the visual data, with a variety of spot parameters used to find the best fit. Clearly though, this analysis cannot be treated as a true solution.

For the system configuration indicated by the visual solution to fit the infrared data, with a spot at some 90° longitude, it was found necessary to increase the system inclination to 78°. This in turn caused the generated fit to the visual data to become too deep around secondary minimum. However, by increasing the radius of the spot in the visual case, it becomes visible behind the secondary component at secondary minimum (taking the form of an annular eclipse), thus providing the "extra" luminosity required.

Hence, by generating various light curves, the system parameters listed in Table 6.7 were obtained, providing reasonable fits to both the visual and infrared data using the same basic system geometry. These generated fits are shown plotted against the V, J, and K light curves, with their corresponding O-C's, in Figures 6.7, 6.8, and 6.9 respectively. Figures 6.10 and 6.11 show a schematic diagram of the SS Ari system configuration, indicating the location and size of the proposed hot spot in the visual (1983) and infrared (1987) cases respectively.

	Visual Data	Infrared Data
q	0.316	0.316
T_1 (K)	6100	6100
$\alpha_{1,2}$	0.5	0.5
$\beta_{1,2}$	0.08	0.08
f	0.931	0.931
i (°)	78.0	78.0
T_2 (K)	6260	6260
Spot Parameters		
longitude (degrees)	20	90
r_s (degrees)	50	60
T_s (above T_2)	160	160

Table 6.7: System and spot parameters used to generate the "best fits" to the visual (1983) and infrared (1987) light curves of SS Ari.

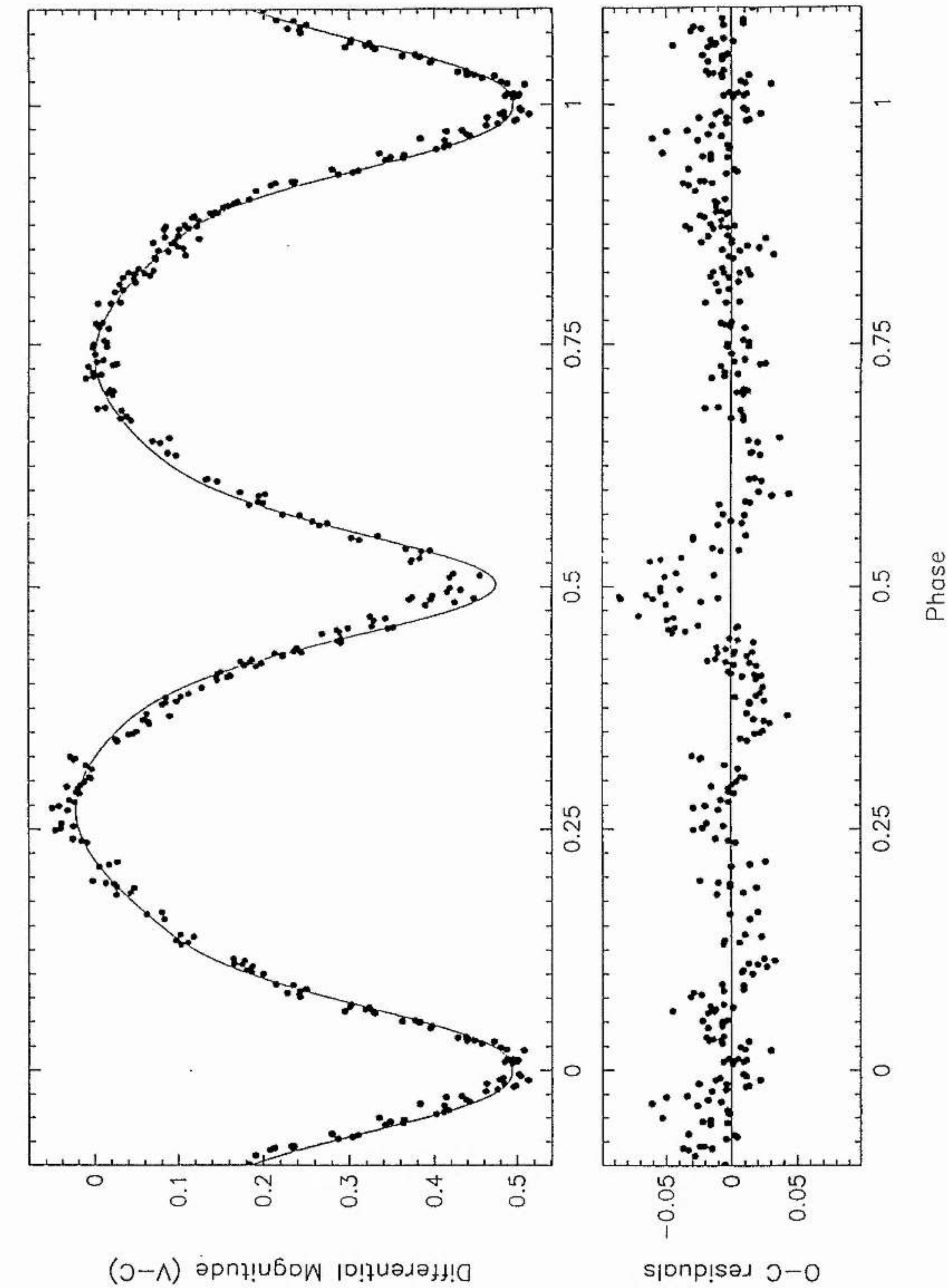

Figure 6.7: The generated "best fit" to the V observations of SS Ari, with the corresponding O-C's shown in the lower plot, using the system and spot parameters given in Table 6.7.

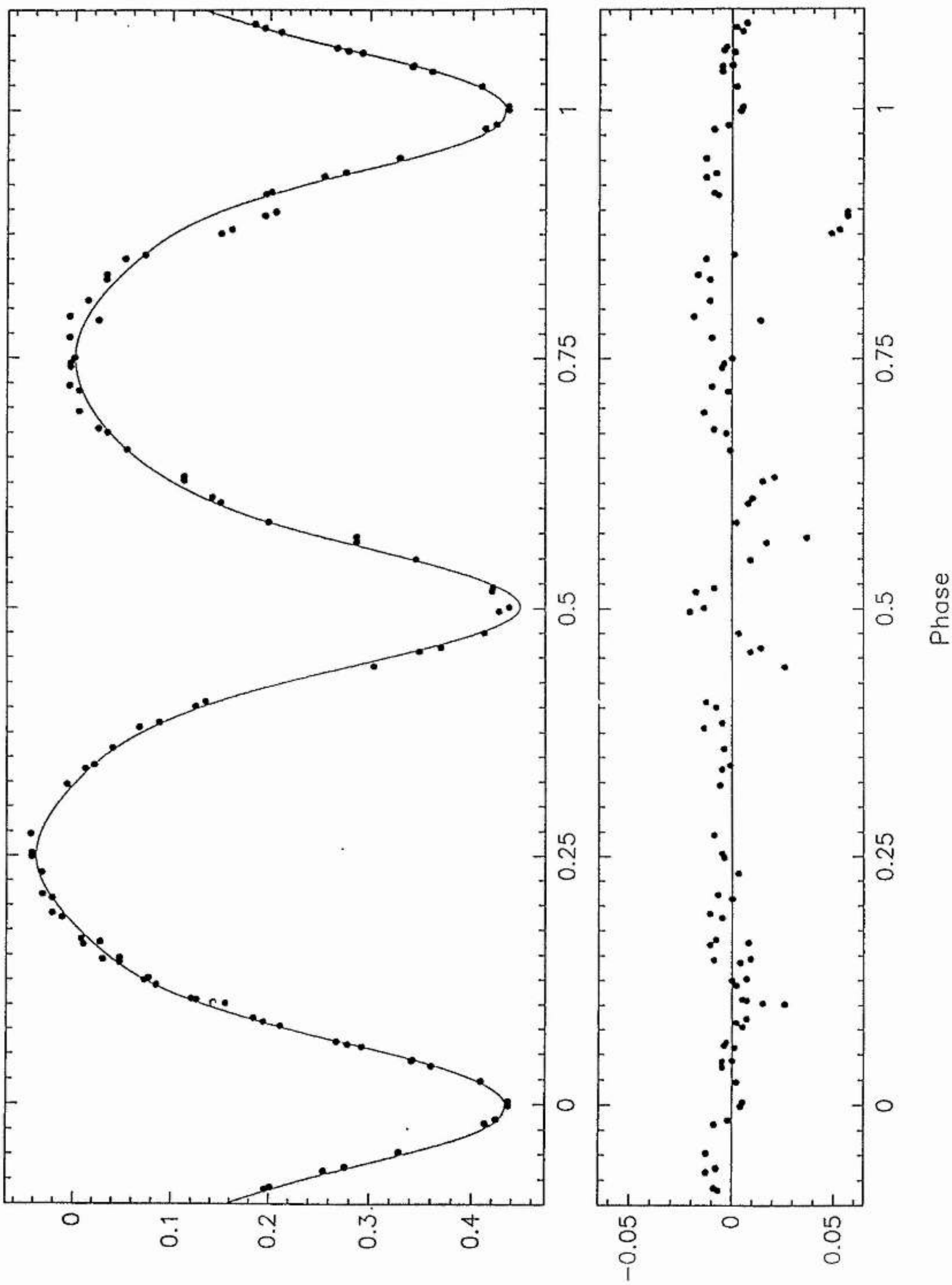

Figure 6.8: The generated "best fit" to the J observations of SS Ari, with the corresponding O-C's shown in the lower plot, using the system and spot parameters given in Table 6.7.

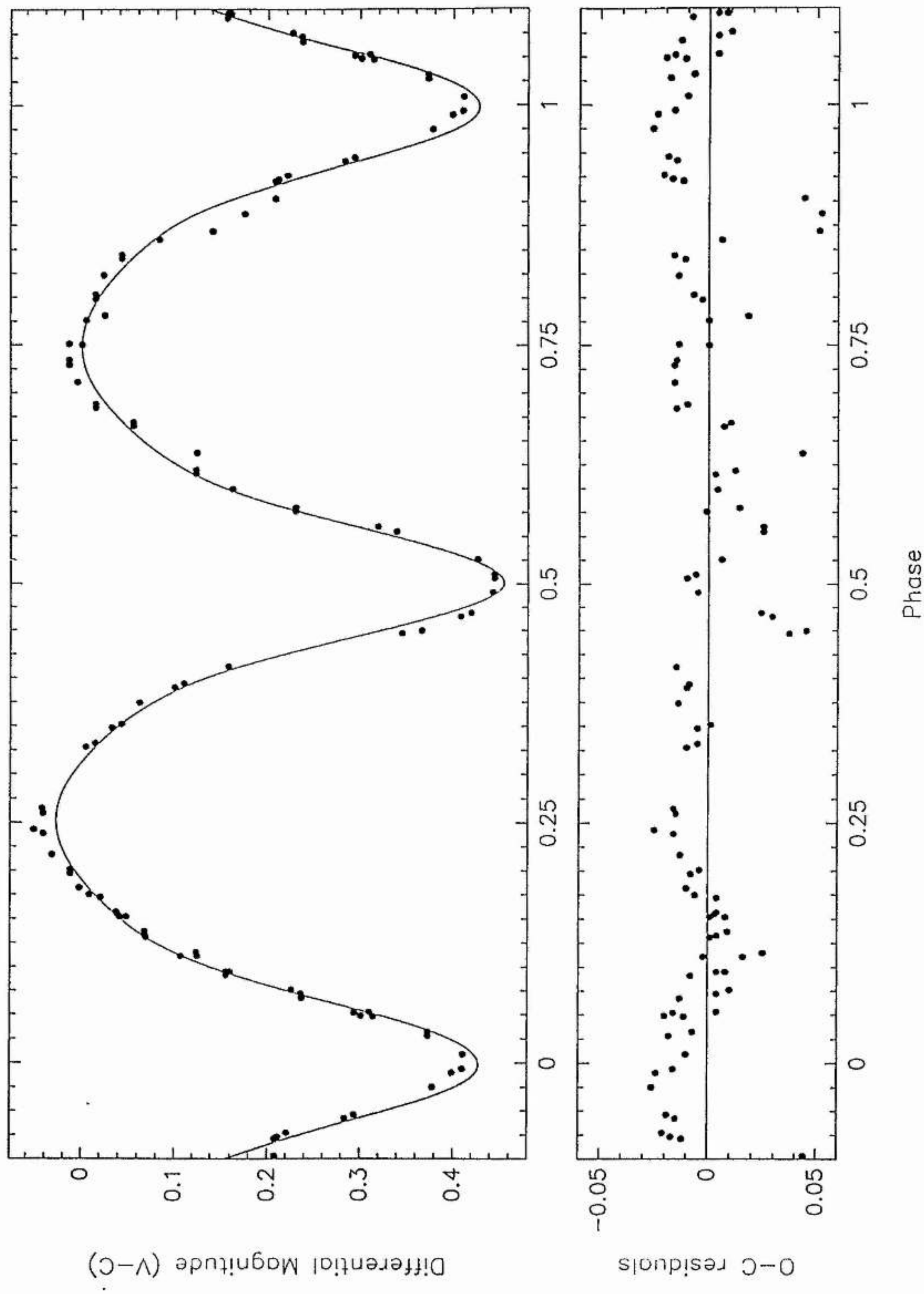

Figure 6.9: The generated "best fit" to the K observations of SS Ari, with the corresponding O-C's shown in the lower plot, using the system and spot parameters given in Table 6.7.

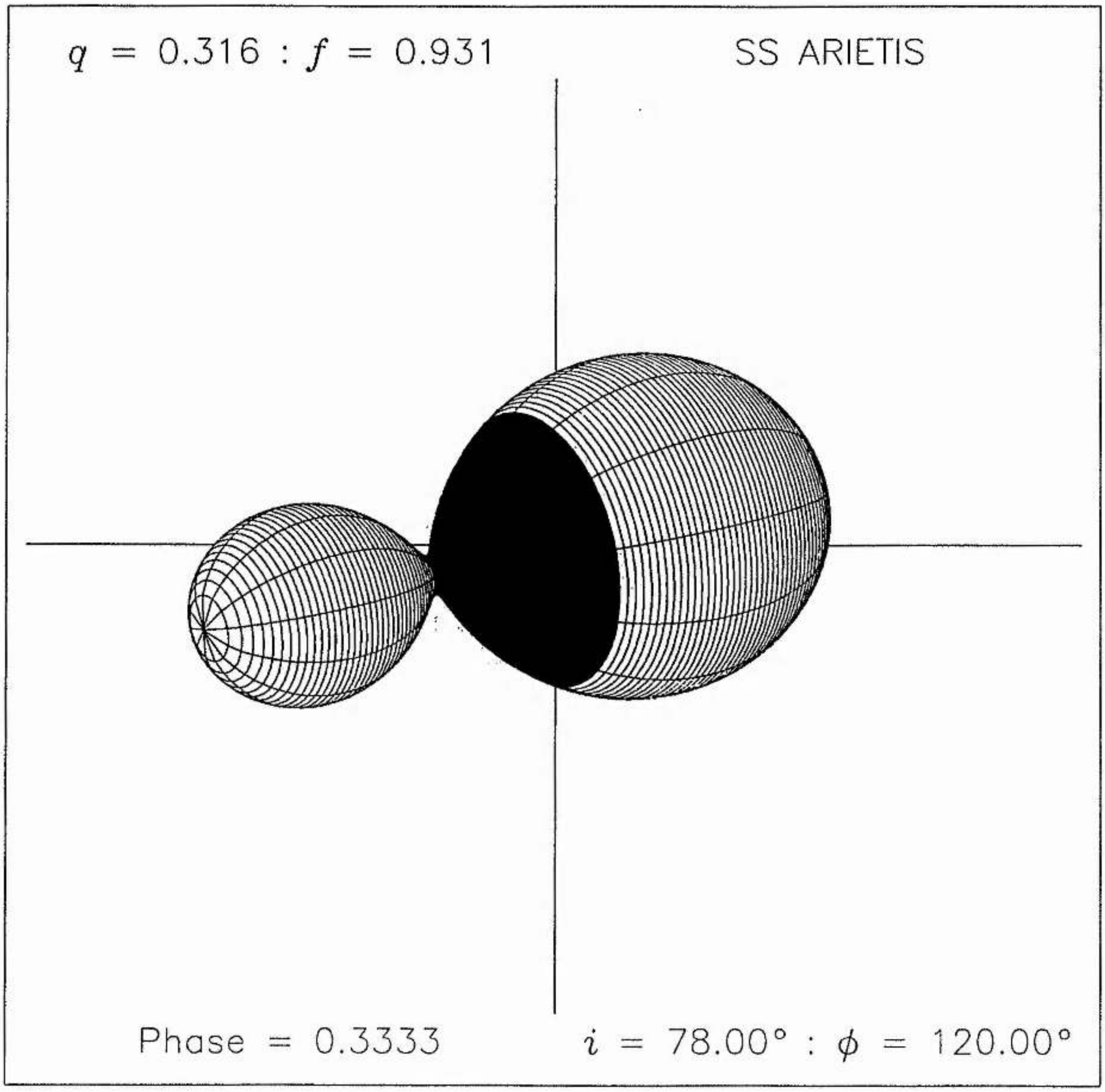

Figure 6.10: A schematic diagram of SS Ari at $0^{\mathrm{P}}.33$, based on the generated "best fit" to the visual data obtained in 1983.

(The location of a hot spot at longitude 20° with a radius of 50°is also shown).

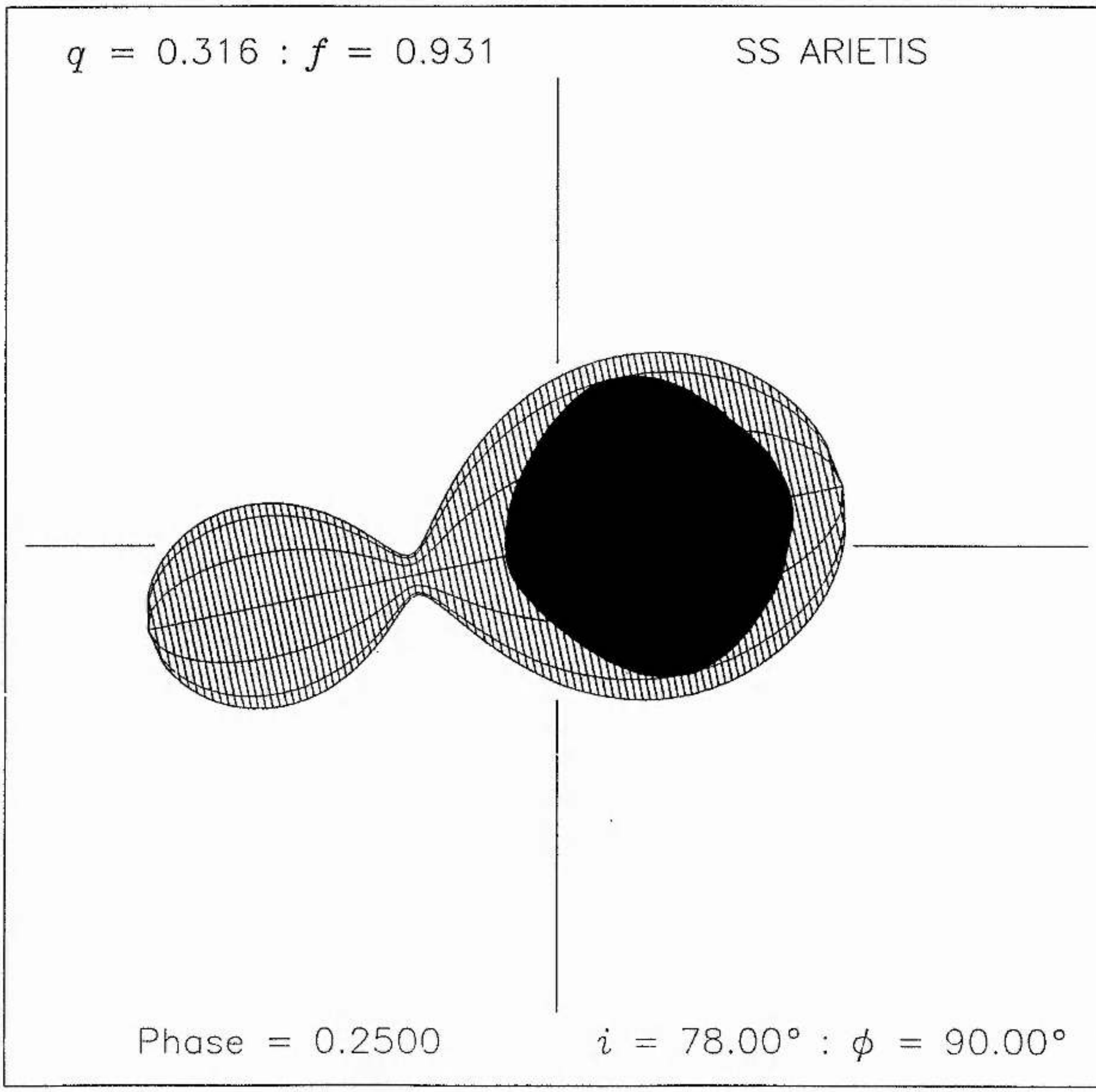

Figure 6.11: A schematic diagram of SS Ari at $0^{P}.25$, based on the generated "best fit" to the infrared data obtained in 1987.
(The system geometry is the same as for the visual case in 1983, but now the location of a hot spot at longitude 90° with a radius of 60°is indicated).

6.5 Discussion

The data and analysis presented here show the difficulty of interpreting a unique spot model for binary systems, particularly those which exhibit light curves with unequal heights of quadrature. (See also Chapter 7).

The true nature of the luminosity distribution on SS Ari is far from certain, with the visual light curve of Kaluzny & Pojmański (1983a) obtained in 1983 apparently indicating a substantially different geometry from that suggested by the infrared light curve obtained in 1987 and presented here. It is encouraging, however, that a common system geometry, modified by the presence of a hot spot, can be found to fit reasonably well both wavelength light curves. This equally, of course, indicates the wide range of solutions which can fit such data, highlighting the problems of obtaining unique solutions. If the possible interpretation presented here is correct, the apparent displacement of the spot to one side of the star needs to be explained, as does the apparent shift of the spot around the star between 1983 and 1987.

The true nature of the system can probably only be resolved by using Doppler Imaging techniques to identify the position of any spot phenomena, and simultaneous infrared and visual photometry to estimate the spot temperature. Also monitoring of the system's light curve over a long time base may reveal any time dependency of the phenomena, and add further photoelectric times of minima which are required to determine the true nature of the apparent sinusoidal period variations.

Assuming the marginal contact, unequal temperature configuration adopted in this analysis is correct, then the astrophysical data for SS Ari, are as listed in Table 6.8. As in previous analyses an error of 200 K has been adopted in the secondary component temperature, and the bolometric corrections have been taken from the compilation of Popper (1980). The system's distance was estimated adopting the colour excess of $E_{(B-V)} = 0\overset{m}{.}035$ (Section 6.4.3).

A comparison of the masses, radii, temperatures, and luminosities of the components of SS Ari (see Chapter 9), with those of other marginal-contact and contact binaries, compiled by Hilditch *et al.* (1988) indicates that the primary and secondary components

Absolute dimensions	Primary	Secondary
$M(M_\odot)$	1.07 ± 0.03	0.34 ± 0.01
$R(R_\odot)$	1.26 ± 0.02	0.75 ± 0.01
$log\,g$ (cgs)	4.26 ± 0.02	4.22 ± 0.02
T_{eff} (K)	6100 ± 200	6260 ± 200
$log\,L/L_\odot$	0.30 ± 0.06	-0.11 ± 0.06
M_{bol}	$4^{m}_{\cdot}01 \pm 0^{m}_{\cdot}14$	$5^{m}_{\cdot}04 \pm 0^{m}_{\cdot}14$
B.C.	$-0^{m}_{\cdot}08$	$-0^{m}_{\cdot}05$
M_V	$4^{m}_{\cdot}09 \pm 0^{m}_{\cdot}14$	$5^{m}_{\cdot}09 \pm 0^{m}_{\cdot}14$
$E_{(B-V)}$	$0^{m}_{\cdot}035$	
Distance (pc)	181 ± 22	

Table 6.8: Astrophysical Data for SS Ari.

lie close to the corresponding components of VW Boo in the M-R and M-L diagrams, occupying the same regions as standard W-type binary systems.

The primary component lies just on the TAMS line of the main-sequence band, whilst the secondary component is over-sized and over-luminous compared with a standard low mass, main-sequence star (Patterson 1984).

On the HR diagram the components of SS Ari are also found to occupy the same regions as the components of standard W-type binary systems.

6.6 References

Bell, S.A., 1990. *Private Communication.*

Braune, W., 1970. *Inf. Bull. Var. Stars*, 440.

Braune, W., & Mundry, E., 1973. *Astr. Nachr.*, **294**, 225.

Braune, W., Hübscher, J., & Mundry, E., 1972. *Astr. Nachr.*, **294**, 123.

Braune, W., Hübscher, J., & Mundry, E., 1977. *Astr. Nachr.*, **298**, 121.

Braune, W., Hübscher, J., & Mundry, E., 1979. *Astr. Nachr.*, **300**, 165.

Braune, W., Hübscher, J., & Mundry, E., 1981. *Astr. Nachr.*, **302**, 53.

Braune, W., Hübscher, J., & Mundry, E., 1983. *BAV Bull.*, No. 36.

Crawford, D.L., 1975. *Astr. J.*, **80**, 995.

Faulkner, D.R., 1986. *Publs astr. Soc. Pacif.*, **98**, 690.

Hilditch, R.W., & Hill, G., 1975. *Mem. R. astr. Soc.*, **79**, 101.

Hilditch, R.W., King, D.J., & McFarlane, T.M., 1988. *Mon. Not. R. astr. Soc.*, **231**, 341.

Hoffmeister, C., 1934. *Astr. Nachr.*, **253**, 195.

Hübscher, J., & Mundry, E., 1984. *BAV Bull.*, No. 38.

Hübscher, J., Lichtenknecker, D., & Meyer, J., 1986. *BAV Bull.*, No. 43.

Hübscher, J., & Lichtenknecker, D., 1988. *BAV Bull.*, No. 50.

Huth, H., 1964. *Mitt. Sonneberg*, **2**, 112.

Isles, J.E., 1985a. *BAA Var. Star Section Circ.*, No. 60.

Isles, J.E., 1985b. *BAA Var. Star Section Circ.*, No. 61.

Isles, J.E., 1986. *BAA Var. Star Section Circ.*, No. 63.

Isles, J.E., 1988. *BAA Var. Star Section Circ.*, No. 66.

Kaluzny, J., & Pojmański, G., 1984a. *Acta Astr.*, **34**, 445.

Kaluzny, J., & Pojmański, G., 1984b. *Inf. Bull. Var. Stars*, 2564.

Keskin, V., & Pohl, E., 1989. *Inf. Bull. Var. Stars*, 3355.

Kholopov, P.N., Samus, N.N., Frolov, M.S., Goranskij, V.P., Gorynya, N.A., Kireeva, N.N., Kukarkin, N.P., Kurochkin, N.E., Medvedeva, G.I., Perova, N.B., & Shugarov, S.Yu., 1985. *General Catalogue of Variable Stars*, Vol 1, Nauka Publishing House, Moscow.

Koornneef, J., 1983. *Astr. Astrophys.*, **128**, 84.

Kramer, E.H., 1948. *Astronomical Circular of the USSR*, **79**, 9.

Kurpiński, M., 1982. *SAC*, **54**, 97.

Locher, K., 1978. *BBSAG Bull.*, No. 39.

Locher, K., 1980a. *BBSAG Bull.*, No. 46.

Locher, K., 1980b. *BBSAG Bull.*, No. 51.

Locher, K., 1981a. *BBSAG Bull.*, No. 52.

Locher, K., 1981b. *BBSAG Bull.*, No. 53.

Locher, K., 1981c. *BBSAG Bull.*, No. 56.

Locher, K., 1981d. *BBSAG Bull.*, No. 57.

Locher, K., 1982a. *BBSAG Bull.*, No. 58.

Locher, K., 1982b. *BBSAG Bull.*, No. 62.

Locher, K., 1983a. *BBSAG Bull.*, No. 64.

Locher, K., 1983b. *BBSAG Bull.*, No. 65.

Locher, K., 1983c. *BBSAG Bull.*, No. 69.

Locher, K., 1984a. *BBSAG Bull.*, No. 70.

Locher, K., 1984b. *BBSAG Bull.*, No. 71.

Locher, K., 1984c. *BBSAG Bull.*, No. 74.

Locher, K., 1985. *BBSAG Bull.*, No. 78.

Locher, K., 1986. *BBSAG Bull.*, No. 79.

Locher, K., 1987a. *BBSAG Bull.*, No. 82.

Locher, K., 1987b. *BBSAG Bull.*, No. 83.

Locher, K., 1988a. *BBSAG Bull.*, No. 86.

Locher, K., 1988b. *BBSAG Bull.*, No. 87.

Locher, K., 1988c. *BBSAG Bull.*, No. 88.

Locher, K., 1989a. *BBSAG Bull.*, No. 90.

Locher, K., 1989b. *BBSAG Bull.*, No. 91.

Odynskaya, O.K., 1949. *Perem. Zvezdy*, **6**, 316.

Patterson, J., 1984. *Astrophys. J. Suppl.*, **54**, 443.

Pohl, E., Hamzaoglu, E., Gudur, N., & Ibanoglu, C., 1983. *Inf. Bull. Var. Stars*, 2385.

Pohl, E., Tunca, Z., Gulmen, O., & Evren, S., 1985. *Inf. Bull. Var. Stars*, 2793.

Pohl, E., Akan, M.C., Ibanoglu, C., Sezer, C., & Gudur, N., 1987. *Inf. Bull. Var. Stars*, 3078.

Popper, D.M., 1980. *Ann. Rev. Astr. Astrophys.*, **18**, 115.

Rucinski, S.M., 1983. *Astr. Astrophys.*, **127**, 84.

Zhukov, G.V., 1975. *Astronomical Circular of the USSR*, **888**, 7.

6.7 Appendix - New Photoelectric Data

This appendix tabulates the new photoelectric data for SS Ari presented in this study.

These infrared observations were obtained with the United Kingdom Infrared Telescope during November 1987 (see Section 6.4.2 and Chapter 2).

Table 6.9 gives the J-filter observations, and Table 6.10 gives the K-filter observations.

Table 6.9: 1987 UKIRT J observations.

H.J.D.	Phase	(V-C)	H.J.D.	Phase	(V-C)	H.J.D.	Phase	(V-C)
2447118.74233	0.4407	+9.276	2447118.90017	0.8294	+9.005	2447119.79083	0.0232	+9.381
2447118.74864	0.4562	+9.320	2447118.90199	0.8339	+9.005	2447119.79695	0.0383	+9.332
2447118.75020	0.4600	+9.341	2447118.90862	0.8502	+9.024	2447119.79870	0.0426	+9.313
2447118.75624	0.4749	+9.384	2447118.91026	0.8543	+9.044	2447119.80472	0.0575	+9.264
2447118.76513	0.4968	+9.399	2447118.93480	0.9147	+9.168	2447119.81467	0.0819	+9.166
2447118.76687	0.5011	+9.409	2447118.98747	0.0445	+9.314	2447119.81626	0.0859	+9.156
2447118.77320	0.5167	+9.392	2447118.99326	0.0587	+9.250	2447119.82244	0.1011	+9.127
2447118.77499	0.5211	+9.393	2447118.99474	0.0624	+9.239	2447119.82405	0.1051	+9.097
2447118.78648	0.5494	+9.317	2447119.00092	0.0776	+9.183	2447119.83295	0.1270	+9.048
2447118.79339	0.5664	+9.259	2447119.01101	0.1024	+9.114	2447119.83941	0.1429	+9.019
2447118.79513	0.5707	+9.259	2447119.01251	0.1061	+9.092	2447119.84105	0.1469	+9.019
2447118.80126	0.5858	+9.171	2447119.01830	0.1204	+9.056	2447119.84774	0.1634	+8.999
2447118.80923	0.6054	+9.122	2447119.02025	0.1252	+9.044	2447119.85771	0.1879	+8.960
2447118.81107	0.6100	+9.113	2447119.02879	0.1462	+9.002	2447119.85930	0.1919	+8.950
2447118.81807	0.6272	+9.084	2447119.03495	0.1614	+8.982	2447119.86543	0.2070	+8.950
2447118.81966	0.6311	+9.084	2447119.03681	0.1660	+8.980	2447119.86722	0.2114	+8.940
2447118.83041	0.6576	+9.026	2447119.73051	0.8746	+9.122	2447119.87620	0.2335	+8.939
2447118.83735	0.6747	+9.006	2447119.73207	0.8785	+9.133	2447119.88261	0.2493	+8.929
2447118.83910	0.6790	+8.997	2447119.73796	0.8930	+9.167	2447119.88426	0.2534	+8.929
2447118.84607	0.6962	+8.977	2447119.73970	0.8973	+9.178	2447119.89174	0.2718	+8.928
2447118.85474	0.7175	+8.977	2447119.74780	0.9172	+9.173	2447119.91215	0.3220	+8.965
2447118.85673	0.7224	+8.967	2447119.75442	0.9335	+9.227	2447119.91870	0.3382	+8.984
2447118.86415	0.7407	+8.968	2447119.75600	0.9374	+9.248	2447119.92036	0.3423	+8.993
2447118.86596	0.7452	+8.968	2447119.76195	0.9521	+9.301	2447119.92704	0.3587	+9.012
2447118.87651	0.7711	+8.967	2447119.77361	0.9808	+9.385	2447119.93589	0.3805	+9.039
2447118.88335	0.7880	+8.997	2447119.77521	0.9847	+9.396	2447119.93758	0.3847	+9.059
2447118.88503	0.7921	+8.967	2447119.78114	0.9994	+9.408	2447119.94411	0.4008	+9.096
2447118.89166	0.8085	+8.986	2447119.78272	0.0032	+9.408	2447119.94616	0.4058	+9.106

Table 6.10: 1987 UKIRT K observations.

H.J.D.	Phase	(V-C)	H.J.D.	Phase	(V-C)	H.J.D.	Phase	(V-C)
2447118.74470	0.4465	+8.964	2447118.89740	0.8226	+8.643	2447119.79289	0.0283	+8.992
2447118.74628	0.4504	+8.985	2447118.90439	0.8398	+8.662	2447119.79446	0.0322	+8.992
2447118.75228	0.4652	+9.027	2447118.90607	0.8440	+8.662	2447119.80077	0.0477	+8.933
2447118.75389	0.4691	+9.038	2447118.91259	0.8600	+8.702	2447119.80237	0.0516	+8.913
2447118.76267	0.4908	+9.061	2447118.93747	0.9213	+8.827	2447119.81232	0.0762	+8.845
2447118.76893	0.5062	+9.063	2447118.98950	0.0495	+8.920	2447119.81832	0.0909	+8.775
2447118.77051	0.5101	+9.063	2447118.99097	0.0531	+8.929	2447119.81994	0.0949	+8.775
2447118.77712	0.5263	+9.045	2447118.99676	0.0673	+8.856	2447119.82662	0.1114	+8.726
2447118.78893	0.5554	+8.958	2447118.99847	0.0716	+8.855	2447119.83522	0.1326	+8.687
2447118.79073	0.5599	+8.938	2447119.00794	0.0949	+8.779	2447119.83704	0.1371	+8.687
2447118.79737	0.5762	+8.849	2447119.01452	0.1111	+8.744	2447119.84318	0.1522	+8.667
2447118.79894	0.5801	+8.849	2447119.01605	0.1148	+8.743	2447119.84499	0.1566	+8.657
2447118.80670	0.5992	+8.781	2447119.02247	0.1307	+8.688	2447119.85529	0.1820	+8.617
2447118.81320	0.6152	+8.742	2447119.03099	0.1516	+8.660	2447119.86143	0.1971	+8.607
2447118.81482	0.6192	+8.742	2447119.03252	0.1554	+8.658	2447119.86305	0.2011	+8.607
2447118.82189	0.6366	+8.743	2447119.03911	0.1716	+8.640	2447119.86954	0.2171	+8.587
2447118.83335	0.6648	+8.674	2447119.04067	0.1755	+8.628	2447119.87839	0.2389	+8.577
2447118.83497	0.6688	+8.674	2447119.72807	0.8686	+8.760	2447119.88014	0.2432	+8.567
2447118.84123	0.6843	+8.634	2447119.73565	0.8873	+8.794	2447119.88702	0.2601	+8.577
2447118.84284	0.6882	+8.634	2447119.74192	0.9028	+8.827	2447119.88914	0.2654	+8.576
2447118.85219	0.7113	+8.614	2447119.75004	0.9228	+8.830	2447119.91441	0.3276	+8.624
2447118.85940	0.7290	+8.605	2447119.75176	0.9270	+8.840	2447119.91612	0.3318	+8.634
2447118.86136	0.7338	+8.605	2447119.75802	0.9424	+8.903	2447119.92268	0.3480	+8.652
2447118.86826	0.7508	+8.605	2447119.75963	0.9464	+8.913	2447119.92430	0.3520	+8.662
2447118.87864	0.7764	+8.624	2447119.77130	0.9751	+8.997	2447119.93344	0.3745	+8.681
2447118.88045	0.7809	+8.644	2447119.77725	0.9898	+9.018	2447119.93986	0.3903	+8.719
2447118.88741	0.7980	+8.634	2447119.77885	0.9937	+9.029	2447119.94151	0.3944	+8.729
2447118.88925	0.8025	+8.634	2447119.78526	0.0095	+9.030	2447119.94871	0.4121	+8.777

Chapter 7

The Binary System AG Virginis

7.1 Introduction

The eclipsing binary AG Vir (HD 104350, BD+13° 2481) has been the subject of several studies during the past sixty years since its discovery by Guthnick & Prager (1929). The period of the system was correctly determined by Dugan (1933) and two photographic studies were subsequently made by Bodokia (1937) and Gaposchkin (1953). Several photoelectric light curves have been presented for this W Ursae–Majoris system by Wood (1946), Szczepanowska (1958), Fliegel (1963), Binnendijk (1969), Blanco & Catalano (1970) and more recently by Niarchos (1985) and Kałużny (1986). Low dispersion spectroscopic observations (≈ 79 Å mm^{-1}) have been made by Sanford (1934) who measured radial velocities for the brighter component only and by Hill & Barnes (1972) who obtained similar observations (≈ 63 Å mm^{-1}) and also found no evidence for the spectrum of the secondary component. They concluded that the orbit of AG Vir was eccentric and presented orbital elements for the system.

In the majority of published light curves, the bottom of primary minimum is somewhat distorted and shows some evidence for night to night variations (e.g. Michaels 1988). Similarly, first quadrature is also considerably brighter than second quadrature by approximately $0^{m}_{\cdot}08$ and secondary minimum occurs shortly after $0^{p}_{\cdot}5$. Binnendijk (1969) has shown that the orbital period of AG Vir abruptly lengthened by $0^{s}_{\cdot}4$ around 1944.

Blanco & Catalano (1970) subsequently suggested that the orbital period of the system shows a variation in an interval of just under 40 yr. However, times of minima obtained since their study suggest that this interpretation is probably no longer applicable. The period of this system appears to have been constant since 1944 although the residuals of the photoelectric times of minima from a specific ephemeris show a scatter of around $0^{d}.005$, more than would normally be expected for photoelectric data. These variations and the distortions in the light curves have been put forward as evidence for gas streams and/or spot activity on one or both of the components of AG Vir (e.g. Kałużny1986). A subsequent study of chromospheric emission from W UMa systems by Eaton (1983) using short wavelength IUE spectra indicated that AG Vir showed little clear evidence of surface activity whereas both A– and W–type systems of similar spectral type showed considerable activity.

7.2 Spectroscopy

Radial velocity spectra of AG Vir, centred on 4200 Å were obtained and reduced as detailed in Chapter 2.

The spectra of AG Vir were cross-correlated against the F6IV standard star HD 89449, and the radial velocity measurements given in Table 7.1 obtained. These observations were phased using the ephemeris specified in Section 7.3.

H.J.D.	Phase	V_1 $km\,s^{-1}$	(O–C) $km\,s^{-1}$	V_2 $km\,s^{-1}$	(O–C) $km\,s^{-1}$
2447280.46673	0.6737	+65	−1.4	−207	−7.2
2447281.45247	0.2075	−74	−0.2	+238	−8.2
2447282.38671	0.6612	+61	−2.5	−195	−4.6
2447282.41375	0.7033	+72	+0.3	−211	+5.6
2447282.42605	0.7225	+74	+0.2	−220	+3.3
2447282.45757	0.7715	+77	+2.7	−221	+3.7
2447282.51917	0.8674	+53	−2.3	−170	−5.7
2447282.53419	0.8907	+51	+3.8	−135	+3.8
2447283.39107	0.2241	−78	−2.5	+248	−3.6
2447283.40571	0.2469	−74	+2.5	+251	−3.7
2447283.42045	0.2698	−75	+0.9	+255	+2.1
2447283.44870	0.3138	−72	−1.5	+248	+12.3
2447283.46098	0.3329	−66	+0.4	+225	+2.2
2447283.53190	0.4432	−26	+1.2	——	——
2447283.59209	0.5369	+15	−1.6	——	——

Table 7.1: Radial velocity data for AG Vir.

The sine wave fits to the radial velocity data are shown in Figure 7.1. The two additional primary velocity measurements around $0^{\rm P}\!.5$, which may have been contaminated by the rotational velocity of the star, have been included in the analysis since they are found to have no effect on the resulting best fit computed for the primary data. The radial velocity semi-amplitudes for the primary and secondary, K_1 and K_2 respectively, the systemic velocity V_0 and the derived mass functions and projected semi-major axes of the orbits and their standard errors are given in Table 7.2.

$K_1\,(\mathrm{km\,s^{-1}})$	=	75.7 ± 0.6
$K_2\,(\mathrm{km\,s^{-1}})$	=	240.8 ± 1.9
$V_{0_1}\,(\mathrm{km\,s^{-1}})$	=	-0.8 ± 0.5
$V_{0_2}\,(\mathrm{km\,s^{-1}})$	=	$+13.9 \pm 1.7$
$\overline{V}_0\,(\mathrm{km\,s^{-1}})$	=	-6.6 ± 1.8
$\sigma_1\,(\mathrm{km\,s^{-1}})$ †	=	2.0
$\sigma_2\,(\mathrm{km\,s^{-1}})$ †	=	6.0
q $(\mathrm{m_2/m_1})$	=	0.314 ± 0.004
e	=	0 (adopted)
$\mathrm{a_1 \cdot \sin i\ (R_\odot)}$	=	0.961 ± 0.008
$\mathrm{a_2 \cdot \sin i\ (R_\odot)}$	=	3.058 ± 0.024
$\mathrm{a \cdot \sin i\ (R_\odot)}$	=	4.019 ± 0.025
$\mathrm{m_1 \cdot \sin^3 i\ (M_\odot)}$	=	1.611 ± 0.024
$\mathrm{m_2 \cdot \sin^3 i\ (M_\odot)}$	=	0.506 ± 0.008

Table 7.2: Orbital elements for AG Vir.

† — r.m.s. scatter of a single observation.

A careful analysis of the limited number of radial velocity data for each component gives no indication of any orbital eccentricity (e). If spot activity is present in the light curve near $0^{\mathrm{P}}\!.5$, it would be unwise to draw any conclusive evidence for orbital eccentricity from the phase delay of secondary minimum. It would appear that the orbital eccentricity calculated by Hill & Barnes (1972) can be explained in terms of the blending of lines from both components of AG Vir caused by the measurement of low dispersion spectroscopy.

The small number of spectra obtained for this study make an accurate determination of the systemic velocity difficult and probably contribute to the difference between the values determined from the primary and secondary component velocity curves. However, there is reasonable agreement between the values of K_1 and $\overline{V}_0$ determined

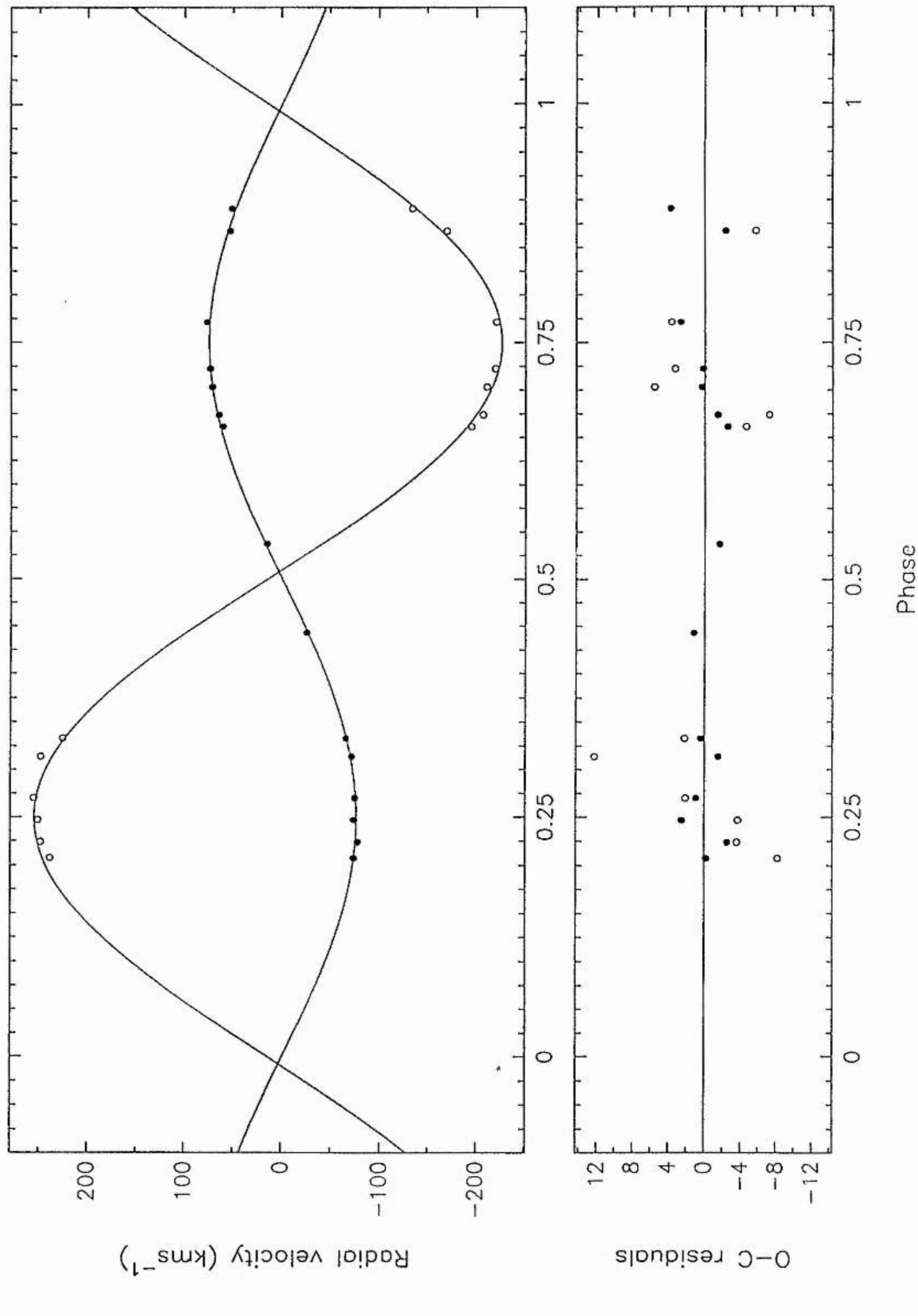

Figure 7.1: Radial velocities of the Primary and Secondary components of AG Vir (closed and open circles respectively), plotted together with their orbital solutions, and corresponding O-Cs (lower plot).

in this study and that of Hill & Barnes.

7.3 Ephemeris

Binnendijk (1969) showed that the period of AG Vir increased abruptly by $0^{s}.4$ around 1944 and noted that secondary minimum generally occurs later than $0^{P}.5$. He deduced that the period had been constant since 1944 and computed the following ephemeris:

$$\text{Pri. min. (H.J.D.)} = 2439946.7472 + 0.64265068 \,.\, E$$

Blanco & Catalano (1970) concluded that the orbital period suffers a slow variation with a period of just less than 40 yr. Subsequently, it was suggested by Niarchos (1985) that if this variation were real then a third body or apsidal motion could be invoked to explain the variation. Michaels (1988) has shown that the displacement of secondary minimum shows evidence of increasing slowly with time over the past 50 yr and that the period change around 1944 was $0^{s}.11$ using times of photoelectric primary minima only. His analysis has also cast doubt on the 40 yr variation suggested by Blanco & Catalano. Kałużny (1986) has suggested that secondary minima may be more appropriate for use in period determinations as the phase interval $0^{P}.41$–$0^{P}.59$ is relatively free from distortion. However, determinations of secondary minima are still few in number and the photometric data presented here do not support this suggestion. Most observers have avoided the distorted section at the bottom of primary minimum for their time of minimum and period determinations and this practice has been continued for this study.

One primary and one secondary minimum have been determined from the new optical observations presented here (Section 7.4.1), using the method of Kwee and van Woerden (1956), and omitting the distorted sections of both minima. A least-squares analysis of 31 times of primary minimum since 1950 was made to calculate the period of AG Vir. This period, adopted for this study, is $0.64265059 \pm 0.00000007$ day and the residuals for this determination are plotted in Figure 7.2. The ephemeris used to phase the spectroscopic and photometric data presented in this study is:

$$\text{Pri. min. (H.J.D.)} = 2447593.64729\,(\pm 0.00011) + 0.64265059\,(\pm 0.00000007) \,.\, E$$

Using this ephemeris, the residuals of 72 visual, photographic and photoelectric times of minima summarized in Table 7.3 are plotted in Figure 7.3. The photoelectric data show a scatter of approximately $0^{d}\!.005$, whereas that for the visual data is some ten times higher. Clearly visual observations of the distorted minima of AG Vir are of limited value and photoelectric determinations offer the only reliable way to evaluate the times of minima for this system.

Table 7.3: Times of minima for AG Vir.

H.J.D.	Cycle	Method	Reference
24585.494	−23903.0	PG	Prager & Dugan (Wood, 1946)
25002.575	−23254.0	PG	Prager & Dugan (Wood, 1946)
25004.520	−23251.0	PG	Prager, 1929
25740.325	−22106.0	VIS	Kukarkin, 1929.
26117.562	−21519.0	PG	Dugan (Wood, 1946)
26119.496	−21516.0	PG	Dugan (Wood, 1946)
26124.660	−21508.0	PG	Dugan (Wood, 1946)
26418.991	−21050.0	PG	Bodokia, 1937
26444.701	−21010.0	PG	Dugan (Wood, 1946)
27157.381	−19901.0	VIS	Kreiner, 1976
27547.499	−19294.0	VIS	Lause, 1937
27888.714	−18763.0	PG	Dugan (Wood, 1946)
27891.610	−18758.5	PG	Dugan (Wood, 1946)
28297.440	−18127.0	VIS	Lause, 1937
28612.341	−17637.0	VIS	Lause, 1937
29329.851	−16520.5	PE	Wood, 1946
29334.993	−16512.5	PE	Wood, 1946
29335.956	−16511.0	PE	Wood, 1946
29337.884	−16508.0	PE	Wood, 1946
29338.851	−16506.5	PE	Wood, 1946
29339.811	−16505.0	PE	Wood, 1946
29346.879	−16494.0	PE	Wood, 1946
29359.734	−16474.0	PE	Wood, 1946
29363.910	−16467.5	PE	Wood, 1946
29368.732	−16460.0	PE	Wood, 1946
31265.173	−13509.0	VIS	Zessewitch, 1944
33387.854	−10206.0	PE	Nason & Moore, 1951
34086.41948	−9119.0	PE	Kwee, 1958
34120.47868	−9066.0	PE	Kwee, 1958
34455.2919	−8545.0	PE	Szczepanowska, 1958
34458.5090	−8540.0	PE	Szczepanowska, 1958
34487.42968	−8495.0	PE	Kwee, 1958
34776.62146	−8045.0	PE	Kwee, 1958
35197.5551	−7390.0	PE	Szczepanowska, 1958

Table 7.3: Times of minima for AG Vir — *continued.*

H.J.D.	Cycle	Method	Reference
35198.5286	−7388.5	PE	Szczepanowska, 1958
35219.4146	−7356.0	PE	Szczepanowska, 1958
35561.2974	−6824.0	PE	Szczepanowska, 1958
35562.2619	−6822.5	PE	Szczepanowska, 1958
35848.5649	−6377.0	PE	Szczepanowska, 1958
37028.47545	−4541.0	PE	Purgathofer & Widorn, 1964
38846.5350	−1712.0	PE	Blanco & Catalano, 1970
39587.5065	−559.0	PE	Blanco & Catalano, 1970
39596.5040	−545.0	PE	Blanco & Catalano, 1970
39618.3520	−511.0	PE	Blanco & Catalano, 1970
39643.4142	−472.0	PE	Blanco & Catalano, 1970
39943.8593	−4.5	PE	Binnendijk, 1969
39944.8190	−3.0	PE	Binnendijk, 1969
39946.7472	0.0	PE	Binnendijk, 1969
39948.6755	3.0	PE	Binnendijk, 1969
41391.4270	2248.0	PE	Kizilirmak & Pohl, 1974
42451.4800	3897.5	PE	Pohl & Kizilirmak, 1976
42892.6620	4584.0	PE	Mallama *et al.*, 1977
44709.4356	7411.0	PE	Pohl *et al.*, 1982
45074.457	7979.0	PE	Locher, 1982
45432.4146	8536.0	PE	Niarchos, 1985
45433.3851	8537.5	PE	Niarchos, 1985
45741.2071	9016.5	PE	Kałużny, 1986
46113.630	9648.5	VIS	Isles, 1989
46180.409	9700.0	VIS	Locher, 1985
46855.8822	10751.0	PE	Michaels, 1988
46859.7378	10757.0	PE	Michaels, 1988
46860.7106	10758.5	PE	Michaels, 1988
46875.8052	10782.0	PE	Michaels, 1988
46892.505	10808.0	VIS	Locher, 1987
46903.42	10825.0	VIS	Locher, 1987
46911.7924	10838.0	PE	Michaels, 1988
47261.3930	11382.0	VIS	Hübscher & Lichtenknecker, 1988
47262.3659	11383.5	PE	Keskin & Pohl, 1989
47270.3876	11396.0	PE	Locher, 1988

Table 7.3: Times of minima for AG Vir — *continued.*

H.J.D.	Cycle	Method	Reference
47270.404	11396.0	VIS	Locher, 1988
47593.6473	11899.0	PE	TPT — this paper
47596.5443	11903.5	PE	TPT — this paper

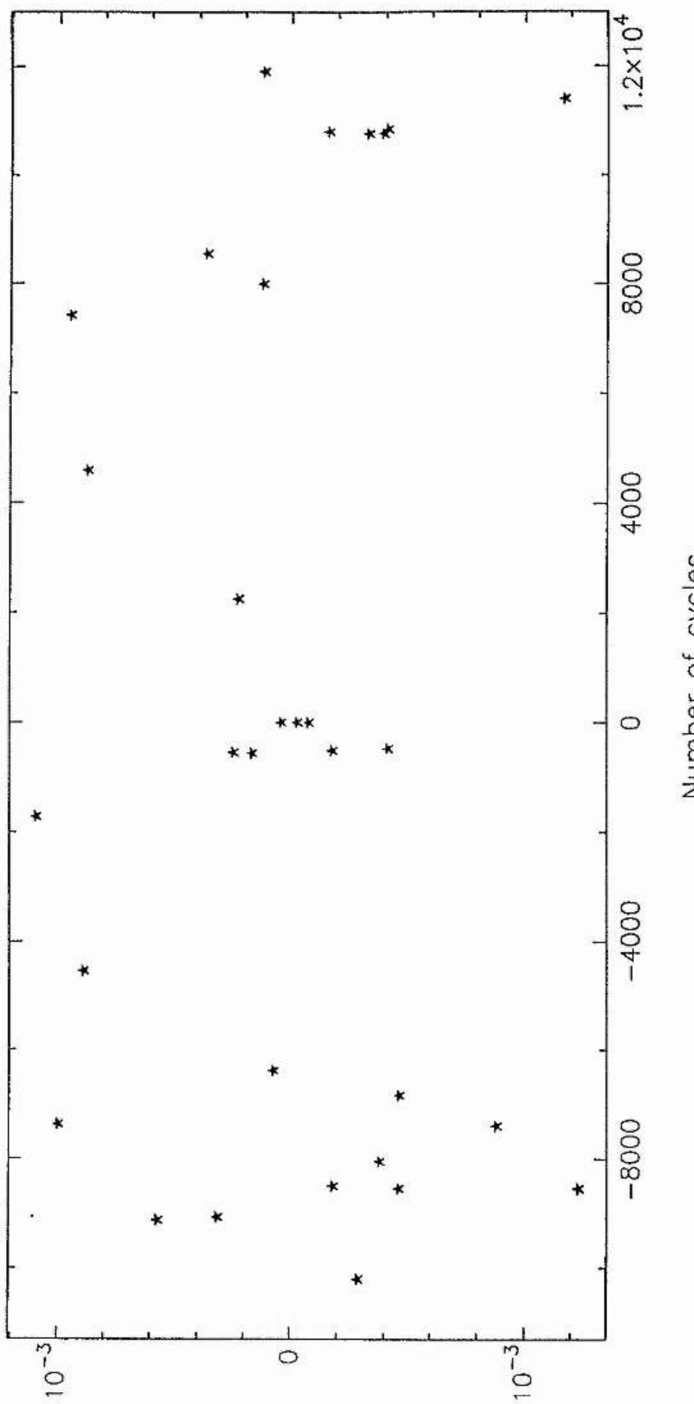

Figure 7.2: Observed minus calculated times of minima in fractions of a day based on the period determined from 31 photoelectric times of primary minima since 1950. Cycle numbers are based on the ephemeris computed by Binnendijk (1969).

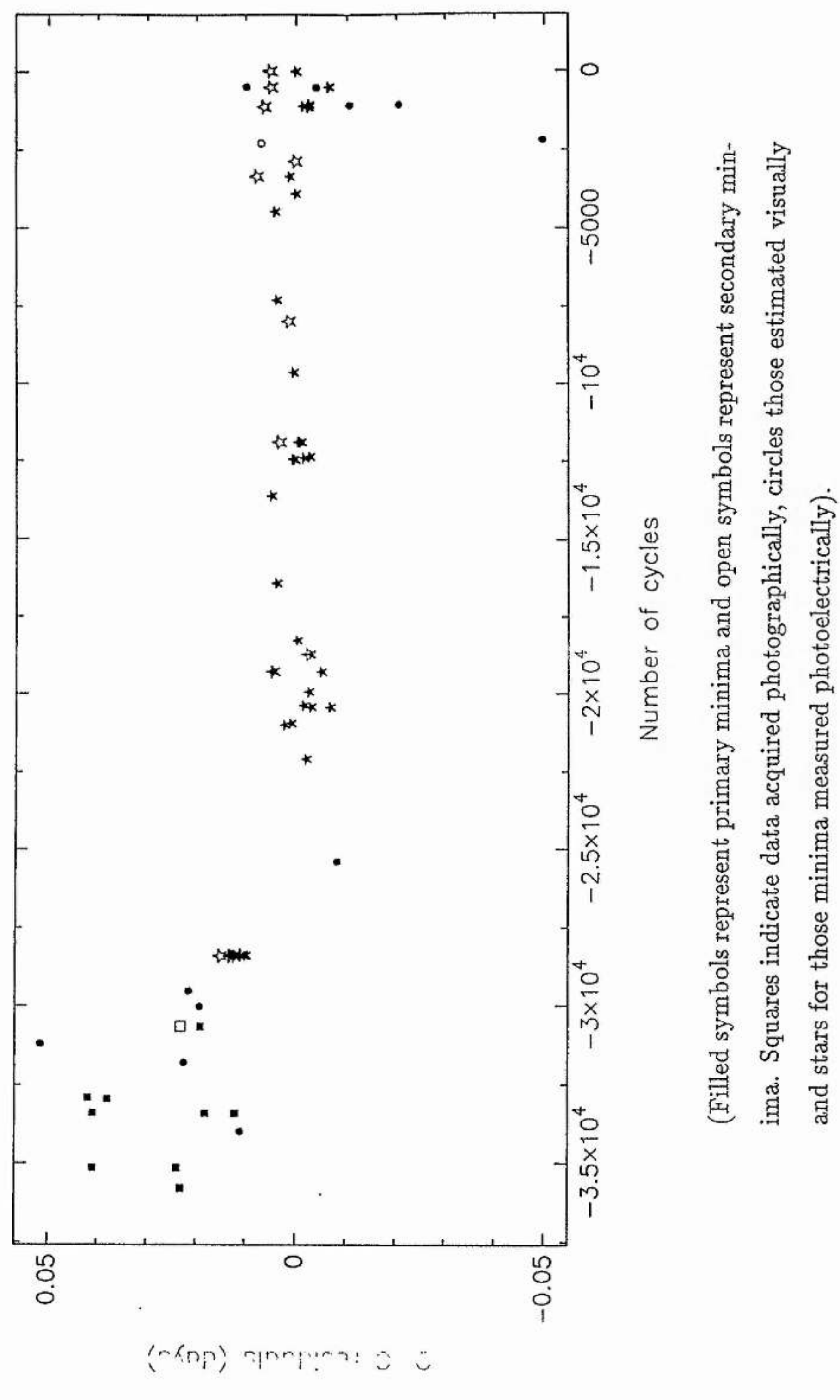

Figure 7.3: Observed minus calculated times of minima in fractions of a day based on the ephemeris computed in Section 7.3 using published data and those minima obtained for this study.

7.4 Photometric Analysis

7.4.1 Optical Observations

New photoelectric photometry of AG Vir in 1989 March was obtained and reduced as outlined in Chapter 2. The filter employed for these observations was comparable to the Johnson V filter. The typical error in the differential magnitudes is approximately $0^{m}\!.006$, and the data were phased using the ephemeris given in Section 7.3. The photoelectric data consisting of 663 observations are listed in the Appendix to this Chapter, and are shown plotted in Figures 7.4, 7.5 and 7.6.

Examination of the light curve reveals several interesting features. The most noticeable is the fact that first quadrature is $0^{m}\!.09$ brighter than secondary quadrature. There is a well defined anomalous brightening of the system during the egress from primary minimum between $0^{p}\!.00$ and $0^{p}\!.04$. On closer examination, the phase of maximum light near first quadrature is displaced by $0^{p}\!.02$ towards primary minimum whereas maximum light at second quadrature occurs at $0^{p}\!.75$. The middle of the 'flat' portion of secondary minimum occurs at $0^{p}\!.515$ although extrapolation of the ingress to and egress from this minimum suggests that secondary minimum occurs at $0^{p}\!.5$. Finally, the 'flat' portion of secondary minimum is not quite flat – there appears to be a very slow increase in brightness through the bottom of the eclipse.

7.4.2 Spectral Type

In his study of AG Vir, Wood (1946) estimated the spectral types of the components of the system to be A2 + A9. Hill & Barnes (1972) were unable to detect the secondary component on their spectra and classified the brighter component to be between A7 and A9. This classification has subsequently been confirmed by Hill *et al.* (1975).

Eggen (1967) published $(B-V)$ colour indices for AG Vir of $0^{m}\!.31$ and $0^{m}\!.29$ for phases close to primary and secondary minimum respectively and determined a colour excess $E_{(B-V)}$ of $+0^{m}\!.03$ for the system. The period–colour relation plotted by Eggen shows that AG Vir lies in an area between regions occupied by detached and contact systems at an age of about 5×10^8 yr. More recently, Hilditch & Hill (1975) have published several Strömgren colour indices at secondary minimum indicating a mean $(b-y)$ of $0^{m}.161$. Similarly, Rucinski & Kałużny (1981) published a mean $(b-y)$ for the system of $0^{m}.156$. Using the spectrum–colour relation given by Rucinski & Kałużny the dereddened $(b-y)$ colour index of Hilditch & Hill would indicate a spectral type of A9 whereas that of Rucinski & Kałużny indicates A8.

Assuming $E_{(b-y)} = 0.74\,E_{(B-V)}$ and the $(B-V)$ colour excess given by Eggen is correct, then $(b-y)_0 = 0^{m}.14$ at secondary minimum. If the contribution of the secondary component to the total light of the system is negligible at secondary minimum then a temperature for the primary component of 7400 K can be inferred using the $(b-y)_0$–temperature tabulation given by Popper (1980). This compares favourably with the spectral classification of between A7 and A9. Using the $(B-V)_0$–effective temperature calibration of Böhm-Vitense (1981), the $(B-V)$ colour index given by Eggen suggests a temperature for the primary component of 7500 ± 200 K. According to Böhm-Vitense, this estimate places the primary component at the limiting temperature for which models incorporating radiative equilibrium are required for single stars. For this study, a temperature estimate for the primary component of 7400 ± 200 K has been adopted.

7.4.3 Light Curve Analysis

The light curve analysis of AG Vir was carried out by Dr. S.A. Bell at St Andrews University Observatory, and follows the analytical approach adopted for the light curve analysis of SS Ari (Section 6.4.4). A summary of the analysis is presented here.

Like SS Ari, each half of the V light curve for AG Vir was analysed separately using the light curve synthesis program LIGHT2. Contact solutions were initiated with an inclination i of 80°, a 'fill-out' factor f of 1.0 (denoting marginal contact), and the mass ratio q fixed at that derived spectroscopically (Section 7.2). Similarly, detached solutions were started with the primary and secondary mean radii, $\overline{r_1}$ and $\overline{r_2}$ respectively, set to 0.45 and 0.25. Bolometric albedos α_1 and α_2 for the primary and secondary components respectively were both fixed at 0.5 and solutions were attempted with the gravity darkening exponents β_1 and β_2 for both the primary and secondary components fixed at their convective values of 0.08 and also their radiative values of 0.25. The primary component temperature T_1 was fixed at 7400 K and solutions were sought for the inclination, fill-out factor or mean radii and secondary component temperature T_2.

The preliminary analysis suggested three methods of solution for each half of the light curve. Two contact solutions were made, one using $\beta_{1,2} = 0.25$ and the other using $\beta_{1,2} = 0.08$. A detached solution using $\beta_1 = 0.25$ and $\beta_2 = 0.08$ was also attempted. The results for the solutions of the first half of the light curve are given in Table 7.4 and those for the second half are given in Table 7.5. The convective contact, radiative contact and detached solutions for each half of the light curve are shown in Figures 7.4, 7.5 and 7.6 respectively. The solutions have been reflected around $0^{\mathrm{p}}.5$ and plotted against the complete set of data. The residuals for each half of the light curve from their respective solutions have also been plotted.

Solution parameter	Contact mode $\beta_{1,2} = 0.08$	Contact mode $\beta_{1,2} = 0.25$	Detached mode $\beta_1 = 0.25$, $\beta_2 = 0.08$
T_2 (K)	7000 ± 11	6683 ± 13	6398 ± 28
i (°)	89.26 ± 0.16	88.96 ± 0.16	$90.00^{(\dagger)}$
f	0.523 ± 0.013	0.712 ± 0.013	see $\overline{r_1}$ & $\overline{r_2}$
$\overline{r_1}$	0.514 ± 0.001	0.503 ± 0.001	0.484 ± 0.003
$\overline{r_2}$	0.315 ± 0.001	0.303 ± 0.001	0.282 ± 0.002
$\alpha_{1,2}$	0.50 (fixed)	0.50 (fixed)	0.50 (fixed)
χ^2	1.783×10^{-4}	1.577×10^{-4}	7.416×10^{-4}
$\overline{O-C}$ & s.d.	0.0000 ± 0.0122	-0.0001 ± 0.0116	-0.0019 ± 0.0256

Table 7.4: LIGHT2 solutions for first half of AG Vir light curve.

† — This quantity was fixed during the solution process.

The solutions obtained for the first half of the light curve indicate a system whose inclination is very close to 90°. The detached solution shown in Figure 7.6 is clearly inadequate as very little of the curve is fitted properly. The contact solutions do appear to be a reasonable fit to the majority of the data with the exception of $0^{\mathrm{p}}.4$ to $0^{\mathrm{p}}.5$ where the fit is in error by up to $0^{\mathrm{m}}.03$. Both of these contact solutions indicate deep contact

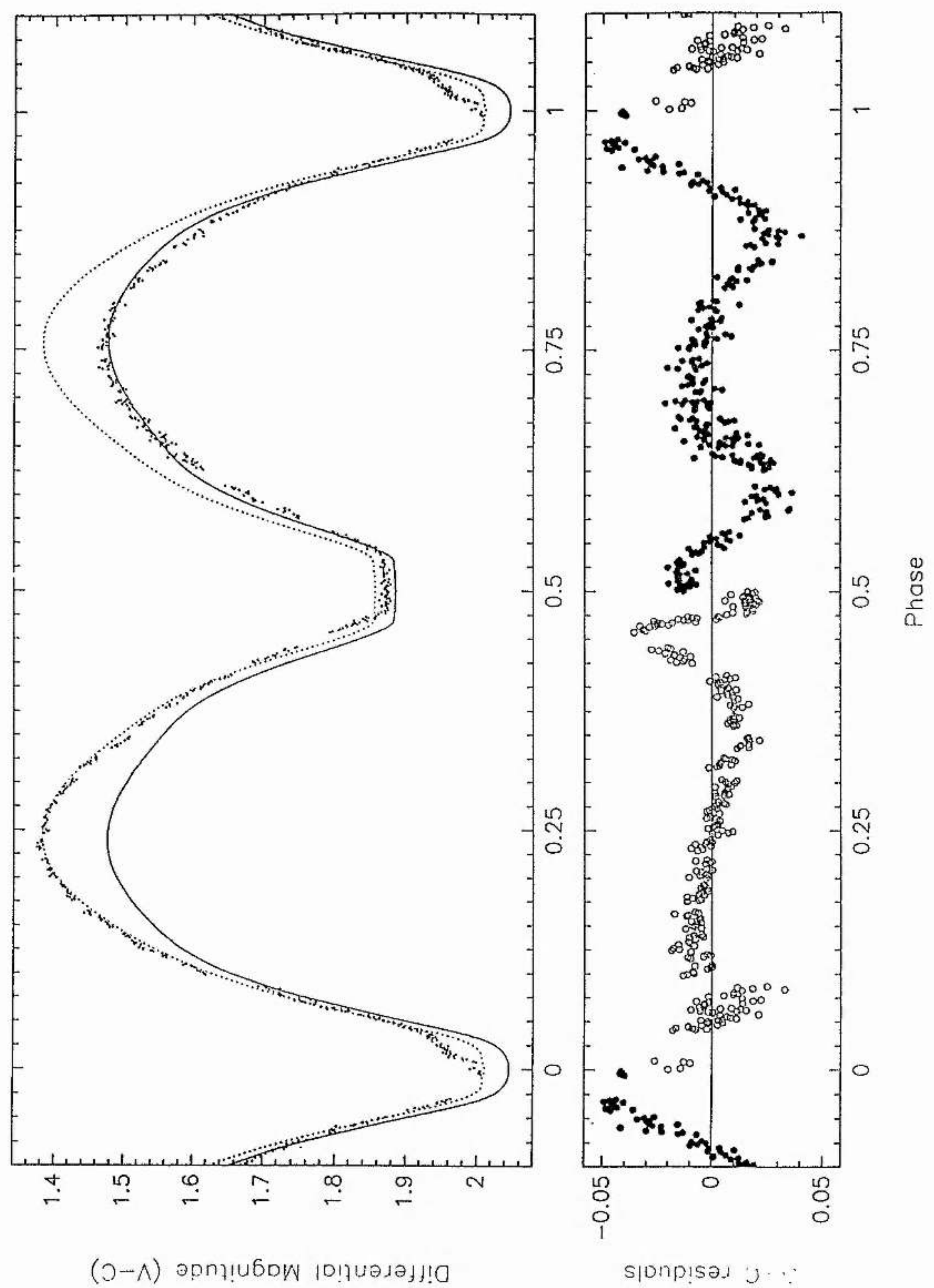

Figure 7.4: TPT *V* observations of AG Vir with two convective contact solutions for each half of the light curve.

(The dotted line is a solution to the light curve from $0^{P}_{.}0$ to $0^{P}_{.}5$ and the solid line is a solution to the light curve from $0^{P}_{.}5$ to $1^{P}_{.}0$. The lower plot shows the residuals of the data from each half of the light curve and its respective solution. The open symbols represent the first half of the light curve and the filled symbols the second half of the light curve).

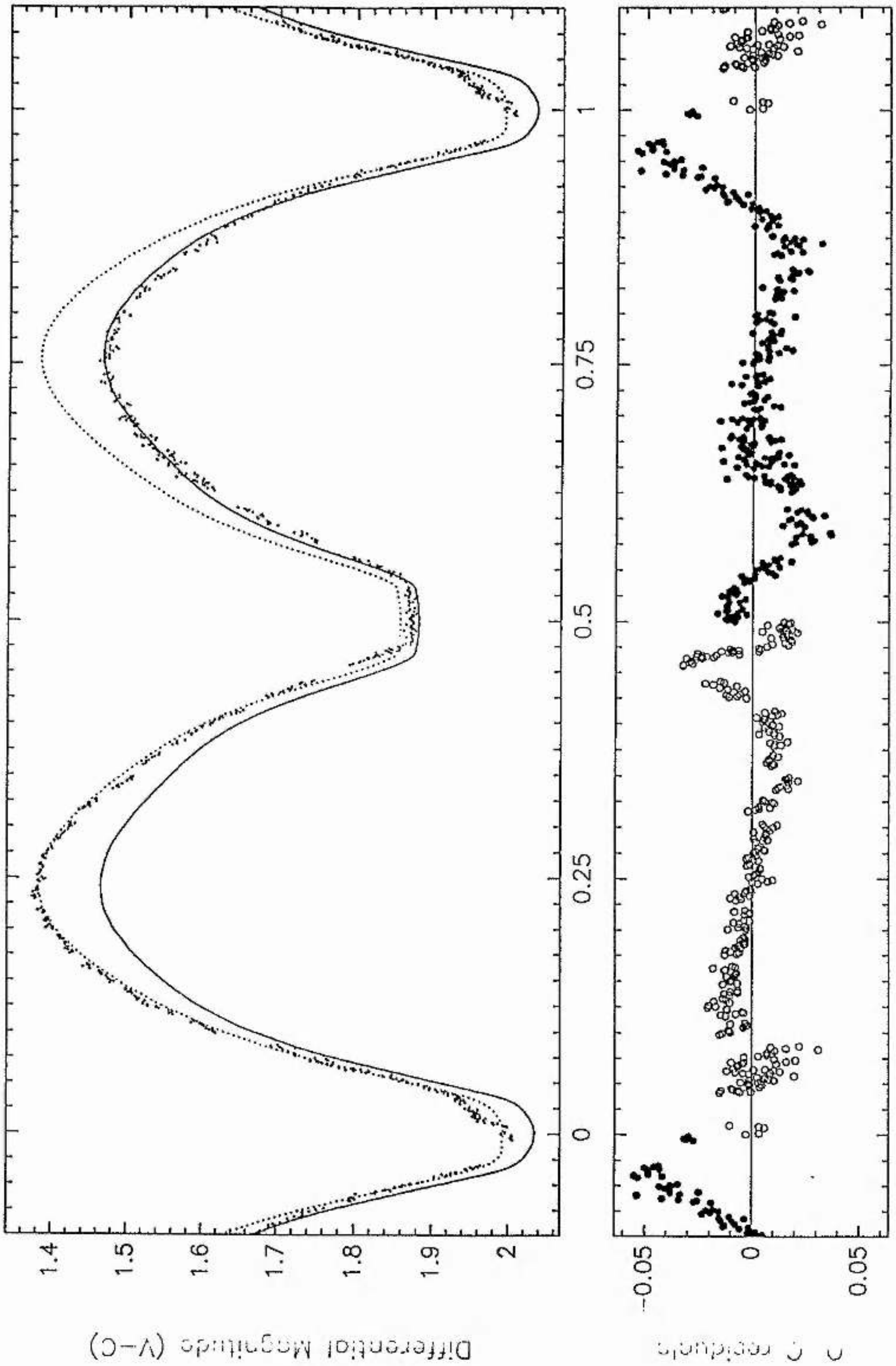

Figure 7.5: TPT *V* observations of AG Vir and two radiative contact solutions for each half of the light curve.

(The dotted line is a solution to the light curve from $0\overset{P}{.}0$ to $0\overset{P}{.}5$ and the solid line is a solution to the light curve from $0\overset{P}{.}5$ to $1\overset{P}{.}0$. The lower plot shows the residuals of the data from each half of the light curve and its respective solution. The open symbols represent the first half of the light curve and the filled symbols the second half of the light curve).

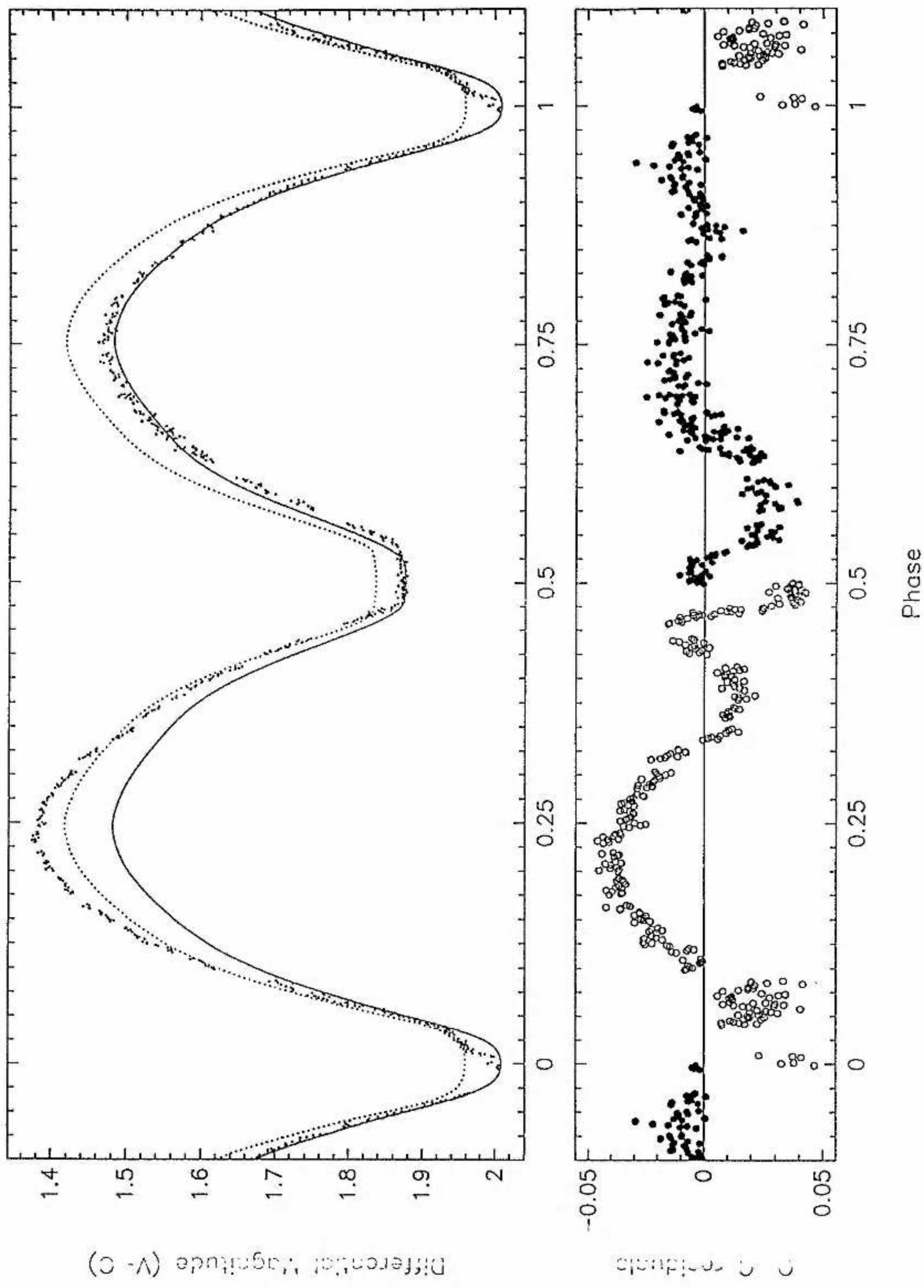

Figure 7.6: TPT *V* observations of AG Vir with two detached solutions for each half of the light curve.

(The dotted line is a solution to the light curve from $0^{P}.0$ to $0^{P}.5$ and the solid line is a solution to the light curve from $0^{P}.5$ to $1^{P}.0$. The lower plot shows the residuals of the data from each half of the light curve and its respective solution. The open symbols represent the first half of the light curve and the filled symbols the second half of the light curve).

Solution parameter	Contact mode $\beta_{1,2} = 0.08$	Contact mode $\beta_{1,2} = 0.25$	Detached mode $\beta_1 = 0.25$, $\beta_2 = 0.08$
T_2 (K)	6879 ± 19	6576 ± 21	6293 ± 21
i (°)	87.35 ± 0.19	89.02 ± 0.26	81.04 ± 0.51
f	0.924 ± 0.022	$1.000^{(\dagger)}$	see $\overline{r_1}$ & $\overline{r_2}$
$\overline{r_1}$	0.491 ± 0.002	0.484 ± 0.001	0.484 ± 0.002
$\overline{r_2}$	0.289 ± 0.001	0.283 ± 0.001	0.280 ± 0.002
$\alpha_{1,2}$	0.50 (fixed)	0.50 (fixed)	0.50 (fixed)
χ^2	3.704×10^{-4}	3.426×10^{-4}	2.088×10^{-4}
$\overline{O-C}$ & s.d.	0.0005 ± 0.0179	$+0.0006 \pm 0.0171$	-0.0003 ± 0.0137

Table 7.5: LIGHT2 solutions for second half of AG Vir light curve.

† — This quantity was fixed during the solution process.

configurations with a secondary component whose temperature is more than 400 K cooler than the primary. As for SS Ari, it is difficult to reconcile these two factors.

The contact solutions to the second half of the light curve are of similar quality. They are both $0^{\mathrm{m}}.02$ too deep at secondary minimum and are up to $0^{\mathrm{m}}.05$ too deep at primary minimum. The contact solutions indicate a marginal contact system at an inclination close to 90° with a temperature difference between the two components of 500 K to 800 K. The detached solution is the most satisfactory overall fit to the data in the second half of the light curve, fitting the depths of the minima better than the contact solutions. This solution indicates that the system is very close to or just at contact with an inclination of 81° and a secondary component 1100 K cooler than the primary. It would appear that the second half of the light curve, like for SS Ari, is probably a more accurate reflection of the geometrical configuration of AG Vir and that the first half of the light curve exhibits varying degrees of excess luminosity.

7.4.4 Modelling a Hot Spot

As with SS Ari, if the detached solution for the second half of the light curve is adopted as the most likely configuration of AG Vir, then the assertion can be made that a hot spot is responsible for the "excess luminosity" observed in the first half of the light curve. Again this spot must be offset to one side of the system, geometric considerations suggesting a spot on the primary component at a longitude of approximately 270° or on the secondary component at a longitude of approximately 90°. For the same reasons outlined in Chapter 6, attempts to solve for a spot radius and temperature using LIGHT2 failed due to the relatively unconstrained model parameters.

However, unpublished *BVR* photometry of AG Vir obtained at the University of Victoria, British Columbia, (Robb 1989) indicates that the $(B - R)$ colour is essentially constant throughout the curve with the exception of a $0\overset{\mathrm{m}}{.}1$ blue peak centred at $0\overset{\mathrm{p}}{.}22$ with a duration of approximately 20% of the orbital cycle. Although the scatter is around $0\overset{\mathrm{m}}{.}04$, this would support the suggestion of a "hot spot" on one of the components. As the secondary component is totally eclipsed at secondary minimum however, and there is still evidence for some distortion of the light curve at this point from the adopted detached solution, it would seem that the hot spot is on the hotter primary component !

Thus as for SS Ari, light curves were generated using the system configuration indicated by the detached solution to the second half of the light curve, and a variety of primary component hot spot radii and temperatures at a longitude of 270°. Assuming that the blue peak in the $(B - R)$ curves is related to the size of the "spot" then a radius of approximately 20° can be inferred. In this case the best match to the light curve can then be obtained with a spot temperature of some 9500 K and this "best fit" is shown plotted in Figure 7.7. Like SS Ari, this cannot be treated as a true solution, but does seem to suggest that this form of "excess luminosity" displaced to one side of the system, may be a different phenomena from the simple energy transfer regions modelled in VW Boo (Chapter 4) and BX And (Chapter 5). The feature at the bottom of primary minimum in AG Vir could also be explained in terms of a spot or stream of material between the two stars.

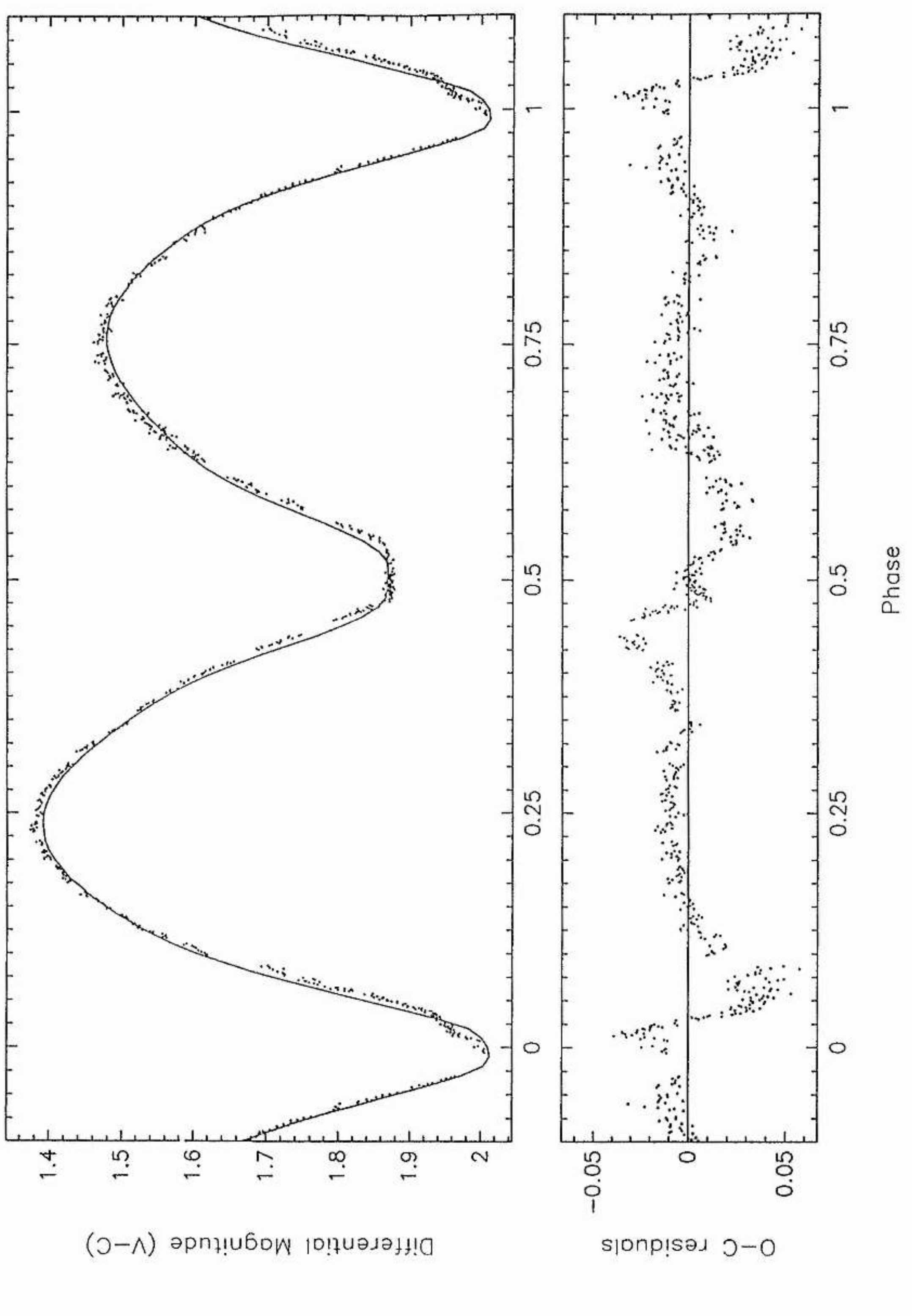

Figure 7.7: Generated "best fit" with hot spot to the TPT V observations of AG Vir with corresponding residuals shown in lower plot.

7.5 Discussion

Assuming the detached photometric solution for the second half of the TPT data given in Table 7.5 is correct, then the astrophysical data for AG Vir are as given in Table 7.6. As in previous analysis, an error of 200 K has been adopted in the secondary component temperature, and the bolometric corrections have been taken from the compilation of Popper (1980). The system's distance was estimated using the colour excess given in Section 7.4.2. Figure 7.8 shows a schematic diagram of the basic "unspotted" system geometry of of AG Vir.

Absolute dimensions	Primary	Secondary
$M\,(M_\odot)$	1.67 ± 0.03	0.53 ± 0.01
$R\,(R_\odot)$	1.97 ± 0.02	1.14 ± 0.01
$log\,g$ (cgs)	4.07 ± 0.01	4.05 ± 0.01
T_{eff}(K)	7400 ± 200	6300 ± 200
$log\,L/L_\odot$	1.02 ± 0.05	0.27 ± 0.06
M_{bol}	$2^{m}_{\cdot}21 \pm 0^{m}_{\cdot}12$	$4^{m}_{\cdot}10 \pm 0^{m}_{\cdot}14$
B.C.	$-0^{m}_{\cdot}01$	$-0^{m}_{\cdot}06$
M_V	$2^{m}_{\cdot}22 \pm 0^{m}_{\cdot}12$	$4^{m}_{\cdot}16 \pm 0^{m}_{\cdot}14$
$E_{(B-V)}$	$+0^{m}_{\cdot}03$	
Distance (pc)	175 ± 15	

Table 7.6: Astrophysical data for AG Vir.

A comparison of the masses, radii, temperatures and luminosities of the components of AG Vir (see Chapter 9), with those of other marginal-contact and contact binaries compiled by Hilditch *et al.* (1988), shows that the primary component is close to the TAMS relationship of Vandenberg (1985) and has properties similar to the A–type contact binaries and the B–type marginal-contact systems. The secondary component is approximately 2.5 times larger than expected for its ZAMS mass and occupies the same region in the M–R and M–L diagrams as other B–type secondaries. AG Vir appears to be in a marginal contact state like the W–type contact systems, however,

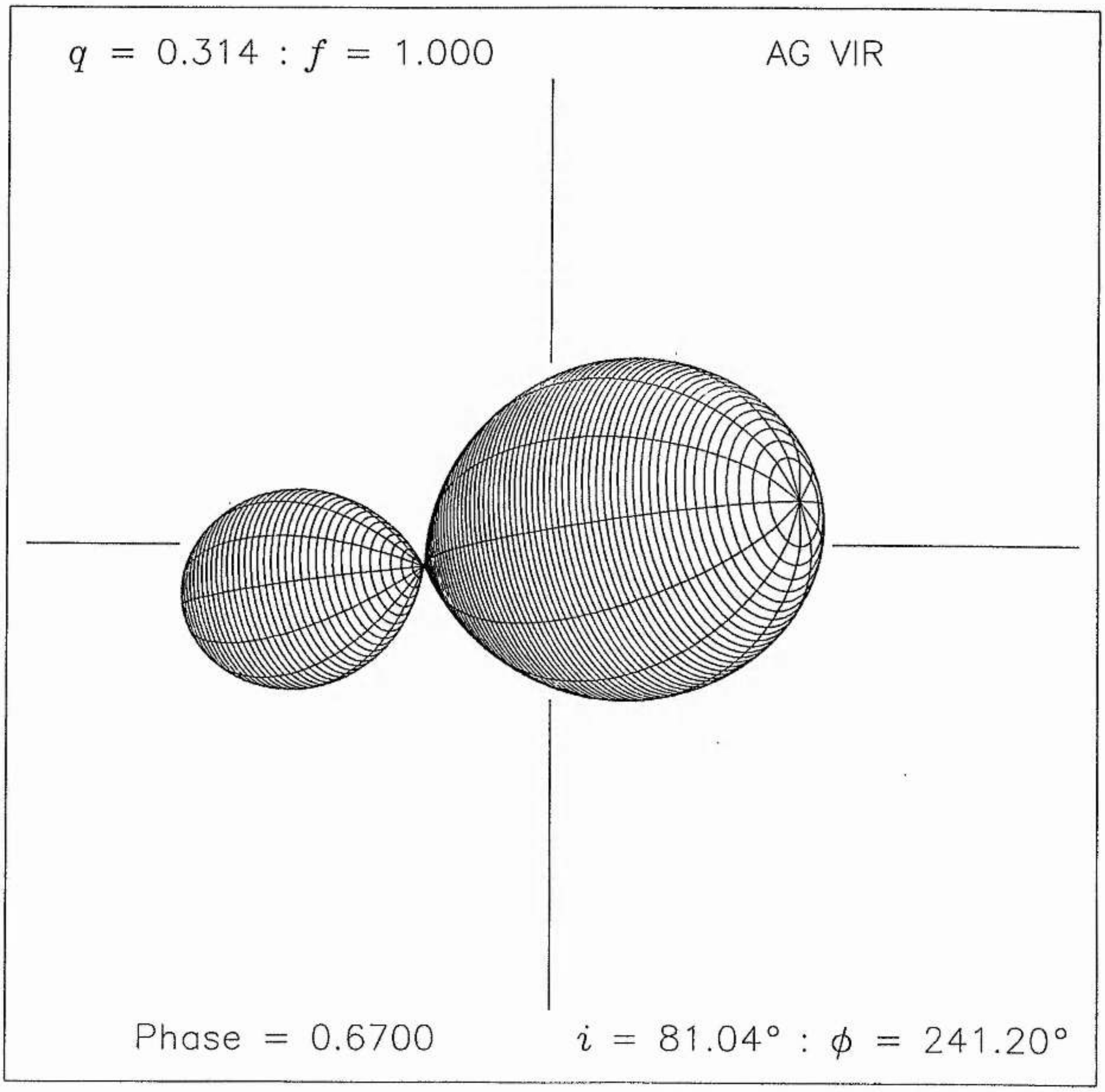

Figure 7.8: Schematic diagram at $0^{\rm p}\!.67$ of the basic system geometry of AG Vir, with no spots shown.

the secondary component does not lie to the left of the ZAMS line in the HR diagram as it would for the secondaries of the W–type systems. It lies on the ZAMS relation which may indicate that the luminosity transfer suggested for the W–type systems is not complete but has progressed further than systems such as BX And where the secondary component lies to the right of the ZAMS line in the HR diagram.

7.6 References

Binnendijk, L., 1969. *Astr. J.*, **74**, 1024.

Blanco, C. & Catalano, F., 1970. *Mem. Soc. astr. Ital.*, **41**, 343.

Böhm-Vitense, E., 1981. *Ann. Rev. Astr. Astrophys.*, **19**, 295.

Bodokia, V.M., 1937. *Abastumani Bull.*, No. 1, 25.

Dugan, R.S., 1933. *Astr. Nachr.*, **247**, 357.

Eaton, J.A., 1983. *Astrophys. J.*, **268**, 800.

Eggen, O.J., 1967. *Mem. R. astr. Soc.*, **70**, 111.

Fliegel, H.F., 1963. Dissertation, University of Pennsylvania, Philadelphia.

Gaposchkin, S., 1953. *Harvard Ann,*, **113**, 69.

Guthnick, P. & Prager, R., 1929. *Beob. Zir.*, No. 11, 32.

Hilditch, R.W. & Hill, G., 1975. *Mem. R. astr. Soc.*, **79**, 101.

Hilditch, R.W., King, D.J. & McFarlane, T.M., 1988. *Mon. Not. R. astr. Soc.*, **231**, 341.

Hill, G. & Barnes, J.V., 1972. *Publs astr. Soc. Pacif.*, **84**, 382.

Hill, G., Hilditch, R.W., Younger, F. & Fisher, W.A., 1975. *Mem. R. astr. Soc.*, **79**, 131.

Hübscher, J. & Lichtenknecker, D., 1988. *BAV Mitt.*, No. 50.

Isles, J.E., 1989. *BAA Var. Star Section Circ.*, No. 69.

Kałużny, J., 1986. *Acta Astr.*, **36**, 121.

Keskin, V. & Pohl, E., 1989. *Inf. Bull. Var. Stars*, No. 3355.

Kizilirmak, A. & Pohl, E., 1974. *Inf. Bull. Var. Stars*, No. 937.

Kreiner, J.M., 1976. *Acta Astr.*, **26**, 341.

Kwee, K.K., 1958. *Bull. Astr. Inst. Neth.*, **14**, 131.

Kwee, K.K., & van Woerden, H., 1956. *Bull. Astr. Inst. Neth.*, **12**, 327.

Kukarkin, B.W., 1929. *Nishni Novgorod Veränd. Sterne*, **1**, No. 12.

Lause, F., 1937. *Astr. Nachr.*, **264**, 107.

Locher, K., 1982. *BBSAG Bull.*, No. 60.

Locher, K., 1985. *BBSAG Bull.*, No. 77.

Locher, K., 1987. *BBSAG Bull.*, No. 83.

Locher, K., 1988. *BBSAG Bull.*, No. 88.

Michaels, E.J., 1988. *Inf. Bull. Var. Stars*, No. 3202.

Nason, M.E. & Moore, R.C., 1951. *Astr. J.*, **56**, 183.

Niarchos P.G., 1985. *Astr. Astrophys. Suppl.*, **61**, 313.

Pohl, E. & Kizilirmak, A., 1976. *Inf. Bull. Var. Stars*, No. 1163.

Pohl, E., Evren, S., Tümer, O. & Sezer, C., 1982. *Inf. Bull. Var. Stars*, No. 2189.

Popper, D.M., 1980. *Ann. Rev. Astr. Astrophys.*, **18**, 115.

Prager, R., 1929. *Kl. Veröff., Berlin-Babelsberg*, No. 6, 35.

Purgathofer, A. & Widorn, T., 1964. *Mitt. Wein.*, **12**, 31.

Robb, R., 1989. *Private Communication.*

Rucinski, S.M. & Kałużny, J., 1981. *Acta Astr.*, **31**, 409.

Sanford, R.F., 1934. *Astrophys. J.*, **79**, 89.

Szczepanowska, A., 1958. *Acta Astr.*, **8**, 36.

Vandenberg, D.A., 1985. *Astrophys. J. Suppl.*, **58**, 711.

Wood, F.B., 1946. *Contrib. Princeton Univ. Obs.*, No. 21, 4.

Zessewitch, W., 1944. *Kasan Astron. Circ.*, No. 35, 9.

7.7 Appendix - New Photoelectric Data

This appendix tabulates the new photoelectric data for AG Vir presented in this study. These V-filter observations were obtained with the St Andrews TPT during March 1989 (see Section 7.4.1 and Chapter 2).

Table 7.7: TPT *V* observations.

H.J.D.	Phase	(V–C)	H.J.D.	Phase	(V–C)	H.J.D.	Phase	(V–C)
2447593.41060	0.6317	+1.598	2447593.47414	0.7306	+1.467	2447593.54136	0.8352	+1.540
2447593.41129	0.6328	+1.602	2447593.47483	0.7316	+1.462	2447593.54205	0.8362	+1.536
2447593.41198	0.6338	+1.591	2447593.47553	0.7327	+1.474	2447593.54275	0.8373	+1.544
2447593.41268	0.6349	+1.588	2447593.47622	0.7338	+1.477	2447593.54417	0.8395	+1.550
2447593.41337	0.6360	+1.588	2447593.47797	0.7365	+1.478	2447593.54487	0.8406	+1.552
2447593.41503	0.6386	+1.563	2447593.47867	0.7376	+1.471	2447593.54556	0.8417	+1.559
2447593.41572	0.6397	+1.574	2447593.47936	0.7387	+1.466	2447593.54626	0.8428	+1.560
2447593.41642	0.6408	+1.570	2447593.48005	0.7398	+1.470	2447593.54695	0.8439	+1.556
2447593.41711	0.6418	+1.576	2447593.48075	0.7409	+1.473	2447593.55578	0.8576	+1.572
2447593.41782	0.6429	+1.566	2447593.48748	0.7513	+1.466	2447593.55649	0.8587	+1.571
2447593.42160	0.6488	+1.561	2447593.48818	0.7524	+1.461	2447593.55717	0.8598	+1.574
2447593.42230	0.6499	+1.552	2447593.48887	0.7535	+1.466	2447593.55786	0.8608	+1.589
2447593.42299	0.6510	+1.561	2447593.48957	0.7546	+1.473	2447593.55856	0.8619	+1.585
2447593.42369	0.6521	+1.553	2447593.49026	0.7557	+1.468	2447593.56128	0.8662	+1.591
2447593.42438	0.6531	+1.557	2447593.49161	0.7578	+1.473	2447593.56197	0.8672	+1.600
2447593.42600	0.6557	+1.537	2447593.49231	0.7588	+1.473	2447593.56267	0.8683	+1.601
2447593.42670	0.6567	+1.546	2447593.49300	0.7599	+1.468	2447593.56336	0.8694	+1.614
2447593.42739	0.6578	+1.544	2447593.49370	0.7610	+1.467	2447593.56406	0.8705	+1.601
2447593.42808	0.6589	+1.553	2447593.49439	0.7621	+1.478	2447593.56518	0.8722	+1.602
2447593.42878	0.6600	+1.539	2447593.49524	0.7634	+1.474	2447593.56587	0.8733	+1.614
2447593.43039	0.6625	+1.541	2447593.49593	0.7645	+1.484	2447593.56657	0.8744	+1.612
2447593.43108	0.6636	+1.538	2447593.49663	0.7656	+1.473	2447593.56726	0.8755	+1.611
2447593.43178	0.6647	+1.538	2447593.49732	0.7666	+1.482	2447593.56797	0.8766	+1.607
2447593.43247	0.6657	+1.535	2447593.49801	0.7677	+1.474	2447593.57282	0.8841	+1.625
2447593.43317	0.6668	+1.531	2447593.50054	0.7716	+1.471	2447593.57351	0.8852	+1.628
2447593.43462	0.6691	+1.518	2447593.50123	0.7727	+1.475	2447593.57421	0.8863	+1.625
2447593.43532	0.6702	+1.526	2447593.50193	0.7738	+1.477	2447593.57490	0.8874	+1.639
2447593.43601	0.6712	+1.530	2447593.50262	0.7749	+1.475	2447593.57560	0.8884	+1.637
2447593.43671	0.6723	+1.529	2447593.50332	0.7760	+1.476	2447593.57792	0.8921	+1.649
2447593.43740	0.6734	+1.528	2447593.50542	0.7792	+1.478	2447593.57862	0.8931	+1.647
2447593.43926	0.6763	+1.520	2447593.50612	0.7803	+1.482	2447593.57931	0.8942	+1.656
2447593.43995	0.6774	+1.516	2447593.50681	0.7814	+1.470	2447593.58001	0.8953	+1.661
2447593.44064	0.6784	+1.510	2447593.50751	0.7825	+1.479	2447593.58070	0.8964	+1.661
2447593.44134	0.6795	+1.515	2447593.50820	0.7836	+1.484	2447593.58317	0.9002	+1.670
2447593.44203	0.6806	+1.508	2447593.51271	0.7906	+1.485	2447593.58386	0.9013	+1.677
2447593.44644	0.6875	+1.507	2447593.51341	0.7917	+1.478	2447593.58455	0.9024	+1.677
2447593.44714	0.6886	+1.506	2447593.51410	0.7927	+1.485	2447593.58525	0.9035	+1.679
2447593.44783	0.6896	+1.512	2447593.51480	0.7938	+1.481	2447593.58594	0.9045	+1.686
2447593.44852	0.6907	+1.510	2447593.51549	0.7949	+1.485	2447593.58800	0.9077	+1.691
2447593.44922	0.6918	+1.504	2447593.51704	0.7973	+1.500	2447593.58870	0.9088	+1.699
2447593.45049	0.6938	+1.496	2447593.51774	0.7984	+1.482	2447593.58939	0.9099	+1.691
2447593.45119	0.6949	+1.487	2447593.51843	0.7995	+1.484	2447593.59010	0.9110	+1.696
2447593.45187	0.6959	+1.499	2447593.51913	0.8006	+1.492	2447593.59078	0.9121	+1.706
2447593.45256	0.6970	+1.490	2447593.51982	0.8016	+1.491	2447593.59276	0.9151	+1.716
2447593.45326	0.6981	+1.503	2447593.52829	0.8148	+1.508	2447593.59345	0.9162	+1.715
2447593.46247	0.7124	+1.481	2447593.52899	0.8159	+1.512	2447593.59415	0.9173	+1.731
2447593.46317	0.7135	+1.482	2447593.52968	0.8170	+1.512	2447593.59484	0.9184	+1.724
2447593.46386	0.7146	+1.484	2447593.53038	0.8181	+1.512	2447593.59554	0.9195	+1.735
2447593.46455	0.7156	+1.487	2447593.53108	0.8192	+1.512	2447593.59735	0.9223	+1.735
2447593.46525	0.7167	+1.482	2447593.53275	0.8218	+1.519	2447593.59805	0.9234	+1.743
2447593.46648	0.7186	+1.486	2447593.53344	0.8228	+1.525	2447593.59874	0.9245	+1.753
2447593.46716	0.7197	+1.480	2447593.53414	0.8239	+1.518	2447593.59944	0.9255	+1.752
2447593.46785	0.7208	+1.479	2447593.53483	0.8250	+1.520	2447593.60013	0.9266	+1.762
2447593.46855	0.7219	+1.476	2447593.53553	0.8261	+1.515	2447593.60433	0.9332	+1.796
2447593.46924	0.7229	+1.476	2447593.53997	0.8330	+1.533	2447593.60503	0.9342	+1.794
2447593.47344	0.7295	+1.475	2447593.54067	0.8341	+1.540	2447593.60572	0.9353	+1.801

Table 7.7: TPT *V* observations — *continued.*

H.J.D.	Phase	(V–C)	H.J.D.	Phase	(V–C)	H.J.D.	Phase	(V–C)
2447593.60642	0.9364	+1.798	2447593.67876	0.0490	+1.883	2447596.53791	0.4980	+1.875
2447593.60711	0.9375	+1.797	2447593.67945	0.0500	+1.870	2447596.53861	0.4991	+1.876
2447593.60902	0.9404	+1.803	2447593.68014	0.0511	+1.868	2447596.54010	0.5014	+1.873
2447593.60972	0.9415	+1.827	2447593.68152	0.0533	+1.863	2447596.54079	0.5025	+1.870
2447593.61041	0.9426	+1.829	2447593.68222	0.0544	+1.855	2447596.54149	0.5035	+1.871
2447593.61110	0.9437	+1.847	2447593.68291	0.0554	+1.847	2447596.54218	0.5046	+1.874
2447593.61180	0.9448	+1.841	2447593.68360	0.0565	+1.837	2447596.54288	0.5057	+1.872
2447593.61333	0.9472	+1.853	2447593.68430	0.0576	+1.849	2447596.54434	0.5080	+1.865
2447593.61402	0.9482	+1.862	2447593.68570	0.0598	+1.815	2447596.54503	0.5091	+1.875
2447593.61472	0.9493	+1.863	2447593.68639	0.0608	+1.820	2447596.54572	0.5101	+1.869
2447593.61541	0.9504	+1.873	2447593.68709	0.0619	+1.818	2447596.54642	0.5112	+1.870
2447593.61610	0.9515	+1.883	2447593.68778	0.0630	+1.809	2447596.54711	0.5123	+1.876
2447593.62028	0.9580	+1.903	2447593.68848	0.0641	+1.799	2447596.54893	0.5151	+1.869
2447593.62098	0.9591	+1.920	2447593.69210	0.0697	+1.774	2447596.54963	0.5162	+1.869
2447593.62167	0.9601	+1.914	2447593.69279	0.0708	+1.753	2447596.55033	0.5173	+1.870
2447593.62237	0.9612	+1.926	2447593.69349	0.0719	+1.767	2447596.55101	0.5184	+1.873
2447593.62307	0.9623	+1.932	2447593.69420	0.0730	+1.765	2447596.55171	0.5194	+1.868
2447593.62491	0.9652	+1.945	2447593.69488	0.0741	+1.751	2447596.55312	0.5216	+1.876
2447593.62561	0.9663	+1.956	2447593.69626	0.0762	+1.724	2447596.55382	0.5227	+1.868
2447593.62630	0.9673	+1.952	2447593.69695	0.0773	+1.726	2447596.55451	0.5238	+1.868
2447593.62700	0.9684	+1.959	2447593.69764	0.0783	+1.725	2447596.55520	0.5249	+1.864
2447593.62770	0.9695	+1.963	2447593.69834	0.0794	+1.722	2447596.55590	0.5260	+1.870
2447593.64363	0.9943	+2.006	2447593.69903	0.0805	+1.715	2447596.55738	0.5283	+1.870
2447593.64431	0.9954	+2.004	2447593.70034	0.0825	+1.709	2447596.55806	0.5293	+1.867
2447593.64501	0.9965	+2.003	2447593.70104	0.0836	+1.724	2447596.55876	0.5304	+1.867
2447593.64570	0.9975	+2.005	2447593.70173	0.0847	+1.705	2447596.55945	0.5315	+1.869
2447593.64639	0.9986	+2.005	2447593.70244	0.0858	+1.693	2447596.56015	0.5326	+1.867
2447593.64759	0.0005	+1.991	2447593.70312	0.0869	+1.702	2447596.56348	0.5378	+1.865
2447593.64827	0.0015	+1.996	2447596.51594	0.4638	+1.823	2447596.56417	0.5388	+1.864
2447593.65174	0.0069	+1.999	2447596.51664	0.4649	+1.831	2447596.56487	0.5399	+1.862
2447593.65244	0.0080	+1.995	2447596.51733	0.4659	+1.829	2447596.56556	0.5410	+1.857
2447593.65313	0.0091	+1.981	2447596.51803	0.4670	+1.835	2447596.56626	0.5421	+1.857
2447593.65382	0.0102	+1.987	2447596.51872	0.4681	+1.846	2447596.56753	0.5441	+1.845
2447593.65452	0.0113	+1.980	2447596.51975	0.4697	+1.843	2447596.56822	0.5451	+1.857
2447593.65695	0.0150	+1.971	2447596.52045	0.4708	+1.856	2447596.56892	0.5462	+1.845
2447593.65764	0.0161	+1.964	2447596.52114	0.4719	+1.847	2447596.56961	0.5473	+1.849
2447593.65834	0.0172	+1.953	2447596.52184	0.4730	+1.857	2447596.57031	0.5484	+1.843
2447593.65903	0.0183	+1.958	2447596.52253	0.4740	+1.857	2447596.57166	0.5505	+1.830
2447593.65973	0.0194	+1.958	2447596.52370	0.4759	+1.861	2447596.57236	0.5516	+1.828
2447593.66121	0.0217	+1.960	2447596.52439	0.4769	+1.871	2447596.57305	0.5527	+1.832
2447593.66190	0.0227	+1.954	2447596.52510	0.4780	+1.865	2447596.57375	0.5537	+1.827
2447593.66260	0.0238	+1.960	2447596.52578	0.4791	+1.871	2447596.57444	0.5548	+1.818
2447593.66329	0.0249	+1.944	2447596.52648	0.4802	+1.874	2447596.57594	0.5571	+1.806
2447593.66400	0.0260	+1.950	2447596.52765	0.4820	+1.874	2447596.57664	0.5582	+1.816
2447593.66800	0.0322	+1.938	2447596.52834	0.4831	+1.873	2447596.57733	0.5593	+1.804
2447593.66869	0.0333	+1.942	2447596.52904	0.4842	+1.871	2447596.57804	0.5604	+1.799
2447593.66938	0.0344	+1.931	2447596.52973	0.4852	+1.871	2447596.57872	0.5615	+1.797
2447593.67009	0.0355	+1.937	2447596.53042	0.4863	+1.876	2447596.58762	0.5753	+1.749
2447593.67077	0.0365	+1.936	2447596.53173	0.4884	+1.871	2447596.58833	0.5764	+1.747
2447593.67226	0.0389	+1.931	2447596.53243	0.4894	+1.878	2447596.58901	0.5775	+1.750
2447593.67296	0.0399	+1.922	2447596.53312	0.4905	+1.878	2447596.58971	0.5786	+1.747
2447593.67365	0.0410	+1.908	2447596.53382	0.4916	+1.873	2447596.59040	0.5796	+1.743
2447593.67435	0.0421	+1.918	2447596.53451	0.4927	+1.877	2447596.59185	0.5819	+1.728
2447593.67504	0.0432	+1.897	2447596.53583	0.4947	+1.873	2447596.59254	0.5830	+1.731
2447593.67737	0.0468	+1.894	2447596.53652	0.4958	+1.872	2447596.59324	0.5841	+1.737
2447593.67807	0.0479	+1.883	2447596.53722	0.4969	+1.875	2447596.59393	0.5851	+1.720

Table 7.7: TPT *V* observations — *continued.*

H.J.D.	Phase	(V–C)	H.J.D.	Phase	(V–C)	H.J.D.	Phase	(V–C)
2447596.59463	0.5862	+1.730	2447596.67340	0.7088	+1.501	2447601.43641	0.1203	+1.556
2447596.59839	0.5921	+1.699	2447596.67409	0.7099	+1.497	2447601.43761	0.1222	+1.543
2447596.59908	0.5932	+1.686	2447601.36639	0.0114	+1.969	2447601.43830	0.1233	+1.539
2447596.59978	0.5942	+1.689	2447601.36709	0.0125	+1.960	2447601.43900	0.1243	+1.528
2447596.60047	0.5953	+1.688	2447601.36778	0.0135	+1.968	2447601.43969	0.1254	+1.528
2447596.60116	0.5964	+1.685	2447601.36848	0.0146	+1.962	2447601.44039	0.1265	+1.522
2447596.60268	0.5988	+1.673	2447601.36917	0.0157	+1.957	2447601.44215	0.1293	+1.525
2447596.60338	0.5998	+1.672	2447601.37130	0.0190	+1.962	2447601.44284	0.1303	+1.515
2447596.60407	0.6009	+1.679	2447601.37198	0.0201	+1.955	2447601.44354	0.1314	+1.518
2447596.60476	0.6020	+1.675	2447601.37268	0.0212	+1.956	2447601.44423	0.1325	+1.514
2447596.60546	0.6031	+1.678	2447601.37337	0.0222	+1.952	2447601.44492	0.1336	+1.511
2447596.60667	0.6050	+1.666	2447601.37407	0.0233	+1.949	2447601.44682	0.1365	+1.508
2447596.60737	0.6061	+1.658	2447601.37785	0.0292	+1.938	2447601.44753	0.1376	+1.503
2447596.60806	0.6071	+1.661	2447601.37855	0.0303	+1.944	2447601.44821	0.1387	+1.506
2447596.60876	0.6082	+1.655	2447601.37924	0.0314	+1.938	2447601.44891	0.1398	+1.499
2447596.60945	0.6093	+1.646	2447601.37994	0.0324	+1.931	2447601.44960	0.1408	+1.500
2447596.62018	0.6260	+1.614	2447601.38063	0.0335	+1.934	2447601.45342	0.1468	+1.479
2447596.62089	0.6271	+1.613	2447601.38186	0.0354	+1.938	2447601.45410	0.1478	+1.484
2447596.62157	0.6282	+1.605	2447601.38255	0.0365	+1.934	2447601.45480	0.1489	+1.479
2447596.62226	0.6292	+1.611	2447601.38325	0.0376	+1.921	2447601.45549	0.1500	+1.476
2447596.62296	0.6303	+1.601	2447601.38394	0.0387	+1.928	2447601.45619	0.1511	+1.476
2447596.62435	0.6325	+1.605	2447601.38465	0.0398	+1.917	2447601.45759	0.1533	+1.473
2447596.62504	0.6336	+1.606	2447601.38601	0.0419	+1.913	2447601.45827	0.1543	+1.467
2447596.62574	0.6346	+1.599	2447601.38670	0.0430	+1.906	2447601.45896	0.1554	+1.467
2447596.62643	0.6357	+1.586	2447601.38739	0.0440	+1.898	2447601.45966	0.1565	+1.466
2447596.62713	0.6368	+1.600	2447601.38808	0.0451	+1.890	2447601.46035	0.1576	+1.464
2447596.62817	0.6384	+1.591	2447601.38878	0.0462	+1.890	2447601.46208	0.1603	+1.452
2447596.62885	0.6395	+1.592	2447601.39075	0.0493	+1.875	2447601.46276	0.1613	+1.450
2447596.62954	0.6406	+1.591	2447601.39144	0.0503	+1.868	2447601.46345	0.1624	+1.442
2447596.63024	0.6416	+1.587	2447601.39214	0.0514	+1.858	2447601.46415	0.1635	+1.451
2447596.63093	0.6427	+1.587	2447601.39283	0.0525	+1.862	2447601.46484	0.1646	+1.448
2447596.63627	0.6510	+1.565	2447601.39352	0.0536	+1.850	2447601.47196	0.1756	+1.425
2447596.63696	0.6521	+1.575	2447601.39792	0.0604	+1.809	2447601.47266	0.1767	+1.429
2447596.63766	0.6532	+1.569	2447601.39862	0.0615	+1.800	2447601.47335	0.1778	+1.428
2447596.63835	0.6543	+1.554	2447601.39931	0.0626	+1.789	2447601.47404	0.1789	+1.422
2447596.63905	0.6554	+1.560	2447601.40001	0.0637	+1.796	2447601.47474	0.1800	+1.418
2447596.64042	0.6575	+1.559	2447601.40070	0.0648	+1.781	2447601.47619	0.1822	+1.423
2447596.64112	0.6586	+1.556	2447601.40215	0.0670	+1.771	2447601.47688	0.1833	+1.419
2447596.64182	0.6597	+1.558	2447601.40284	0.0681	+1.766	2447601.47758	0.1844	+1.419
2447596.64251	0.6607	+1.556	2447601.40354	0.0692	+1.759	2447601.47827	0.1855	+1.418
2447596.64320	0.6618	+1.560	2447601.40423	0.0702	+1.755	2447601.47896	0.1865	+1.419
2447596.64473	0.6642	+1.551	2447601.40492	0.0713	+1.744	2447601.48054	0.1890	+1.416
2447596.64829	0.6697	+1.528	2447601.42217	0.0982	+1.619	2447601.48123	0.1901	+1.411
2447596.65154	0.6748	+1.535	2447601.42286	0.0992	+1.617	2447601.48193	0.1912	+1.413
2447596.65223	0.6759	+1.535	2447601.42356	0.1003	+1.615	2447601.48262	0.1922	+1.410
2447596.65294	0.6770	+1.536	2447601.42426	0.1014	+1.611	2447601.48332	0.1933	+1.409
2447596.65362	0.6780	+1.529	2447601.42495	0.1025	+1.607	2447601.48747	0.1998	+1.402
2447596.65431	0.6791	+1.528	2447601.42672	0.1052	+1.604	2447601.48817	0.2009	+1.393
2447596.66336	0.6932	+1.502	2447601.42742	0.1063	+1.601	2447601.48886	0.2019	+1.401
2447596.66406	0.6943	+1.507	2447601.42811	0.1074	+1.598	2447601.48955	0.2030	+1.396
2447596.66475	0.6953	+1.507	2447601.42880	0.1085	+1.586	2447601.49025	0.2041	+1.398
2447596.66545	0.6964	+1.501	2447601.42950	0.1096	+1.591	2447601.49189	0.2066	+1.393
2447596.66614	0.6975	+1.494	2447601.43363	0.1160	+1.562	2447601.49259	0.2077	+1.390
2447596.67132	0.7056	+1.493	2447601.43432	0.1171	+1.557	2447601.49328	0.2088	+1.396
2447596.67201	0.7066	+1.491	2447601.43502	0.1182	+1.561	2447601.49398	0.2099	+1.393
2447596.67270	0.7077	+1.493	2447601.43571	0.1192	+1.561	2447601.49738	0.2152	+1.389

Table 7.7: TPT V observations — *continued.*

H.J.D.	Phase	(V–C)	H.J.D.	Phase	(V–C)	H.J.D.	Phase	(V–C)
2447601.49807	0.2163	+1.390	2447601.55392	0.3032	+1.426	2447601.62255	0.4100	+1.651
2447601.49877	0.2174	+1.390	2447601.56203	0.3158	+1.436	2447601.62325	0.4111	+1.646
2447601.49946	0.2184	+1.382	2447601.56273	0.3169	+1.442	2447601.62394	0.4121	+1.655
2447601.50016	0.2195	+1.386	2447601.56342	0.3180	+1.445	2447601.63207	0.4248	+1.689
2447601.50653	0.2294	+1.377	2447601.56411	0.3190	+1.451	2447601.63276	0.4259	+1.685
2447601.50723	0.2305	+1.379	2447601.56481	0.3201	+1.448	2447601.63345	0.4269	+1.694
2447601.50792	0.2316	+1.374	2447601.56609	0.3221	+1.452	2447601.63415	0.4280	+1.692
2447601.50862	0.2327	+1.378	2447601.56679	0.3232	+1.460	2447601.63484	0.4291	+1.703
2447601.50931	0.2338	+1.383	2447601.56748	0.3243	+1.460	2447601.63585	0.4307	+1.707
2447601.51060	0.2358	+1.375	2447601.56818	0.3254	+1.459	2447601.63656	0.4318	+1.717
2447601.51129	0.2368	+1.380	2447601.56887	0.3264	+1.460	2447601.63724	0.4328	+1.714
2447601.51198	0.2379	+1.382	2447601.57519	0.3363	+1.482	2447601.63793	0.4339	+1.719
2447601.51268	0.2390	+1.380	2447601.57589	0.3374	+1.489	2447601.63863	0.4350	+1.719
2447601.51339	0.2401	+1.382	2447601.57658	0.3384	+1.487	2447601.63992	0.4370	+1.735
2447601.51700	0.2457	+1.385	2447601.57727	0.3395	+1.489	2447601.64062	0.4381	+1.729
2447601.51769	0.2468	+1.382	2447601.57797	0.3406	+1.494	2447601.64133	0.4392	+1.731
2447601.51839	0.2479	+1.390	2447601.58005	0.3438	+1.500	2447601.64201	0.4402	+1.744
2447601.51908	0.2490	+1.392	2447601.58075	0.3449	+1.507	2447601.64270	0.4413	+1.747
2447601.51977	0.2500	+1.387	2447601.58144	0.3460	+1.504	2447601.65255	0.4566	+1.793
2447601.52126	0.2524	+1.381	2447601.58214	0.3471	+1.505	2447601.65325	0.4577	+1.797
2447601.52195	0.2534	+1.384	2447601.58283	0.3482	+1.508	2447601.65394	0.4588	+1.805
2447601.52264	0.2545	+1.385	2447601.59011	0.3595	+1.521	2447601.65464	0.4599	+1.806
2447601.52334	0.2556	+1.386	2447601.59080	0.3606	+1.525	2447601.65533	0.4610	+1.811
2447601.52403	0.2567	+1.387	2447601.59150	0.3616	+1.526	2447601.65638	0.4626	+1.817
2447601.52585	0.2595	+1.389	2447601.59219	0.3627	+1.525	2447601.65708	0.4637	+1.816
2447601.52654	0.2606	+1.389	2447601.59289	0.3638	+1.529	2447601.65777	0.4648	+1.826
2447601.52724	0.2617	+1.388	2447601.59444	0.3662	+1.533	2447601.65847	0.4659	+1.825
2447601.52795	0.2628	+1.384	2447601.59514	0.3673	+1.537	2447601.65916	0.4669	+1.828
2447601.52863	0.2638	+1.386	2447601.59583	0.3684	+1.542	2447601.66040	0.4689	+1.826
2447601.53129	0.2680	+1.392	2447601.59653	0.3695	+1.542	2447601.66109	0.4699	+1.841
2447601.53198	0.2690	+1.390	2447601.59722	0.3705	+1.543	2447601.66179	0.4710	+1.839
2447601.53269	0.2701	+1.388	2447601.60222	0.3783	+1.561	2447601.66248	0.4721	+1.845
2447601.53337	0.2712	+1.390	2447601.60291	0.3794	+1.567	2447601.66318	0.4732	+1.843
2447601.53407	0.2723	+1.394	2447601.60361	0.3805	+1.566	2447601.67020	0.4841	+1.865
2447601.53599	0.2753	+1.395	2447601.60430	0.3816	+1.567	2447601.67090	0.4852	+1.873
2447601.53668	0.2763	+1.396	2447601.60499	0.3826	+1.577	2447601.67159	0.4863	+1.874
2447601.53738	0.2774	+1.402	2447601.60841	0.3880	+1.586	2447601.67229	0.4874	+1.872
2447601.53807	0.2785	+1.402	2447601.60911	0.3891	+1.586	2447601.67298	0.4884	+1.873
2447601.53877	0.2796	+1.400	2447601.60980	0.3901	+1.581	2447601.67426	0.4904	+1.863
2447601.54273	0.2858	+1.404	2447601.61049	0.3912	+1.592	2447601.67496	0.4915	+1.872
2447601.54342	0.2868	+1.409	2447601.61119	0.3923	+1.592	2447601.67565	0.4926	+1.873
2447601.54411	0.2879	+1.412	2447601.61315	0.3953	+1.600	2447601.67635	0.4937	+1.870
2447601.54481	0.2890	+1.407	2447601.61385	0.3964	+1.601	2447601.67704	0.4948	+1.870
2447601.54550	0.2901	+1.413	2447601.61454	0.3975	+1.611	2447601.67832	0.4967	+1.866
2447601.54687	0.2922	+1.415	2447601.61524	0.3986	+1.611	2447601.67901	0.4978	+1.875
2447601.54756	0.2933	+1.417	2447601.61593	0.3997	+1.614	2447601.67970	0.4989	+1.873
2447601.54826	0.2944	+1.418	2447601.61727	0.4017	+1.616	2447601.68040	0.5000	+1.873
2447601.54895	0.2954	+1.413	2447601.61797	0.4028	+1.622	2447601.68109	0.5011	+1.870
2447601.54965	0.2965	+1.422	2447601.61866	0.4039	+1.623	2447601.68209	0.5026	+1.871
2447601.55114	0.2988	+1.424	2447601.61936	0.4050	+1.627	2447601.68279	0.5037	+1.872
2447601.55183	0.2999	+1.427	2447601.62005	0.4061	+1.627	2447601.68348	0.5048	+1.875
2447601.55253	0.3010	+1.424	2447601.62116	0.4078	+1.639	2447601.68417	0.5058	+1.874
2447601.55322	0.3021	+1.432	2447601.62186	0.4089	+1.645	2447601.68487	0.5069	+1.878

Chapter 8

Other Spectroscopic Observations

8.1 Introduction

As detailed in Section 1.5, this chapter contains other spectroscopic observations which were made during this project, but which failed to yield sufficient information to enable detailed study. As a result, these observations are briefly noted here for completeness, but further analysis is not presented as part of this work.

8.2 The W UMa-type Binary System TZ Bootis

The variability of the binary system TZ Boo was discovered by Guthnick & Prager (1927), and due to its unusual light curve, has been well studied photoelectrically and to some extent spectroscopically.

Carr (1971) showed that the system exhibited interchanging depths of primary and secondary minima, a phenomenon known only in a very few systems (eg. AC Boo and AM Leo). This was confirmed and extensively studied by Hoffmann (1978a,b & 1980), who suggested that the repetitive interchanges of the minima depths exhibited a period of some 3.5 years, explained as a solar-like activity cycle.

McLean & Hilditch (1983) obtained limited spectroscopic observations of TZ Boo around first and second quadratures which gave the first, and so far only, spectroscopic mass ratio for the system of $q = 0.13 \pm 0.03$. However, no attempt has been made to use this mass ratio with a light curve synthesis program to model the basic "unperturbed" geometry of the system. Clearly the magnitude of distortions observed in the light curve, certainly at visual wavelengths at least, would make this a complex task.

Figure 8.1 shows the B light curves of TZ Boo in 1970 and 1978 (Hoffmann 1978b) clearly indicating the interchange of minima depths. It is difficult to see how such perturbations (which are clearly very different from the regions of "excess luminosity" considered so far in this work) can be explained by anything other than large-scale dark spot activity in the system.

High dispersion radial velocity spectra of TZ Boo, centred on 4200 Å, were obtained and reduced as detailed in Chapter 2.

The observations were phased using the photoelectric ephemeris given by Hoffmann (1980), and cross-correlated against a range of radial velocity standard stars of spectral type G0 to K0. The best results were produced using the G0V standard star HD140913, and the cross-correlation functions thus obtained for each spectrum are shown plotted in order of increasing orbital phase in Figure 8.2.

The cross-correlation functions for TZ Boo show no clear, consistent sign of the secondary component. In addition a "bump"-like distortion is present to the varying degrees on the left-hand side of each primary correlation peak. This distortion made it

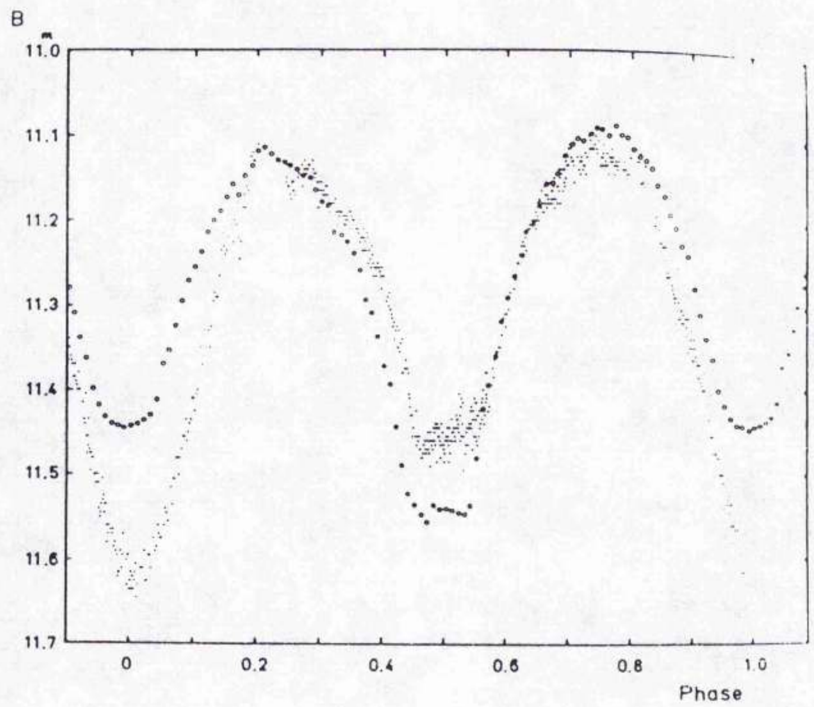

Figure 8.1: B light curves of TZ Boo (Hoffmann 1978b). Open circles represent normal points of 1970 observations, and dots represent 1978 observations.

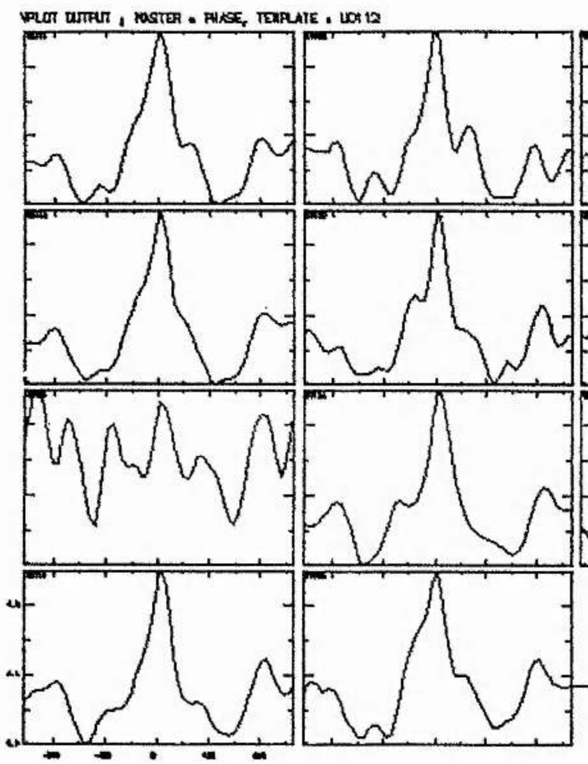

Figure 8.2: Cross-correlation functions for 4200 Å spectra of TZ Boo in order of increasing orbital phase. ($0^{P}\!.02$ top left to $0^{P}\!.97$ bottom right).

difficult to obtain measurements for even the primary component velocities from these data, and it was not possible to produce a consistent set of results using this analytical technique. (The ninth c.c.f. in Figure 8.2 (at $0^{P}\!.38$) is contaminated by a cosmic ray which can be "windowed out" during individual spectrum analysis, but not during the multiple plotting routine used to produce this figure).

8.3 The RS CVn-type Binary System XY Ursae Majoris

The short period eclipsing binary XY UMa (SAO27143) exhibits erratic light curve changes typical of RS CVn stars.

The bulk of the observational work on this system has been done by E.H. Geyer. The primary component is a G2-G5V star, and the secondary a K5 star (Geyer 1980). Like TZ Boo (Section 8.2), the erratic light curve changes can only be explained by invoking dark starspot activity. These distortions appear to show up on three different timescales ; from orbit to orbit, from symmetrical to asymmetrical light curve shape over about four years (Geyer 1980), and total system brightness variations over about 30 years (Geyer 1976). No spectroscopic mass ratio for the system is available.

Hall & Kreiner (1980) published the most recent period analysis for XY UMa, which showed small erratic changes on top of a long-term period change, which was attributed to an enhanced stellar wind flowing isotropically from the active component. Although several light curves have been published since this study, their analysis has concentrated purely on interpreting and modelling the light curve distortions observed in terms of the spot activity on the primary component, and so more recent period study has not been possible (eg. Jassur 1986 and Zeilik & Budding 1987).

Recently, EXOSAT observations of the coronal X-ray emission from the primary component of XY UMa have been published (Bedford *et al.* 1990), which support the model of great photospheric activity on the primary component.

Radial velocity spectra of XY UMa centred on 4200 Å were obtained and reduced as detailed in Chapter 2.

Using the G1 radial velocity standard star HD84441 for cross-correlation, the radial velocity measurements listed in Table 8.1 were obtained. Only primary component velocities were obtained, as the secondary component could not be seen in the cross-correlation functions, even when a later type K2 standard star template was used to try and "bring out" the secondary component cross-correlation peak.

The corresponding orbital phasing of the primary component measurements given in Table 8.1 were calculated using the ephemeris :-

HJD 2435216.5011($\pm$20) + 0.478994587E($\pm$83) which was derived in the period study by Hall & Kreiner (1980).

H.J.D.	Phase	V_1 $km\,s^{-1}$	(O-C) $km\,s^{-1}$
2447197.49458	0.8049	+104	−6.5
2447197.51636	0.8504	+97	−3.4
2447198.69644	0.3140	−124	−0.4
2447198.72072	0.3647	−110	−0.3
2447200.42801	0.9291	+68	+5.0
2447200.45323	0.9817	+43	+15.1
2447200.63315	0.3573	−115	−2.6
2447200.65759	0.4084	−85	+4.4
2447201.46989	0.1042	−73	−11.7
2447202.54253	0.3436	−118	−1.1
2447202.62674	0.5194	−11	+3.6
2447202.65090	0.5698	+26	+3.1
2447202.71411	0.7018	+93	−5.2

Table 8.1: Radial Velocity data for the Primary Component of XY UMa.

Assuming circular orbits, the sine wave fit and corresponding residuals to the radial velocity data for the primary component of XY UMa is shown in Figure 8.3.

This fit gives a radial velocity semi-amplitude for the primary component of $K_1 = (118.3 \pm 3.1)\,\mathrm{km\,s^{-1}}$ and a systemic velocity for the system of $V_0 = (-7.2 \pm 2.0)\,\mathrm{km\,s^{-1}}$. The resultant mass function is then $f(m)$=0.082 $M_\odot$. If a mass of 1 $M_\odot$ is adopted for the G2V primary, then the secondary must be at least 0.6 $M_\odot$ (for i=90°) which is consistent with the classification by Geyer (1980) of K5 for the secondary component, given that this mass estimate is a lower limit.

Clearly there is a small phase shift in the radial velocity data in Figure 8.3 with respect to the ephemeris of Hall & Kreiner (1980) used to derive the orbital phasing. This highlights the need for continuing times of minima to be published for new observations of the system, so that the period behaviour can be constantly reviewed.

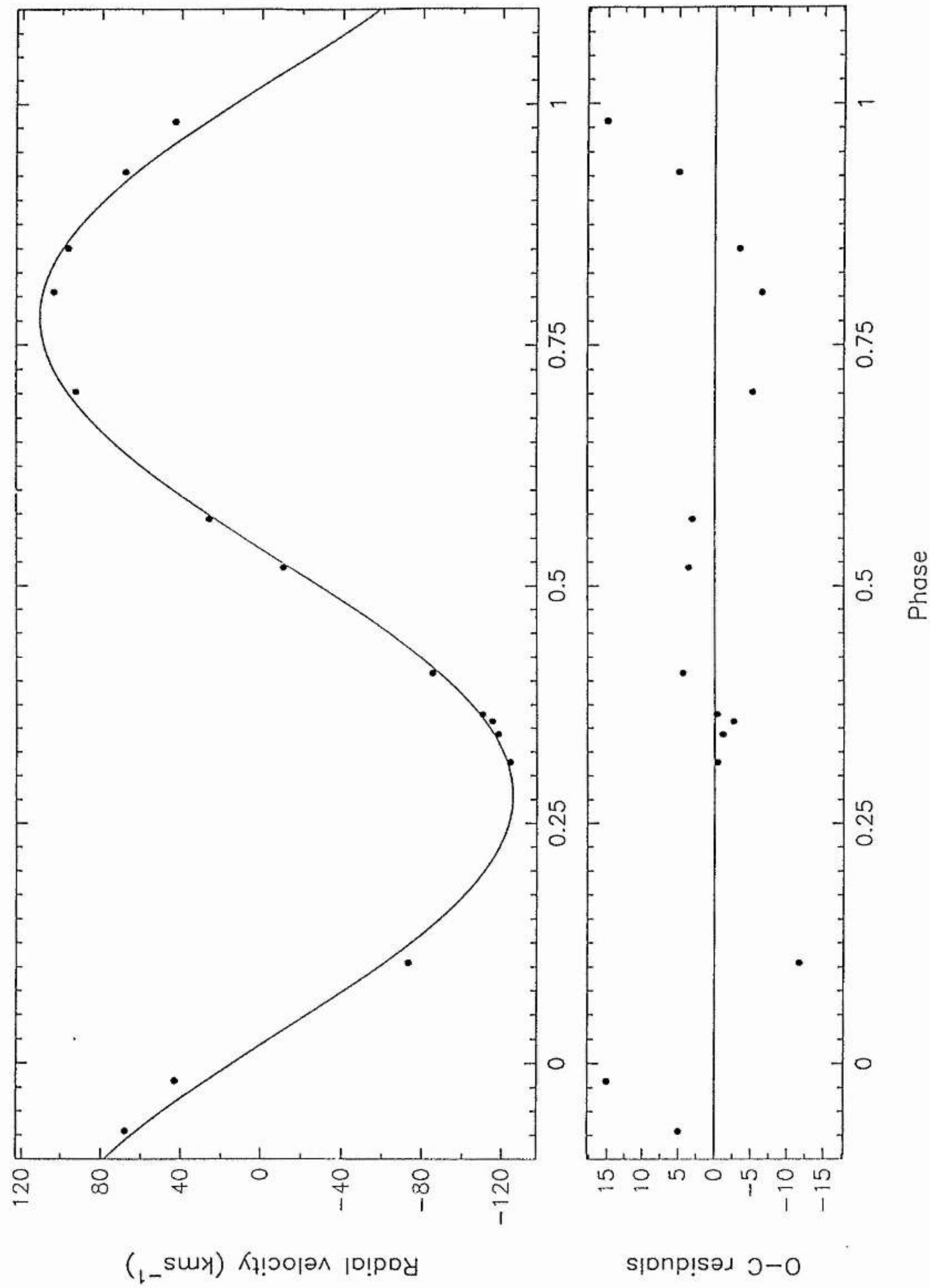

Figure 8.3: Radial Velocities for the Primary Component of XY UMa, plotted with the orbital solution, and corresponding O-Cs (lower plot).

8.4 The RS CVn-type Binary System SV Camelopardalis

The short-period RS CVn-type eclipsing binary SV Cam (HD44982), like XY UMa (Section 8.3), also exhibits erratic light curve changes (see Figure 1.1), presumably due to dark starspot activity (eg. Zeilik *et al.* 1988). Indeed, observed infrared flux excesses for SV Cam (Cellino *et al.* 1985) suggest the presence of cool regions, some 1500K cooler than the quiet photosphere.

Like XY UMa, the light curve of SV Cam has been well observed in recent years. Hilditch *et al.* (1979), showed that SV Cam is composed of a G3V primary component which is slightly evolved above the main sequence, and a K4V secondary component.

Frieboes-Conde & Herczeg (1973) surveyed the extensive series of published times of minima, and concluded that the observed variations suggested a light-time effect due to orbital motion about a third body with a period of some 72.8 years. This was supported by Hilditch *et al.* (1979) who calculated a period of some 64 years, and Cellino *et al.* (1985) who calculated a period of some 74.7 years.

Spectroscopic observations of SV Cam were made by Hiltner (1953), and more recently analysis by Lucy & Sweeney (1971), yielded a radial velocity semi-amplitude for the primary component of $K_1 = 121.6\,\mathrm{km\,s^{-1}}$ and a systemic velocity for the system of $V_0 = -15.0\,\mathrm{km\,s^{-1}}$.

Radial velocity spectra of SV Cam centred on 4200 Å were obtained and reduced as detailed in Chapter 2.

Using the G1 radial velocity standard star HD84441 for cross-correlation, the radial velocity measurements listed in Table 8.2 were obtained. Like XY UMa (Section 8.3), only primary component velocities could be measured from the cross-correlation functions, and even using later type standard star templates, the secondary component could not be seen in the cross-correlation peaks.

The corresponding orbital phasing of the primary component measurements given in Table 8.2 were calculated using the ephemeris :-

$$\mathrm{HJD}\ 2447258.5326\,(\pm 17) + 0.59307121\,(\pm 5)\,\mathrm{E}$$

This ephemeris (Pollard 1988a) was derived by Dr.C.Pollard and the author following photoelectric observations of several primary minima of SV Cam made in October 1987 and

February 1988, using the TPT and James Gregory telescopes at St Andrews, as part of the commissioning of a new 8-channel photometer built at St Andrews (Pollard 1988b).

Assuming circular orbits, the sine wave fit and corresponding residuals to the radial velocity data for the primary component of SV Cam is shown in Figure 8.4.

This fit gives a radial velocity semi-amplitude for the primary component of $K_1 = (122.7 \pm 2.0)\,\mathrm{km\,s^{-1}}$ and a systemic velocity for the system of $V_0 = (-9.7 \pm 1.5)\,\mathrm{km\,s^{-1}}$. The primary component semi-amplitude shows good agreement with the value obtained by Lucy & Sweeney (1971), and the clearly changing value of systemic velocity supports the suggestions from period studies of orbit about a third body.

H.J.D.	Phase	V_1 $km\,s^{-1}$	(O-C) $km\,s^{-1}$
2447107.75733	0.7721	+113	+1.3
2447108.73657	0.4232	−69	−2.6
2447109.55225	0.7986	+103	−4.1
2447109.58345	0.8512	+90	+1.3
2447109.62343	0.9186	+42	−8.0
2447109.65283	0.9686	+36	+21.7
2447109.71235	0.0685	−71	−9.7
2447109.75929	0.1476	−112	−3.9
2447109.77371	0.1720	−118	+0.1
2447110.66357	0.6724	+96	−2.8
2447196.57477	0.5305	+12	−2.0
2447197.59132	0.2445	−132	+0.4
2447197.61714	0.2881	−129	−0.2
2447197.64096	0.3283	−117	+0.7
2447198.36402	0.5475	+38	+11.4
2447198.39341	0.5970	+58	−2.8
2447198.46834	0.7234	+108	−3.3
2447198.49299	0.7649	+108	−4.3
2447200.53073	0.2008	−123	+3.7
2447200.55914	0.2487	−130	+2.4
2447201.37219	0.6197	+89	+14.7
2447201.40231	0.6704	+92	−6.1
2447202.43560	0.4127	−79	−5.6
2447202.45903	0.4522	−48	−2.3

Table 8.2: Radial Velocity data for the Primary Component of SV Cam.

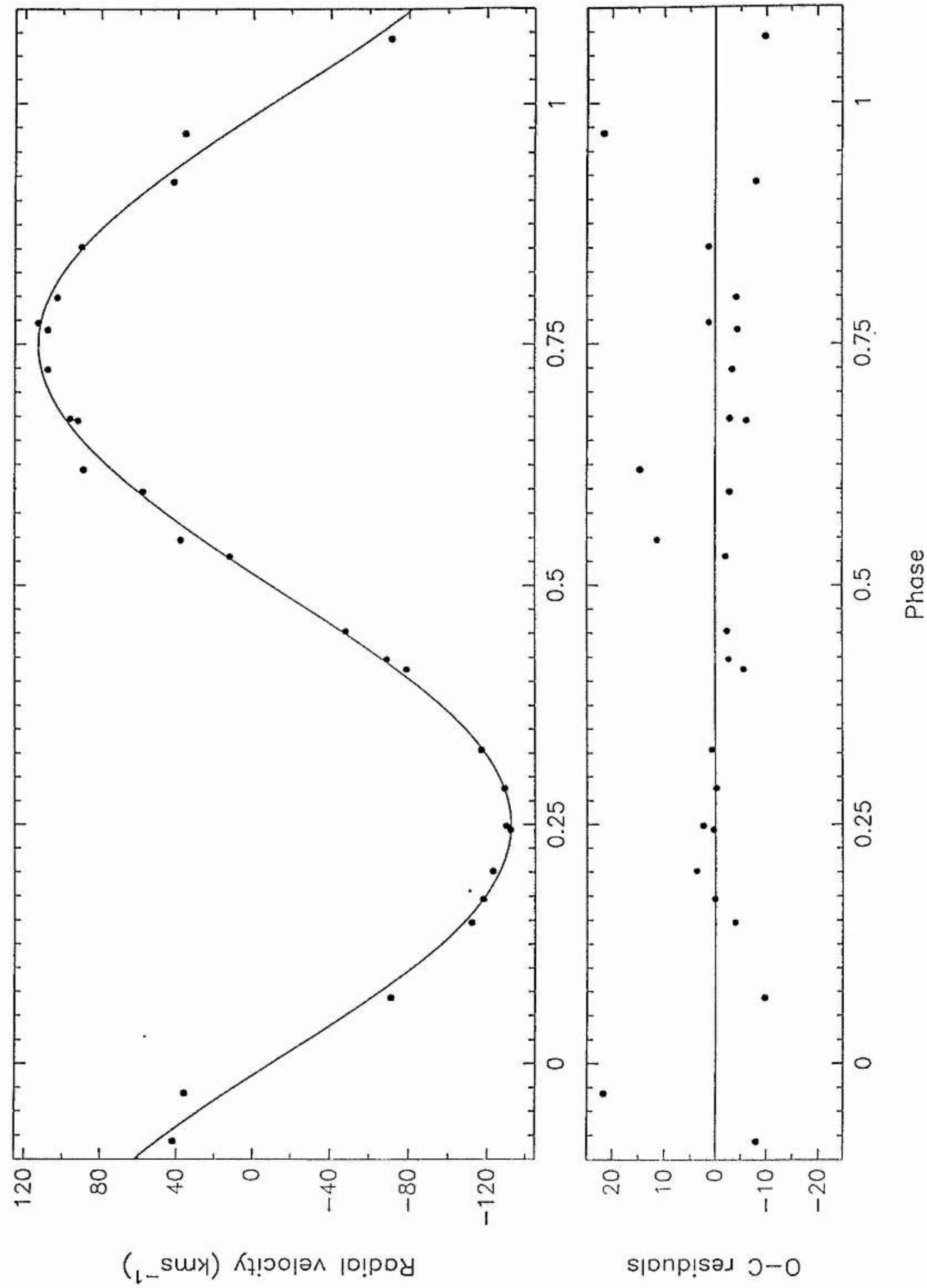

Figure 8.4: Radial Velocities for the Primary Component of SV Cam, plotted with the orbital solution, and corresponding O-Cs (lower plot).

8.5 *H-α* Line Profiles with Orbital Phase for 7 Binary Systems.

Spectra centred on 6563 Å were obtained and reduced as outlined and discussed in Chapter 2.

The attempts to analyse these line profiles are also detailed in Chapter 2, but here the data are simply presented as a compilation of the *H-alpha* line profiles with orbital phase for each binary system.

Each spectrum is shown in its rectified "R-file" format, plotted over the wavelength range 6510 Å to 6630 Å and place in order of increasing orbital phase. The orbital phasing of these observations for each binary system were calculated using the appropriate ephemerides already discussed in this work, and summarised in Table 8.3 (no errors quoted).

Figures 8.5 to 8.11 show the 6563 Å data for the binary systems TY Boo, VW Boo, BX And, SS Ari, AG Vir, TZ Boo and SV Cam respectively. Only the RS CVn-type system XY UMa was not observed at 6563 Å since it was the only object solely observed with the JKT.

Object	Ephemeris
TY Boo	HJD 2446589.7906 + 0.31714964E
VW Boo	HJD 2441091.8840 + 0.34219634E
BX And	HJD 2447117.9279 + 0.61011258E
SS Ari	HJD 2447119.7814 + 0.4059899E
AG Vir	HJD 2447593.6473 + 0.64265059E
TZ Boo	HJD 2439632.8418 + 0.2971620E
SV Cam	HJD 2447258.5326 + 0.59307121E

Table 8.3: Summary of ephemerides used to phase the 6563Å data (no errors quoted - see appropriate preceeding Section).

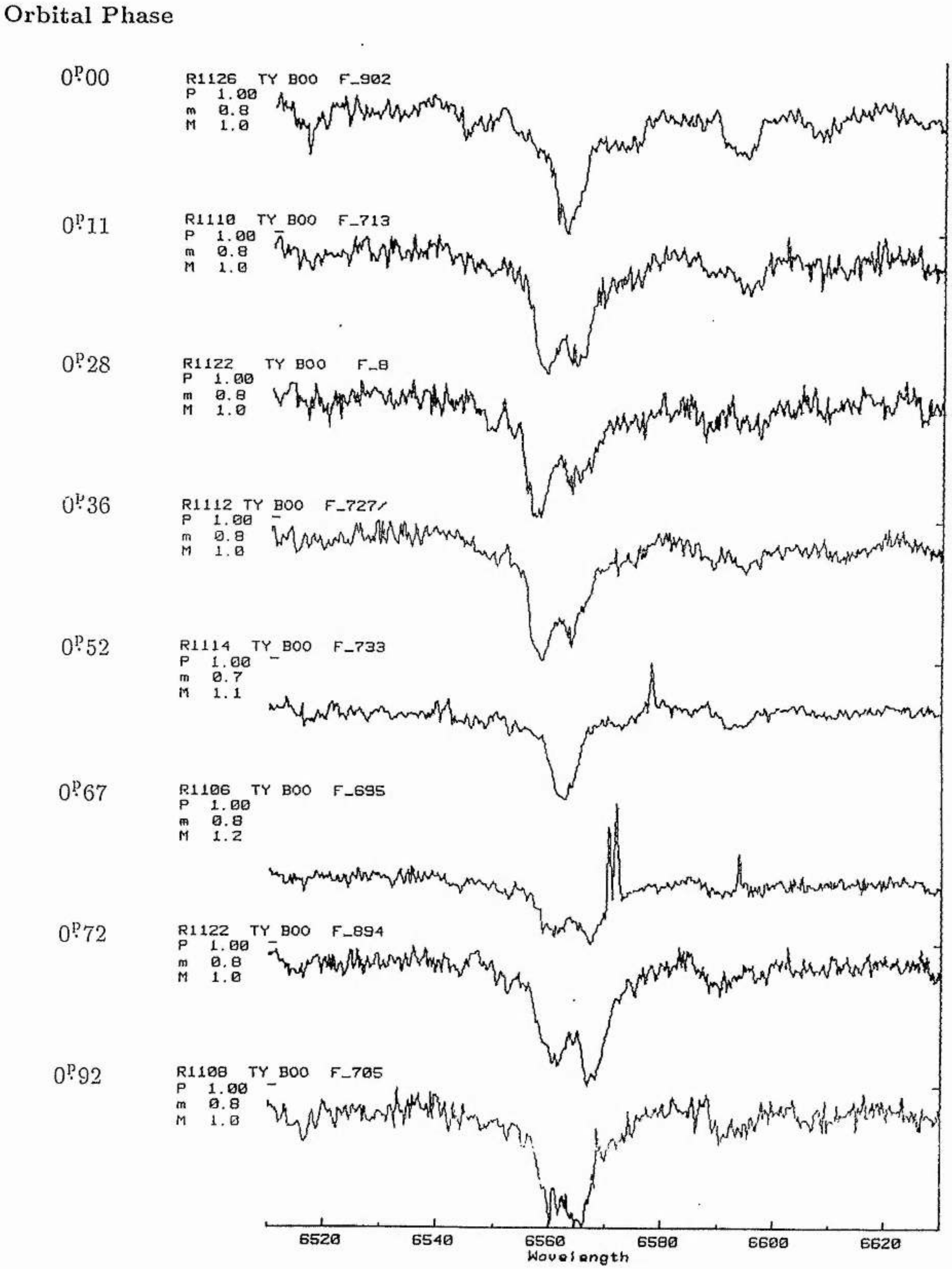

Figure 8.5: 6563 Å spectra of TY Boo showing the *H-alpha* line profile against increasing orbital phase.

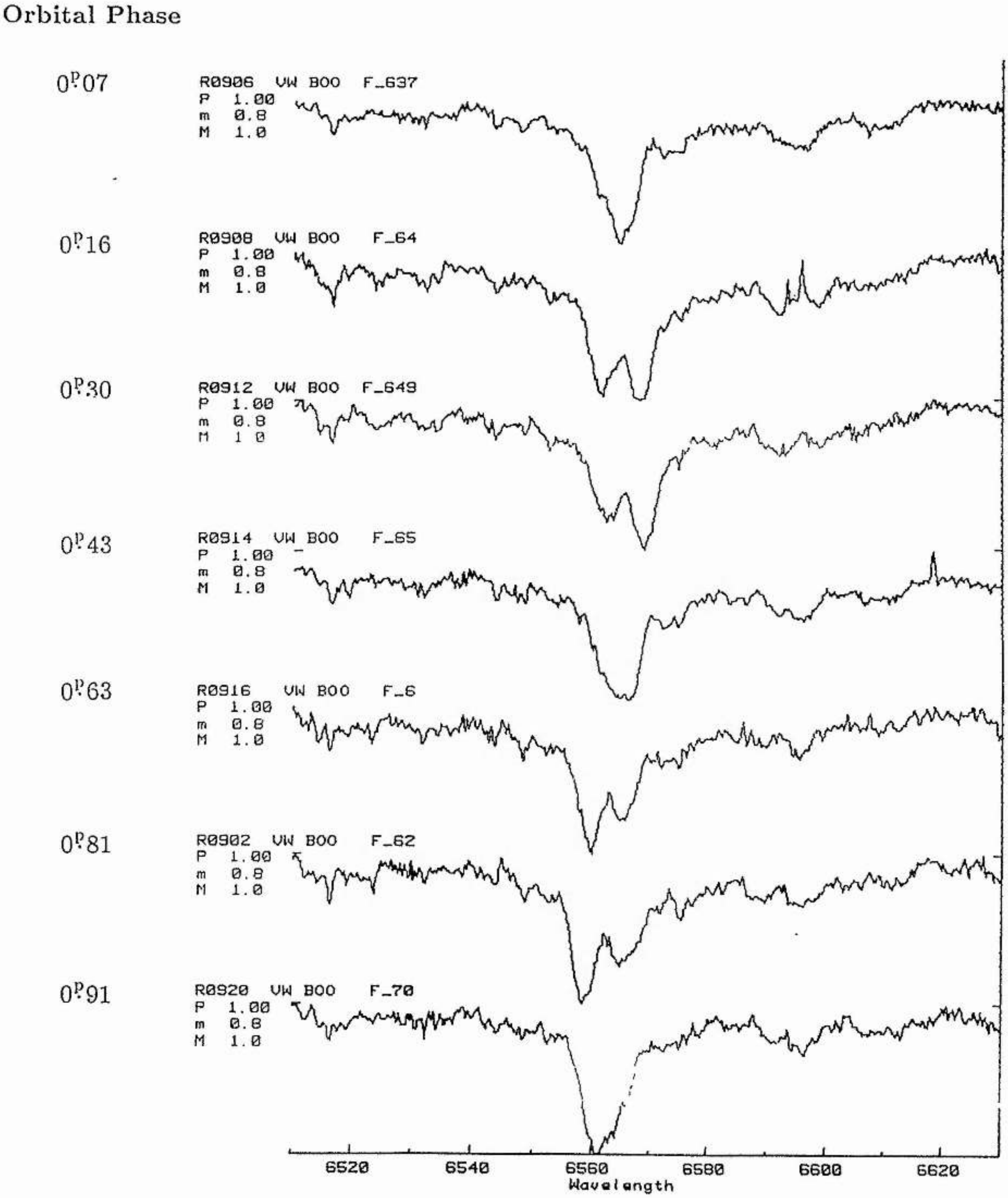

Figure 8.6: 6563 Å spectra of VW Boo showing the *H-alpha* line profile against increasing orbital phase.

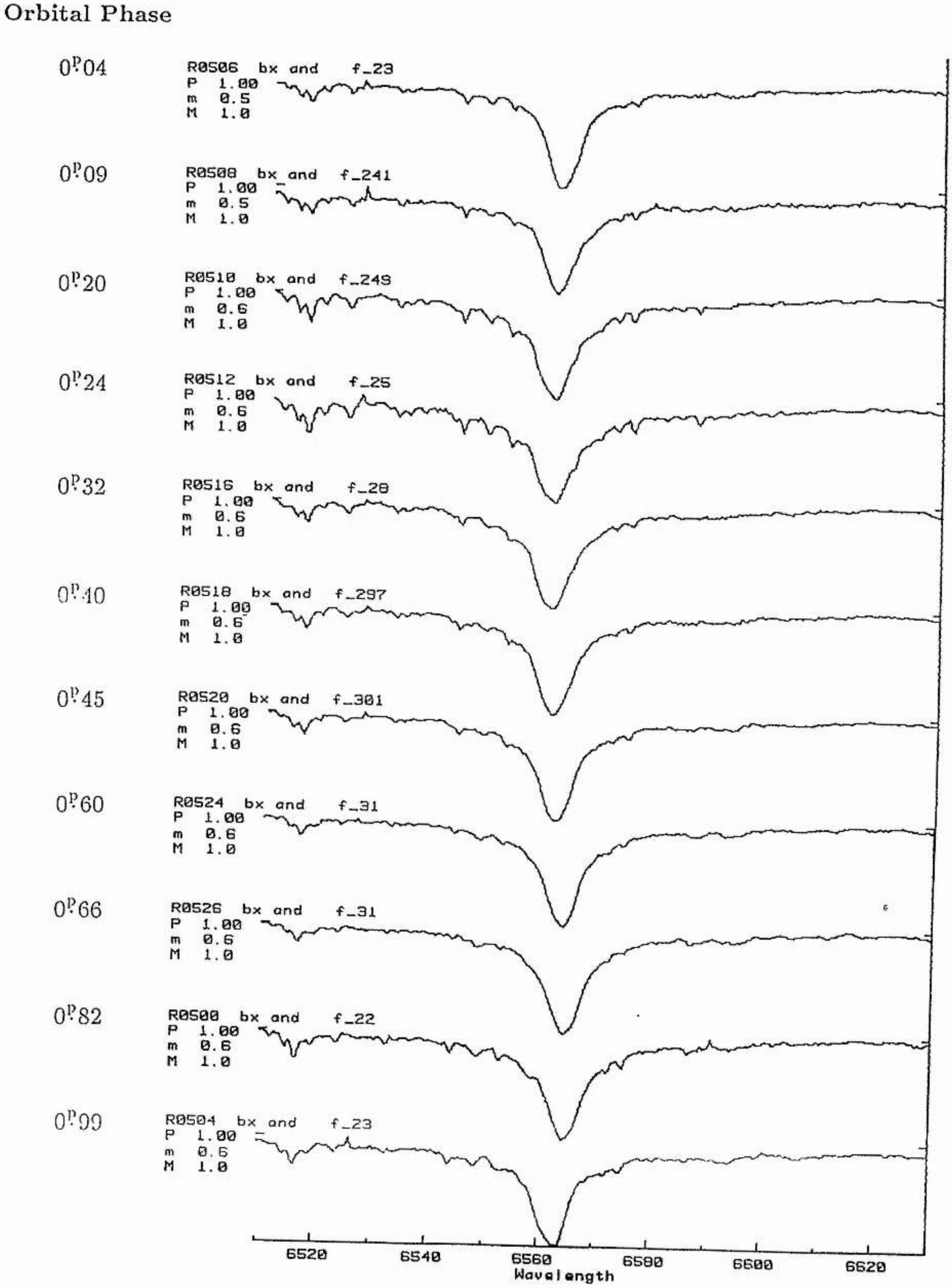

Figure 8.7: 6563 Å spectra of BX And showing the *H-alpha* line profile against increasing orbital phase.

Orbital Phase

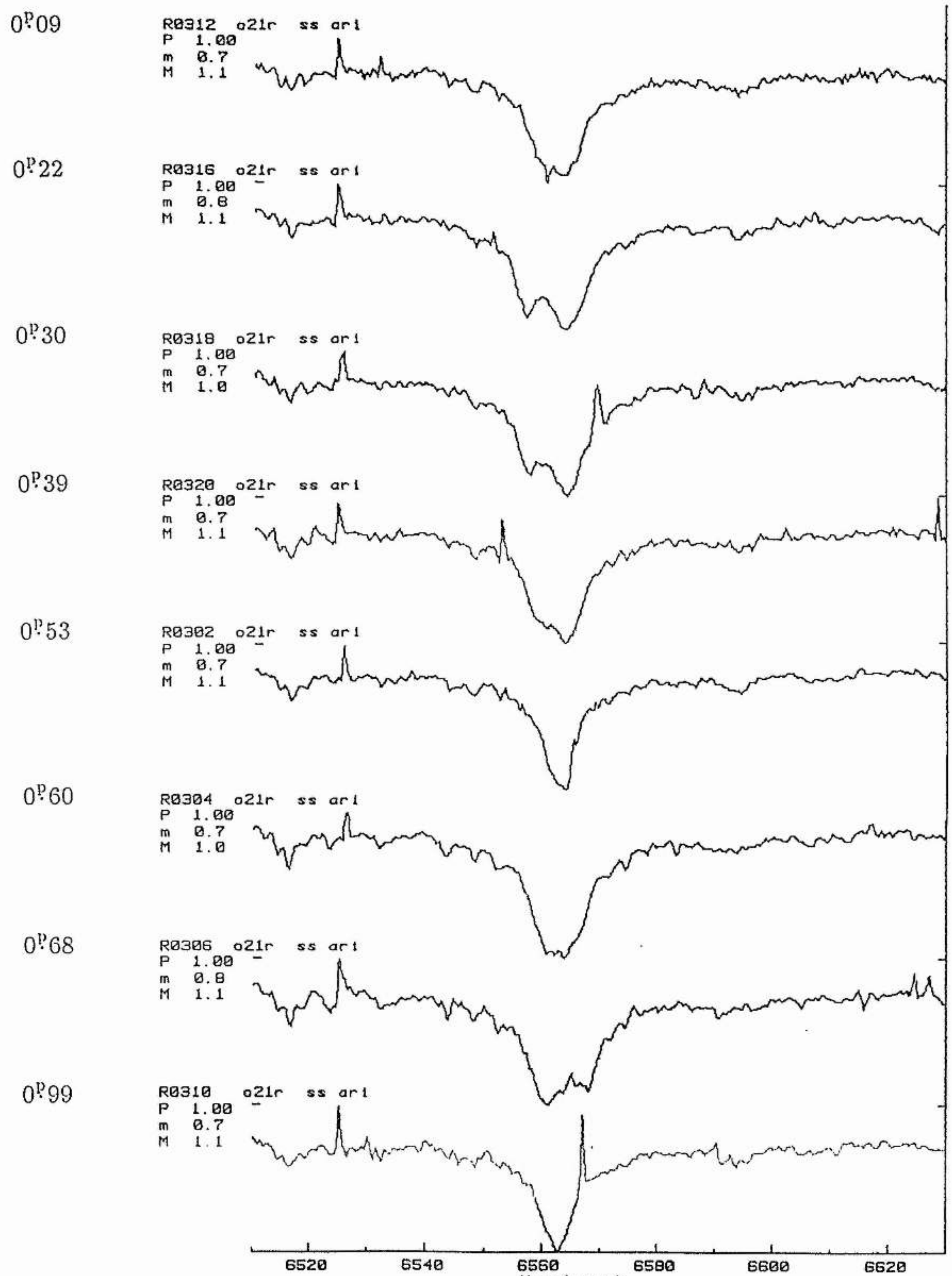

Figure 8.8: 6563 Å spectra of SS Ari showing the *H-alpha* line profile against increasing orbital phase.

Orbital Phase

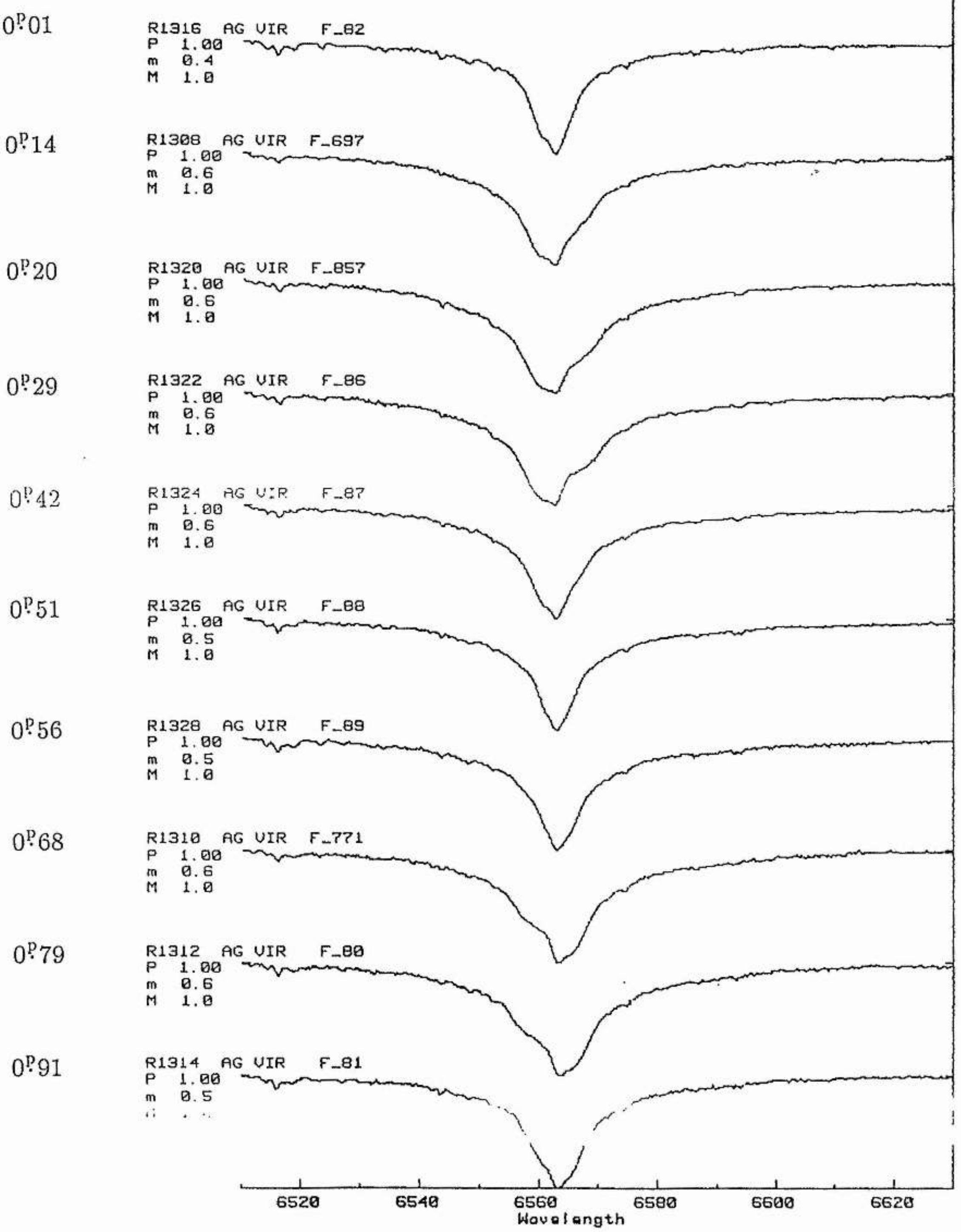

Figure 8.9: 6563 Å spectra of AG Vir showing the *H-alpha* line profile against increasing orbital phase.

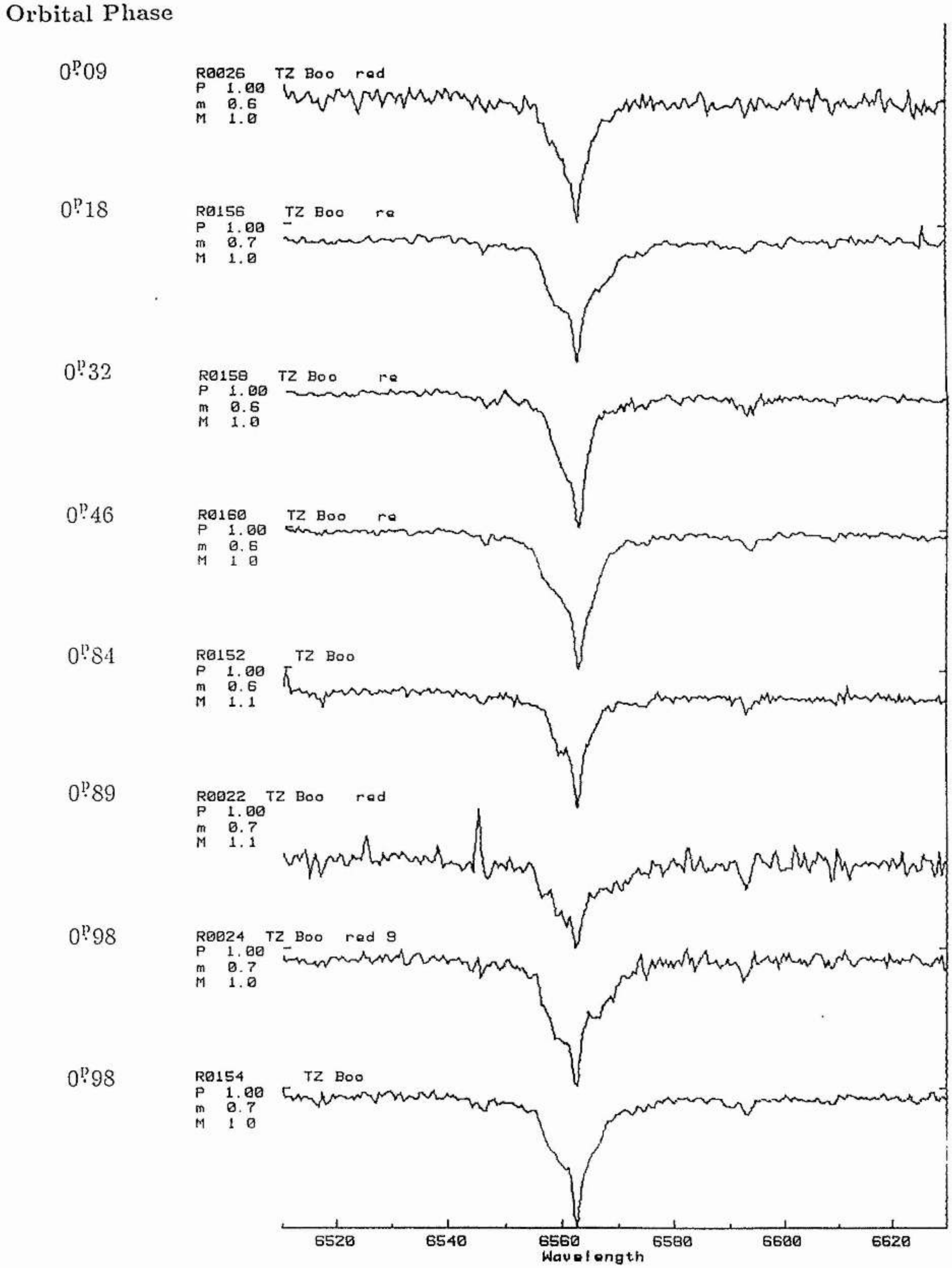

Figure 8.10: 6563 Å spectra of TZ Boo showing the *H-alpha* line profile against increasing orbital phase.

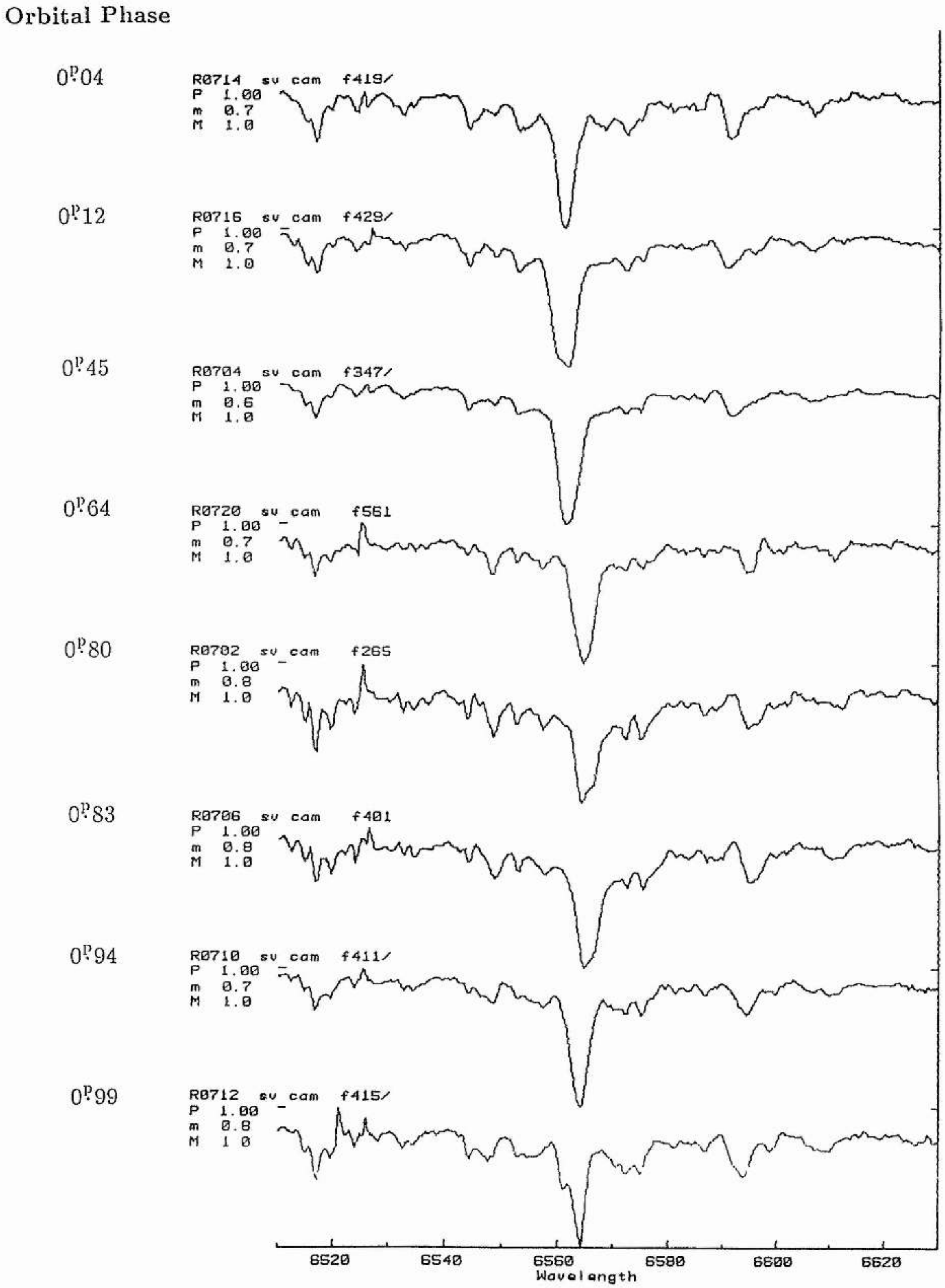

Figure 8.11: 6563 Å spectra of SV Cam showing the *H-alpha* line profile against increasing orbital phase.

8.6 References

Bedford, D.K., Jeffries, R.D., Geyer, E.H., & Vilhu, O., 1990. *Mon. Not. R. astr. Soc.*, **243**, 557.

Carr, R.B., 1971. *Publications of the Goodsell Observatory*, No. 16.

Cellino, A., Scaltriti, F., & Busso, M., 1985. *Astr. Astrophys.*, **114**, 315.

Frieboes-Conde, H., & Herczeg, T., 1973. *Astr. Astrophys. Suppl.*, **12**, 1.

Geyer, E.H., 1976. *I.A.U. Colloquium No.42*, Page 292.

Geyer, E.H., 1980. *I.A.U. Symposium No.88*, Page 423.

Guthnick, P., & Prager, R., 1927. *Kl. Veröff. Berlin-Babelsberg*, No. 4.8.

Hall, D.S., & Kreiner, J.M., 1980. *Acta Astr.*, **30**, 501.

Hilditch, R.W., Harland, D.M., & McLean, B.J., 1979. *Mon. Not. R. astr. Soc.*, **187**, 797.

Hiltner, W.A., 1953. *Astrophys. J.*, **118**, 262.

Hoffmann, M., 1978a. *Astr. Astrophys. Suppl.*, **33**, 63.

Hoffmann, M., 1978b. *Inf. Bull. Var. Stars*, 1487.

Hoffmann, M., 1980. *Astr. Astrophys. Suppl.*, **40**, 263.

Jasser, D.M.Z., 1896. *Astrophys. Space Sci.*, **128**, 369.

Lucy, L.B., & Sweeney, M.A., 1971. *Astr. J.*, **76**, 544.

McLean, B.J., & Hilditch, R.W., 1983. *Mon. Not. R. astr. Soc.*, **203**, 1.

Pollard, C.A., 1988a. *Private Communication.*

Pollard, C.A., 1988b. *PhD Thesis*, St Andrews University.

Zeilik, M., & Budding, E., 1987. *Astrophys. J.*, **319**, 827.

Zeilik, M., DeBlasi, C., Rhodes, M., & Budding, E., 1988. *Astrophys. J.*, **332**, 293.

Chapter 9

Conclusions

9.1 Summary

In this study, a detailed analysis of five low-mass, interacting binary systems has been presented, with spectroscopic mass ratios for these systems derived for the first time.

TY Boo appears to be a straight forward, shallow contact, W-type contact binary, whose light curve shows no signs of distortions due to anomalous luminosity distributions. Like other W-type systems, the primary and secondary components of TY Boo occupy regions in the M-R, M-L, and H-R diagrams (Figures 9.1, 9.2 and 9.3 respectively) that indicate the primary component lies within the main-sequence band, whilst the secondary component is over-sized and over-luminous (Hilditch *et al.* 1988).

The physical parameters of VW Boo are similar to those for TY Boo, with only some 100K additional temperature difference between the components of VW Boo. (Also VW Boo is an "A-type" in terms of eclipsed components). However, light curve analysis of VW Boo suggests a region of excess luminosity around the neck joining the two components. Again the primary component of VW Boo lies on the main-sequence band, whilst the secondary component is over-sized and over-luminous on the M-R and M-L diagrams, occupying similar regions as the secondary components of other marginal contact "B-type" binaries. However, on the H-R diagram, the secondary component is found to lie in the main-sequence band, between other B-type secondary components, and the secondary components of the W-type systems.

The binary system BX And, whilst being in marginal contact, exhibits a substantial temperature difference between the components. Like VW Boo, light curve analysis of BX And suggests a region of excess luminosity around the neck joining the two components. The components show similar properties to other B-type binary components, the primary lying close to the TAMS relationship (Vandenberg 1985) in the main-sequence band, and the secondary being over-sized and over-luminous.

Although there is only a small temperature difference of some 150K between the components of the marginal contact system SS Ari, an anomalous luminosity distribution is immediately evident from the unequal heights of quadrature observed in the light curve. However, with this type of distortion, geometric considerations suggest that the distorting feature in this case must reside on the side of the affected component rather than around the neck joining the system. Like TY Boo, the components of SS Ari are found to occupy the same regions on the M-R, M-L and H-R diagrams as the components of standard W-type binary systems.

AG Vir has a similar light curve to that of SS Ari (but with a much greater temperature difference between the components), suggesting a similar distorting anomalous luminosity distribution. Like BX And, the components of AG Vir show similar properties to other B-type binary components. However, in the H-R diagram the secondary component of AG Vir is found to lie on the ZAMS relationship of the main-sequence band, rather than to the left or right of it, as do the secondary components of the W-type and B-type systems respectively (compare with VW Boo).

9.2 Spot Models

This study represents the first attempts at a quantitative analysis of the regions of excess luminosity observed in some binary systems. Until now, the basic contact binary light curve generating model has been used to provide the best fit to the observed light curves, the presence of spots inferred from the regions of anomalous luminosity (Figure 1.6), and in some cases, the use of the secondary albedo as a free parameter employed to synthesize a better fit (eg. McFarlane *et al.* 1986 and Kaluzny 1983). A quantitative analysis is now possible as the "next generation" of light curve synthesis routines begin to include the ability to add spots to the basic binary model. However, the problems of obtaining unique solutions must always be borne in mind with any attempts at modelling spots.

It now seems increasingly clear that the variety of different distortions observed in binary light curves are due not to a single phenomenon, but rather a variety of different phenomena.

The semi-detached RS CVn-type binaries, briefly discussed in Chapter 8, and contact systems like TZ Boo (also Chapter 8), show strong and convincing evidence for erratic light curve distortions produced by dark starspots on one of the components. Such starspots also have a strong theoretical base, being analogous to Sunspots, but magnified by the "spinning up" of components in a close binary system.

The rather different regions of "excess luminosity" investigated in this study appear to fall into two groups, VW Boo and BX And exhibiting a different type of phenomenon from SS Ari and AG Vir.

The excess luminosity observed in VW Boo and BX And around the ingress and egress to secondary minima is only really revealed when a basic light curve analysis is applied, since the light curves at first glance appear similar to those of standard contact systems like TY Boo. Since geometric considerations suggest that these regions of excess luminosity must reside around the neck joining the two components, and such systems also exhibit a temperature difference between components, it seems natural to conclude that these systems are in poor thermal contact, and the excess luminosity is due to the expected energy transfer from the hotter to the cooler component. In this case, the term "hot spot" could be misleading, since the region is more of a "warm puddle" at a temperature between that of the two components as the two components thermalize out. The analysis of such systems therefore provides an immediate test on the theory, since the modelled spot temperature cannot be hotter than the temperature of the hottest component in the system. Both VW Boo and BX And analysed here fulfill this constraint.

The anomalous luminosity distribution in SS Ari and AG Vir is immediately obvious in the shape of the light curve. The analysis presented here of these two systems attempts to apply the same energy transfer scenario seen in VW Boo and BX And to model a hot spot in these systems. However, this form of distortion causes several problems for this model. Firstly why should the energy transfer be "shifted" from the neck to one side of the component ? Secondly, in the more extreme light curve distortion of AG Vir, there is some evidence that the distorting phenomenon actually resides on the hotter component ! Alternatively it could be argued that dark starspots on the opposite hemisphere are responsible for this distortion, but neither scenario really provides a convincing model for these systems. It is possible therefore that this form of distortion is due to a third type of phenomenon, like for example Faculae (Rucinski 1985), which like starspots are analogous to the solar examples, but magnified due to the "spinning up" of components in a close binary system.

9.3 Evolutionary Status

As detailed in Chapter 1, an important reason for studying marginal contact systems in poor thermal contact is the lack of observed systems in the "broken contact state" predicted by the TRO Theory. As a result of evolution through angular momentum loss, it is reasonable to expect those binaries which are undergoing TRO-like oscillations to exhibit lower specific orbital angular momentum than those systems which are reaching contact for the first time.

Hilditch *et al.* (1988) complied the first evolutionary data base for late-type contact and near contact binaries, using the masses, radii, and luminosities for the 31 well studied systems available (Section 1.4.2). Angular momentum considerations, and other properties of the three B-type systems in this compilation, suggested that these systems were reaching contact for the first time rather than being in the broken contact state of the TRO process.

Since the compilation of Hilditch *et al.* good photoelectric and spectroscopic data have been published for two more of systems (AB And and OO Aql) and improved data published for the system VW Cep, already in the data base. These new and revised data are presented in Table 9.1, along with the data for the five new systems analysed in this study. This brings the evolutionary data base up to 38 well observed systems, the work presented here providing 13% of the data, and more importantly adds four more B-type systems to the sample.

Object	Type	P(days)	logM(pri)	(sec)	logR(pri)	(sec)	logT(pri)	(sec)	logL(pri)	(sec)	Reference
AB And	W	0.332	+0.00	−0.31	+0.02	−0.12	+3.74	+3.77	−0.06	−0.23	Hrivnak 1988
OO Aql	A	0.507	+0.02	−0.06	+0.14	+0.11	+3.76	+3.75	+0.26	+0.17	Hrivnak 1989
VW Cep	W	0.278	−0.05	−0.61	−0.03	−0.30	+3.69	+3.72	−0.34	−0.78	Hill 1989
TY Boo	W	0.317	−0.04	−0.40	+0.00	−0.16	+3.76	+3.79	+0.01	−0.21	Chapter 3
VW Boo	B	0.342	−0.01	−0.38	+0.03	−0.13	+3.76	+3.71	+0.05	−0.45	Chapter 4
BX And	B	0.610	+0.18	−0.12	+0.25	+0.11	+3.83	+3.65	+0.79	−0.20	Chapter 5
SS Ari	B	0.406	+0.03	−0.47	+0.10	−0.12	+3.79	+3.80	+0.30	−0.11	Chapter 6
AG Vir	B	0.643	+0.22	−0.28	+0.29	+0.06	+3.78	+3.80	+1.02	+0.27	Chapter 7

Table 9.1: New mass, radii and luminosity data for 8 contact binaries, updating the compilation of Hilditch *et al.* (1988).

The data in Table 9.1 were added to the original compilation of Hilditch *et al.* and evolutionary M-R, M-L and H-R diagrams produced for the 38 system data base. These are shown plotted in Figures 9.1, 9.2 and 9.3 respectively. A discussion of the results for each system studied here is given in the corresponding Chapter, and summarized in Section 9.1.

Finally, Figure 9.4 shows a plot of q verse $\log(q(1+q)^{-2}P^{\frac{1}{3}})$, where q is the mass ratio and P the orbital period (in days) of the system, for the 38 system data base. This provides a relative easy measure of the specific orbital angular momentum of each well observed system, since :-

$$q.(1+q)^{-2}.P^{1/3} \propto J_{orb}/M_{tot}^{5/3}$$

where J_{orb} is the orbital angular momentum, and M_{tot} is the total mass of the binary.

Of the four B-type systems presented in this work, the angular momentum considerations shown in Figure 9.4, and the other properties of these systems, tend to suggest that these systems too could well be reaching contact for the first time rather than being in the broken contact phase of the TRO process.

Both BX And and AG Vir exhibit greater specific orbital angular momentum than W-type contact binaries of the same mass ratios.

SS Ari is much closer to the W-type systems, with a lower angular momentum than AG Vir, but not sufficiently low for conclusive conclusions to be reached. Since the temperature difference between the components of SS Ari is only small it may be that in this case thermal contact is almost complete after having come into contact for the first time. On the other hand, the period behaviour of SS Ari suggests past cyclic periods of mass transfer. (However it should be noted that the period behaviour of BX And, which does seem to be coming into contact for the first time also suggests past cyclic activity !). Hence the evolutionary position of SS Ari is far from certain, and clearly warrants further study.

Like SS Ari, the position of VW Boo is not entirely clear, and warrants further study. VW Boo does have a specific orbital angular momentum close to the W-type systems, but again no firm conclusions can be drawn. VW Boo further raises curiosity because its secondary component lies, in the H-R diagram, between the B-types and W-types, suggesting it is in transition between the two, either for the first time or

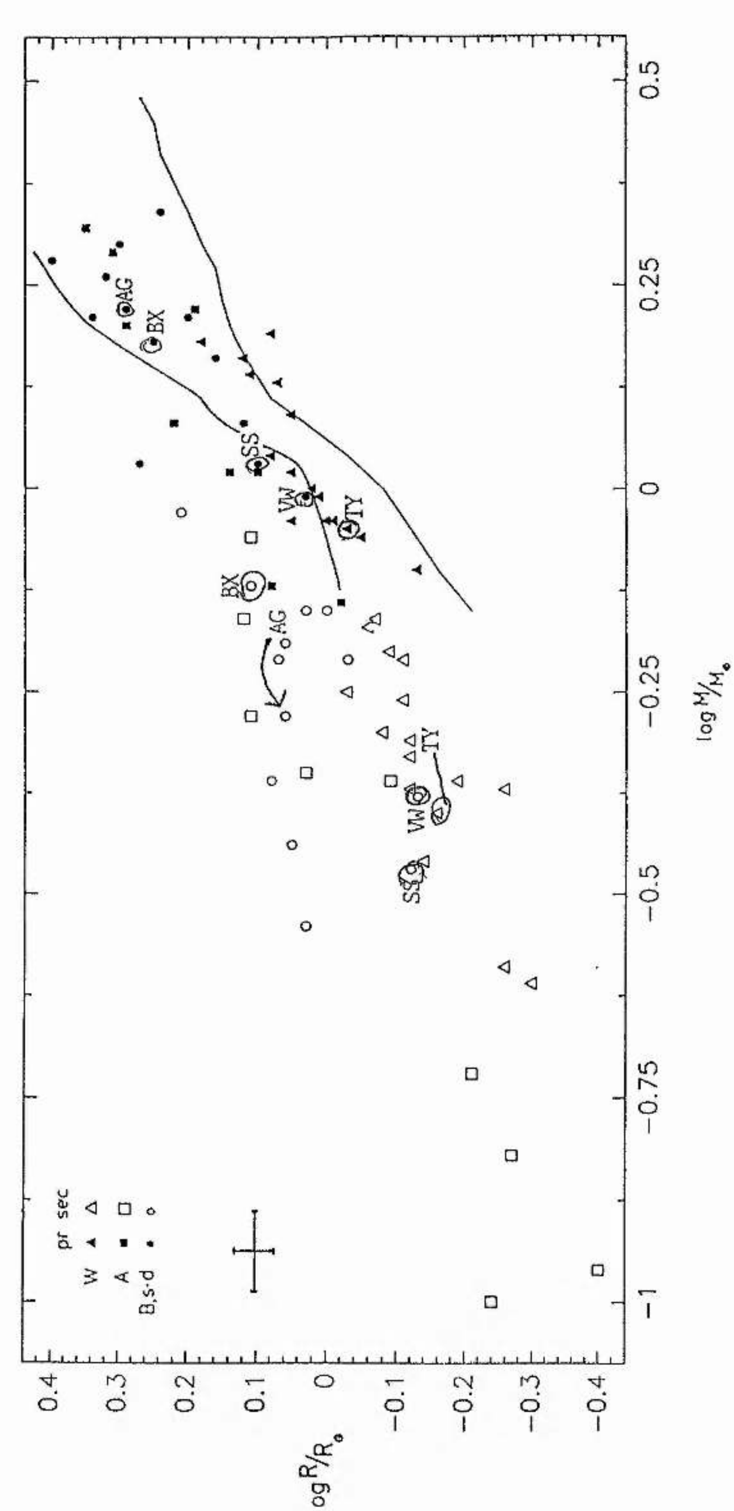

Figure 9.1: Location of primary and secondary components of 38 well observed contact/near-contact binary stars in the mass-radius plane. Also shown are the ZAMS and TAMS lines from VandenBerg (1985), and error bars typical for the sample.

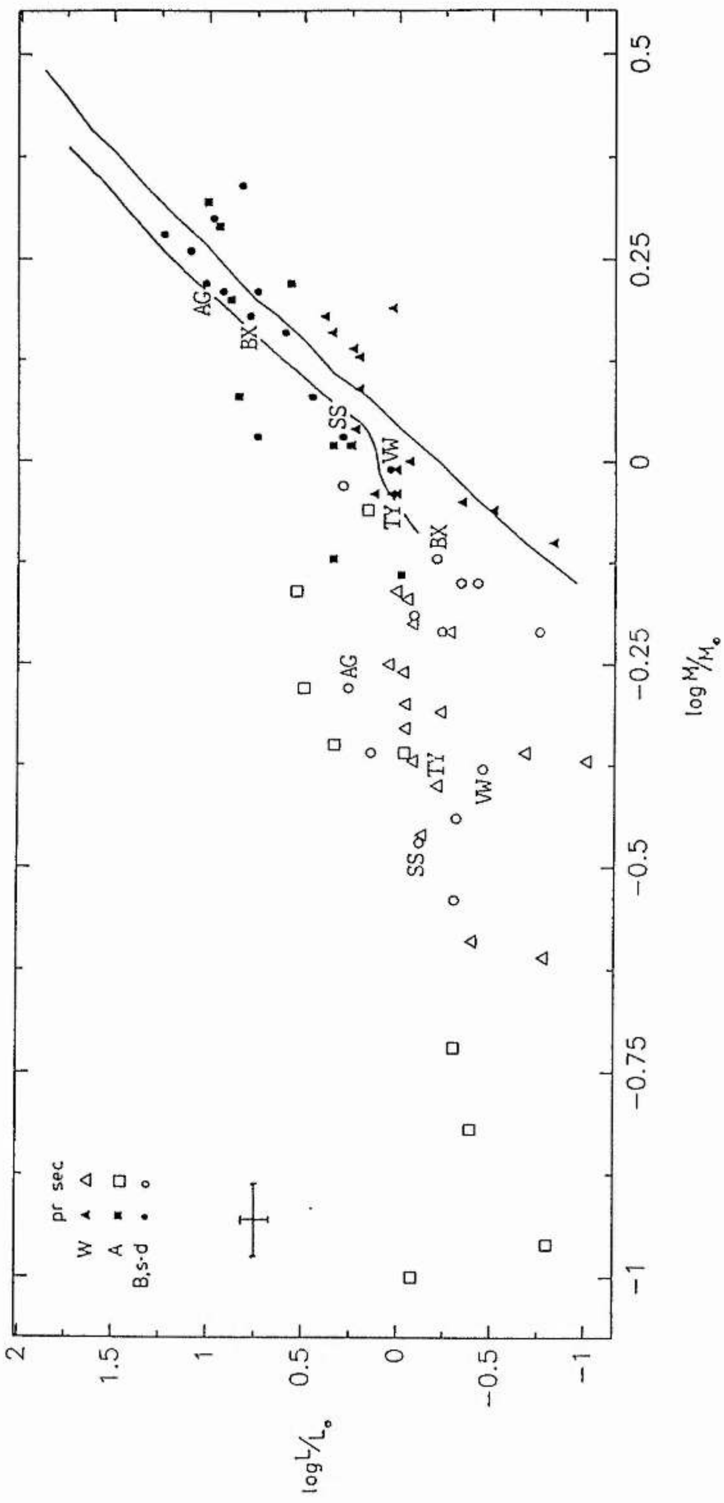

Figure 9.2: Location of primary and secondary components of 38 well observed contact/near-contact binary stars in the mass-luminosity plane. Also shown are the ZAMS and TAMS lines from VandenBerg (1985), and error bars typical for the sample.

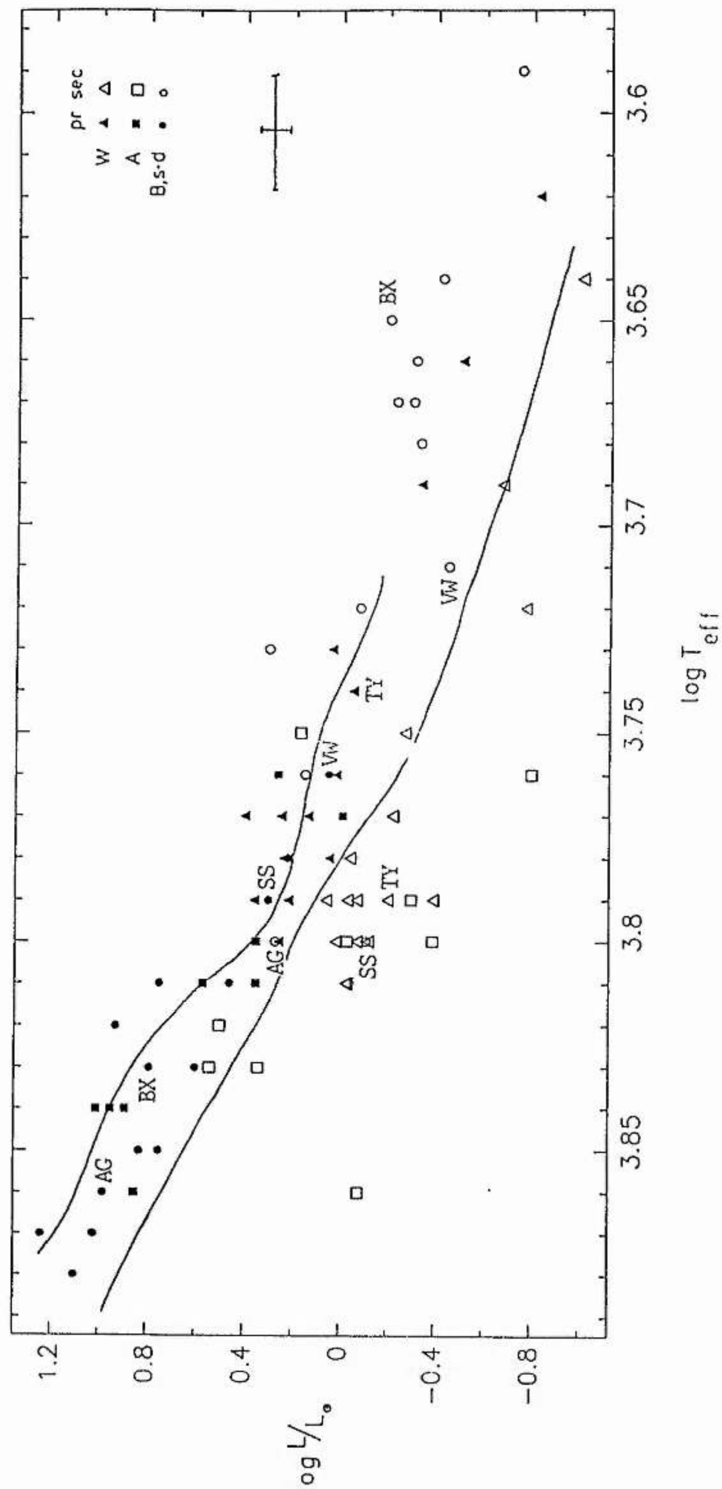

Figure 9.3: Location of primary and secondary components of 38 well observed contact/near-contact binary stars in the H-R diagram. Also shown are the ZAMS and TAMS lines from VandenBerg (1985), and error bars typical for the sample.

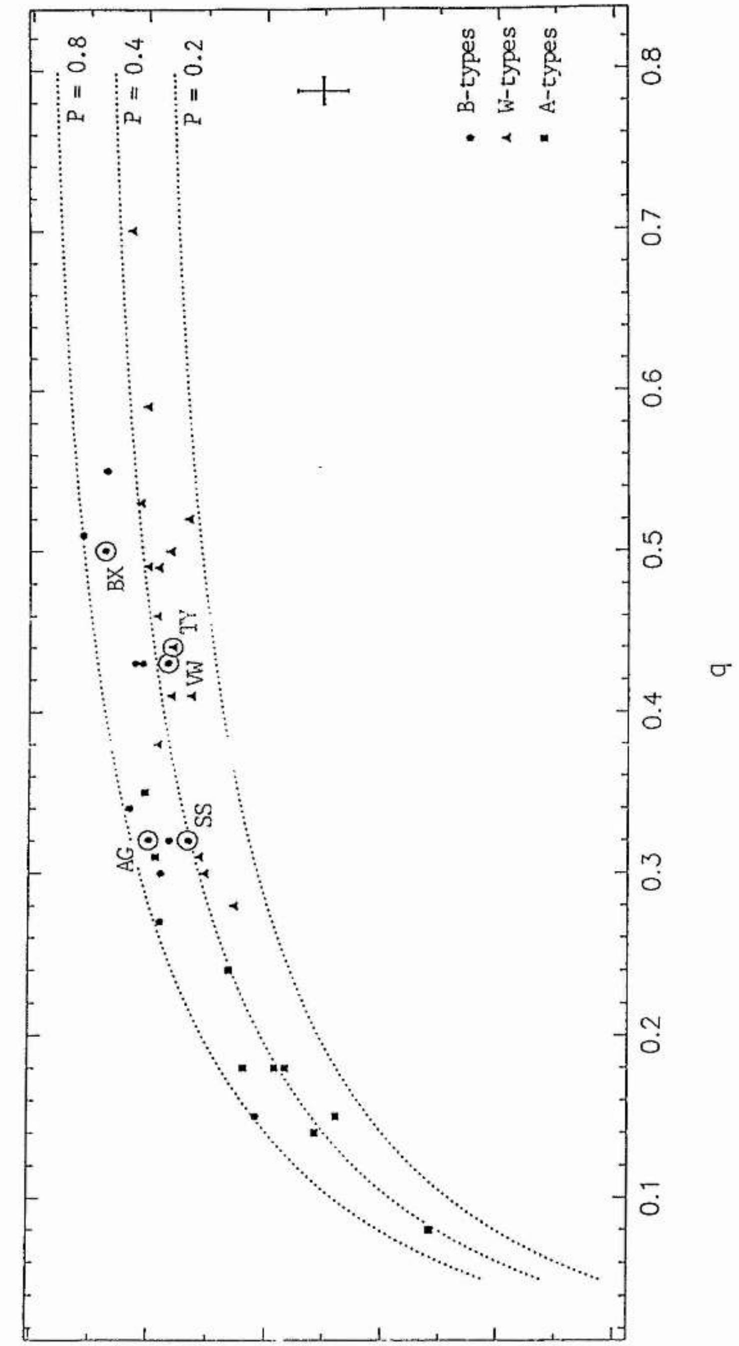

Figure 9.4: Relative orbital angular momenta of 38 well observed contact/near-contact binary stars. The dashed lines indicate the dependence of the ordinate on mass ratio at constant orbital period.

cyclically. However, again a note of caution should be sounded, since the secondary component of AG Vir, which does seem to be coming into contact for the first time, also occupies a similar position in the main-sequence band on the H-R diagram. Further, the orbital period of VW Boo is the least certain of the systems studied in this work, and a "shift" in position on the H-R diagram can be caused by uncertainty in assigning an effective temperature to the primary component.

9.4 Concluding Remarks

Clearly then the TRO Theory, unless critically "dampened" by angular momentum loss via magnetic braking, still suffers from a lack of systems in the broken state of contact. This work has made a significant improvement to the size of the evolutionary data base, particularly by adding four more B-type systems. Although the trend for such systems to be reaching contact for the first time continues, the uncertainty surrounding the evolutionary status of SS Ari and VW Boo is a clear marker for further study. In this regard however, it must be questioned whether theoretically the loss of angular momentum with time expected from a system undergoing TRO-like oscillations, would be significant enough to distinguish it observationally from a system which is just reaching contact for the first time.

The position surrounding some of the distortions seen in binary light curves due to anomalous surface luminosity distributions, seems to suggest that different distortions are produced by different phenomena. In particular the model of a hot spot around the neck in some systems, due to energy transfer between components has been quantitatively modelled for the first time, proving that such "warm" spots due to energy transfer can be responsible for the magnitude of distortions observed. Equally the lack of success of dark and "warm" spots to explain the distortions in systems like SS Ari and AG Vir, where the light curve quadrature heights are unequal, suggests that a third distorting mechanism may be active in such systems.

Finally it is gratifying to note that this work is already being followed up by the St Andrews group, in collaboration with others, and that further observations of some of these objects (and others) are planned to provide further quantitative analysis of the "spot" phenomena. Clearly simultaneous observations over a wide wavelength range, as attempted in this work but sunk by instrument malfunction, are still likely to be a useful tool in determining spot temperatures, and to some extent positions, thus reducing the number of free parameters in the model. But most of all, the extension of "Doppler Imaging" techniques (Section 1.5.3.2) to contact binaries will clearly provide a powerful tool in accurately analysing all types of spot phenomena. Whilst it is disappointing that the 6563 Å observations in this work were not quite of high enough resolution and signal to noise to reveal such features, the St Andrews group have been able to use the bench mark laid down by these observations, along with the magnitude of spot phenomena now expected from this quantitative analysis, to plan new observations with the "new generation" of larger optical telescopes and detectors. Such observations and analysis will hopefully go a long way towards finally unravelling the true nature of distorting phenomena which are active in these late-type contact binaries.

9.5 References

Hilditch, R.W., King, D.J., & McFarlane, T.M., 1988. *Mon. Not. R. astr. Soc.*, **231**, 341.

Hill, G., 1989. *Astr. Astrophys.*, **218**, 141.

Hrivnak, B.J., 1988. *Astrophys. J.*, **335**, 319.

Hrivnak, B.J., 1989. *Astrophys. J.*, **340**, 458.

Kaluzny, J., 1983. *Acta Astr.*, **33**, 345.

McFarlane, T.M., Hilditch, R.W., & King, D.J., 1986. *Mon. Not. R. astr. Soc.*, **223**, 595.

Rucinski, S.M., 1985. *Interacting Binaries*, **17**, Reidel Publishing Company.

Vandenberg, D.A., 1985. *Astrophys. J. Suppl.*, **58**, 711.